

PREPARATION AND CHARACTERIZATION OF RECYCLED  
POLYPROPYLENE BASED NANOCOMPOSITES

A THESIS SUBMITTED TO  
THE GRADUATE SCHOOL OF NATURAL AND APPLIED SCIENCES  
OF  
MIDDLE EAST TECHNICAL UNIVERSITY

BY

FİLİZ CENGİZ

IN PARTIAL FULFILLMENT OF THE REQUIREMENTS  
FOR  
THE DEGREE OF MASTER OF SCIENCE  
IN  
CHEMICAL ENGINEERING

SEPTEMBER 2008

Approval of the thesis:

**PREPARATION AND CHARACTERIZATION OF RECYCLED POLYPROPYLENE  
BASED NANOCOMPOSITES**

submitted by **FİLİZ CENGİZ** in partial fulfillment of the requirements for the degree of  
**Master of Science in Chemical Engineering Department, Middle East Technical  
University** by,

Prof. Dr. Canan Özgen  
Dean, Graduate School of **Natural and Applied Sciences** \_\_\_\_\_

Prof. Dr. Gürkan Karakaş  
Head of Department, **Chemical Engineering** \_\_\_\_\_

Prof. Dr. Ülkü Yılmaz  
Supervisor, **Chemical Engineering Dept., METU** \_\_\_\_\_

**Examining Committee Members:**

Prof. Dr. Duygu Kısakürek  
Chemistry Dept., METU \_\_\_\_\_

Prof. Dr. Ülkü Yılmaz  
Chemical Engineering Dept., METU \_\_\_\_\_

Prof. Dr. Leyla Aras  
Chemistry Dept., METU \_\_\_\_\_

Prof. Dr. Erdal Bayramlı  
Chemistry Dept., METU \_\_\_\_\_

Assoc. Prof. Dr. Göknur Bayram  
Chemical Engineering Dept., METU \_\_\_\_\_

**Date:** 05.09.2008  
\_\_\_\_\_

**I hereby declare that all information in this document has been obtained and presented in accordance with academic rules and ethical conduct. I also declare that, as required by these rules and conduct, I have fully cited and referenced all material and results that are not original to this work.**

Name, Last name: Filiz Cengiz

Signature:

## ABSTRACT

### PREPARATION AND CHARACTERIZATION OF RECYCLED POLYPROPYLENE BASED NANOCOMPOSITES

Cengiz, Filiz

M.S., Department of Chemical Engineering

Supervisor: Prof. Dr. Ülkü Yılmaz

September 2008, 207 pages

The aim of this study was to improve the mechanical properties of a recycled grade polypropylene. Polymer blends and nanocomposites were prepared by melt compounding method in a twin screw extruder. Cloisite® 15A, Cloisite® 25A and Cloisite® 30B were used as organoclays, and ethylene-methyl acrylate-glycidyl methacrylate (E-MA-GMA) and maleic anhydride grafted polypropylene (PP-MAH) were used as compatibilizers. The effects of additive concentrations, types of organoclays and compatibilizers, processing conditions, and the compatibilizer to organoclay ratio on the morphology and mechanical, thermal and flow properties were investigated.

Organoclay loading over 2 wt% prevented the intercalation mechanism and material properties, even in the presence of compatibilizer, as a consequence of large clay agglomerate formation. E-MA-GMA compatibilizer improved the intercalation ability of the polymer; however a substantial increase in mechanical properties was not obtained. PP-MAH is found to be a better compatibilizer.

Processing conditions significantly affected both mechanical properties and morphology. When the processing temperature was decreased and screw speed was increased simultaneously, tensile and impact properties were improved owing to enhanced shear and dispersive forces.

TEM analysis revealed that intercalated and delaminated structures were formed with the addition of PP-MAH compatibilizer. In addition to that, as the ratio of PP-MAH to organoclay was increased, more effective dispersion of organoclay was observed and hence resultant improvements in both tensile and impact properties were greater at compatibilizer to organoclay ratio of three.

Cloisite® 15A exhibited the highest improvements in mechanical properties, although the degree of organoclay dispersion was better for Cloisite® 25A and particularly for Cloisite® 30B. Melt flow index values were lower compared to pure recycled polypropylene in the presence of organoclay and compatibilizers. DSC analysis indicated no significant change in the melting behavior of the matrix materials.

**Keywords:** Recycled Polypropylene; Nanocomposite; Organoclay; Compatibilizer; Extrusion

## ÖZ

### GERİ KAZANILMIŞ POLİPROPİLEN BAZLI NANOKOMPOZİTLERİN HAZIRLANMASI VE KARAKTERİZASYONU

Cengiz, Filiz

Yüksek Lisans, Kimya Mühendisliği

Tez Yöneticisi: Prof. Dr. Ülkü Yılmaz

Eylül 2008, 207 sayfa

Bu çalışmanın amacı, geri kazanılmış polipropilen malzemenin mekanik özelliklerinin iyileştirilmesidir. Polimer karışımları ve nanokompozitleri, çift vidalı bir ekstrüderde eriyik karıştırma metoduyla hazırlanmışlardır. Organik kil olarak Cloisite® 15A, Cloisite® 25A ve Cloisite® 30B, uyumlaştırıcı olarak etilen-metil akrilat-glisidil metakrilat (E-MA-GMA) ve maleik anhidrit aşılınmış polipropilen (PP-MAH) kullanılmıştır. Katkı maddesi konsantrasyonlarının, organik kil ve uyumlaştırıcı tiplerinin, işlem koşullarının, ve uyumlaştırıcının organik kile oranının morfoloji ile, mekanik, ısı ve akış özelliklerine etkileri araştırılmıştır.

Kütlece %2'den fazla organik kil eklenmesi, büyük kil topaklarının oluşumu sonucu, uyumlaştırıcının var olduğu durumlarda dahi araya sokulma mekanizmasını ve malzeme özelliklerini kötüleştirmiştir. E-MA-GMA uyumlaştırıcısı polimerin araya sokulma kabiliyetini iyileştirmiş, ancak mekanik özelliklerde önemli bir artış elde edilmemiştir. PP-MAH'ın daha iyi bir uyumlaştırıcı olduğu bulunmuştur.

İşlem koşulları, mekanik özellikleri ve morfolojiyi önemli ölçüde etkilemiştir. Eş zamanlı olarak, işlem sıcaklığı azaltıldığında ve vida dönüş hızı artırıldığında, çekme ve darbe özellikleri artan kesme ve dağıtma kuvvetlerine bağlı olarak iyileşmiştir.

TEM analizi, PP-MAH uyumlaştırıcısının eklenmesiyle araya sokulmalı ve açılmış yapıların oluştuğunu ortaya çıkarmıştır. Buna ek olarak, PP-MAH'ın organik kile oranı

arttıkça, daha etkili organik kil dağılımı gözlenmiş ve böylelikle çekme ve darbe dayanımında sonuç olarak meydana gelen iyileşmeler, uyumlaştırıcının kile oranının üç olduğu durumlarda daha fazla olmuştur.

Organik kil dağılım derecesi Cloisite® 25A ve özellikle Cloisite® 30B'de daha iyi olmasına rağmen, Cloisite® 15A mekanik özelliklerde en fazla iyileşmeyi göstermiştir. Eriyik akış indeksi değerleri geri kazanılmış polipropilene kıyasla, organik kil ve uyumlaştırıcı varlığında daha düşük olmuştur. DSC analizleri, matris malzemelerinin erime davranışlarında kayda değer bir değişiklik olmadığını göstermiştir.

**Anahtar Kelimeler:** Geri Kazanılmış Polipropilen; Nanokompozit; Organik Kil; Uyumlaştırıcı; Ekstrüzyon

***Dedicated to my parents***

## ACKNOWLEDGEMENTS

I would like to express my deepest gratitude to my supervisor, Prof. Dr. Ülkü Yılmaz, for his continuous support, guidance, constructive criticism, invaluable advice, and insight throughout my thesis study. It was a pleasing honor for me to work with him and I sincerely appreciate the time and effort he has taken to train me and the opportunities he provided.

I am grateful to Assoc. Prof. Dr. Göknur Bayram from Department of Chemical Engineering for permitting to use the instruments in her laboratory and also her kind advice.

Special thanks go to Cengiz Tan from Department of Metallurgical and Materials Engineering for SEM analysis, Mihrican Açıkgöz from Department of Chemical Engineering for DSC analysis, and Necmi Avcı from Department of Metallurgical Engineering for XRD analysis.

I would like to thank my dear friends Canan Yeniova, Damla Erođlu and Canan Gücüyener for their valuable friendship, endless support and for making my graduate study special and enjoyable.

I sincerely thank to Sertan Yeşil for his help, advice and contributions during my study. Friendly and helpful support of all my friends in Polymer Laboratory including Dr. Özcan Köysüren, Dr. Işıl Işık, Tijen Seyidođlu and Mert Kılınç are also greatly acknowledged.

I am forever grateful to my parents Nahide Cengiz, Erhan Cengiz and my sister Funda Cengiz Pekperdahcı for their endless love, encouragement and support throughout my life.

Above all, I am greatly indebted to my fiancée Orkun Öztürk for his unconditional love, care, support, patience and being with me all the time.

This study was supported by SAN-TEZ 00112.STZ.2007-1.

## TABLE OF CONTENTS

ABSTRACT.....	iv
ÖZ.....	vi
ACKNOWLEDGEMENTS.....	ix
TABLE OF CONTENTS .....	ix
LIST OF TABLES.....	xiii
LIST OF FIGURES.....	xiv
NOMENCLATURE.....	xxiv
CHAPTER	
1. INTRODUCTION .....	1
2. BACKGROUND .....	5
2.1 Composite Materials.....	5
2.1.1 Reinforcement in Composites.....	7
2.1.2 Types of Composites .....	7
2.1.3 Polymer Matrix Composites .....	8
2.2 Nanocomposites.....	9
2.2.1 Polymer Layered Silicate Nanocomposites (PLSN) .....	10
2.2.1.1 Layered Silicate Structure.....	10
2.2.2 Nanocomposite Types .....	12
2.2.3 Nanocomposite Preparation Methods.....	14
2.2.3.1 In-situ Polymerization Method .....	15
2.2.3.2 Solution Intercalation .....	16
2.2.3.3 Sol-Gel Technology .....	16
2.2.3.4 Melt Intercalation.....	17
2.3 Polymer Blends .....	18
2.4 Recycling Polymers.....	20
2.5 Polymer Matrix of the Study .....	21
2.5.1 Polypropylene.....	22
2.5.1.1 Polymerization, Structure and Tacticity of Polypropylene .....	22
2.5.1.2 Polypropylene Recycling.....	24
2.5.2 Polyethylene.....	25
2.6 Polypropylene Nanocomposites.....	27

2.6.1 Glycidyl Methacrylate (GMA) Functionality.....	29
2.6.2 Maleic Anhydride (MAH) Functionality.....	31
2.7 Polymer Processing.....	32
2.7.1 Extrusion .....	32
2.7.1.1 Screw Design .....	33
2.7.1.2 Extruder Types.....	35
2.7.2 Injection Molding .....	36
2.8 Characterization of Nanocomposites .....	37
2.8.1 Mechanical Properties.....	38
2.8.1.1 Tensile Test.....	38
2.8.1.2 Impact Test .....	41
2.8.2 Thermal Analysis.....	43
2.8.2.1 Differential Scanning Calorimetry (DSC) .....	43
2.8.3 Morphological Analysis .....	45
2.8.3.1 X-Ray Diffraction (XRD) Analysis .....	45
2.8.3.2 Scanning Electron Microscopy (SEM) .....	46
2.8.3.3 Transmission Electron Microscopy (TEM).....	48
2.8.4 Flow Characteristics.....	48
2.8.4.1 Melt Flow Index .....	49
2.9 Previous Studies.....	50
3. EXPERIMENTAL.....	54
3.1 Materials .....	54
3.1.1 Polymer Matrix.....	54
3.1.2 Organoclays .....	55
3.1.2.1 Cloisite® 15A .....	55
3.1.2.2 Cloisite® 25A .....	56
3.1.2.3 Cloisite® 30B .....	57
3.1.2.4 Organoclay Hydrophobicity.....	58
3.1.3 Compatibilizers.....	59
3.2 Equipment and Processing .....	61
3.2.1 Melt Compounding .....	61
3.2.1.1 Drying.....	62
3.2.1.2 Processing Parameters.....	63
3.2.1.3 Addition Order .....	64
3.2.1.3.a Simultaneous Feeding (All-S).....	65

3.2.1.3.b Masterbatch Method (MB) .....	65
3.2.2 Injection Molding .....	68
3.3 Characterization .....	70
3.3.1 Morphological Testing Procedure and Equipment.....	70
3.3.1.1 X-Ray Diffraction Analysis .....	70
3.3.1.2 Scanning Electron Microscopy (TEM) Analysis.....	70
3.3.1.3 Transmission Electron Microscopy (TEM) Analysis .....	70
3.3.2 Mechanical Properties.....	71
3.3.2.1 Tensile Test.....	72
3.3.2.2 Impact Test .....	73
3.3.3 Thermal Analysis.....	73
3.3.3.1 Differential Scanning Calorimetry (DSC) Analysis .....	73
3.3.4 Flow Characteristics.....	74
3.3.4.1 Melt Flow Index.....	74
4. RESULTS AND DISCUSSION.....	75
4.1 Morphological Analysis.....	75
4.1.1 X-RAY Diffraction Analysis.....	75
4.1.2 TEM Analysis .....	94
4.1.3 Scanning Electron Microscopy Analysis (SEM).....	104
4.2 Mechanical Properties.....	129
4.2.1 Tensile Tests .....	129
4.2.1 Impact Tests.....	151
4.3 Differential Scanning Calorimetry Analysis.....	158
4.4 Melt Flow Index Analysis.....	164
5. CONCLUSIONS .....	168
REFERENCES .....	171
APPENDICES	
A. MECHANICAL TEST RESULTS.....	181
B. DSC ANALYSIS .....	191

## LIST OF TABLES

Table 3.1 Properties of the polymer matrix.....	54
Table 3.2 Properties of Cloisite® 15A.....	56
Table 3.3 Properties of Cloisite® 25A.....	57
Table 3.4 Properties of Cloisite® 30B.....	58
Table 3.5 General characteristics of Lotader® AX8900 (E-MA-GMA).....	60
Table 3.6 General characteristics of Bondyram® 1001.....	61
Table 3.7 Properties of twin screw extruder.....	62
Table 3.8 Drying conditions.....	63
Table 3.9 Compositions prepared in experiments.....	67
Table 3.10 Injection molding parameters.....	69
Table 3.11 Dimensions of the tensile test specimens.....	72
Table 3.12 Dimensions of impact test specimens.....	73
Table 4.1 XRD results of P- Cloisite® 15A- Lotader® AX8900 nanocomposites.....	81
Table 4.2 XRD results, effects of processing conditions.....	84
Table 4.3 XRD results, effects of PP-MAH to organoclay ratio.....	88
Table 4.4 XRD results, effects of clay types.....	94
Table 4.5 SEM results.....	105
Table 4.6 DSC results, Lotader® AX8900 (E-MA-GMA) compatibilizer.....	160
Table 4.7 DSC results, effect of processing conditions.....	161
Table 4.8 DSC results, effect of PP-MAH to organoclay ratio.....	162
Table 4.9 DSC results, effect of organoclay type.....	163
Table 4.10 MFI results, Lotader® AX8900 (E-MA-GMA) compatibilizer.....	165
Table 4.11 MFI results, effect of processing conditions.....	166
Table 4.12 MFI results, effect of PP-MAH to organoclay ratio and organoclay type.....	167
Table A.1 Young's Modulus data and standard deviations for all compositions.....	181
Table A.2 Tensile stress at yield data and standard deviations for all compositions.....	183
Table A.3 Tensile strength data and standard deviations for all compositions.....	185
Table A.4 Elongation at break (%) data and standard deviations for all compositions.....	187
Table A.5 Impact strength data and standard deviations for all compositions.....	189

## LIST OF FIGURES

Figure 2.1 Structure of 2:1 layered silicates.....	11
Figure 2.2 Idealized structures of organically modified silicates.....	12
Figure 2.3 Nanocomposite types.....	13
Figure 2.4 Proposed model for the torturous zigzag diffusion path in an exfoliated polymer–clay nanocomposite when used as a gas barrier.....	14
Figure 2.5 In-situ polymerization method.....	15
Figure 2.6 Solution intercalation method.....	16
Figure 2.7 Melt intercalation method.....	17
Figure 2.8 Polymerization of polypropylene.....	23
Figure 2.9 Stereochemical configurations of polypropylene.....	24
Figure 2.10 Structure of polyethylene.....	26
Figure 2.11 Types of polyethylene.....	27
Figure 2.12 Structure of GMA.....	29
Figure 2.13 Typical GMA reactions.....	30
Figure 2.14 Structure of maleic anhydride grafted polypropylene and it's reaction with hydroxyl groups.....	31
Figure 2.15 Schematic representation of the intercalation process of PP-MAH.....	32
Figure 2.16 A simple extruder scheme and representation of the sections.....	33
Figure 2.17 General purpose extruder screw.....	34
Figure 2.18 Screw configurations for twin screw extruders.....	36
Figure 2.19 Tensile test machine and dog bone shaped specimen.....	39
Figure 2.20 Idealized stress-strain curve for a polymer that undergoes ductile failure.....	40
Figure 2.21 Stress–strain curves at various temperatures (increasing from a to e): (a) low extensibility followed by brittle fracture at the lowest temperature; (b) localized yielding followed by fracture; (c) necking and cold drawing; (d) homogeneous deformation with indistinct yield; (e) rubber-like behavior.....	41
Figure 2.22 Charpy and Izod impact tests.....	42
Figure 2.23 Differential scanning calorimeter.....	43
Figure 2.24 Typical DSC curves.....	44
Figure 2.25 Diffraction of X-Rays.....	46

Figure 2.26 Schematic diagram representing the main components of a scanning electron microscope.....	47
Figure 2.27 Melt flow index measurement.....	49
Figure 3.1 Chemical structure of organic modifier and anion (Cl-) of Cloisite® 15A.....	56
Figure 3.2 Chemical structure of organic modifier and anion (methyl sulfate) of Cloisite® 25A.....	57
Figure 3.3 Chemical structure of organic modifier and anion (Cl-) of Cloisite® 30B..	58
Figure 3.4 Chemical structure of Lotader® AX8900.....	59
Figure 3.5 Chemical structure of maleic anhydride grafted polypropylene.....	60
Figure 3.6 Thermoprism TSE 16 TC twin-screw extruder.....	62
Figure 3.7 Schematic diagram of processing parameters; barrel temperature and screw speed.....	64
Figure 3.8 Flow chart for nanocomposite production and characterization.....	66
Figure 3.9 Injection molding equipment.....	69
Figure 3.10 Specimens used in morphological analysis.....	71
Figure 3.11 Tensile test specimen.....	72
Figure 3.12 Impact test specimen.....	73
Figure 4.1 X-Ray Diffraction pattern of recycled polypropylene.....	76
Figure 4.2 XRD pattern of Cloisite® 15A in powder form.....	79
Figure 4.3 XRD patterns of P- Cloisite® 15A- Lotader® AX8900 nanocomposites at 2 wt% organoclay loading.....	79
Figure 4.4 XRD patterns of P- Cloisite® 15A- Lotader® AX8900 nanocomposites at 4 wt% organoclay loading.....	80
Figure 4.5 XRD patterns of P- Cloisite® 15A- Lotader® AX8900 nanocomposites at 6 wt% organoclay loading.....	80
Figure 4.6 XRD patterns of P- Cloisite® 15A- Lotader® AX8900 at 2 wt% organoclay and 5 wt% compatibilizer loading, effect of processing conditions.....	83
Figure 4.7 XRD patterns of P- Cloisite® 15A- PP-MAH at 1 wt% organoclay and 2 wt% compatibilizer loading, effect of processing conditions.....	83
Figure 4.8 Binary nanocomposites of P and Cloisite® 15A at various compositions.....	86
Figure 4.9 Ternary nanocomposites of P- Cloisite® 15A- PP-MAH prepared at compatibilizer to organoclay ratio of 1.....	86

Figure 4.10 Ternary nanocomposites of P- Cloisite® 15A- PP-MAH prepared at compatibilizer to organoclay ratio of 2.....	87
Figure 4.11 Ternary nanocomposites of P- Cloisite® 15A- PP-MAH prepared at compatibilizer to organoclay ratio of 3.....	87
Figure 4.12 XRD pattern of Cloisite® 25A in powder form.....	91
Figure 4.13 XRD pattern of Cloisite® 30B in powder form.....	91
Figure 4.14 Binary nanocomposites of P- Cloisite® 25A at various clay loadings.....	92
Figure 4.15 Ternary nanocomposites of P- Cloisite® 25A- PP-MAH prepared at compatibilizer to organoclay ratio of 2 and various clay loadings.....	92
Figure 4.16 Binary nanocomposites of P- Cloisite® 30B at various clay loadings.....	93
Figure 4.17 Ternary nanocomposites of P- Cloisite® 30B- PP-MAH prepared at compatibilizer to organoclay ratio of 2 and various clay loadings.....	93
Figure 4.18 TEM images at different magnifications of the binary nanocomposite containing recycled polypropylene and 2wt% Cloisite® 15A prepared with MB method.....	96
Figure 4.19 TEM micrographs at different magnifications of the ternary nanocomposite, containing recycled polypropylene, 2 wt% Cloisite® 15A and 5 wt% E-MA-GMA prepared with All-S method at 180 °C and 350 rpm screw speed.....	98
Figure 4.20 TEM micrographs at different magnifications of the ternary nanocomposite containing recycled polypropylene, 2 wt% Cloisite® 15A and 6 wt% PP-MAH prepared with MB method at 180 °C and 350 rpm screw speed.....	99
Figure 4.21 TEM micrographs at different magnifications of the ternary nanocomposite containing recycled polypropylene, 1 wt% Cloisite® 15A and 2 wt% PP-MAH prepared with MB method at 180 °C and 350 rpm screw speed.....	101
Figure 4.22 TEM micrographs at different magnifications of the ternary nanocomposite containing recycled polypropylene, 1 wt% Cloisite® 25A and 2 wt% PP-MAH prepared with MB method at 180 °C and 350 rpm screw speed.....	102
Figure 4.23 TEM micrographs at different magnifications of the ternary nanocomposite containing recycled polypropylene, 1 wt% Cloisite® 30B and 2 wt% PP-MAH prepared with MB method and 180 °C and 350 rpm screw speed.....	103
Figure 4.24 SEM micrographs of recycled polypropylene a) Not extruded (x3000) b) Not extruded (x10000) c) Extruded once (x3000) d) Extruded once (x10000) e) Extruded twice (x3000) f) Extruded twice (x10000).....	108
Figure 4.25 SEM micrographs of binary blends of E-MA-GMA a) 5 wt% (x250) b) 5 wt% (x3000) c) 10 wt% (x250) d) 10 wt% (x3000).....	110

Figure 4.26 SEM micrographs of binary nanocomposites of P and Cloisite® 15A prepared by All-S method a) 2 wt% (x250) b) 2 wt% (x3000) c) 4 wt% (x250) d) 4 wt% (x3000) e) 6 wt% (x250) f) 6 wt% (x3000).....	112
Figure 4.27 SEM micrographs of ternary nanocomposites containing 5 wt% E-MA-GMA and Cloisite® 15A at various compositions a) 2 wt% 15A (x250) b) 2 wt% (x3000) 15A c) 4 wt% 15A (x250) d) 4 wt% 15A(x3000) e) 6 wt% 15A (x250) f) 6 wt% 15A (x3000).....	113
Figure 4.28 SEM micrographs of ternary nanocomposites containing 10 wt% E-MA-GMA and Cloisite® 15A at various compositions a) 2 wt% 15A (x250) b) 2 wt% (x3000) 15A c) 4 wt% 15A (x250) d) 4 wt% 15A(x3000) e) 6 wt% 15A (x250) f) 6 wt% 15A (x3000).....	114
Figure 4.29 SEM micrographs of ternary nanocomposites containing 2 wt% Cloisite® 15A and 5 wt% E-MA-GMA prepared by All-S method and at various processing conditions a) 200°C-350rpm (x250) b) 200°C-350rpm (x3000) c) 180°C-250rpm (x250) d) 180°C-250rpm (x3000) e) 180°C-350rpm (x250) f) 180°C-350rpm (x3000).....	116
Figure 4.30 SEM micrographs of ternary nanocomposites containing 1 wt% Cloisite® 15A and 2 wt% PP-MAH prepared by All-S method and at various processing conditions a) 200°C-250rpm (x250) b) 200°C-250rpm (x3000) c) 200°C-350rpm (x250) d) 200°C-350rpm (x3000) e) 180°C-250rpm (x250) f) 180°C-250rpm (x3000).....	117
Figure 4.31 SEM micrographs of binary blends containing PP-MAH at various contents a) 2 wt% (x250) b) 2 wt% (x3000) c) 4 wt% (x250) d) 4 wt% (x3000) e) 6 wt% (x250) f) 6 wt% (x3000).....	121
Figure 4.32 SEM micrographs of ternary nanocomposites prepared with Cloisite® 15A at PP-MAH to organoclay ratio of 1 a)P+0.5wt%PP-MAH+0.5wt%15A (x250) b)P+0.5wt%PP-MAH+0.5wt%15A(x3000) c)P+1.0wt%PP-MAH+1.0wt%15A (x250) d)P+1.0wt%PP-MAH+1.0wt%15A (x3000) e)P+2.0wt%PP-MAH+2.0wt%15A (x250) f)P+2.0wt%PP-MAH+2.0wt%15A (x3000).....	122
Figure 4.33 SEM micrographs of ternary nanocomposites prepared with Cloisite® 15A at PP-MAH to organoclay ratio of 2 a)P+1.0wt%PP-MAH+0.5wt%15A (x250) b)P+1.0wt%PP-MAH+0.5wt%15A (x3000) c)P+2.0wt%PP-MAH+1.0wt%15A (x250) d)P+2.0wt%PP-MAH+1.0wt%15A (x3000) e)P+4.0wt%PP-MAH+2.0wt%15A (x250) f)P+4.0wt%PP-MAH+2.0wt%15A (x3000).....	123

Figure 4.34 SEM micrographs of ternary nanocomposites prepared with Cloisite® 15A at PP-MAH to organoclay ratio of 3	
a) P+1.5wt%PP-MAH+0.5wt%15A (x250)	
b) P+1.5wt%PP-MAH+0.5wt%15A (x3000)	
c) P+3.0wt%PP-MAH+1.0wt%15A (x250)	
d) P+3.0wt%PP-MAH+1.0wt%15A (x3000)	
e) P+6.0wt%PP-MAH+2.0wt%15A (x250)	
f) P+6.0wt%PP-MAH+2.0wt%15A (x3000)	124
Figure 4.35 SEM micrographs of binary nanocomposites containing 1 wt% different types of organoclays	
a) 15A (x250)	
b) 15A (x3000)	
c) 25A (x250)	
d) 25A (x3000)	
e) 30B (x250)	
f) 30B (x3000)	125
Figure 4.36 SEM micrographs of binary nanocomposites containing 2 wt% different types of organoclays	
a) 15A (x250)	
b) 15A (x3000)	
c) 25A (x250)	
d) 25A (x3000)	
e) 30B (x250)	
f) 30B (x3000)	126
Figure 4.37 SEM micrographs of ternary nanocomposites prepared with Cloisite® 25A at PP-MAH to organoclay ratio of 2	
a) P+1.0wt%PP-MAH+0.5wt%25A (x250)	
b) P+1.0wt%PP-MAH+0.5wt%25A (x3000)	
c) P+2.0wt%PP-MAH+1.0wt%25A (x250)	
d) P+2.0wt%PP-MAH+1.0wt%25A (x3000)	
e) P+4.0wt%PP-MAH+2.0wt%25A (x250)	
f) P+4.0wt%PP-MAH+2.0wt%25A (x3000)	127
Figure 4.38 SEM micrographs of ternary nanocomposites prepared Cloisite® 30B at PP-MAH to organoclay ratio of 2	
a) P+1.0wt%PP-MAH+0.5wt%30B (x250)	
b) P+1.0wt%PP-MAH+0.5wt%30B (x3000)	
c) P+2.0wt%PP-MAH+1.0wt%30B (x250)	
d) P+2.0wt%PP-MAH+1.0wt%30B (x3000)	
e) P+4.0wt%PP-MAH+2.0wt%30B (x250)	
f) P+4.0wt%PP-MAH+2.0wt%30B (x3000)	128
Figure 4.39 Typical stress-strain curve of recycled polypropylene	130
Figure 4.40 Young's Modulus of blends and nanocomposites prepared with E-MA-GMA compatibilizer (200° C, 250 rpm, All-S)	132
Figure 4.41 Tensile stress at yield of blends and nanocomposites prepared with E-MA-GMA compatibilizer (200° C, 250 rpm, All-S)	132
Figure 4.42 Tensile strength of blends and nanocomposites prepared with E-MA-GMA compatibilizer (200° C, 250 rpm, All-S)	133
Figure 4.43 Elongation at break (%) of blends and nanocomposites prepared with E-MA-GMA compatibilizer (200° C, 250 rpm, All-S)	133
Figure 4.44 Young's Modulus of nanocomposites containing 5 wt% E-MA-GMA and 2 wt% Cloisite® 15A (on the left) and 2 wt% PP-MAH and 1 wt% Cloisite® 15A (on the right) prepared under different processing conditions	135

Figure 4.45 Tensile stress at yield of ternary nanocomposites containing 5 wt% E-MA-GMA and 2 wt% Cloisite® 15A (on the left) and 2 wt% PP-MAH and 1 wt% Cloisite® 15A (on the right) prepared under different processing conditions.....	135
Figure 4.46 Tensile strength of nanocomposites containing 5 wt% E-MA-GMA and 2 wt% Cloisite® 15A (on the left) and 2 wt% PP-MAH and 1 wt% Cloisite® 15A (on the right) prepared under different processing conditions.....	136
Figure 4.47 Elongation at break (%) of nanocomposites containing 5 wt% E-MA-GMA and 2 wt% Cloisite® 15A (on the left) and 2 wt% PP-MAH and 1 wt% Cloisite® 15A (on the right) prepared under different processing conditions.....	136
Figure 4.48 Young's Modulus of binary blends containing PP-MAH.....	139
Figure 4.49 Tensile stress at yield of binary blends containing PP-MAH.....	139
Figure 4.50 Tensile strength of binary blends containing PP-MAH.....	140
Figure 4.51 Elongation at break (%) of binary blends containing PP-MAH.....	140
Figure 4.52 Young's Modulus of binary nanocomposites containing different types of organoclays.....	141
Figure 4.53 Tensile stress at yield of binary nanocomposites containing different types of organoclays.....	142
Figure 4.54 Tensile strength of binary nanocomposites containing different types of organoclays.....	142
Figure 4.55 Elongation at break at break (%) of binary nanocomposites containing different types of organoclays.....	143
Figure 4.56 Young's Modulus of ternary nanocomposites prepared with PP-MAH to organoclay ratios of 1, 2 and 3.....	145
Figure 4.57 Tensile stress at yield of ternary nanocomposites prepared with PP-MAH to organoclay ratios of 1, 2 and 3.....	145
Figure 4.58 Tensile strength of ternary nanocomposites prepared with PP-MAH to organoclay ratios of 1, 2 and 3.....	146
Figure 4.59 Elongation at break (%) of ternary nanocomposites prepared with PP-MAH to organoclay ratios of 1, 2 and 3.....	146
Figure 4.60 Young's Modulus of ternary nanocomposites prepared with PP-MAH to organoclay ratio of 2 and different types of organoclays (180 °C, 350 rpm, MB).....	149
Figure 4.61 Tensile stress at yield of ternary nanocomposites prepared with PP-MAH to organoclay ratio of 2 and different types of organoclays (180 °C, 350 rpm, MB).....	149

Figure 4.62 Tensile strength of ternary nanocomposites prepared with PP-MAH to organoclay ratio of 2 and different types of organoclays (180 °C, 350 rpm, MB).....	150
Figure 4.63 Elongation at break (%) of ternary nanocomposites prepared with PP-MAH to organoclay ratio of 2 and different types of organoclays (180 °C, 350 rpm, MB).....	150
Figure 4.64 Impact strength of blends and nanocomposites prepared with E-MA-GMA compatibilizer (200° C, 250 rpm, All-S).....	153
Figure 4.65 Impact strength of nanocomposites containing 5 wt% E-MA-GMA and 2 wt% Cloisite® 15A (on the left) and 2 wt% PP-MAH and 1 wt% Cloisite® 15A (on the right) prepared under different processing conditions.....	154
Figure 4.66 Impact strength of blends containing PP-MAH.....	155
Figure 4.67 Impact strength of binary nanocomposites containing different types of organoclays. The ratios given are those of PP-MAH to organoclay.....	156
Figure 4.68 Impact strength of ternary nanocomposites prepared with PP-MAH to organoclay ratios of 1, 2 and 3.....	157
Figure 4.69 Impact strength of ternary nanocomposites prepared with PP-MAH to organoclay ratio of 2 and different types of organoclays (180 °C, 350 rpm, MB).....	158
Figure B.1 DSC thermogram of recycled polypropylene.....	191
Figure B.2 DSC thermogram of Lotader® AX8900 (E-MA-GMA).....	191
Figure B.3 DSC thermogram of PP-MAH.....	192
Figure B.4 DSC thermogram of binary blend containing 5 wt% E-MA-GMA.....	192
Figure B.5 DSC thermogram of binary blend containing 10 wt% E-MA-GMA.....	192
Figure B.6 DSC thermogram of binary nanocomposite containing 2 wt% Cloisite® 15A (All-S).....	193
Figure B.7 DSC thermogram of binary nanocomposite containing 4 wt% Cloisite® 15A.....	193
Figure B.8 DSC thermogram of binary nanocomposite containing 6 wt% Cloisite® 15A.....	193
Figure B.9 DSC thermogram of ternary nanocomposite containing 2 wt% Cloisite® 15A and 5 wt% E-MA-GMA prepared at 200 °C temperature and 250 rpm.....	194
Figure B.10 DSC thermogram of ternary nanocomposite containing 2 wt% Cloisite® 15A and 10 wt% E-MA-GMA.....	194
Figure B.11 DSC thermogram of ternary nanocomposite containing 4 wt% Cloisite® 15A and 5 wt% E-MA-GMA.....	194

Figure B.12 DSC thermogram of ternary nanocomposite containing 4 wt% Cloisite® 15A and 10 wt% E-MA-GMA.....	195
Figure B.13 DSC thermogram of ternary nanocomposite containing 6 wt% Cloisite® 15A and 5 wt% E-MA-GMA.....	195
Figure B.14 DSC thermogram of ternary nanocomposite containing 6 wt% Cloisite® 15A and 10 wt% E-MA-GMA.....	195
Figure B.15 DSC thermogram of ternary nanocomposite containing 2 wt% Cloisite® 15A and 5 wt% E-MA-GMA prepared at 200 °C temperature and 350 rpm.....	196
Figure B.16 DSC thermogram of ternary nanocomposite containing 2 wt% Cloisite® 15A and 5 wt% E-MA-GMA prepared at 180 °C temperature and 250 rpm.....	196
Figure B.17 DSC thermogram of ternary nanocomposite containing 2 wt% Cloisite® 15A and 5 wt% E-MA-GMA prepared at 180 °C temperature and 350 rpm.....	196
Figure B.18 DSC thermogram of ternary nanocomposite containing 1 wt% Cloisite® 15A and 2 wt% PP-MAH prepared at 200 °C temperature and 250 rpm.....	197
Figure B.19 DSC thermogram of ternary nanocomposite containing 1 wt% Cloisite® 15A and 2 wt% PP-MAH prepared at 200 °C temperature and 350 rpm.....	197
Figure B.20 DSC thermogram of ternary nanocomposite containing 1 wt% Cloisite® 15A and 2 wt% PP-MAH prepared at 180 °C temperature and 250 rpm.....	197
Figure B.21 DSC thermogram of binary blend containing 0.5 wt% PP-MAH.....	198
Figure B.22 DSC thermogram of binary blend containing 1 wt% PP-MAH.....	198
Figure B.23 DSC thermogram of binary blend containing 2 wt% PP-MAH.....	198
Figure B.24 DSC thermogram of binary blend containing 3 wt% PP-MAH.....	199
Figure B.25 DSC thermogram of binary blend containing 4 wt% PP-MAH.....	199
Figure B.26 DSC thermogram of binary blend containing 6 wt% PP-MAH.....	199
Figure B.27 DSC thermogram of binary nanocomposite containing 0.5 wt% Cloisite® 15A.....	200
Figure B.28 DSC thermogram of binary nanocomposite containing 1 wt% Cloisite® 15A.....	200
Figure B.29 DSC thermogram of binary nanocomposite containing 2 wt% Cloisite® 15A.....	200
Figure B.30 DSC thermogram of binary nanocomposite containing 0.5 wt% Cloisite® 25A.....	201
Figure B.31 DSC thermogram of binary nanocomposite containing 1 wt% Cloisite® 25A.....	201

Figure B.32 DSC thermogram of binary nanocomposite containing 2 wt% Cloisite® 25A.....	201
Figure B.33 DSC thermogram of binary nanocomposite containing 0.5 wt% Cloisite® 30B.....	202
Figure B.34 DSC thermogram of binary nanocomposite containing 1 wt% Cloisite® 30B.....	202
Figure B.35 DSC thermogram of binary nanocomposite containing 2 wt% Cloisite® 30B.....	202
Figure B.36 DSC thermogram of ternary nanocomposite containing 0.5 wt% Cloisite® 15A and 0.5 wt% PP-MAH.....	203
Figure B.37 DSC thermogram of ternary nanocomposite containing 1 wt% Cloisite® 15A and 1 wt% PP-MAH.....	203
Figure B.38 DSC thermogram of ternary nanocomposite containing 2 wt% Cloisite® 15A and 2 wt% PP-MAH.....	203
Figure B.39 DSC thermogram of ternary nanocomposite containing 0.5 wt% Cloisite® 15A and 1 wt% PP-MAH.....	204
Figure B.40 DSC thermogram of ternary nanocomposite containing 1 wt% Cloisite® 15A and 2 wt% PP-MAH, prepared at 180 °C and 350 rpm.....	204
Figure B.41 DSC thermogram of ternary nanocomposite containing 2 wt% Cloisite® 15A and 4 wt% PP-MAH.....	204
Figure B.42 DSC thermogram of ternary nanocomposite containing 0.5 wt% Cloisite® 15A and 1.5 wt% PP-MAH.....	205
Figure B.43 DSC thermogram of ternary nanocomposite containing 1 wt% Cloisite® 15A and 3 wt% PP-MAH.....	205
Figure B.44 DSC thermogram of ternary nanocomposite containing 2 wt% Cloisite® 15A and 6 wt% PP-MAH.....	205
Figure B.45 DSC thermogram of ternary nanocomposite containing 0.5 wt% Cloisite® 25A and 1 wt% PP-MAH.....	206
Figure B.46 DSC thermogram of ternary nanocomposite containing 1 wt% Cloisite® 25A and 2 wt% PP-MAH.....	206
Figure B.47 DSC thermogram of ternary nanocomposite containing 2 wt% Cloisite® 25A and 4 wt% PP-MAH.....	206
Figure B.48 DSC thermogram of ternary nanocomposite containing 0.5 wt% Cloisite® 30B and 1 wt% PP-MAH.....	207

Figure B.49 DSC thermogram of ternary nanocomposite containing 1 wt% Cloisite® 30B and 2 wt% PP-MAH.....	207
Figure B.50 DSC thermogram of ternary nanocomposite containing 2 wt% Cloisite® 30B and 4 wt% PP-MAH.....	207

## NOMENCLATURE

$\bar{A}$	Average area of domains in SEM analysis, $\mu\text{m}^2$
$A_i$	Area of a number of domains in SEM analysis, $\mu\text{m}^2$
$A_0$	Cross-sectional area of the gauge region, $\text{mm}^2$
$d$	Interlayer spacing, $\text{\AA}$
$d_{\text{av}}$	Average domain size, nm
$\bar{d}$	Average domain size, nm
$D$	Distance between grips of tensile test specimen, mm
$D$	Diameter of the screws, mm
$E$	Young's Modulus, MPa
$F$	Force, N
$g$	Gauge length of tensile test specimen, mm
$\Delta H_f$	Heat of fusion, J/g
$\Delta H_f^\circ$	Heat of fusion for pure crystalline form of polymer, J/g
$\Delta H_{f, \text{PE}}^\circ$	Heat of fusion for pure crystalline form of polyethylene, J/g
$\Delta H_{f, \text{PE}}^\circ$	Heat of fusion for pure crystalline form of polypropylene, J/g
$L$	Length of the Extruder Barrel, mm
$L$	Total length of impact test specimen, mm
$L_0$	Initial gauge length, mm
$L_0$	Overall length of tensile test specimen, mm
$\Delta L$	Change in sample length, mm
$n$	Degree of diffraction
$n$	Notch length (v type, $45^\circ$ ), mm
$N_i$	Number of domains analyzed in SEM analysis
$t$	Thickness of tensile test specimen, mm
$t$	Thickness of impact test specimen, mm
$T_g$	Glass Transition Temperature, $^\circ\text{C}$
$T_m$	Melting Temperature, $^\circ\text{C}$
$T_c$	Crystallization Temperature, $^\circ\text{C}$
$X_c$	Crystallinity, %
$w$	Unnotched width of impact test specimen, mm
$W$	Width of narrow section of tensile test specimen, mm

### ***Greek Letters***

$\sigma$	Stress, MPa
$\varepsilon$	Strain, mm/mm
$\theta$	Diffraction angle, °
$\lambda$	Wavelength, nm

### ***Abbreviations***

All-S	Melt mixing sequence in which all materials are fed into extruder simultaneously
CCC	Carbon-Carbon Matrix Composites
CEC	Cation Exchange Capacity
CMC	Ceramic Matrix Composites
COOH	Carboxyl
CRT	Cathode Ray Tube
DSC	Differential Scanning Calorimetry
E-MA-GMA	Ethylene-Methyl Acrylate-Glycidyl Methacrylate
FTIR	Fourier Transform Infrared Spectroscopy
GMA	Glycidyl Methacrylate
HDPE	High Density Polyethylene
iPP	Isotactic Polypropylene
ISO	International Organization for Standardization
LDPE	Low Density Polyethylene
LLDPE	Linear Low Density Polyethylene
MAH	Maleic Anhydride
MB	Melt mixing sequence in which organoclay and PP-MAH are fed into extruder first and added into recycled polypropylene in the second extrusion
MDPE	Medium Density Polyethylene
MFI	Melt Flow Index
MMC	Metal Matrix Composites
MMT	Montmorillonite
NH <sub>2</sub>	Amine
OH	Hydroxyl
OMLS	Organically Modified Layered Silicate

PA	Polyamide
PC	Polycarbonate
PE	Polyethylene
PE-MAH	Maleic Anhydride Grafted Polyethylene
PET	Polyethyleneterephthalate
PLSN	Polymer Layered Silicate Nanocomposites
PMC	Polymer Matrix Composites
PP	Polypropylene
PP-MAH	Maleic Anhydride Grafted Polypropylene
PS	Polystyrene
PVC	Polyvinylchloride
SAXS	Small Angle X-ray Scattering
SEM	Scanning Electron Microscopy
TEM	Transmission Electron Microscopy
XRD	X-Ray Diffraction
VLDPE	Very Low Density Polyethylene
WAXS	Wide Angle X-ray Scattering
15A	Cloisite® 15A
25A	Cloisite® 25A
30B	Cloisite® 30B
8900	E-MA-GMA

# CHAPTER 1

## INTRODUCTION

Composites are emerged from combinations of two or more distinctly insoluble phases at macroscopic level by a synthetic assembly. The new material exhibits unique properties that can not be achieved by a single component while carrying the identity of each constituent [1-3]. Composites are preferred and widely used for their versatility in unlimited selection of characteristic properties, design flexibility and superior mechanical, thermal, electrical etc. properties compared to their single phase counterparts [4].

Polymer matrices are the most commonly used matrix type in composite applications regarding to their low cost and weight, low heat-pressure requirement and ease of processing advantages [3]. However, their inadequate mechanical strength, impact resistance, electrical conductivity or permeability brings in need for filling and compounding with inorganic, synthetic and/or natural compounds [5].

Over the past decade, polymer matrices are started to being used effectively in nanocomposite applications. Nanocomposites are multiphase materials whose at least one of the constituent phases is in nanometer range ( $10^{-9}$  m). At this scale, materials exhibit different characteristic properties than observed in the bulk and they offer new advances for material design even with a small nanofiller addition owing to large surface area to volume ratio of nanoadditives [6, 7].

Intercalation chemistry of polymers that was developed by compounding with properly modified layered silicates was known for a long time. However, after the report published by Toyota research group regarding to significant improvements in thermal and mechanical properties of nanocomposites prepared with a small amount of montmorillonite (MMT) loaded to Nylon-6 matrix and the observations of Vaia et al. [8] on the possible melt intercalation mechanism in the absence of solvent renewed the interest for layered silicates [9, 10].

Layered silicates belong to the 2:1 phyllosilicates family and their crystal lattice consists of a central octahedral sheet of alumina or magnesia fused to two external tetrahedral sheet of silica by the tip. The layer thickness is around 1 nm, and layers arrange themselves in a parallel manner to form stacks with regular van der Waals gaps between them called interlayer or gallery. Negative charge which is generated by the isomorphic substitution within the layers is counterbalanced by the alkali or alkaline earth cations inside the layers [11]. In addition to those, the partial charge for each cation within the interlayer creates a hydrophilic environment in the phyllosilicates structure [12]. Therefore, a cation exchange process is required with alkylammonium or alkylphosphonium type cations in order to obtain a hydrophobic/organophilic character promoting compatibility with many polar polymers and also a larger interlayer spacing which increases the intercalation ability [13].

Synthesis of nanocomposites can be implemented with in situ polymerization, solution intercalation and melt intercalation techniques. Among all three methods, melt intercalation offer great advantages for its solvent free operation type, compatibility with the current industrial processes, such as extrusion and injection molding, and ease of application proper for any type of polymer matrices including polar ones. The final properties of nanocomposite produced by melt intercalation are strongly affected by the state of dispersion and interactions between the filler and polymer matrix. Depending on the strength of interfacial interactions between layered silicates (modified or not) and the matrix, three types of polymer layered silicate nanocomposites are thermodynamically achievable; intercalated, intercalated-flocculated, and exfoliated-delaminated. The degree of dispersion increases as the morphology deviates from an intercalated form to an exfoliated structure owing to enhanced surface area and interactions between the matrix and silicate layers [9].

There are several factors affecting the state of dispersion such as organic modifier of the nanoclay, polarity of the polymer matrix and the type of compatibilizer used during melt intercalation. In addition to these, the state of exfoliation is strongly affected by the processing conditions such as mean residence time, amount of shear applied during melt intercalation and processing temperatures as well as type of the processing equipment and mixing protocol [14].

Polypropylene is a thermoplastic linear hydrocarbon polymer that has excellent physical, mechanical and thermal properties for room temperature applications [15].

However, polyolefins such as polypropylene and polyethylene do not contain any polar groups and a high level of dispersion of the silicate layers is not possible with direct melt intercalation. Therefore, compatibilizers with functional groups are incorporated to facilitate exfoliation in addition to modifying clay surfaces [16].

Every year millions of tones of polypropylene are being consumed together with other plastic materials, and tones of plastic wastes are collected in the landfills. Therefore, recycling processes are required for their reuse in the industry. The major problem in polypropylene recycling is the contamination of the matrix with other polymers especially with polyethylene. Regarding to separation difficulties, two polymers are often recycled together. Immiscibility between two phases causes poor mechanical properties and instability as present in this study [15]. Interfacial adhesion and rigidity can be improved by using proper compatibilizers and also fillers such as talc, mica and layered silicates [17].

The aim of this study was to improve the mechanical properties of recycled polypropylene by using montmorillonite type layered silicate and compatibilizers having functional groups. Cloisite® 15A, Cloisite® 25A and Cloisite® 30B were used as organoclays and Lotader® AX8900, random terpolymer of ethylene (E), methyl acrylate- glycidyl methacrylate (E-MA-GMA) and Bondyram® 1001, maleic anhydride grafted polypropylene (PP-MAH) were used as compatibilizers. Throughout the study, the effects of organoclay and compatibilizer content, types, processing parameters, such as processing temperature and screw speed, and compatibilizer to organoclay ratio on the final properties of the nanocomposites were investigated. Components of nanocomposites containing E-MA-GMA were simultaneously fed to extruder at 200 °C temperature and 250 rpm screw speed. After studying the effects of processing conditions in the preparation of nanocomposites including PP-MAH compatibilizer, processing parameters were set to 180 °C temperature and 350 rpm screw speed. In addition to that, masterbatch method was applied in order to process nanocomposites with low organoclay contents and increase the interactions between PP-MAH and organoclay.

All materials except recycled polypropylene were dried before extrusion and injection molding processes at proper temperatures and durations. Standard test specimens were prepared according to the standard of ISO 527-2 5A for characterization, and specimens were conditioned for specified durations prior to analysis.

Finally, tensile and impact tests were conducted to determine the mechanical properties. Morphological characterization and organoclay dispersion were evaluated by Scanning Electron Microscopy (SEM), Transmission Electron Microscopy TEM and X-Ray Diffraction (XRD) analysis. Melting and crystallization behavior of the composites were examined by Differential Scanning Calorimetry (DSC) and flow properties were studied with Melt Flow Index (MFI) measurements.

## CHAPTER 2

### BACKGROUND

#### 2.1 Composite Materials

Composites are structural materials that are combined at macroscopic level by a synthetic assembly from two or more distinct phases which are insoluble in each other and separated by a distinct interface [1, 3]. Synthesized material exhibits the characteristics of each individual element in the system by introducing new special properties which can not be achieved by a single component. Despite the fact that the designed material may be in homogeneous phase, each constituent dominates its distinct structural features while remaining their identity in the mixture [2].

Composite materials existed in nature for millions of years. Wood, bamboo and bone are very commonly known natural composites. Mud blocks reinforced with bamboo shoots and glued laminated wood are the first historical examples of man made composites. Modern composites were started to be used in 1930's with the invention of fiber glass reinforced resins. After 1970's composite applications significantly increased with the development of new fibers such as carbon, boron and aramids and also new composite systems with metal and ceramic matrices [1]. Today aircraft, automobile, leisure, electronic and medical industries depend on fiber reinforced plastics. Also, mineral filled plastics are widely used in industry because of associated cost reduction [3, 18]

Increasing interest and demand for composite materials are mainly related to the advantages provided by their unique structures and designing flexibility that provides unlimited selection of characteristics for the invented material [4]. According to design considerations, they may offer improved strength, stiffness, fatigue and impact resistance, thermal conductivity, corrosion resistance and many other properties [1].

Most of the composites consist of two phases, and one of the components which is continuous and often, but not always, in greater quantity is designated as the *matrix*.

The second constituent is referred as the *reinforcing phase*, and reinforcement is incorporated into the matrix to enhance the properties of the surrounding phase. In many cases, the reinforcement is harder, stronger and stiffer than the matrix like the sand particles in cement, whereas there are some exceptions such as ductile metal reinforcement in a ceramic matrix or rubber phase reinforcement in a brittle polymer matrix [3, 18].

The behavior of a composite material is a result of combined effects of matrix, reinforcing phase, and the reinforcing phase-matrix interface. Interface is a region with finite thickness through which material parameters such as concentration, crystal structure, atomic registry, elastic modulus, density, coefficient of thermal expansion etc. can vary from one side to another. For composite structure, interface is a bonding surface between reinforcement and matrix with possible sharp and gradual discontinuities. Effective transmission of load from one constituent to another through interface is extremely important for the performance of the composite [18].

Wettability, surface roughness, interface interactions and bonding are very important parameters for an optimum interfacial interaction [18]. Wettability is described as the ability of a liquid to spread on a solid surface and exhibits the extent of intimate contact between two phases. Surface roughness is related with specific surface area of the reinforcement and it can contribute to mechanical bonding strength if adequate matrix wetting is available [18].

Interfacial bonding can be classified as mechanical, physical and chemical bonding where one or more of them can be present between the phases. Mechanical bonding is formed between two surfaces due to mechanical keying or interlocking effect. Generally, it is a low energy bond compared to a chemical bond and efficient in load transfer when the applied force is parallel to the interface. Physical bonding involves weak, secondary or van der Waals forces, dipolar interactions, and hydrogen bonding. Chemical bonding is a result of atomic or molecular transport by diffusion processes. Compound formation can occur at the reinforcement-matrix interface with a certain thickness, and all types of covalent, ionic, and metallic bonding may exist in the reaction zone. Consequently, interfacial bonding should be optimized for enhanced mechanical properties, since a weak matrix interface can prevail if no matrix is present, whereas a too strong bond can cause embrittlement due to low strain capability of the interface and can fail when cracking occurs [18].

### **2.1.1 Reinforcement in Composites**

The mechanical properties of composites are a function of the shape and dimension of the reinforcing phase since the geometry of the reinforcement is one of the major parameters in determining the effectiveness of the reinforcing material [3, 18]. Composites can be classified according to their matrix as previously mentioned and also for their geometry of reinforcement: particulate, flake and fibers [1].

In particulate composites, particles are immersed in the matrices, and load is carried primarily by the matrix phase. Reinforcing particles which have approximately equal dimensions in all directions can be spherical, cubic, platelet or in any regular or irregular geometry with a random or preferred orientation [1, 3]. Typical examples are aluminum particles in rubber and silicon carbide particles in aluminum. Flake particles consist of flat reinforcements of matrices and they offer high out-of-plane flexural modulus, higher strength, and low cost, whereas only a limited number of materials are available since they can not be oriented easily. Mica, glass and aluminum are the typical examples of flake materials [1]. Fibrous reinforcements can be characterized by their high particle length to cross-sectional proportion, namely the aspect ratio, which can vary considerably. In these types of reinforcement, fiber is the major phase that carries the load. Long fibers with high aspect ratio are called continuous fiber reinforced composites, while short fibers of low aspect ratio that can be encountered either in random or preferred orientations are called discontinuous fiber composites [3].

### **2.1.2 Types of Composites**

Composites can be investigated under three subcategories for their matrices: Metal matrix composites (MMC), ceramic matrix composites (CMC), carbon-carbon matrix composites (CCC), and polymer matrix composites (PMC).

Metals are naturally strong and tough, they can be plastically deformed and strengthened by variety of methods and these important structural characteristics make metals very versatile engineering materials [18]. Metals are mainly reinforced to provide the advantages over monolithic metals such as aluminum and steel. The elastic stiffness and strength of metals can be increased, while weight, large coefficient of thermal expansion and thermal electric conductivity of metals can be

reduced by the addition of fibers such as silicon carbide. Many examples of MMCs are available in aerospace engineering, military and transportation applications and one of them is the usage of MMCs in gas turbine engines for their high strength and low weight [1].

Ceramics are very hard and brittle. Their high strength and high stiffness at very high temperatures, chemical inertness, low density etc. make them very important in industry. However, ceramics have strong covalent and ionic bonds and very few slip systems available compared to metals, causing low failure strains and toughness or fracture energies. CMCs are produced to toughen the ceramics by incorporating fibers and hence to use their attractive high-temperature strength and environmental stability by preventing failure damage [18]. CMCs are generally applied in high temperature areas where PMCs and MMCs can not be used like aircraft engines [1].

In carbon-carbon composites, carbon fibers are embedded in a carbon matrix. Carbon-carbon composites are used in very high temperature environments up to 3315°C and they are 20 times stronger and 30% lighter than carbon structured graphite. Like ceramics, carbons are very brittle and flaw sensitive, and gradual failing property is provided in addition to resistance to high temperatures, low creep at high temperatures, low density, good tensile and compressive strengths, high fatigue resistance, high thermal conductivity and high coefficient of friction with the reinforcement of a carbon matrix. However, some disadvantages of these types of composites are also present such as susceptibility to oxidation and high cost [1].

### **2.1.3 Polymer Matrix Composites**

In order to increase the several properties of the polymeric matrices which are inadequate for industrial applications, like heat resistance, mechanical strength and impact resistance, or to decrease other properties like electrical conductivity or permeability for gases like oxygen, they have been filled with many inorganic synthetic and/or natural compounds [5]. Low cost, low heat-pressure requirement and ease of processing of the designed material make PMCs the most common composite type [3].

The matrix material of PMCs can be thermoplastic or thermosetting according to their response to temperature. Thermoplastic polymers can soften upon heating and flow

repeatedly when a heating process is applied, therefore their scrap can be recycled. They are formable at high temperatures and pressures due to Van der Waals type weak bonds. Thermosetting polymers can flow under stress only once after the heat treatment. Heating causes a curing reaction and crosslinking because of their rigidly attached chains with strong covalent bonds and further heating leads only to degradation [1, 19].

Epoxy, polyester and urethane reinforced with thin diameter fibers such as graphite, aramids and boron are the most widely used PMCs due to their enhanced mechanical properties. As an example, graphite-epoxy composites are almost five times stronger than steel on weight base [1]. PMCs have extensive application area in industry including automotive, aerospace, civil construction etc.

## **2.2 Nanocomposites**

Nanocomposites are multiphase materials whose one of the constituent phase is less than 100nm, at least in one dimension [6]. At this scale, the behavior and the properties of the materials differ from the bulk phase [1], and in most cases multifunctional behavior for any specific property of the material is more than the sum of the individual components. The possibility of realizing unique combinations of properties unachievable with traditional materials is the motivation behind researches on nanocomposite field [6].

Polymer nanocomposites have attracted considerable interest in both academia and industry over the past decade as a consequence of outstanding mechanical properties achieved with only small amount of nanofiller addition. Large surface area to volume ratio of nanoadditives compared to conventional fillers is the main reason behind these improvements. In addition to enhanced mechanical properties, superior barrier resistance, flame retardancy, scratch-wear resistance, optical, magnetic and electrical properties of polymer can also be improved by nanocomposite applications [7].

Polymer nanocomposites can be distinguished by a three-dimensional nanosize distribution structure of dispersed phase. When all three dimensions are in the nanometer size, isodimensional particle structure exists as in the case of spherical silica nanoparticles obtained by in situ sol-gel method. Elongated structures are

formed when two dimensions of the particles are in nanometer level and the third is larger like nanotubes or whiskers. Finally, if one dimension is in the nanometer scale and nanofillers are present in the form of sheets of one to a few nanometer thick to hundreds to thousands nanometers long, this family of composites can be recognized under the name of polymer-layered crystal nanocomposites [11].

### **2.2.1 Polymer Layered Silicate Nanocomposites (PLSN)**

Intercalation chemistry of the polymers due to their mixing with appropriately modified layered silicates has been known for a long time, however the interest on PLSN nanocomposites has recently been amplified. A report published by the Toyota research group regarding to the significant enhancements of thermal and mechanical properties which was achieved with small amount of MMT loading to Nylon-6 matrix and the observations of Vaia et al. [8] on the possibility of melt mixing polymer with layered silicates without using solvents stimulated the renewal of interest to PLSN nanocomposites. Today, almost all types of polymer matrices are being studied for the development of these promising organic-inorganic mixtures [9].

#### **2.2.1.1 Layered Silicate Structure**

Layered silicates used in nanocomposite applications belong to the 2:1 phyllosilicates family, as the better known minerals, talc and mica. Their crystal lattice is arranged with a two dimensional layer where a central octahedral sheet of alumina or magnesia is fused to two external silica tetrahedron by the tip, so that the oxygen ions of the octahedral sheet are also shared by the tetrahedral sheets. The layer thickness is around 1 nm, and depending on the particular silicate, the lateral dimensions of these layers can vary from 300 Å to several microns. The regular van der Waals gap between the layers are called *interlayer* or *gallery* and layers organize themselves in a parallel manner to form stacks with these interspace distances. Negative charges generated owing to the isomorphic substitution within the layers are counterbalanced by alkali or alkaline earth cations which are occupied in the interlayer.  $\text{Al}^{3+}$  replaced by  $\text{Mg}^{2+}$  or by  $\text{Fe}^{2+}$ , or  $\text{Mg}^{2+}$  replaced by  $\text{Li}^+$  can be given as an example to these isomorphic substitutions [11].

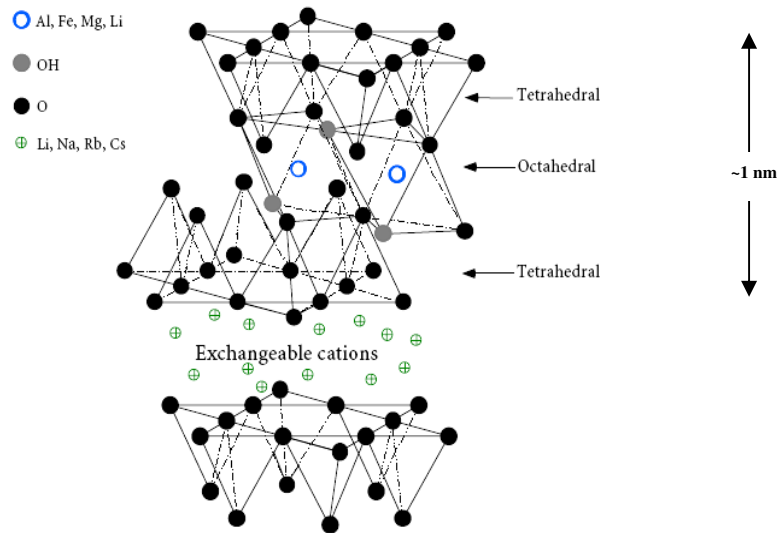


**Figure 2.1** Structure of 2:1 layered silicates [13].

Montmorillonite, hectorite and saponite are the most commonly used layered silicates and their detailed structure is given in Figure 2.1. These types of silicates are characterized by their large surface area (700-800 m<sup>2</sup>/g for montmorillonite), moderate negative surface charge namely cation exchange capacity (CEC, expressed in meq/100g) and their layer morphology considered as hydrophobic colloids of the constant-charge type.

The negative charge varies from layer to layer within certain bounds, and the value indicated by the chemical formula is only an average number over the whole crystal. The major proportion of the charge balancing cations is located in the interlayer while only a small quantity is located at the external crystal surface and they are exchangeable for others in solution [13]. The distance between the atoms in an ordinary Na-O bond is of the order 2.1-2.2 Å, whereas it is 3.6 Å in a gallery. According to this arrangement, almost 60% of the bonding strength between the cation and oxygen is not used regarding to the Coulombic interactions. Thus, the partial charge formed for each cation within a gallery makes phyllosilicates highly hydrophilic [12].

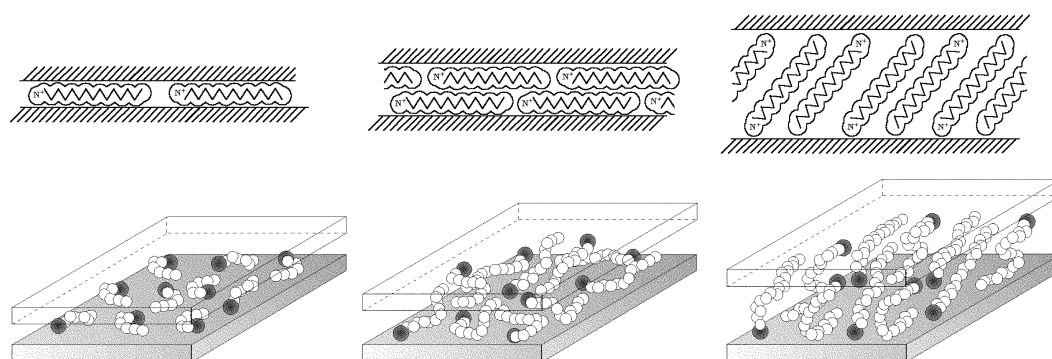


**Figure 2.2** Idealized structures of organically modified silicates [13].

Replacing the hydrated metal cations from the interlayers with organic alkylammonium and alkylphosphonium cations, the layered silicates can attain a hydrophobic/organophilic character and result in a larger interlayer spacing. The cationic head group of the alkylammonium molecule preferentially resides at the layer surface and the aliphatic tail radiates away from the surface due to the negative charge generated in the silicate layer. The equilibrium layer spacing depends on two conditions; the cation exchange capacity of the layered silicate and the chain length of the organic cation. As represented in Figure 2.2, the silicate layers can form mono or bilayers or radiate away from the surface forming mono or bimolecular tilted arrangements depending on the packing density, temperature and the chain length [13].

### 2.2.2 Nanocomposite Types

Proper dispersion of the layered silicates which have remarkably high aspect ratio (e.g. 10-1000) throughout the polymer matrix may create an increased surface area for polymer filler interaction which promotes enhancements in material properties [9]. Besides the conventional microcomposites for which the polymer and the inorganic host remain immiscible [13] three types of polymer layered silicate nanocomposites are thermodynamically achievable: intercalated, intercalated-flocculated and exfoliated-delaminated depending on the strength of these interfacial interactions between the matrix and layered silicates. These structures are shown in Figure 2.3 [9].

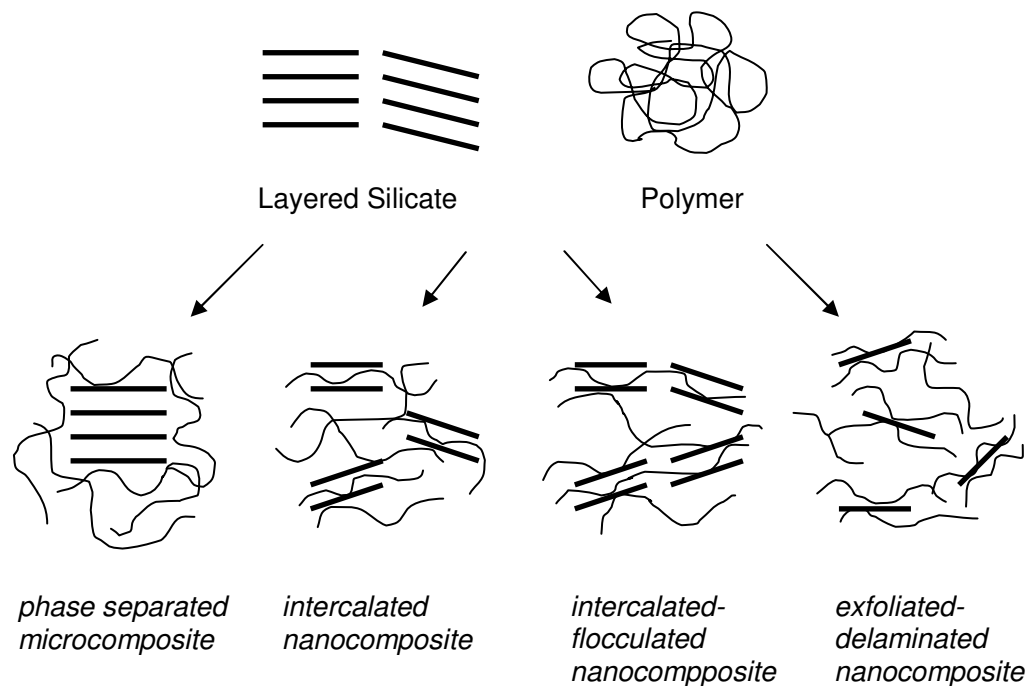


**Figure 2.3** Nanocomposite types.

In *intercalated* structures, extended polymer chains are inserted into the gallery space between parallel individual clay layers, and self-assembled, well ordered multilayer structures are formed [20]. Insertion is achieved in a crystallographically regular fashion and initially about 1 nm interlayer spacing is expanded to a few nanometers (2-3 nm) at the end of the process [9]. Basically, the same properties are observed in *flocculated* nanocomposites however, the silicate layers are flocculated due to hydroxylated edge–edge interactions of the silicate layers. When the individual silicate layers are no longer close enough to interact with the adjacent layers' gallery cations, the silicate layers can not maintain their ordered form, thus a total dispersion of silicate layers in the polymer matrix is observed and the resultant structures are called *exfoliated* or *delaminated* [20]. The ordered structure is lost, and the layer distance becomes of the order of the radius of gyration of the polymer. While in intercalated nanocomposites the polymer matrix and the silicate layers have limited miscibility, in exfoliated hybrids the components are totally miscible [12] and coexistence of these two extreme structures is possible, especially in the case of smectite silicates and clay minerals [20].

The most significant changes in material properties are observed in exfoliated nanocomposite structures. The number of available reinforcing elements for carrying an applied load and deflecting cracks are optimized by the complete dispersion of clay nanolayers in a polymer matrix due to enhanced polymer-layer interactions. Stress transfer to the reinforcing phase is facilitated due to the coupling between the tremendous surface area of the clay and the polymer matrix and thereby tensile and toughening improvements are allowed. Aggregated nanolayer tactoids contained in conventional polymer-clay composites ordinarily improves rigidity. However, in most cases strength, elongation and toughness properties are sacrificed. On the contrary, exfoliated clay nanocomposites represent improvements in all aspects of their mechanical performance. Variety of properties that is not possible for large scaled composites can be achieved regarding the high aspect ratio of the nanolayers. Moreover, the hindered diffusion pathways through exfoliated nanocomposites promote enhanced barrier characteristics, chemical resistance, and reduced solvent uptake and flame retardancy of the polymer layered silicate nanocomposites. See Figure 2.4 [21].

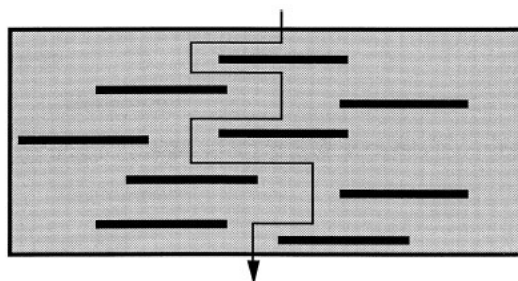


**Figure 2.4** Proposed model for the tortuous zigzag diffusion path in an exfoliated polymer–clay nanocomposite when used as a gas barrier [21].

### **2.2.3 Nanocomposite Preparation Methods**

Polymer intercalation in layered hosts such as layered silicates is a successful method in synthesis of polymer layered silicate nanocomposites. According to the selected materials and processing techniques, preparation methods can be

investigated under four main categories: in-situ polymerization, solution intercalation, sol-gel technology and melt intercalation [9, 12].

### 2.2.3.1 In-situ Polymerization Method

In the past, in-situ polymerization has been used for the synthesis of stereospecific polymers, which are constituted from the monomers entrapped in interlayer spacing [12]. In this technique, the layered silicate is swollen within a liquid monomer or a monomer solution, and the polymer formation takes place in between host layers. Initiation of the polymerization process can be implemented by heat or radiation, by diffusion of a suitable initiator or by an organic initiator or catalyst residing inside the interlayer [11].

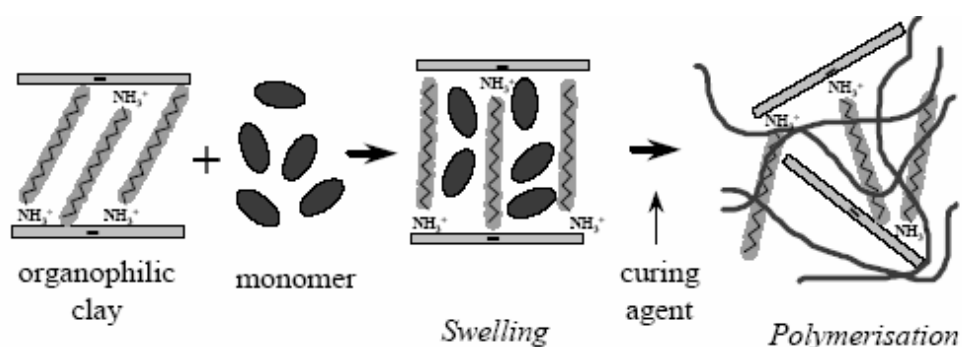


**Figure 2.5** In-situ polymerization method [22].

Depending on polarity of monomer molecules, the surface treatment of the organoclay, and the temperature, the monomer swelling step may require certain amount of time. Diffusion of monomer molecules between the layers occurs depending on the attraction between high surface energy of clay and the polar monomer until an equilibrium state is reached. After the initiation step, monomer starts to react with curing agent, and overall polarity of the intercalated molecules is lowered due to the reactions, since the thermodynamic equilibrium is achieved more polar molecules are driven between the layers, and organic molecules can eventually delaminate the clay layers. In-situ polymerization can effectively be applied to

polymer-clay nanocomposites based on epoxy, unsaturated polyester, polyurethanes and polyethylene terephthalate [22].

### 2.2.3.2 Solution Intercalation

In solution intercalation, the layered silicates are dispersed and exfoliated into single layers by the aid of an appropriate solvent, such as water, chloroform or toluene, in which the polymer (or a prepolymer in case of insoluble polymers such as polyamides) is also soluble. Since the forces, stacking the layers together are weak, the layers can easily be dispersed in a proper solvent. The solvated polymer and swelled layered silicates are then mixed and the polymer chains are replaced with the solvent molecules within the expanded silicate layers. Finally, the solvent is evaporated (or mixture is precipitated) and the polymer is adsorbed onto the delaminated sheets, and sheets are reassembled by sandwiching the polymer to form an ordered multilayer structure [9, 11]. The intercalation process is represented in Figure 2.6.

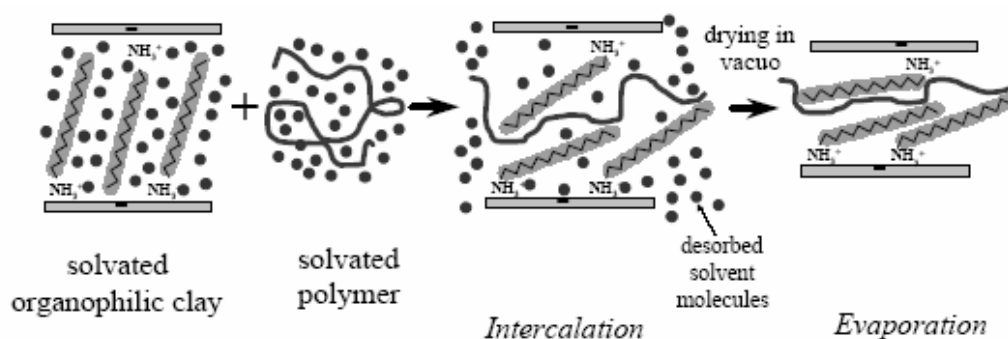


**Figure 2.6** Solution intercalation method [22].

### 2.2.3.3 Sol-Gel Technology

Sol-Gel technology is applied for the direct crystallization of the silicate clays via hydrothermal treatment of a gel, which contains organics and organometallics including the polymer. Silica sol, magnesium hydroxide sol and lithium fluoride are

used as a precursor for the clay. In this method, high dispersion of the silicate layers is promoted without requiring the presence of the onium ions [12].

#### 2.2.3.4 Melt Intercalation

In this method, annealing of a polymer and a layered silicate is employed above the glass transition or the softening point of the selected polymer under static or flow conditions [9]. Usually, organically modified clays are used to promote intercalation to increase the interlayer spacing of modified clays or to render the incompatibility between the polymer and layered silicate aroused due to polarity. Depending on the degree of penetration, polymer chains are spread from the mass in molten state into the silicate galleries to form either intercalated or delaminated hybrids [12].

A spontaneous process can be explained by postulating a gain in entropy owing to the greater conformational energy of the aliphatic chains of the alkylammonium cations, since insertion of polymer increases the size of the galleries [12].

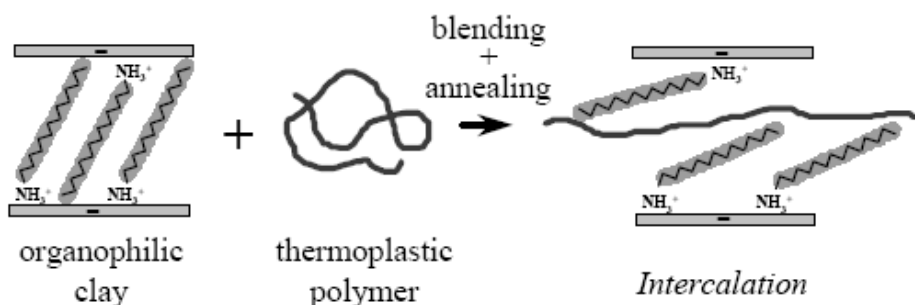


**Figure 2.7** Melt intercalation method [22].

According to the experimental observations, the result of polymer intercalation depends critically on silicate functionalization and interactions between constituents. One of the important parts for constructing the new hybrid is selecting the potentially compatible polymer organically modified layered silicate (OMLS) systems. In order to maximize the configurational freedom of the functionalizing chains upon layer separation and to maximize the potential interaction sites at the interlayer surface,

the structure of the OMLS should be optimized. As an example, polymers containing polar groups are capable of associative interactions such as Lewis-acid/base interactions or hydrogen bonding and thus their structure may lead to intercalation. The functional groups in the OMLS should be short in order to minimize the unfavorable interactions between the aliphatic chains and the polymer in the presence of polar or hydrophilic polymer [9].

When all three methods are compared, melt intercalation offers great advantages. Since this method does not require an organic solvent, it is environmentally benign and economically favorable. Moreover, it is compatible with many current industrial processes such as extrusion and injection molding, and it also authorizes the use of polymers which is previously not proper for solution intercalation or in situ polymerization [9].

### **2.3 Polymer Blends**

Blending technology began fifty years ago in plastic industry [23] and today polymer blends constitute 36 wt% of the total polymer consumption with a continuously increasing demand [24].

The idea behind developing the polymer blending technology is combining properties of two different polymers whose final properties can satisfy the requirements of a particular application [23].

The material related benefits of polymer blending can be mentioned as:

- i. Providing new materials with the required properties at the lowest price
- ii. Enhancing the resin performance
- iii. Improving the specific material properties such as solvent resistance and impact strength
- iv. Employing waste recycling for industrial plastics

In addition to these advantages, blending offers benefits for the manufacturer, such as improved processability, scrap reduction, flexibility for formulation changes, reduction of the number of grades that need to be manufactured and stored, and inherent recyclability [24].

Blending was applied historically for improving impact strength of early resins, such as toughening of polystyrene (PS), polyvinylchloride (PVC), polyamide (PA) and polyethyleneterephthalate (PET) etc. In time, blending was used for producing multi-polymer systems for impact modification and compatibilization. Various types of blends have been formulated with a multicomponent modifier that compatibilizes and provides impact modification simultaneously [24].

Polymer blends can be prepared by five major techniques: melt, solution and latex blending, partial, block or graft copolymerization, and synthesis of interpenetrating networks. Creation of homogeneous mixtures by means of mechanical effects can be implemented in a twin or single screw extruder, batch mixers or two roll mills [23].

The morphology of the polymer blends is very important and basically depends on the blend concentration. When the concentration of one of the components is low, the dispersed phase arranges in the continuous matrix in nearly spherical drops, whereas at higher loadings, formation can be in the shape of cylinders, fibers or sheets. Besides these two distinct morphologies a co-continuous structure may also be formed at the phase inversion concentration, where the distinction between the matrix and the dispersed phase disappears [24].

Miscibility of the polymer blends has also a significant effect on blend morphology and physical properties of the product. Miscibility behavior is significantly affected by preparation method. Various problems may arise regarding to weak interfacial strength between the two phases which affects the performance of the material [23]. During processing, the hydrostatic and shear stresses can diverge to a lower critical solubility temperature resulting with a miscible blend. In contrast, the blend coming out of the extruder may have phase separation by a spinodal decomposition mechanism into a co-continuous structure as in the case of PET- polycarbonate (PC) blends [24].

Considering the blend rheology, presence of specific interactions may change the free volume and degree of entanglement upon mixing, which affects the flow behavior. For immiscible blends, flow is affected in a similar fashion but there exist at least three contributing phases: blend components and the interphase in-between [24].

Thermal behavior of a polymer blends also gives information on miscibility. While a miscible polymer exhibits a single glass transition temperature ( $T_g$ ) between the pure components'  $T_g$  values, a partially miscible represents two  $T_g$  values that closer to each other but not identical [23].

Quality of the compounded blend is greatly affected by the processing conditions and performance. Layering, poor weld lines in injection molding parts, skin-core extrudate with low notched impact strength indicate the poor blend quality owing to inadequate dispersion or poor stabilization morphology. Therefore, precise controlling the processing parameters during blend preparation is essential [24].

## **2.4 Recycling Polymers**

Recycling is both an economical and an environmental issue. Each year millions of tones of plastic scraps are collected in landfills causing environmental threats affecting ecology. Moreover, environmental legislations and the economical potential of plastic post consumer products are supporting the interest on the recycling technologies.

Recycling processes are necessary to transform the collected materials into raw materials to manufacture new products. Type of the recycling is often specific to the individual plastic and can be classified into three major categories: Physical recycling, chemical recycling and thermal recycling.

Physical recycling process is basically related with changing the appearance of the material without altering (at least not to a large extent) it's main chemical structure such as removing contaminants, changing size and shape of the materials, and blending with additives if required. Some of the examples are grinding, air classification, washing, gravity separation in water, and often melting and pelletization by adding colorants, heat stabilizers etc. Today, physical recycling constitutes the major part of plastic recycling.

Chemical recycling involves breaking down the molecular structure of the polymers by the aid of chemical reactions. Recycled materials are purified and used as raw materials for producing the same or a related polymer. Glycolysis can be given as an example for chemical recycling, and condensation polymers such as PET, PA are more amenable in this technique than polyolefins or PS.

Thermal recycling also involves breaking down the chemical structure; however, heat is used as the driving force for reactions instead of chemical reactions. As an example, in pyrolysis, the polymer (or mixture of polymers) is subjected to high temperatures in the absence of sufficient oxygen for combustion. Thermal recycling can be applied to all types of polymers. When reasonably pure compounds can be recovered, they can be used as raw materials, whereas when the products are a complex mixture and separation is difficult, products are often used as fuel [25].

When the structures of the components are preserved and no significant degradation occurs during recycling and lifetime, recycling can be a good option. Degradation may cause some deteriorating effects such as decrease in molecular weight, branching formation of chemical groups etc., and the new created material from the recycled plastic may have reduced physical properties and hence value. Then, the most important part of plastic recycling is avoiding further degradation. This is possible with the correct selection of processing conditions and by addition of stabilizers and other additives before melt compounding [26].

The presence of contaminants and solid particles in the polymer matrix may also adversely affect the physical performance of the molded parts and hence the quality of the final recycled product, since material may experience a premature failure. Therefore, separation is a very important part of polymer recycling. In addition to that, since most polymers are mutually insoluble, a blend of resins is likely to consist of domains of one resin embedded in a matrix of the other resin at a microscopic scale. While this sometimes results in desirable properties, more often it does not. Various techniques are also applied for separation of different polymer grades and types [25].

## **2.5 Polymer Matrix of the Study**

Polymer matrix used in this study was a recycled grade polypropylene with polyethylene phase embedded in the continuous polypropylene matrix. Recycling process was implemented by the producer from the post consumer polymers by melt blending method in a single screw extruder. Besides recycling, about 5 wt% talc addition was also applied by the producer in order to increase the stiffness properties of the final blend product.

### **2.5.1 Polypropylene**

Polypropylene (PP) is a thermoplastic polyolefin that is produced by polymerizing propylene monomer, which is a gaseous byproduct of petroleum refining, in the presence of a catalyst under controlled heat and pressure [15, 27].

Polypropylene was initially produced in 1954 by G. Natta's group following the work of K. Ziegler regarding to successful development of a suitable stereo-specific catalyst, which conferred polypropylene a kind of structural characteristics useful for rigid items [15, 28].

Polypropylene is widely used in the world owing to the widespread availability, low cost monomer, low manufacturing cost and desirable properties. Moreover, processability in variety of different processing equipment, ranging from injection molding, calendaring and blown film equipment due to its proper melt rheology and thermal behavior supports the industrial demand, and approximately 30 million tones of polypropylene was consumed worldwide in 2001 [15, 29].

Structure of polypropylene resembles polyethylene however the rigidity of the PP is higher than low density polypropylene. Polypropylene has excellent physical, mechanical and thermal properties for room temperature uses. Characteristic properties of polypropylene such as low density, relatively high stiffness, impact resistance and high melting point make PP desirable for industrial applications. Polypropylene is used in production of many industrial products the main application areas are packaging, fibers, crates, pipes and automobile applications (often with reinforcing fillers) [30].

PP also has the ability to form integral hinges with an unlimited repeated bending resistance [30]. Moreover, properties of PP can simply be varied and improved by altering the chain regularity (tacticity), distribution or content, adding comonomers such as ethylene into the polymer chains and incorporation of an impact modifier [15].

#### **2.5.1.1 Polymerization, Structure and Tacticity of Polypropylene**

Polypropylene is synthesized from propylene monomer by Ziegler-Natta polymerization or metallocene catalyst polymerization as previously mentioned.

Polypropylene is also a vinyl polymer and its structure resembles that of polyethylene. However, the special feature of propylene polymerization compared to ethylene synthesis is the symmetry of the monomer addition into the growing polymer chain due to presence of the methyl group in the propylene monomer. This unique property provides orientation to the monomer insertion and a stereochemical configuration (regularity of the methyl group replacement relative to other methyl groups) compared to other units in the chain backbone (see Figure 2.8) [29].

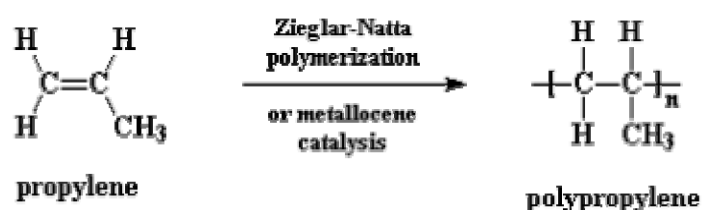


**Figure 2.8** Polymerization of polypropylene [31].

In polypropylene polymerization, stereochemical isomerism is possible regarding to linkage of the monomers according to the varying spatial arrangement of the methyl groups. *Isotactic* arrangement occurs if the methyl groups are all accommodated in one side of the chain [15]. Isotactic polypropylene (iPP) is a polymorphic material with various crystal modifications and a modification with intermediate crystalline order [28]. *Syndiotactic* structure is formed when methyl groups arrange at the alternate sides of the chain. In addition to these, random arrangement of methyl groups is also possible and *atactic* polypropylene structure is obtained in this case (see Figure 2.9). Homopolymer PP consists of two phases in its structure; crystalline and noncrystalline regions. Both isotactic PP and atactic PP contain crystalline and noncrystalline regions. However, amorphous regions of isotactic PP are crystallizable and they crystallize slowly over time as entanglements allow [15].

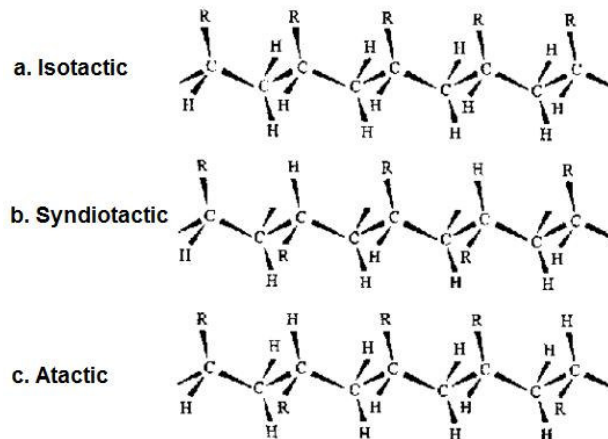


**Figure 2.9** Stereochemical configurations of polypropylene [28]

Stereochemical features of polypropylene are discussed in terms of tacticity. Commonly, polypropylene is known with its high tacticity in marketplace namely, the high isotactic content. While high tacticity polypropylene materials represent desirable physical, mechanical and thermal properties in solid state, atactic materials are sticky, soft and gummy and they are usually used in applications where stickiness is required. Syndiotactic PP is not used widely and it is less crystalline than isotactic PP [15].

### 2.5.1.2 Polypropylene Recycling

Considering the entire lifecycle, polypropylene is recognized as a preferred polymer for the manufacturers and various recycling techniques have been developed for recycling polypropylene.

Besides the environmental concerns, the production cost of polypropylene has led to conversion of waste polymer to monomer. As a consequence, depolymerization of polypropylene has become one of the most preferred methods for polypropylene recycling, especially pyrolysis. Another technique is selective dissolution process. Plastic wastes consists different types and grades of polymers, and by applying selective dissolution process with a controlled sequence of proper solvents, regaining pure polypropylene and other plastics is possible [15].

Extrusion and compounding based technologies are also widely applied in plastic recycling for upgrading of commingled plastics to marketable properties for their economical and technical aspects. By blending with virgin polypropylene, different grades of polypropylene and other polymers in the waste stream can also be processed in twin or single screw extruders for their reuse [15]. The polypropylene grade used in this study was prepared by this method.

The challenge in recycling polypropylene by compounding method is contamination of the matrix with other polymers which is often polyethylene. Detergent bottles (a body of high density polyethylene and a spout or cap of polypropylene) or disposable diapers can be given as examples (PE outer liner and PP inner liner). It is physically impossible to separate these polymers into pure components [32]. Immiscibility of the two phases causes poor interfacial adhesion resulting in poor blend mechanical properties and the lack of stability in the morphology and hence separation or stratification during later processing or use. Mostly, compatibilizers in the form of block and graft copolymers are used for improving interfacial adhesion and reducing interfacial tension [15]. Also, reinforcing materials such as talc, mica, calcium carbonate etc. may be incorporated in order to reduce the material cost and improve rigidity as in the case of other blends [17].

### **2.5.2 Polyethylene**

The simplest form of a polyethylene (PE) chain contains a long backbone of even numbered carbon atoms which are covalently linked with a pair of hydrogen atoms attached to each carbon atom (see Figure 2.10) [33].

Polyolefin synthesis began in 1890's with polymethylene, and polyethylene (as in the form of low density polyethylene) was the first commercially used thermoplastic polyolefin [29]. In 1933, R. Gibson and E. Fawcett at Imperial Chemical Industries (ICI) investigated the high pressure reaction of ethylene with benzaldehyde and discovered polyethylene polymer [33]. After the discovery, PE was immediately utilized for electrical cable sheeting for radar applications during the World War.

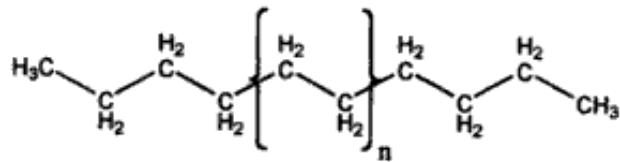


**Figure 2.10** Structure of polyethylene [29].

Chemically pure polyethylene chains consist of alkanes in  $C_nH_{n+2}$  formula where  $n$  represents the degree of polymerization. Typically the degree of polymerization is more than 100 and the molecular weight of the polymer may vary from 1400 to 3,500,000. There are many types of polyethylene exists with identical backbone structure of covalently linked carbon atoms with pendant hydrogens and distinct branches whose variations modify the nature of the material. Types of polyethylene can be classified as:

- Low density polyethylene (LDPE)
- Linear low density polyethylene (LLDPE)
- Very low density polyethylene (VLDPE)
- Medium density polyethylene (MDPE)
- High density polyethylene (HDPE) [33]

Crystallization process is hindered in LDPE chains by existing branches at substantial concentrations and that causes relatively low densities usually varying between 0.90-0.94 g/cm<sup>3</sup>. VLDPE has much higher concentrations of branching which inhibits crystallization effectively. High levels of branching and predominantly noncrystalline form result lower densities in between 0.86 to 0.90 g/cm<sup>3</sup>. LLDPE resins have linear polyethylene backbones attached to short alkyl groups at random intervals and they are in the same density range with LDPE.

MDPE is less dense and notch sensitive than HDPE. HDPE which is most widely used form of PE has primarily unbranched molecules with a very few defects affecting its linearity. Owing to low defects that may cause hindering the organization, high level of crystallinity is obtained [33]. HDPE is generally taken to mean the product of ethylene polymerization and it has the highest density between PE types

that is above  $0.94 \text{ g/cm}^3$  [29]. The chain structures of PE types are represented in Figure 2.11.

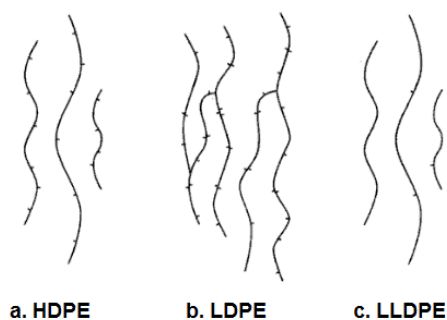


**Figure 2.11** Types of polyethylene [33].

Polyethylene has extensive industrial application areas such as the usage of LDPE in textile products, moisture barriers, cable insulation and bags; also HDPE is used in bottle production, pails, tubes, caps, complex mold shapes for injection, film, sheet wire etc. [34].

## 2.6 Polypropylene Nanocomposites

As previously mentioned, polypropylene has many desirable properties such as low density, high thermal stability and good solvent resistance that provide a great potential for nanocomposite applications. However, its lower modulus compared to engineering polymers and brittle nature bring in some limitations for many applications. Inorganic fillers such as talc, mica and layered silicates can improve stiffness, reduce mold shrinkage and thermal expansion properties while an elastomeric phase can compensate for the reduction in toughness emerged regarding to filler incorporation [35-38].

In polypropylene nanocomposites, the dispersion of the filler and elastomer phases as well as processing conditions play an important role in determination of toughness and stiffness properties [37-39]. Conventional fillers such as talc has low aspect ratio, therefore, high amount of additive loading is required to obtain significant

improvements in stiffness that may result in poor processability, low ductility and a rough surface finish. On the other hand, fillers with high aspect ratio, such as layered silicates can potentially solve these issues particularly when high degree of filler dispersion is present [40].

The dispersion of the silicate layers in the molten polymer basically depends on the thermal diffusion of the polymer chains inside the clay galleries and the mechanical action and shear applied during compounding. Nanofillers are naturally hydrophilic since they have polar hydroxyl groups in their structure. Whereas, polypropylene has no polar groups in its backbone and one of the most hydrophobic polymers, therefore direct intercalation or exfoliation of silicate galleries is quite difficult [41-43]. One of the attempts to solve this problem includes modification of the clay surface with organic cations, such as alkylammonium ion or alkylamine as previously mentioned [44, 45]. Thermal diffusion can be favored by this method and clay galleries can become chemically compatible with the polymer owing to more organophilic-hydrophobic character [46, 47].

Another method is adding compatibilizers having functional groups such as maleic anhydride or acrylic acid grafted onto a polymer matrix or elastomer to improve the miscibility and adhesion between polymer-filler and also polymer-elastomer [48, 49]. In order to satisfy necessary interaction, firstly the compatibilizer should have certain amount of polar groups to effectively intercalate between the silicate layers through hydrogen bonding. Secondly, the structure of the compatibilizer should be miscible with polypropylene. In addition to that, since the presence of polar functional groups in the compatibilizers affects the miscibility with polypropylene: an optimum content of polar functional groups is required to form hybrids [45].

Maleic anhydride grafted polypropylene (PP-MAH) is one of the most commercially used compatibilizers in preparation of polypropylene based nanocomposites. Maleic anhydride functionality of the PP-MAH is capable of forming hydrogen bonding with the clay while providing compatibility with the matrix through its polypropylene backbone. There are some studies available in the literature for the effect of PP-MAH to organoclay ratio on the morphology and the performance of the PP based nanocomposites [16, 45]. Several studies are also available for degree of functionality and effect of maleic anhydride content of PP-MAH on the nanocomposite structure [42, 50].

The role of organoclay and compatibilizers are also essential for blend morphology. In this study, the recycled polypropylene used in nanocomposite preparation contains some amount of polyethylene dispersed in the matrix. The mixture of these two polyolefins forms an immiscible blend with poor mechanical properties as a consequence of low interfacial adhesion, phase coalescence, coarse and unstable morphology [51, 52]. The well dispersed organoclay layers create a barrier effect and avoid agglomeration of the elastomeric domains and positively affect the mechanical properties, particularly toughness [40, 53]. Moreover, it is a known fact that the presence of an interfacial agent or a compatibilizer can stabilize the blend morphology by reducing the interfacial tension, hindering and coarsening by forming a protecting layer as in the case of organoclays [54, 55]. Some studies in the literature suggested that PP-MAH can provide an interfacial interaction between two phases even for immiscible blends such as polyethylene and polypropylene [56].

In this study, two types of compatibilizers were used: a terpolymer of ethylene-methyl acrylate-glycidyl methacrylate (E-MA-GMA) and maleic anhydride grafted polypropylene.

### 2.6.1 Glycidyl Methacrylate (GMA) Functionality

Glycidyl Methacrylate (GMA) monomer shown in Figure 2.12 contains both acrylic and epoxy groups, and both of the groups can react readily with a wide range of monomers and functionalized molecules that provide performance and flexibility in polymer design. Moreover, desirable properties of both methacrylics and epoxies can be used owing to dual functionality of the GMA.

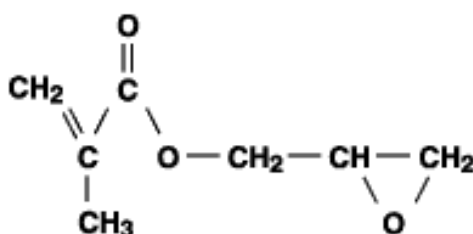


**Figure 2.12** Structure of GMA [57].

Epoxy functionality of the elastomer enables crosslinking reactions with amines, carboxylic acids, anhydrides and hydroxyl groups. Moreover, proper accelerator-catalyst choice employs wide ranges of cure temperatures and schedules. Structural modification of the polymer backbones can be implemented by the epoxy groups and hence differentiated properties and higher performance can be provided.

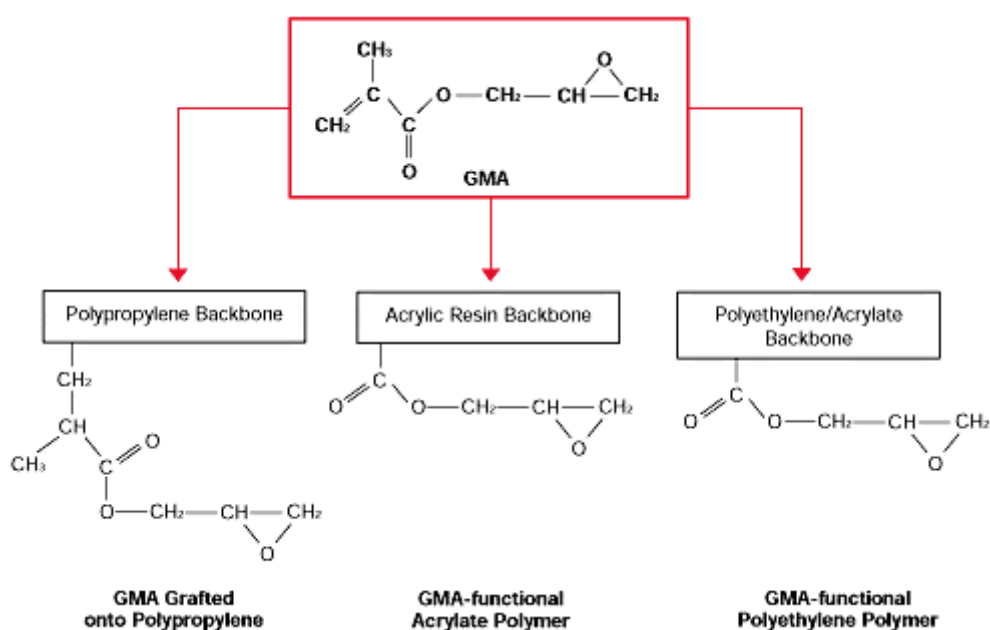


**Figure 2.13** Typical GMA reactions [57].

Acrylic and vinyl functionalities allow copolymerization with a variety of other vinyl monomers in aqueous and nonaqueous systems. A unique combination of epoxy functionality with an acrylic backbone can be obtained in the synthesized polymer. Easy control of physical and chemical properties such as  $T_g$  and solution viscosity are provided with a wide co-monomer selection. Typical GMA reactions are shown in Figure 2.13.

Finally, both acrylic and epoxy functionalities provide enhanced impact resistance, improved adhesion strength, acid resistance (only with epoxy groups), improved water and heat resistance and thermoplastic polymer blend compatibility [57].

### 2.6.2 Maleic Anhydride (MAH) Functionality

Maleic anhydride functionality is used to obtain compatibility between the matrix and the filler. Polar character of anhydride is believed to cause an affinity for the silicate surface [16].

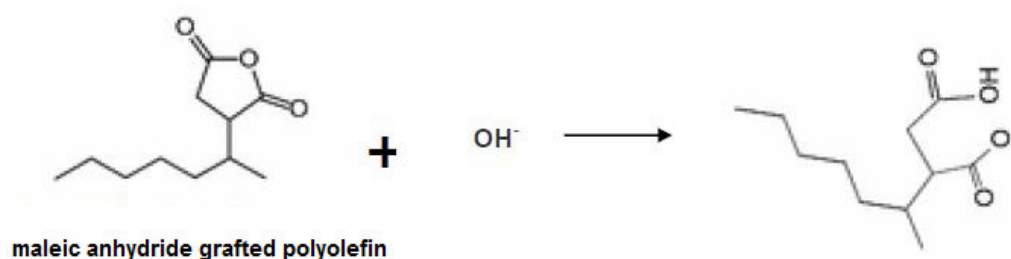


**Figure 2.14** Structure of maleic anhydride grafted polypropylene and its reaction with hydroxyl groups.

The main driving force for intercalation is originated from the strong hydrogen bonding between the maleic anhydride group, more specifically the carboxyl (COOH) or hydroxyl (OH) groups generated from the hydrolysis of the maleic anhydride group, and the oxygen group of the silicates as represented in Figure 2.14 [58, 59].

Figure 2.15 represents the intercalation process of PP-MAH inside clay galleries. Owing to polar affinity, the PP-MAH can intercalate between the silicate layers and expand the galleries for the entrance of polypropylene macromolecules and it also provides compatibility between the phases.

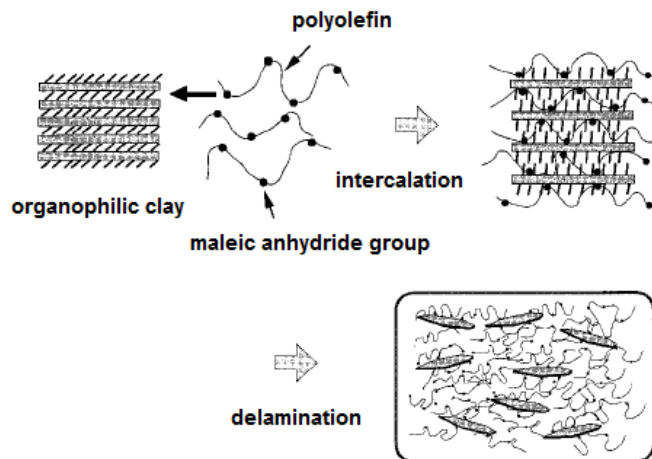


**Figure 2.15** Schematic representation of the intercalation process of PP-MAH [60].

## 2.7 Polymer Processing

The main concern of polymer processing is conversion of raw polymeric materials into value-added products by means of shaping, compounding and reacting to lead macromolecular modifications and morphology stabilization.

Modern polymer processing methods and machines emerged in the 19<sup>th</sup> century rubber industry by the processing of natural rubber. Today, numerous applications are being applied to polymer industries such as extrusion, injection molding, calendaring, fiber spinning, tubular film blowing etc. [61].

### 2.7.1 Extrusion

An extruder is a multifunctional machine capable of performing various operations through its pumping function. In any type of operation, the main objective of extruder is producing a homogeneous molten material at a certain flow rate, pressure and temperature proper for the subsequent operation in the process line which is usually the formation of a solid polymer article [62]. A typical extruder consists of a feed section, a downstream unit and a die section. A diagram of a simple extruder is shown in Figure 2.16.

The first ram extruders were developed in 1845 for wire coating production in rubber industry. Extruders became the most important processing devices since they involve a whole array of units for cooling, stretching and cutting directed to handle infinitely long elements such as rods, fibers, pipes, sheets, films wire coating etc. [63].

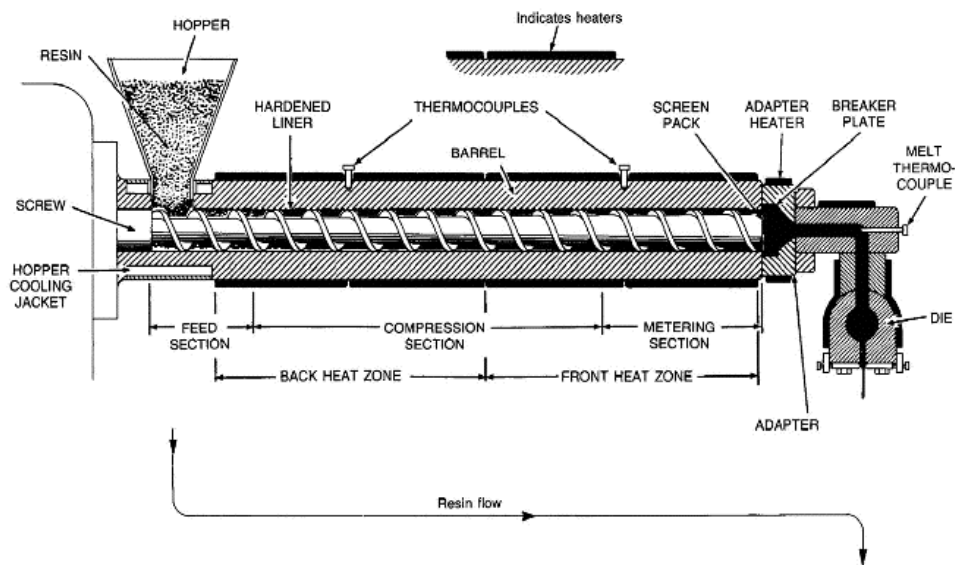


**Figure 2.16** A simple extruder scheme and representation of the sections [25].

### 2.7.1.1 Screw Design

The screw of an extruder is the most important part of the machine and it is divided into several sections such that each one is designed and used for a specific purpose. During extrusion process, solid resins, which are in the pellet or powder form, are introduced from the hopper through the feeding port into the feed throat of the extruder. Solid resins, which are propelled onto the rotating screw, are packed into a solid bed in the first screw section, which is called the *feed zone*. Then the solid particles are melted and conveyed through the *transition zone* in the middle of the downstream unit. Finally, the melt mixture is purged through the die with the aid of the generated pressure in the final *metering section* (see Figure 2.17).

Extruder barrels consist of heater bands and cooling units in order to provide the required temperature profile. However, the heat conduction from the walls of the barrels provides only 10-30% of the energy needed for melting the resin. The remaining part of the heat is supplied from the friction originating from the mechanical motion of the screw called viscous dissipation [25].

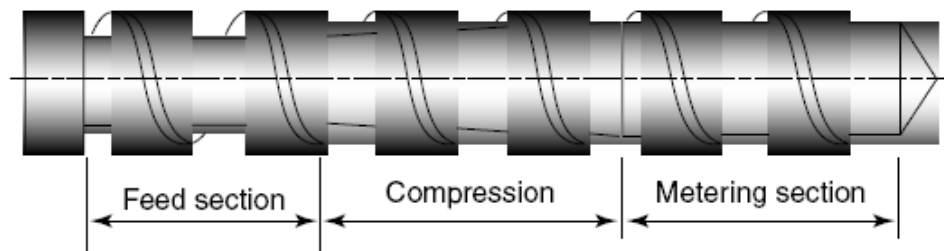


**Figure 2.17** General purpose extruder screw [29].

Screws of the extruders are designed to fulfill the required packing, melting and pressure generation. Outside diameter of the screw which is measured from the top parts of the screw flights remains constant, while the root diameter of the screw changes. The root diameter is small in the feed section, so that the large channel depth (distance between the outside and root diameters) can accommodate the packed solid resin particles. The root diameter increases, diverging from the feed zone to transition zone, to generate a change in the channel depth. Difference in the channel depth can force solid particles into better contact with the barrel wall and promote melting and apply compression on molten polymer. In the metering zone, the root diameter becomes constant with small channel depth, which facilitates pressure generation and helps maintain the temperature of the polymer melt [25].

Geometrical parameters, which characterize the process, are controlled by the screw diameter namely the length to diameter ratio ( $L/D$ ). Usually, extruder screws have length to diameter ( $L/D$ ) ratios of about 30:1. Barrier screws are used to improve melting performance while an assortment of mixing elements incorporated into the metering zone enhances mixing and provide temperature uniformity of the melt [25].

### 2.7.1.2 Extruder Types

Variety of different extruders has been designed for plenty of plastic types since the first invention of extruders. Extruders can be classified as:

- Continuous with single screws (single and multi-stage) or multiscrew (twin-screw etc.)
- Continuous disk or drum
- Discontinuous ram extruders [64].

Single screw extruders account for the 90% of the all extruder types while twin-screw extruders with different type of screw design and configurations constitute the rest 10 percent [25]. Most twin-screw extruders perform the similar elementary polymer processing steps as single screw extruders do. However, compared to single screw extruders, unique time-varying screw-to-screw interaction properties involved in twin-screw extruders particularly affect the melting and mixing steps. Owing to these additional mechanisms that enable enhanced melting and mixing actions, twin-screw extruders offer important advantages over single screw extruders [61].

Twin-screw extruders can be classified as counter-rotating intermeshing or non-intermeshing (tangential) and co-rotating intermeshing according to their screw design and screw configurations (see Figure 2.18). In nonintermeshing extruders, the polymer is conveyed by drag flow. These types of extruders provide tight control of heat and shear, and thus they are preferred in devolatilization, coagulation, reactive extrusion operations and halogenation of polyolefins. In twin-screw extruders with intermeshing design, the screws are interlocked with each other and the polymer is being transferred from one screw to the other, and therefore positive conveyance of the polymer and increased mixing is achieved. They are usually used in applications where mixing and compounding is required simultaneously and they are also used in compounding of small agglomerates such as carbon black since they are highly capable of dispersing [25].

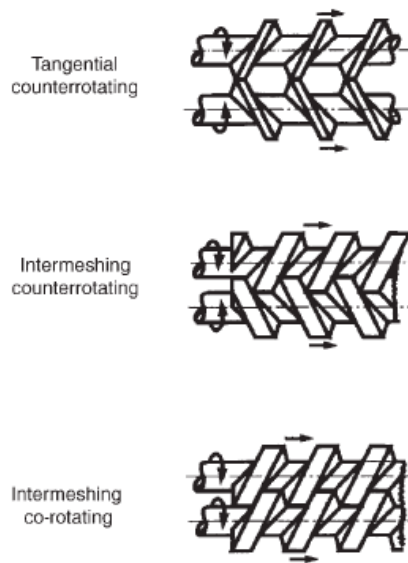


**Figure 2.18** Screw configurations for twin screw extruders [65].

In counter-rotating twin screw extruders, a part of the polymer flows between the screws and the barrel wall and the remaining part resides between two screws. The longer flow path in counter-rotating intermeshing twin-screw extruder causes increased residence time but the degree of elongational flow also increases and hence the mixing is enhanced [25].

### 2.7.2 Injection Molding

Injection molding process is used for producing plastic parts with required shapes and dimensions. An injection molding device consists of four major parts: injection unit, control systems, drive system and clamping unit [25].

The first injection machine is invented in 1872 for the processing of cellulose nitrate and today the processing of thermoplastics by injection molding comprises the major part of the industry representing almost 50% of the processing machinery. The major difference of injection molding compared to extrusion process is being a batchwise-cyclic process where the final shape is obtained in a cooled mold made of two parts that alternatively open and close [63]. The main processing parameters are the cycle time, temperature and pressure.

Plunger type is the simplest molding machine and the plastic is pushed forward through a heated region by a plunger. The more commonly used type is the reciprocating screw injection-molding machine. The function of the screw is melting and mixing the feed material. The entire screw moves forward as a plunger for injection and a special valve prevents backflow [62].

Two distinct processes are performed during injection molding. The first one is performed in the injection unit and involves the heating and melting of the polymer, injecting the melt into the cavity and applying pressure during cooling phase. The second one is related with the structuring and it takes place in the mold cavity. The injection mold unit gives the material the shape of the cavity, distributes the polymer melt to the cavities through a runner system and finally cools and ejects the part.

During one cycle of injection molding process, the polymer melt flows from the nozzle on the injection unit through the sprue, then to the runners where the melt is distributed to each of the cavities. The entrance of the cavity is called the gate and usually it is small to provide easy removal of runner system [25]. Cooling time principally depends on the thickness of the molded piece and typically changes in the range of 10 to 100 seconds [62]. In the case of heat sensitive materials, especially during the processing of thermosets, the residence time in the barrel should be minimized. Usually, a fast cycle time and mold temperature with the lowest possible value is preferred for economic reasons; however, too low mold temperature may end up with inadequate surface finish and crystallization which affects performance of the article negatively. Moreover, the injection speed and pressure should be determined according to the types of the materials and the nature of the mold. High injection speed is generally preferred to avoid the formation of premature freezing due to crystallization, especially when the parts are complicated [66].

## **2.8 Characterization of Nanocomposites**

In development of new products, evaluating the properties and structure of the new material and comparing them with the other materials whose properties are already known is quite important for validation of the improvements and service performance. In order to provide all the necessary information, a combination of different test methods is required since only one single test method is inadequate for analyzing the resulting characteristics as a whole. In this study, mechanical, morphological, thermal

and rheological analyses were conducted to evaluate the properties of nanocomposites.

### **2.8.1 Mechanical Properties**

Mechanical properties are concerned with evaluation of load deformation or stress-strain relationship. Applied forces may be in the form of tension, shear, torsion, compression and bending. Mechanical behavior of polymer-based materials depends on composition, structure and interactions at molecular and supermolecular levels. Structures are mainly determined by primary chemical bonding (mostly covalent) inside chains and secondary bonding (dispersion: hydrogen bonding, van der Waals, induction and electrostatic) forces between chains. Moreover, the characteristic stress-strain curve, stress relaxation or impact behavior is very important in determining the applications and limitations of a polymer [29].

#### **2.8.1.1 Tensile Test**

Tensile test is conducted on a machine that can apply uniaxial tensile or compressive loads to the test specimen and also capable of registering the value of applied load and the amount of deformation on the test specimen.

Tensile properties are analyzed according to standard test methods, by using specimens of a specified shape (typically dog bone shape) and dimensions. Tensile test specimen may be round cylinder or a flat strip with reduced cross section, which is called the gauge section, at the midlength, in order to ensure that fracture does not occur at the holding grips [67]. Schematic representation of tensile test is given in Figure 2.19.

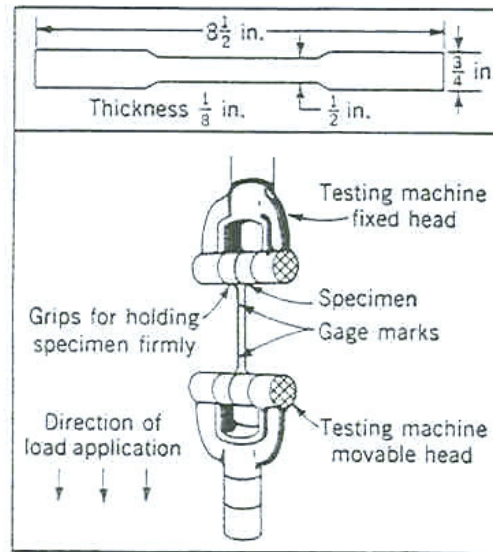


**Figure 2.19** Tensile test machine and dog bone shaped specimen [68].

During the test, a specimen is deformed under gradually increasing tensile load applied uniaxially along the long axis of a specimen at a previously determined strain rate. The applied strain is determined according to the response of the material to the load and usually selected between the ranges of 1-100 %/min. As the strain rate increases (up to  $10^6$  %/min), tensile properties such as tensile strength and modulus usually increase significantly while elongation at break decreases [68]. Moreover, the temperature and other environmental factors can affect mechanical behavior, thus polymers can represent the features of a glassy brittle solid, elastic rubber or a viscous liquid depending on the temperature and time scale of measurements [29].

In tensile test, stress is plotted against strain, in order to calculate the required tensile properties. *Stress* (nominal) is the condition of a material due to applied load and determined by dividing the load at any time by the original cross sectional area.

$$\sigma = F / A_0 \quad [2.1]$$

where the stress is  $\sigma$  (MPa), applied force measured at the fixed end as a function of elongation is  $F$  (N) and the original cross sectional area is  $A_0$  ( $\text{mm}^2$ ) [67].

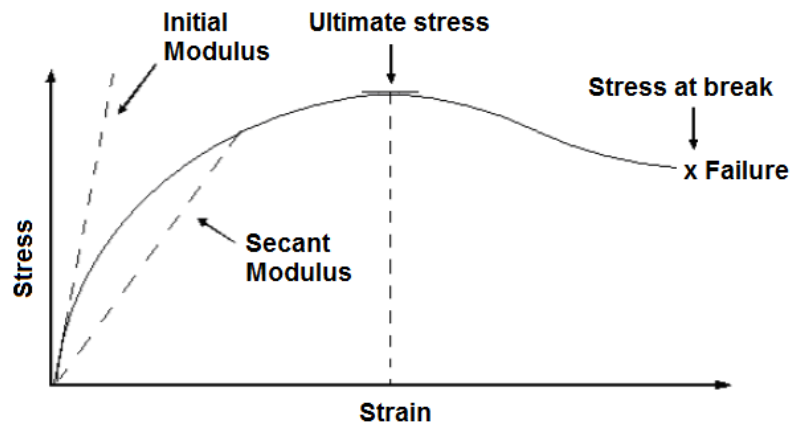


**Figure 2.20** Idealized stress-strain curve for a polymer that undergoes ductile failure [69].

*Strength* is the load carrying capacity of a material and the numerical value is determined at the specific load. While stress during a tensile test varies from zero to maximum with infinite number of stresses, test gives only three values of strength: yield, ultimate, and fracture [67].

*Elastic strain* ( $\epsilon$ ) is the unit of elongation when the change in length ( $\Delta L$ ) is divided by the length of the central section of the specimen namely the initial gauge length ( $L_0$ ).

$$\epsilon = \Delta L / L_0 \quad [2.2]$$

$$\sigma = E \epsilon \quad [2.3]$$

Young's Modulus or modulus of elasticity ( $E$ ) is the ratio of stress to corresponding strain during elastic deformation or briefly the material's resistance to deformation [29]. Elastic deformation occurs in the elastic strain region of the stress strain curve and it is the recoverable strain in which stressed chains are capable of returning their original state without any permanent deformation upon removal of the load [68]. Young's Modulus is calculated via the straight line of the stress-strain curve and also known as the proportionality constant in Hooke's Law which relates stress to strain

for uniaxial deformation of the ideal elastic isotropic solid as represented in equation 2.3 [29, 67]. The unit of the Young's Modulus is expressed in MPa, and materials which have high Young's Modulus values, represent hard and rigid behavior.

Finally, tensile test also gives information regarding to the stress-strain behavior of the material and typical behaviors of polymers under load are shown in Figure 2.21.

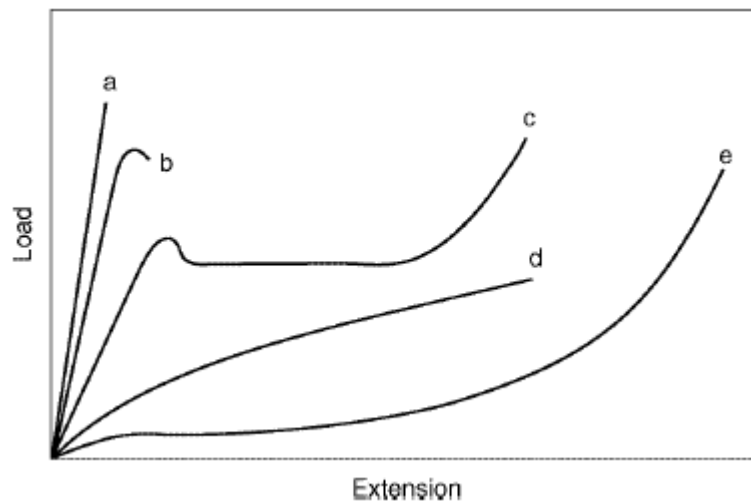


**Figure 2.21** Stress–strain curves at various temperatures (increasing from a to e): (a) low extensibility followed by brittle fracture at the lowest temperature; (b) localized yielding followed by fracture; (c) necking and cold drawing; (d) homogeneous deformation with indistinct yield; (e) rubber-like behavior [29].

### 2.8.1.2 Impact Test

Impact resistance is the capacity of a material or specimen to resist a sudden load without failure. It is a complex function of intrinsic factors such as mechanical properties of the material but also dependent on extrinsic factors such as geometry, mode of loading, environment [29].

There are two types of impact test instruments: pendulum type instruments and falling-weight impact instruments. Specimens can be unnotched or notched, and

have different sizes. An arm which rotates about a pivot point is attached to the end of the machine. When the arm is released it swings and strikes the specimen. There are two types of pendulum type machines that are designed according to the specimen support: Izod and Charpy impact tests, which are also standardized according to ISO and ASTM designations.

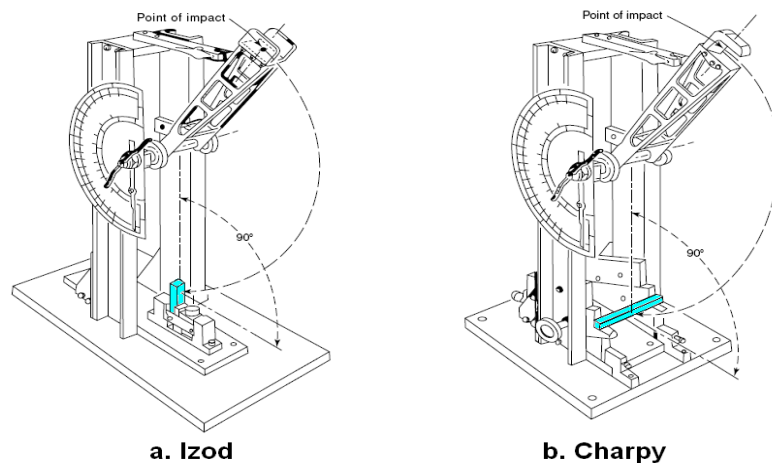


**Figure 2.22** Charpy and Izod impact tests [29].

In Izod test, a notched bar specimen which acts as a stress concentrator and promotes the brittle failure is supported as a cantilever. Unnotched Izod impact strength can be obtained by reversing the specimen in the vice. Charpy impact test is applied to an unnotched or oppositely notched specimen, which is supported at its ends.

Toughness and impact resistance are correlated with each other. Impact resistance measures the response of the specimen to a high and sudden load while fracture toughness is determined at low strain rate testing conditions. Toughness can be calculated from the area under the curve of the stress-strain diagram and can be improved by the incorporation of a soft, elastomeric phase into the rigid polymer matrix. Enhancements of the toughness improve impact strength [29].

## 2.8.2 Thermal Analysis

Heating a polymeric material sample provides observation of the physical property changes associated with the changes in the degree of packing and chain-chain interactions. Thermal analyses are applied to measure and monitor the thermal properties of a sample as a function of temperature or time at constant temperature. [29]. Various techniques are being applied in thermal analysis of polymeric materials such as differential scanning calorimetry (DSC), differential thermal analysis (DTA), thermogravimetry (TG), thermomechanical analysis (TMA), dynamic mechanical analysis (DMA), and in this study DSC analysis was conducted for determination of thermal properties of the nanocomposites.

### 2.8.2.1 Differential Scanning Calorimetry (DSC)

In DSC analysis, the power requirement (heat energy per unit time) of a small weighed sample of polymer (e.g. 10 mg) in a sealed aluminum pan referenced to an empty pan is measured by maintaining a zero temperature differential between two pans during previously programmed heating and cooling temperature scans (See Figure 2.23) [70]. When the polymer undergoes a thermal transition, the power which is given to the two heaters is adjusted to keep constant their temperatures and a signal proportional to the power variation is plotted on the axis of the recorder [71].

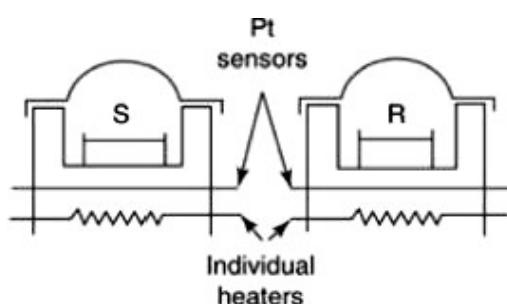


**Figure 2.23** Differential scanning calorimeter [29].

DSC techniques are often applied for determination of glass transition temperature ( $T_g$ ), melting temperature ( $T_m$ ), crystallization temperature ( $T_c$ ) and heat of fusion of

polymers ( $\Delta H_f$ ). DSC analysis also used in kinetics of chemical reactions such as oxidation and decomposition studies. In addition to these, measured heat of fusion (area under the curve) can be converted to % crystallinity when the heat of fusion for the 100% crystalline polymer is known [70]. In Figure 2.24 schematic representation of typical DSC curves is given.

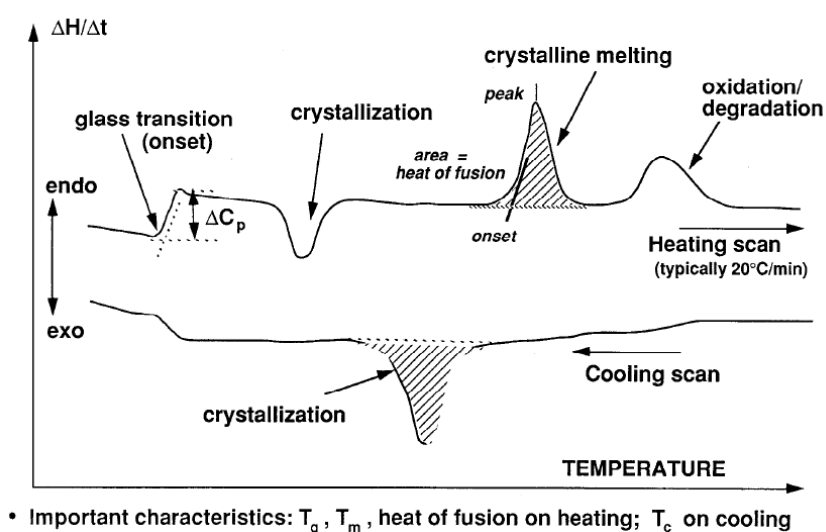


**Figure 2.24** Typical DSC curves [70].

$T_g$  and  $T_m$  appear on the endothermic side of the DSC diagram whereas  $T_c$  resides on the exothermic plane since heat is required upon glass transition and melting while heat is evolved during formation of crystals. In glass transition point ( $T_g$ ), the temperature of the polymer sample is reduced relative to the reference and thus heat capacity is increased. Relatively large amounts of heats are required to melt the crystals in the polymer at constant temperature, therefore compared to the smooth dip of  $T_g$ , a sharper dip is observed at  $T_m$  [19].

In DSC instruments, response of the system depends on the resistance between the holders and surroundings. Therefore, the thermal mass of the sample and reference holders are kept minimum, thermal resistances are reduced as much as possible and

a high loop gain from the differential power control circuit is used to ensure that the response of the system is short [72].

### **2.8.3 Morphological Analysis**

Polymer morphology is related with seeking the information contained in the physical form of the prepared specimen and hence interpreting the physical processes involved in the creation of the material [29]. Numerous changes associated with the morphological and chemical composition may occur in the surface region of the polymer and these differences can significantly influence the properties of the material. Therefore, a complete morphological characterization of the surface and interfacial regions of the polymer is required to analyze and enhance the surface, interfacial or thin-film properties of the polymers [73].

#### **2.8.3.1 X-Ray Diffraction (XRD) Analysis**

XRD has been used for a long time as a very important experimental method to understand variety of issues regarding to crystal structure of solids such as lattice constants and geometry, identification of unknown materials, orientation of single crystals, defects etc. [74].

During XRD analysis, a collimated X-Ray beam with a wavelength typically in the range of 0.7 to 2 Å is impinged on a slowly rotating specimen and diffracted by the crystalline phases in the material.

Diffraction occurs according to the Bragg's law and at any given position a multiplicity of Bragg's reflections is excited with the crystalline sample and gathered data are recorded [74, 75].

$$n\lambda=2d \sin\theta \quad [2.4]$$

where,  $d$  is the distance between successive identical planes of atoms in the crystal,  $\lambda$  is the X-ray wavelength,  $\theta$  is the angle between the X-ray beam and the atomic planes, and  $n$  represents the order of diffraction [76].

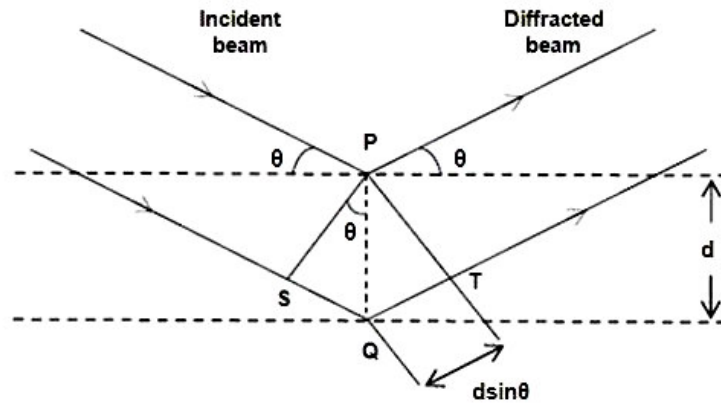


**Figure 2.25** Diffraction of X-Rays [77].

Recorder gives a signal proportional to the X-ray intensity. The signal is amplified and displayed on a meter and a continuous trace of intensity versus  $2\theta$  is provided [75]. The collected diffraction pattern is used to measure the structural properties of the specimen and identify its crystalline phases [74].

Peak positions on the recorded plots may give valuable information about d-spacings and nanocomposite type. An increased d spacing can be determined by a left shifted peak position corresponding to a lower  $2\theta$  value in Bragg's law. While a decreased  $2\theta$  value and new basal spacing may be a representation of an intercalated structure due to layer expansion, usually disappearance of the peaks in a polymer layered nanocomposite designated to extensive delamination and exfoliation.

Depending on the scale of the studied features, two types of X ray scattering are available: wide angle X-Ray scattering (diffraction) (WAXS) and small angle X ray scattering (SAXS). While WAXS analysis is used for detection of changes in crystallinity and orientation of the atoms, in SAXS method fibrillar and lamellar structures and cavities are investigated [68].

### **2.8.3.2 Scanning Electron Microscopy (SEM)**

SEM is primarily used for examining the surface, near surface morphology and structure of the bulk specimens. Fracture surfaces, crack initiation and propagation,

microdomains of blends and nanodispersion of fillers can be detected by this technique. The magnification of the SEM images is in between the optical microscope and transmission electron microscope (TEM). More specifically, 10 to more than 50000 times magnification is possible in SEM images.

In an SEM instrument, an electron source (gun) accelerates the electrons to a higher energy level and after proper magnifications is done, detected low energy secondary electrons and other radiation reflected from specimen surface are recorded. Meanwhile, the spot of a cathode ray tube (CRT) is scanned across the screen and brightness is modulated. Finally, electron beam and CRT spot are both scanned and resultant three dimensional images are obtained [78]. Schematic diagram of SEM is shown in Figure 2.26.

Electron microscopy techniques usually requires specimen coating with a conducting media such as silver, gold and platinum to avoid the loss of resolution as a consequence of the build up of trapped charge [29]. Contrast in the 3-D specimen images can be achieved by using *solvent etching* when there is a large solubility difference in a particular solvent of the polymers being studied or staining can be applied regarding to unsaturation in the polymers under investigation.

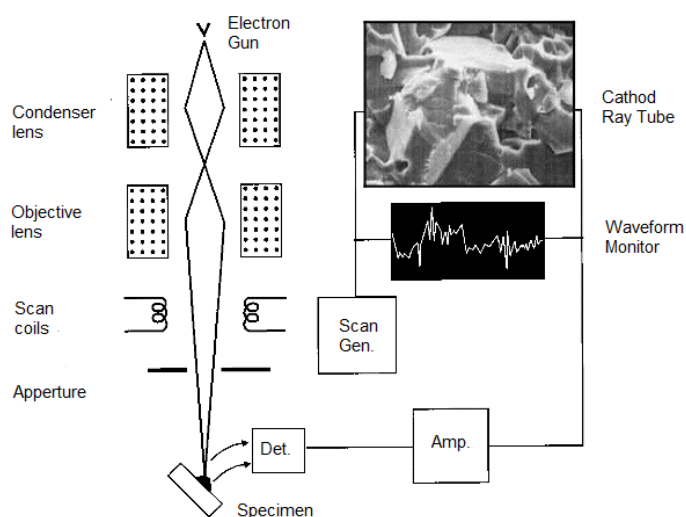


**Figure 2.26** Schematic diagram representing the main components of a scanning electron microscope [78].

SEM can also be used to study liquids or temperature sensitive polymers on a Cryostage. Moreover, qualitative elemental analysis by Energy Dispersive X-ray Spectroscopy (EDS) is also possible during SEM analysis. Identification of inorganic fillers and their dispersion in compounds as well as inorganic impurities on surfaces can be detected via this method [70].

### **2.8.3.3 Transmission Electron Microscopy (TEM)**

Transmission electron microscope (TEM) is similar to the SEM, since they both employ a beam of electrons directed at specimen. While many certain features such as electron gun, condenser lenses and vacuum system are similar in both instruments, methods in which the images are produced and magnified are completely distinct. As previously mentioned, SEM is used to study the surface morphology, whereas TEM provides information about the internal structure of thin specimens in much higher magnifications.

In TEM analysis the illumination is provided by an electron microscope and all lenses are electromagnetic. The first image produced by the objective lens has usually a magnification of 50 to 100 times and the image is further magnified by a series of intermediate and projector lenses such that a magnification of up to one million is easily achieved. Images are viewed through a lead glass window and digital data are recorded [78].

The specimen prepared for TEM analysis is required to be thinned to dimensions (typically 100 nm) which allow the passage of electron beam through the material. The provided electron diffraction data can be used to calculate the molecular spacing of the crystalline phases in the polymer. This type of information is quite complimentary to that obtained in X-Ray diffraction analysis in which the gathering a precise definition of the chain-packing dimensions and orientation is not possible [29].

### **2.8.4 Flow Characteristics**

Rheology of filled polymers is basically associated with the description of deformation under applied stress. The response to deformation of the softened or molten filled polymers varies in extent between viscous liquids and elastic solids [79]. Therefore, in order to understand the flow characteristics of the polymers which are under high

shear medium during extrusion, the rheological analysis are quite important. In this study, Melt Flow Index (MFI) analysis was conducted for evaluation of flow properties.

#### 2.8.4.1 Melt Flow Index

MFI is basically the measured weight of a polymer (g) which is extruded in 10 minutes through a capillary of specific diameter and length with an applied pressure through a dead weight under specified temperature [79].

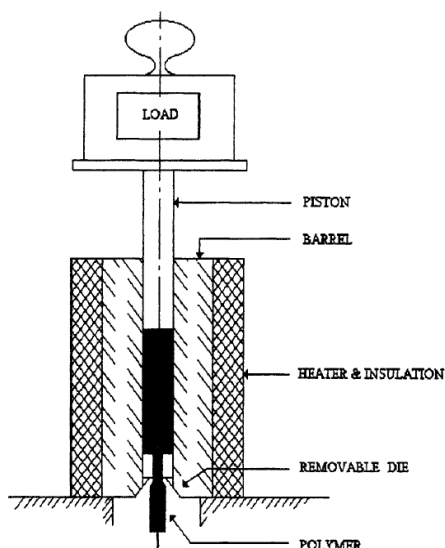


**Figure 2.27** Melt flow index measurement [79].

In Figure 2.27 schematic drawing of an MFI analysis is shown. During characterization, the temperature of the MFI instrument is set to a value which allows polymer to flow. After replacing the die to the cylinder and feeding the polymer, an appropriate dead weight is fixed onto the piston. Then, the material is allowed to flow at specified time intervals. Finally, the collected samples are weighed and their average value is reported in gram per ten minutes.

MFI tests are applied in temperature range of 125 to 300°C with respect to the type of the polymer and, the applied dead load weights may change from 0.325 to 21.6 kg providing pressures of 0.46 to 30.4 kgf /cm<sup>2</sup> [79].

## 2.9 Previous Studies

Deshmane et al. [80] investigated the reinforcement and impact toughness behaviors of nanocomposites with polypropylene and polyethylene matrices at similar clay loadings. Under identical processing conditions, 4 wt% clay loading resulted in improvement of impact strength of polypropylene based nanocomposites, while polyethylene based nanocomposites experienced the opposite. Tensile properties such as Young's Modulus and yield strength were improved for both matrices. However, improvement was more significant for polypropylene. These adverse observations were attributed to the strong interactions between PP and clay which were absent between PE and clay causing significant changes in both physical and structural characteristics such as crystallization and glass transition temperature, increased intergallery spacing and decreased spherulite size.

Zhang et al. [81] prepared polypropylene- montmorillonite nanocomposites with PP-MAH compatibilizer in a twin screw extruder. XRD and TEM analysis revealed that, silicate layers were dispersed in the matrix at nanometer level. Tensile properties were not improved significantly compared to conventionally filled polypropylene nanocomposites. However, the impact properties were greatly improved at low MMT content.

Gianelli et al. [82] studied the effects of resin type on the properties of organoclay filled nanocomposites prepared in a twin screw extruder. Polypropylene homopolymers and heterophasic copolymers of ethylene and propylene having different MFI values were used in nanocomposite preparation, in the presence of PP-MAH compatibilizer. Significant increase in tensile properties was obtained for both matrices. However, the improvements were much remarkable for the homopolymer polypropylene matrix. In addition to that, the delamination of organoclays was favored at high MFI for both homopolymers and heterophasic copolymers in accordance with the dominating thermal diffusion control.

Thon-That et al. [83] prepared nanocomposites with three different types of organoclay, two grades of PP-MAH and two different processing methods in a twin screw extruder. Analysis revealed that the presence of coupling agent increases the degree of the clay intercalation. Tensile and impact properties were significantly improved and enhancements were more pronounced for the nanocomposites prepared with organoclay having high thermal stability and PP-MAH coupling agent with high molecular weight and low grafting content. Mixing procedures did not alter the results significantly.

Kim et al. [16] reported the structure-property relationship of melt blended nanocomposites composed of thermoplastic polyolefin, organoclay and PP-MAH by mainly focusing on the effect of PP-MAH to organoclay ratio. Tensile properties such as Young's Modulus and yield strength values were enhanced by increasing the PP-MAH to clay ratio. Moreover, quantitative analysis pointed that the aspect ratio of dispersed clay particles were decreased as clay content increased and increased as the amount of PP-MAH was increased. Rheological properties revealed that percolation networks caused by physical interaction of clay particles were enhanced by increasing the amount of clay stacks, at fixed ratio of PP-MAH and by increasing the degree of exfoliation at fixed clay content.

Lertwimolnun et al. [84] investigated the effects of compatibilizer and processing conditions on nanoclay dispersion. Nanocomposites were prepared in a twin screw extruder with PP-MAH compatibilizer. Results indicated that, degree of dispersion was improved by incorporating PP-MAH, and clay aggregates became smaller as the ratio of PP-MAH was increased. Moreover, exfoliation was enhanced by increasing shear stress and mixing time, and decreasing mixing temperature. Rheological measurements also revealed that improvement of yield stress value was directly related with degree of exfoliation.

Modesti et al. [43] investigated the effects of processing conditions on mechanical properties of polypropylene based nanocomposites prepared with PP-MAH compatibilizer and organoclay. The role of the compatibilizer was also studied. Results revealed that, barrel temperature was a very important parameter owing to increased shear applied on polymer, as a consequence of low melt viscosity. Tensile properties were increased due to organoclay and compatibilizer addition, and the most remarkable improvements were obtained at low processing temperature and

high screw speed for all compositions. In addition to that, even in the case of optimized processing conditions, the exfoliation of clay platelets was achieved only when PP-MAH compatibilizer was present.

In a subsequent paper, Modesti et al. [85] investigated effects of processing conditions on the thermal properties of melt blended nanocomposites prepared under similar conditions. Results indicated that all properties were strongly influenced by the composition of the nanocomposites, and the effects of processing conditions were remarkable only on the dynamic mechanical properties. It was observed that crystallinity, thermal stability and fire behavior of nanocomposites were greatly improved in the presence of MMT and PP-MAH, independent from the processing conditions.

Deenadayalan et al. [86] conducted studies with nanocomposites of polypropylene impact copolymer, MMT, PP-MAH and maleic anhydride grafted polyethylene (PE-MAH) compatibilizers, and mechanical properties of the nanocomposites were investigated with respect to the effect of compatibilizer. In the presence of PP-MAH, clay particles were dispersed in the matrix phase and resulted in enhancements in modulus and strength, but decreasing ductility at low strain rates. On the other hand, PE-MAH formed an immiscible phase in the matrix, encapsulated the clay platelets and increased the low strain ductility, while suppressing a considerable increase in modulus and strength.

Lim et al. [87] investigated the effects of elastomer polarity on the mechanical and structural properties of rubber toughened polypropylene nanocomposites. Polyethylene octane rubber as a nonpolar elastomer and polyethylene octane grafted maleic anhydride as a polar elastomer were incorporated into the matrix with increasing elastomer content, in the presence of montmorillonite organoclay and PP-MAH compatibilizer. Decrease in tensile properties was observed with incorporation of elastomeric phases, whereas impact strength increased particularly in the presence of the polar elastomer. In addition to it, a more uniform distribution of the particles was observed in presence of the polar elastomer.

Zhu et al. [88] studied the effects of clay chemical modifiers, mixing protocols and screw configurations on clay dispersion. Considering the MFI results, generally two step mixing process, where a previously prepared masterbatch of clay and PP-MAH

was used, represented better exfoliation compared to one step mixing process of simultaneous addition of all components. Residence time was determined as the critical factor in preparation of nanocomposites, and it was observed that long residence times combined with high shear may break the exfoliated structures and stacks of the nanoclay.

## CHAPTER 3

### EXPERIMENTAL

#### 3.1 Materials

##### 3.1.1 Polymer Matrix

In this study, a recycled grade polypropylene was used. Polymer matrix also contained polyethylene phase dispersed in the continuous polypropylene matrix as a consequence of recycling. Recycled polypropylene was purchased from Plastiform Company, Bursa, Turkey which was supplied at 25 kg polyethylene bags. Trade name of the polypropylene was CHIRALENE PPRIG219. For the sake of simplicity CHIRALENE PPRIG219 is abbreviated as P in the report. Material properties are shown in Table 3.1.

**Table 3.1** Properties of the polymer matrix.

Characteristics	Unit	Value	Test Method
<b>Physical Properties</b>			
Density	g/cm <sup>3</sup>	0.89-0.92	ISO 1183
Melt Flow Index	g/10 min	3.9	ISO 1133
Rockwell Hardness	-	80	ISO 2039-2
<b>Mechanical Properties</b>			
Young's Modulus (at 23°C)	MPa (N/mm <sup>2</sup> )	879.7	ISO 527 (15 mm/min)
Max. Load (at 23°C)	MPa (N/mm <sup>2</sup> )	34.8	ISO 527 (15 mm/min)
Elongation (at 23°C)	%	524.4	ISO 527 (15 mm/min)
Notched Charpy Impact Strength (at 23°C)	kJ/m <sup>2</sup>	8.8	ISO179

**Table 3.1** Properties of polymer matrix (Cont'd)

<b>Characteristics</b>	<b>Unit</b>	<b>Value</b>	<b>Test Method</b>
<b>Thermal Properties</b>			
Distortion temperature under load (load=1.8 MPa)	°C	50	ISO 75
Vicat softening temperature	°C	70	ISO 360
Thermal oxidation (Exposure to direct sunlight)	h	>150	ISO 4577
Thermal oxidation (Exposure to indirect sunlight or other heat sources)	h	>100	ISO 4577

### 3.1.2 Organoclays

In this study three types of layered silicates were used; Cloisite® 15A, Cloisite® 25A, and Cloisite® 30B. They were purchased from Southern Clay Products, Texas, USA and they were used as reinforcing agents. They are natural off-white montmorillonites produced by a cation exchange reaction with different organic modifiers. The tallow (long alkyl chain) structures in the organoclay compositions constitute of primarily 18 carbon chains (~%65) and the rest of the components are chains with 16 carbons (~30 %) and 14 carbons (~5 %).

#### 3.1.2.1 Cloisite® 15A

Cloisite® 15A is a natural montmorillonite modified by a dimethyl, dihydrogenated tallow, and quaternary ammonium cation with chloride anion. The Chemical structure of the modifier is shown in Figure 3.1 and the properties of Cloisite® 15A in Table 3.2.

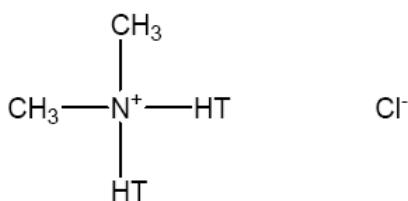


**Figure 3.1** Chemical structure of organic modifier and anion (Cl-) of Cloisite® 15A.

**Table 3.2** Properties of Cloisite® 15A [89].

Properties	Unit	Value
Ion Exchange Capacity	meq/100g clay	125
d-spacing ( $d_{001}$ )	Å	31.5
Moisture Content	%	<2
Weight Loss on Ignition	%	43
<b>Density</b>		
Loose Bulk Density	lbs/ft <sup>3</sup>	10.79
Packed Bulk Density	lbs/ft <sup>3</sup>	18.64
Specific Gravity	g/cc	1.66
<b>Typical Dry Particle Sizes</b>		
10%	μ, by volume	<2
50%	μ, by volume	<6
90%	μ, by volume	<13

### 3.1.2.2 Cloisite® 25A

The organic modifier of Cloisite® 25A is a dimethyl, hydrogenated tallow, 2-ethylhexyl quaternary ammonium cation with methyl sulfate anion. The chemical structure of the modifier and the properties of Cloisite® 25A are shown in Figure 3.2 and Table 3.3, respectively.

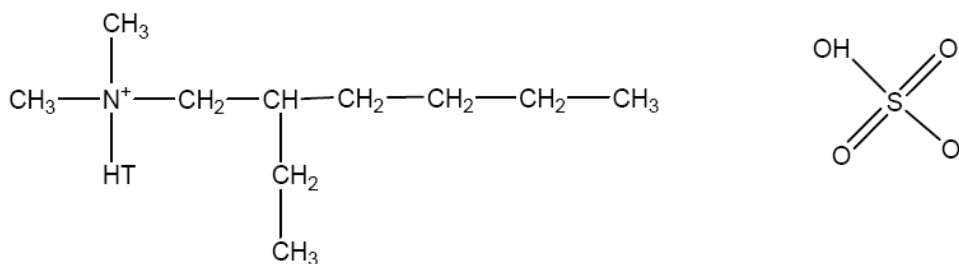


**Figure 3.2** Chemical structure of organic modifier and anion of Cloisite® 25A.

**Table 3.3** Properties of Cloisite® 25A [89].

Properties	Unit	Value
Ion Exchange Capacity	meq/100g clay	95
d-spacing ( $d_{001}$ )	Å	18.6
Moisture Content	%	<2
Weight Loss on Ignition	%	34
<b>Density</b>		
Loose Bulk Density	lbs/ft <sup>3</sup>	12.08
Packed Bulk Density	lbs/ft <sup>3</sup>	20.48
Specific Gravity	g/cc	1.87
<b>Typical Dry Particle Sizes</b>		
10%	μ, by volume	<2
50%	μ, by volume	<6
90%	μ, by volume	<13

### 3.1.2.3 Cloisite® 30B

Modification of Cloisite® 30B is implemented by a methyl, tallow, bis-2-hydroxyethyl quaternary ammonium cation and chloride anion. Chemical structure of the modifier is shown in Figure 3.3 and properties of Cloisite® 30B are given in Table 3.4.

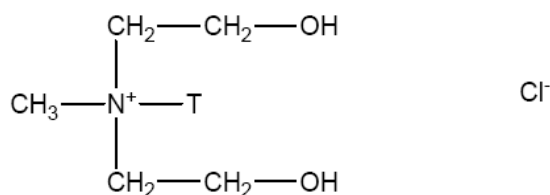


**Figure 3.3** Chemical structure of organic modifier and anion (Cl<sup>-</sup>) of Cloisite® 30B.

**Table 3.4** Properties of Cloisite® 30B [89].

Properties	Unit	Value
Ion Exchange Capacity	meq/100g clay	90
d-spacing (d <sub>001</sub> )	Å	18.5
Moisture Content	%	<2
Weight Loss on Ignition	%	30
<b>Density</b>		
Loose Bulk Density	lbs/ft <sup>3</sup>	14.25
Packed Bulk Density	lbs/ft <sup>3</sup>	22.71
Specific Gravity	g/cc	1.98
<b>Typical Dry Particle Sizes</b>		
10%	μ, by volume	<2
50%	μ, by volume	<6
90%	μ, by volume	<13

#### 3.1.2.4 Organoclay Hydrophobicity

Owing to the nature of the organic modifiers, organoclays have different hydrophobicities. According to information supplied by the production company, Cloisite® 15A has the highest hydrophobicity, while Cloisite® 30B has the lowest and Cloisite® 25A is in the middle of two.

### 3.1.3 Compatibilizers

In this study, Lotader® AX8900, a terpolymer of ethylene, methyl acrylate and glycidyl methacrylate (E-MA-GMA) and Bondyram® 1001, a Maleic Anhydride Modified Polypropylene (PP-MAH) were used as compatibilizing agents.

Lotader® AX8900 was purchased from Arkema Inc., France and the acrylic ester in the structure provides softness and polarity while maintaining high thermal stability. Moreover, GMA functionality is capable of giving reactivity with the hydroxyl (OH), carboxyl (COOH) and amine (NH<sub>2</sub>) groups whereas ethylene groups in the structure bring in flexibility [90]. Chemical structure and properties of the material are shown in Figure 3.4 and Table 3.5 respectively.

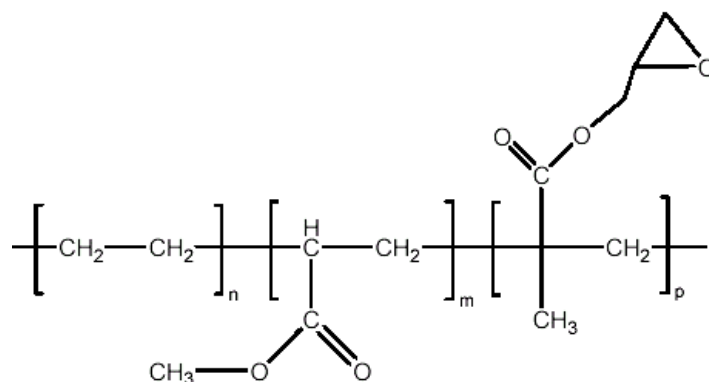


**Figure 3.4** Chemical structure of Lotader® AX8900.

**Table 3.5** General characteristics of Lotader® AX8900 (E-MA-GMA) [90].

Properties	Unit	Value	Test Method
Melt Index (190°C, 2.16Kg)	g/10 min	6	ISO 1133
Methyl Acrylate content	%	24	FTIR
Glycidyl Methacrylate content	%	8	FTIR
Melting temperature	°C/ °F	60/ 140	DSC (ISO 306)
Vicat Temperature	°C/ °F	<40/ 104	DSC (ISO 306)
Hardness Shore A / Shore D	-	64/ 18	ISO 868
Young Modulus	MPa/ Psi	8/ 1160	ISO R527
Tensile Strength	MPa/ Psi	4/ 580	ISO R527
Elongation at break	%	1100	ISO R527
Density	g/cm <sup>3</sup>	0.95	ISO R1183

Bondyram® 1001 was purchased from EMAŞ Plastik, Bursa, Turkey. Maleic anhydride group in the structure can react with the hydroxyl and amine groups and polar character of the anhydride causes an affinity for the silicate surface. Chemical structure of Bondyram® 1001 is shown in Figure 3.5 and material properties are given in Table 3.6.

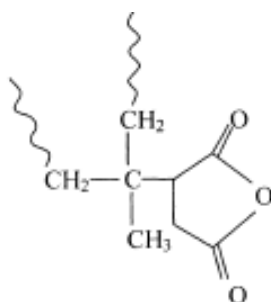


**Figure 3.5** Chemical structure of maleic anhydride grafted polypropylene.

**Table 3.6** General characteristics of Bondyram® 1001 [91].

<b>Properties</b>	<b>Unit</b>	<b>Value</b>	<b>Test Method</b>
Melt Index (190°C, 2.16Kg)	g/10 min	100	ASTM D-1238
Maleic Anhydride content	%	1	FTIR
Young's Modulus	MPa	991	ISO 527
Tensile Strength	MPa	32	ISO 527
Elongation at Break	%	506	ISO 527
Density	g/cm <sup>3</sup>	0.90	ASTM D-792
Melting temperature	°C	160	DSC

## **3.2 Equipment and Processing**

### **3.2.1 Melt Compounding**

Melt compounding was conducted with a Thermoprism TSE 16 TC fully intermeshing and co-rotating twin screw extruder having an L/D ratio of 24 with diameter of 16 mm and screw length of 384 mm. Extruder has maximum 12 Nm torque capability and 500 rpm maximum screw speed.

Barrel temperatures were set to the desired processing temperatures by using temperature controllers on the control panel and allowed to stabilize prior to experiments. A picture of the twin screw extruder is shown in Figure 3.6 and properties are summarized in Table 3.7.

During melt compounding, materials were fed from the main and side feeders according to their addition orders. Materials were melt and mixed inside the extruder and the molten product was purged from the die and passed through the water bath for cooling. Wet product was subjected to air through an air knife attached to the end of the water bath in order to remove the excess water. Then, the product was pelletized and packed in plastic bags for subsequent processes.



**Figure 3.6** Thermo Prism TSE 16 TC twin-screw extruder.

**Table 3.7** Properties of twin screw extruder.

Property	Definition	
Model	Thermo Prism 16 TC	
Type	Twin screw	
Screw type	Co-rotating	
Property	Unit	Value
Twin Bore Diameter	mm	16
Screw Diameter	mm	15.6
Barrel length	mm	284 (24 D)
Die length	mm	16 (1 D)
Maximum screw speed	rpm	500
Maximum Torque	Nm	12

### 3.2.1.1 Drying

In order to prevent hydrolytic degradation caused by moisture all the materials except recycled polypropylene were dried under vacuum at proper temperatures before feeding to extruder. Drying temperatures are shown in Table 3.8.

**Table 3.8** Drying conditions.

<b>Materials</b>	<b>Drying Temperature (°C)</b>	<b>Duration (h)</b>
<b>Before 1<sup>st</sup> Extrusion</b>		
Organoclays	80	12-16
Compatibilizers	40	12-16
<b>Before 2<sup>nd</sup> Extrusion</b>		
P (extruded once)	100	4
P+ Compatibilizers	100	4
P+ Organoclay+ Lotader® AX8900	100	4
Organoclay+ PP-MAH (Masterbatch)	40	4
<b>Before Injection Molding</b>		
Products	100	12-16

### 3.2.1.2 Processing Parameters

In this study, the main processing parameters were feeding rate, barrel temperature profile and screw speed. The total feed rate was kept constant at 25 g/min during all experiments. Temperature profile and screw speeds were changed in order to optimize the processing conditions. Extruder parameters were kept at 200°C constant barrel temperature and 250 rpm screw speed in the earliest experiments. Then, in order to investigate the effect of low temperature profile and higher screw speed, 180°C barrel temperature and 350 rpm screw speed were also added as processing parameters. After performing experiments with different processing conditions for two compositions, it was concluded that low temperature profile and high screw speed provided improvements on nanocomposite properties. Finally, rest of the experiments was performed at 180°C constant barrel temperature and 350 rpm screw speed. Representation of processing parameters is given in Figure 3.7.

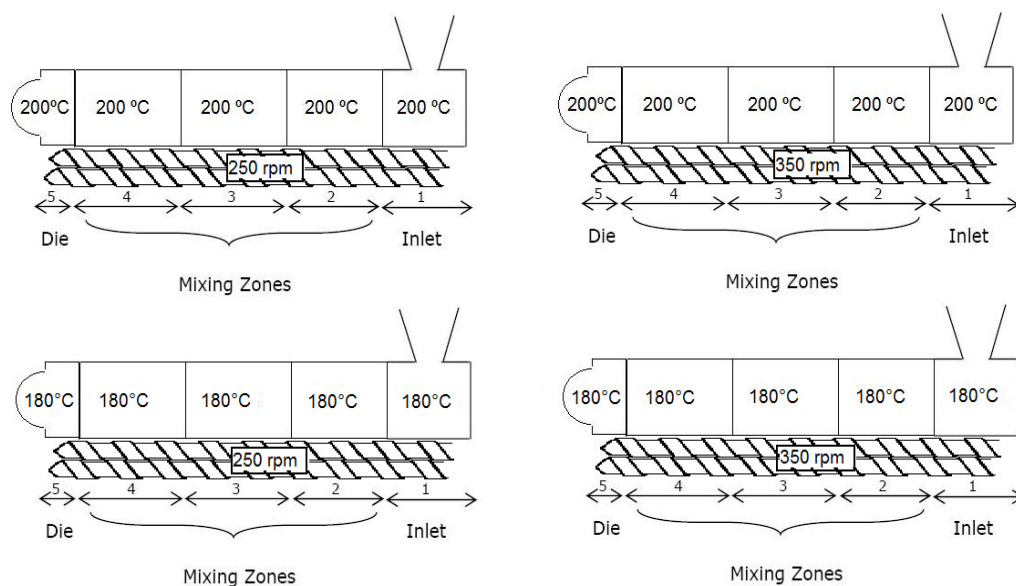


**Figure 3.7** Schematic diagram of processing parameters; barrel temperature and screw speed.

### 3.2.1.3 Addition Order

Two different addition orders were used in preparation of ternary nanocomposites: simultaneous feeding and masterbatch methods. Materials were dried under vacuum at proper temperatures and durations before the extrusion steps (as explained in section 3.2.1.1). In addition to preparing ternary nanocomposites, binary blends of polymer-compatible and binary polymer-organoclay nanocomposites were also prepared in order to investigate the effects of compatibilizer and organoclay when added as a third component. Moreover, pure matrix polymer was also extruded for once and twice, in order to compensate the mechanical and thermal histories added during extrusion, and thus make a better comparison while evaluating the improvements. Finally, processing parameters were set prior to experiments and kept constant during all steps of compounding. Flow chart for this two step melt compounding process is shown in Figure 3.8 and nanocomposite compositions prepared in this study are given in Table 3.9

### **3.2.1.3.a Simultaneous Feeding (All-S)**

This addition order was applied to nanocomposites that were prepared by using Lotader® AX8900 compatibilizer.

1<sup>st</sup> Extrusion: Dry blended pellets of recycled polypropylene and Lotader® AX8900 were fed to the extruder from the main feeder while the organoclay was fed from the second feeder. Simultaneous feeding of all components was achieved by this method.

2<sup>nd</sup> Extrusion: In this run, only the main feeder was utilized. After drying the composites obtained in the first extrusion, pellets were extruded for a second time in order to achieve a better dispersion.

### **3.2.1.3.b Masterbatch Method (MB)**

This method was used in preparation of ternary nanocomposites containing PP-MAH compatibilizer. The aim of applying this method was to achieve a previous reaction between the polymer and the compatibilizer and provide expansion in interlayer spacings of organoclay particulates for enhanced polymer intercalation. Moreover, considering the extruder conditions, one advantage of this method was providing flexibility for feeding organoclays at even very low concentrations (under 2 wt %).

1<sup>st</sup> Extrusion: Masterbatches of organoclay and PP-MAH compatibilizer at three different weight ratios of 1, 2, and 3 (compatibilizer to organoclay) were prepared by this method. PP-MAH pellets inside the main feeder and organoclays inside the second feeder were fed to the extruder simultaneously. Moreover, in order to investigate the effect of compatibilizer, this method was also applied to prepare a masterbatch containing 4 wt. % organoclay in the polymer matrix.

2<sup>nd</sup> Extrusion: Dried masterbatch pellets were dry blended with recycled polypropylene and fed to the extruder from the main feeder and nanocomposites with desired compositions were completed.

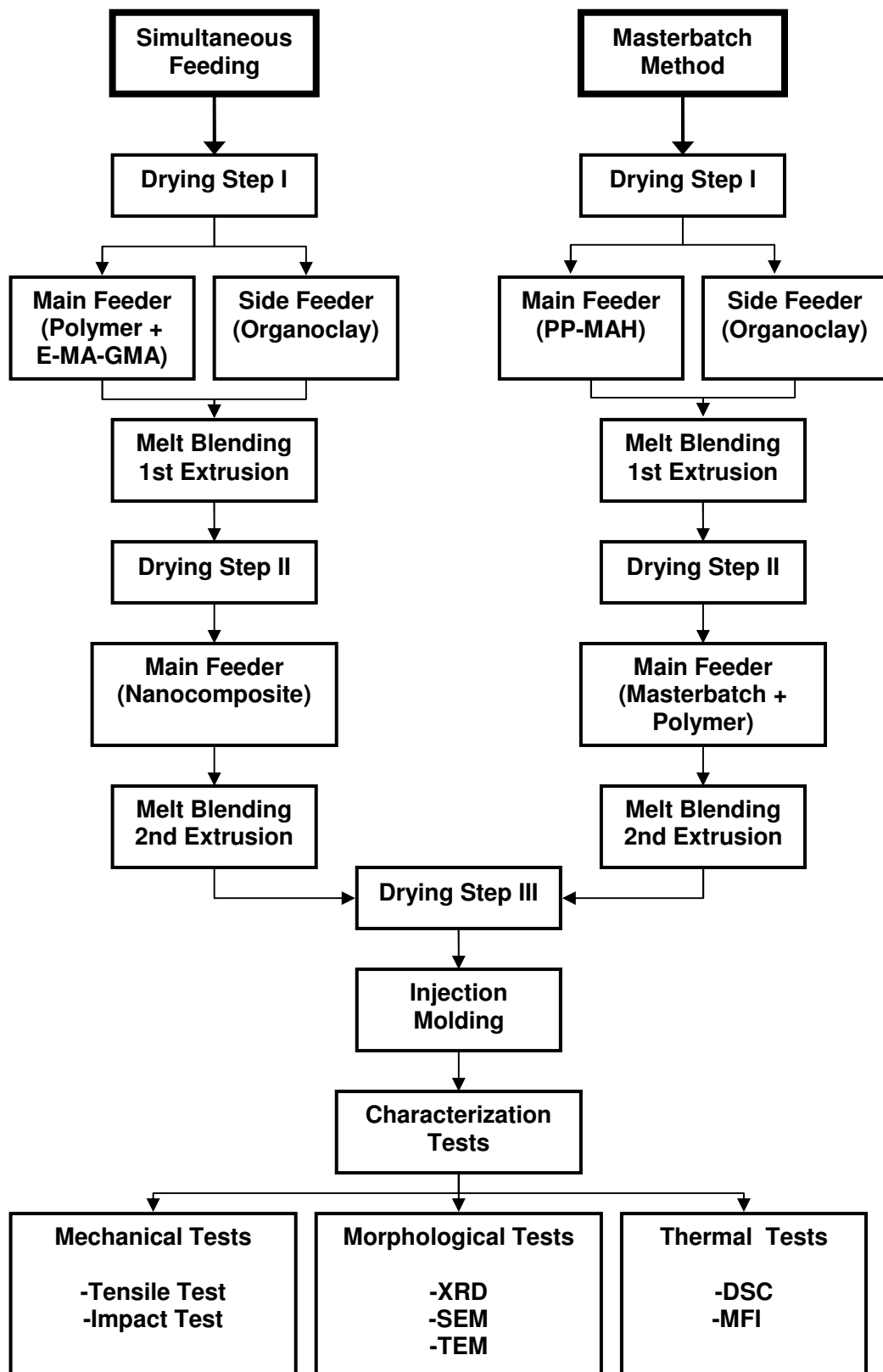


**Figure 3.8** Flow chart for nanocomposite production and characterization.

**Table 3.9** Compositions prepared in experiments.

Components	Addition Order	Processing Parameters	
		°C	rpm
P	-	-	-
<b>P- Compatibilizer Blends</b>			
P+ 5 wt% E-MA-GMA	All-S	200	250
P+ 10 wt% E-MA-GMA	All-S	200	250
P+ 0.5 wt% PP-MAH	All-S	180	350
P+ 1.0 wt% PP-MAH	All-S	180	350
P+ 1.5 wt% PP-MAH	All-S	180	350
P+ 2.0 wt% PP-MAH	All-S	180	350
P+ 3.0 wt% PP-MAH	All-S	180	350
P+ 4.0 wt% PP-MAH	All-S	180	350
P+ 6.0 wt% PP-MAH	All-S	180	350
<b>P- Clay Nanocomposites</b>			
P+ 2 wt% 15A	All-S	200	250
P+ 4 wt% 15A	All-S	200	250
P+ 6 wt% 15A	All-S	200	250
P+ 0.5 wt% 15A	MB	180	350
P+ 1.0 wt% 15A	MB	180	350
P+ 2.0 wt% 15A	MB	180	350
P+ 0.5 wt% 25A	MB	180	350
P+ 1.0 wt% 25A	MB	180	350
P+ 2.0 wt% 25A	MB	180	350
P+ 0.5 wt% 30B	MB	180	350
P+ 1.0 wt% 30B	MB	180	350
P+ 2.0 wt% 30B	MB	180	350
<b>Ternary Nanocomposites (Effect of Processing Conditions)</b>			
P+ 2 wt% 15A+ 5 wt% E-MA-GMA	All-S	200	350
P+ 2 wt% 15A+ 5 wt% E-MA-GMA	All-S	180	250
P+ 2 wt% 15A+ 5 wt% E-MA-GMA	All-S	180	350
P+ 1 wt% 15A+ 2 wt% PP-MAH	MB	200	250
P+ 1 wt% 15A+ 2 wt% PP-MAH	MB	200	350
P+ 1 wt% 15A+ 2 wt% PP-MAH	MB	180	250

**Table 3.9** Compositions prepared in experiments (Cont'd.)

Components	Addition Order	Processing Parameters	
		°C	rpm
<b>P- Compatibilizer-Clay Ternary Nanocomposites</b>			
P+ 2wt% 15A+ 5wt% E-MA-GMA	All-S	200	250
P+ 4wt% 15A+ 5wt% E-MA-GMA	All-S	200	250
P+ 6wt% 15A+ 5wt% E-MA-GMA	All-S	200	250
P+ 2wt% 15A+ 10wt% E-MA-GMA	All-S	200	250
P+ 4wt% 15A+ 10wt% E-MA-GMA	All-S	200	250
P+ 6wt% 15A+ 10wt% E-MA-GMA	All-S	200	250
P+ 0.5wt% 15A+ 0.5wt% PP-MAH	MB	180	350
P+ 1.0wt% 15A+ 1.0wt% PP-MAH	MB	180	350
P+ 2.0wt% 15A+ 2.0wt% PP-MAH	MB	180	350
P+ 0.5wt% 15A+ 1.0wt% PP-MAH	MB	180	350
P+ 1.0wt% 15A+ 2.0wt% PP-MAH	MB	180	350
P+ 2.0wt% 15A+ 4.0wt% PP-MAH	MB	180	350
P+ 0.5wt% 15A+ 1.5wt% PP-MAH	MB	180	350
P+ 1.0wt% 15A+ 3.0wt% PP-MAH	MB	180	350
P+ 2.0wt% 15A+ 6.0wt% PP-MAH	MB	180	350
P+ 0.5wt% 25A+ 1.0wt% PP-MAH	MB	180	350
P+ 1.0wt% 25A+ 2.0wt% PP-MAH	MB	180	350
P+ 2.0wt% 25A+ 4.0wt% PP-MAH	MB	180	350
P+ 0.5wt% 30B+ 1.0wt% PP-MAH	MB	180	350
P+ 1.0wt% 30B+ 2.0wt% PP-MAH	MB	180	350
P+ 2.0wt% 30B+ 4.0wt% PP-MAH	MB	180	350

### 3.2.2 Injection Molding

DSM Xplore laboratory scale of 10 cc micro injection molding equipment is used in preparation of samples, as shown in Figure 3.9. The barrel temperature was adjusted to 220 °C and the mold temperature was set to 30 °C for all experiments. Hold time was 3 minutes and 30 seconds including the feeding time of 10 seconds. Molding cycle of the injection machine had three distinct steps; each was performed at

different pressures and durations. Filling step was conducted at 10 bars for 5 seconds, and then pressure was amplified to 15 bars for 10 seconds during packing in order to offset shrinkage. Throughout the cooling step no pressure was applied and finally specimens were taken out of the mold at room temperature and further cooling and crystallization was allowed for 24 h before conducting characterization tests. Molding parameters are represented in Table 3.10.



**Figure 3.9** Injection molding equipment.

**Table 3.10** Injection molding parameters.

<b>Molding Parameters</b>	<b>Unit</b>	<b>Value</b>
Nozzle temperature	°C	220
Mold temperature	°C	30
Hold time	min	3.5
Injection pressure	bar	15

### **3.3 Characterization**

#### **3.3.1 Morphological Testing Procedure and Equipment**

##### **3.3.1.1 X-Ray Diffraction Analysis**

XRD analysis were conducted on Rigaku D/Max-2200/PC X-Ray diffractometer with monochromatic Cu K $\alpha$  radiation source ( $\lambda = 1.5418$ ) at 40 kV and 40 mA. Diffraction angle  $2\theta$  was scanned from  $1^\circ$  to  $8^\circ$  at a scan rate of  $1^\circ$  per minute with a step size of  $0.01^\circ$ . Peak positions were used to calculate the basal spacings of organoclay layers by using Bragg's Law. Dog bone shaped tensile bars were used in performing analysis.

##### **3.3.1.2 Scanning Electron Microscopy (SEM) Analysis**

The surface morphologies, failure mechanisms, and phase structures of the fractured specimens were examined by a JEOL JSM-6400 low voltage scanning electron microscope (see Figure 3.10). Specimens were coated with gold prior to experiments to avoid the loss of resolution as a consequence of the build up of trapped charge. Solvent etching was conducted for removing the polyethylene and compatibilizer phases. Fractured surfaces of the specimens were immersed in toluene at  $90^\circ\text{C}$  for 30 minutes to accomplish selective etching. Average domain sizes of discarded phase were calculated by Image J program.

##### **3.3.1.3 Transmission Electron Microscopy (TEM) Analysis**

Philips CM200 Transmission Electron Microscope (TEM) at an acceleration voltage of 120 kV in DSM Research, Holland was used to analyze the samples. This method was used to investigate the approximate basal spacing of the organoclay layers after applied processing. Specimens were prepared by cryogenically cutting of ultra thin sections of 70 nm in thickness with a diamond knife at  $-100^\circ\text{C}$  temperature (see Figure 3.10). All samples were trimmed in the molding direction.

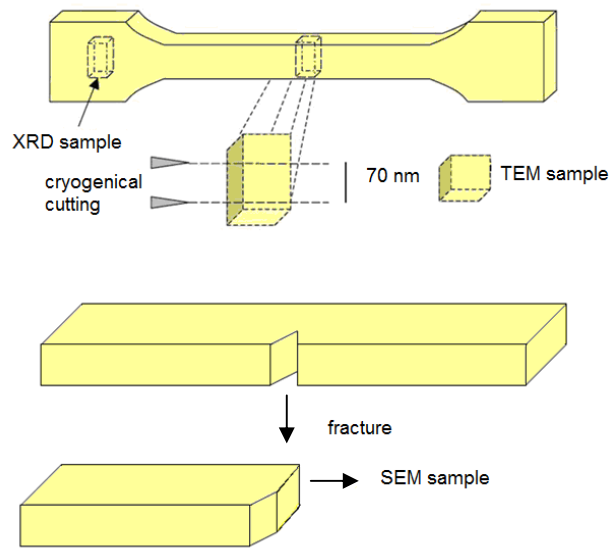


**Figure 3.10** Specimens used in morphological analysis.

### 3.3.2 Mechanical Properties

In this study, mechanical properties of the samples were analyzed by tensile and impact tests. Effects of composition and processing parameters on material performance could easily be detected by mechanical testing since the reinforcement, degree of organoclay dispersion and compatibility between the matrix material and the additives have direct correlations with mechanical properties. While stiffness and strength properties were examined with tensile test, impact tests provided information on impact toughness properties of the materials.

Specimens were prepared according to the standards of ISO 527-5A for tensile tests and ISO 179 for impact test. Samples were conditioned in desiccators for at least 24 hours prior to mechanical testing to allow specimens to complete their cooling and crystal formation. All tests were conducted at 23°C and at least five specimens were tested for each set of experiments. Mechanical test results were calculated by averaging the results and their standard deviations were also computed in order to evaluate the consistency between the test results.

### 3.3.2.1 Tensile Test

A Lloyd 30K universal testing machine was used to conduct tensile testing of molded specimens for all compositions. Tensile test was performed according to the ISO 527 [92] standards at  $23 \pm 2^\circ\text{C}$ . Tensile test specimens were ISO 527-2/5A type and dimensional properties of the samples are given in Figure 3.11 and Table 3.11. The crosshead speed was 15 mm/min and considering the gauge length of 30 mm, the applied strain rate was  $0.5 \text{ min}^{-1}$ . From the collected stress-strain data, Young's Modulus, tensile stress at yield, tensile strength and percent elongation at break values were calculated.

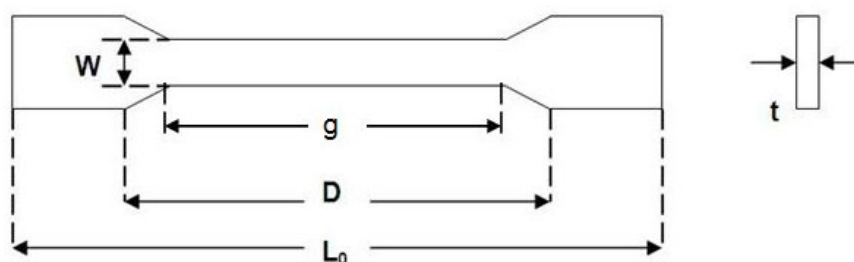


**Figure 3.11** Tensile test specimen.

**Table 3.11** Dimensions of the tensile test specimens.

Symbol	Definition	Value (mm)
$W$	Width of narrow section	4
$D$	Distance between grips	50
$L_0$	Overall length	75
$g$	Gauge Length	30
$t$	Thickness	$>2$

### 3.3.2.2 Impact Test

Charpy impact test was applied to one side notched specimens with a pendulum Ceast Resil Impactor according to the ISO 179 standards [93]. Tests were performed at room temperature and schematic representation of impact test specimen is given in Figure 3.12 and dimensions of the test specimen is given in Table 3.12.

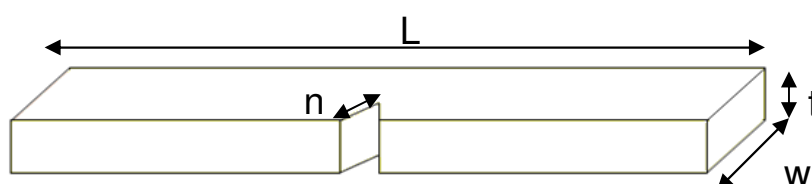


**Figure 3.12** Impact test specimen.

**Table 3.12** Dimensions of impact test specimens.

Symbol	Definition	Value (mm)
L	Total length	80
w	Unnotched width	10
n	Notch length (v type, 45°)	2
t	Thickness	4

### 3.3.3 Thermal Analysis

Differential scanning calorimetry (DSC) was used as thermal analysis in determination of melting and crystallinity behaviors of the nanocomposites.

#### 3.3.3.1 Differential Scanning Calorimetry (DSC) Analysis

Differential scanning calorimetry (DSC) measurements were carried out with DSC-60 Shimadzu differential scanning calorimeter in order to evaluate the deviations in

melting point ( $T_g$ ) and percent crystallinity value due to addition of reinforcing and elastomer phases.

Sample preparations for DSC analysis were implemented by cutting a piece of material from the middle section of the injection molded dog bone specimens. For each composition, about 3.3 mg material was placed in aluminum pans and heated from 30 °C to 250 °C at a rate of 5 °C/min under nitrogen atmosphere. From the gathered data, percent crystallinity values were calculated as the proportion of the heat of fusion ( $\Delta H_f$ ) values of the specimens divided by weight fraction of polymer ( $w$ ) in the nanocomposite and the heat of fusion of the pure crystalline form of the polymer ( $\Delta H_f^0$ ). Since there are two polymer phases available in the blend, two distinct crystallinity values were calculated, crystallinity of polyethylene and crystallinity of polypropylene. Heat of fusion values of 100% crystalline polypropylene was taken as 209 J/g and polyethylene as 293 J/g [94].

### **3.3.4 Flow Characteristics**

Melt flow index analysis (MFI) was used in determination of flow properties. Since the melt viscosity of the polymer is inversely proportional to MFI, examining MFI values of nanocomposites may provide information on changes in viscosity and thus shear intensity properties which are directly related with organoclay dispersion in melt compounding.

#### **3.3.4.1 Melt Flow Index**

Melt flow index (MFI) test was performed according to ISO 1133 [95] using an Omega Melt Flow Indexer. The measurements were carried out at 180 °C with an applied load of 2.16 kg. Melt flow index is the weight of polymer passing through the die in ten minutes. For each composition, at least five specimens were taken and their average values were reported.

## CHAPTER 4

### RESULTS AND DISCUSSION

#### 4.1 Morphological Analysis

##### 4.1.1 X-RAY Diffraction Analysis

In characterization of polymer layered nanocomposite structures, XRD is a very useful and a traditional technique. X-Ray Diffraction is widely employed in determination of interlayer spacing of intercalated nanocomposites regarding to repetitive multilayer structure and periodic arrangement of silicate layers [11, 13].

Degree of intercalation and exfoliation as well as the changes in interlayer spacing were determined by using Bragg's Law. Interlayer spacing of the organoclay usually increases with the intercalation of polymer chains, representing a shift of the diffraction peak toward lower angle values [11]. Moreover, change in intensity and the shape of the basal reflections also indicate the effect of polymer intercalation. More specifically, when an intercalated structure is formed, the concentration of the intercalated clay layers with a given spacing is proportional to the area under the corresponding XRD peak [96].

X-Ray Diffraction peaks disappear in the case of exfoliated structures owing to large interlayer spacing as a consequence of disordered silicate layers and loss of structural registry [11, 20]. Since only the periodically stacked MMT layers are detected by XRD analysis, especially in exfoliated structures, TEM analysis are applied for direct observation of the exfoliated layers [10].

Intermediate structures may also exist constituting the characteristics of both intercalated and exfoliated morphologies besides the two well defined structures. Generally, decrease in intensity and broadening of the diffraction peaks are observed in this case as a representation of partially exfoliated or delaminated structures [11].

Figure 4.1 shows the X-Ray Diffraction pattern of pristine recycled polypropylene. Interestingly, a diffraction peak was observed at  $2\theta=6.34^\circ$  which did not belong to polypropylene or polyethylene in the matrix. The peak position does not belong to any kind of known material in the matrix, and hence presence of this peak is attributed to the unknown impurities inside the polymer as a common consequence of recycling process.

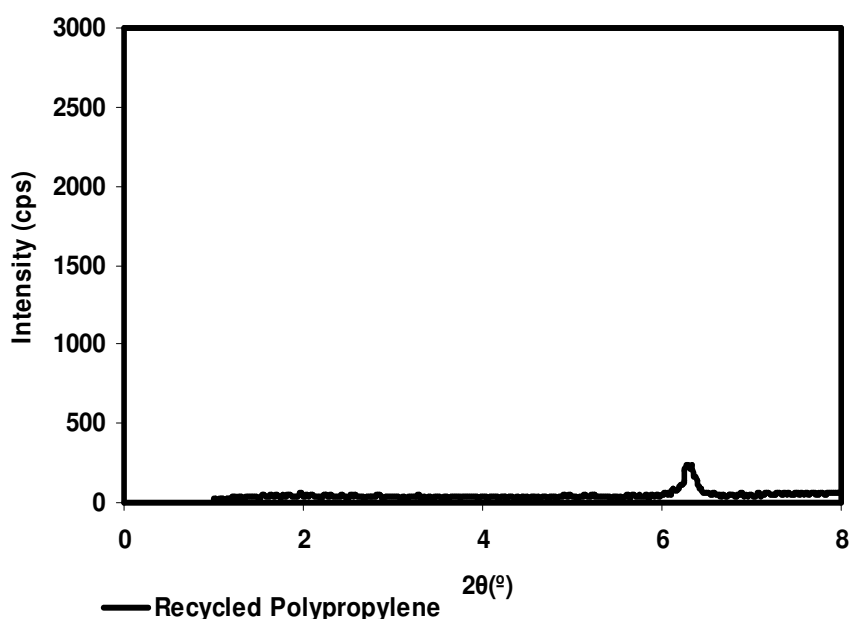


**Figure 4.1** X-Ray Diffraction pattern of recycled polypropylene.

XRD of organoclay Cloisite® 15A in powder form exhibits two distinct diffraction peaks between  $1^\circ$  to  $8^\circ$  consistent with the data provided by Southern Clay Products as shown in Figure 4.2. The first basal reflection exists at  $d_{001}=32 \text{ \AA}$  and  $2\theta=2.76^\circ$  and represents the characteristic peak of the organoclay silicate layer by which intercalated and exfoliated morphologies are determined. Existence of a second peak can result from another silicate layer when  $2\theta$  is about twice the value of the first characteristic peak or it can be attributed to the inorganic cations of the smectite clay that are not fully replaced by organic ions [97-99]. Cloisite®  $\text{Na}^+$  which is an unmodified natural MMT has characteristic peak at  $2\theta$  which is equal to the value of

the second peak in Cloisite® 15A; therefore, presence of the second peak in Cloisite® 15A could be assigned for a portion of clay that was not properly modified.

X-Ray Diffraction patterns of binary and ternary composites, prepared with Cloisite® 15A and Lotader® AX8900 (E-MA-GMA) compatibilizer at 2 wt% clay loadings are shown in Figure 4.3 and d-spacing values are given in Table 4.1. Polypropylene has no polar groups in its backbone, and it is one of the most hydrophobic polymers; therefore, it is difficult for polypropylene macromolecules to diffuse between silicate layers due to thermodynamic restrictions [41, 81]. Usually compatibilizers are added to enhance the intercalation between MMT and polypropylene, or high shear and dispersive forces are applied during compounding [42, 50]. In binary nanocomposite of P and Cloisite® 15A, relatively a slight increase in basal spacing, from 32 Å to 34.2 Å, was observed even when no compatibilizer was added. This result indicates that, although the polymer and clay are incompatible, presence of sufficient shear over an adequate residence time allowed intercalation of polymer chains at this clay loading [100]. Moreover, twice extrusion of all components also contributed to overcome the cohesive forces between clay layers and enhanced diffusion mechanism of polymer chains into the clay layers. TEM images shown later are also in agreement with the presence of some intercalated zones in binary nanocomposites at 2 wt % organoclay loading.

Addition of 5 wt% Lotader® AX8900 (E-MA-GMA) resulted in shifting diffraction peaks to lower angles with an increased d-spacing value up to 39.4 Å and a significant reduction of intensity peak amplitude. Both results indicate that E-MA-GMA acted as a compatibilizer and resulted in the intercalation of polymer chains inside the organoclay interlayer. Increased interlayer distance and decreased intensity of the characteristic peaks indicate the presence of the partially delaminated layers of Cloisite® 15A in the polymer matrix. However, incorporation of more compatibilizer (10 wt%) did not significantly contribute to further expansion of the galleries. Epoxy function of GMA groups has capability of reacting with hydroxyl, carboxyl and amine ends [90]. Polypropylene and polyethylene do not have these types of polar groups in their structures. However, the surface of Cloisite® 15A may have hydroxyl groups. As a general observation, even if the hydrophilic clay surfaces are modified with long alkyl groups, they may remain polar, and non polar polyolefins can not enter the clay galleries without the aid of a compatibilizing agent. The polarity difference between organoclay surface and polymer matrix could be balanced by a

special interaction between the polar group of the compatibilizer and the oxygen group of the organoclay surface. Thus resulting mediated polarity could be the reason of compatibilization effect [101]. MFI value of the E-MA-GMA shown later is higher than the polymer matrix and therefore diffusion of the compatibilizer could be easier owing to its lower viscosity. Moreover, the ethylene group present in the E-MA-GMA compatibilizer could be providing miscibility with the polyethylene particles in the matrix owing to their structural similarity.

According to the XRD diagram, the second peak of the clay also shifted to lower angles and shifting was more remarkable with compatibilizer addition. This movement was also a consequence of intercalation of the polymer chains between the unmodified silicate layers and breakage of large clay agglomerates into small tactoids under applied shear and compatibilization effect.

Figure 4.4 and Figure 4.5 show the X-Ray Diffraction patterns of binary and ternary composites prepared with Cloisite® 15A and Lotader® AX8900 compatibilizer at 4 wt% and 6 wt% clay loadings, respectively. Considering the binary mixtures of polypropylene and Cloisite® 15A, diffraction peaks were shifted to higher angles with increasing peak intensity when the clay content exceed 2 wt%. Even particle-particle attractions were rendered by surface treatment of organoclays, and interlayer gallery was expanded, there are some other factors affecting the polymer intercalation such as polarity and dispersive forces, chemical compatibility etc. [41]. Cloisite® 15A does not have any functional groups and therefore dispersive forces applied during compounding are more effective in delamination of the organoclay. When the clay loading was increased up to a certain point (in this case 2 wt%) the hydrodynamic separation force or shear stress applied by the matrix polymer may not overcome the cohesive forces between the clay platelets, and silicate layers break down to larger agglomerates [102]. Besides hindering the intercalation of polymer chains between clay layers, the decrease in basal spacing with respect to pure clay powder could be a consequence of collapsed clay sheet owing to displacement of ammonium compounds during thermal and mechanical treatment [103]. The positive effect of compatibilization was also observed for the nanocomposites containing compatibilizer at 4 wt% and 6 wt% organoclay loadings due to relatively increased interlayer spacing and decreased intensity. However, at these clay loadings intercalation was still poor even when compatibilizer was present.

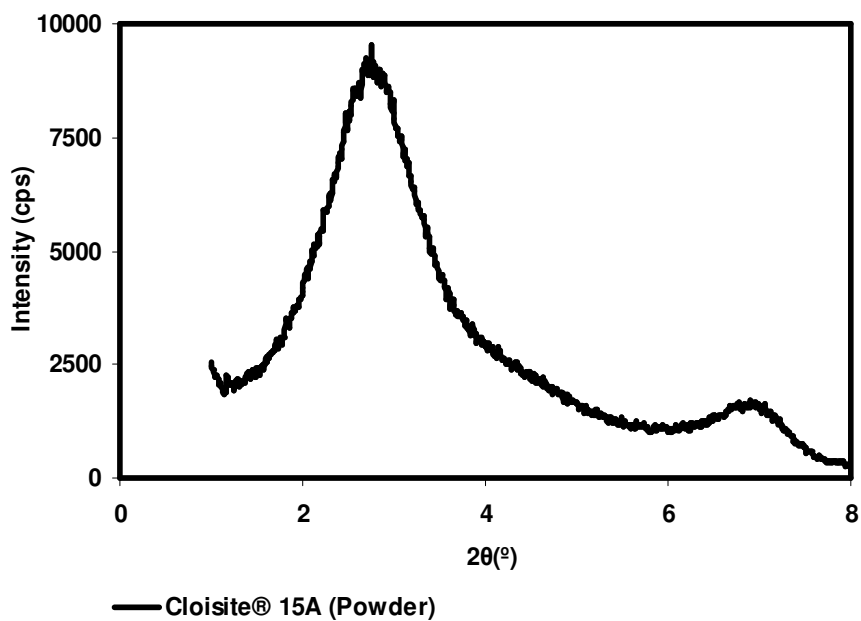


Figure 4.2 XRD pattern of Cloisite® 15A in powder form.

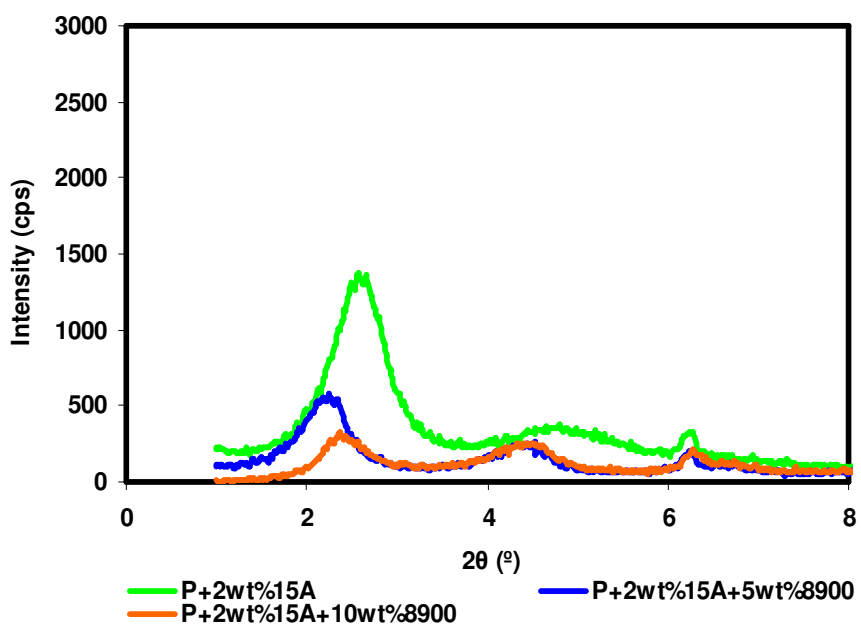
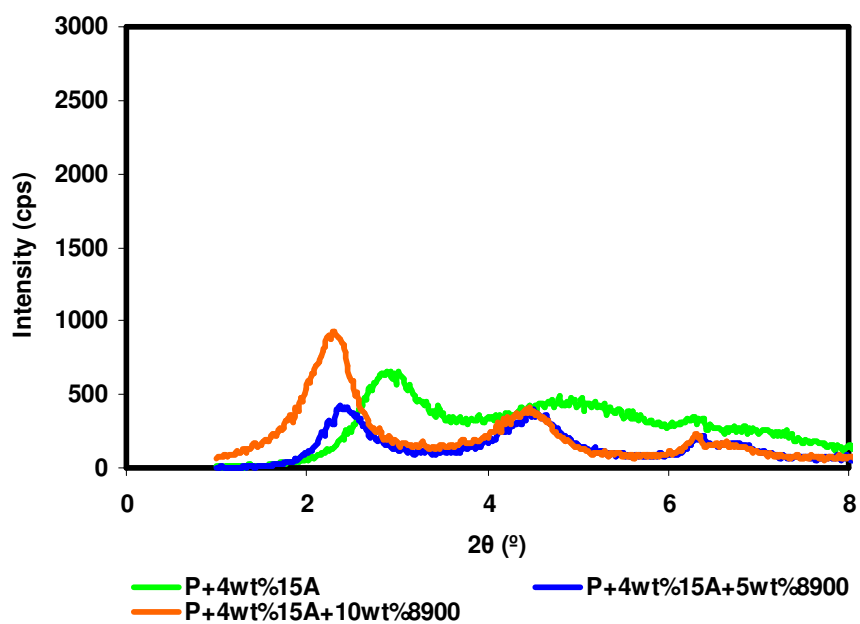
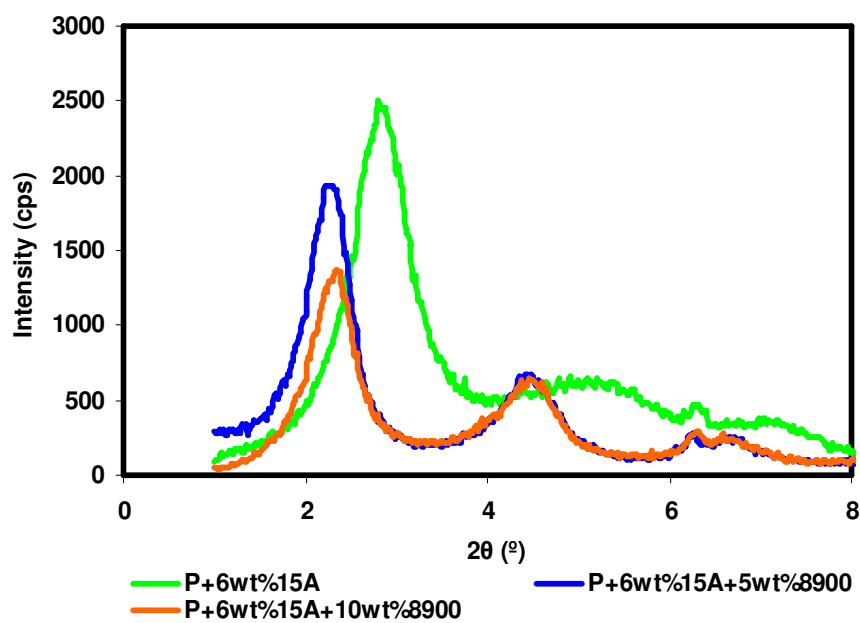


Figure 4.3 XRD patterns of P- Cloisite® 15A- Lotader® AX8900 nanocomposites at 2 wt% organoclay loading.



**Figure 4.4** XRD patterns of P- Cloisite® 15A- Lotader® AX8900 nanocomposites at 4 wt% organoclay loading.



**Figure 4.5** XRD patterns of P- Cloisite® 15A- Lotader® AX8900 nanocomposites at 6 wt% organoclay loading.

**Table 4.1** XRD results of P- Cloisite® 15A- Lotader® AX8900 nanocomposites.

Sample	Peak-I		Peak-II	
	2 $\theta$ (°)	d <sub>001</sub> (Å)	2 $\theta$ (°)	d <sub>002</sub> (Å)
<b>Polymer Matrix</b>				
<b>Recycled Polypropylene (P)</b>	6.34	14.0	-	-
<b>Organoclay</b>				
<b>Cloisite® 15A</b>	2.76	32.0	6.90	12.8
<b>Binary nanocomposites (All-S)</b>				
<b>P+ 2 wt% 15A</b>	2.58	34.2	4.80	18.4
<b>P+ 4 wt% 15A</b>	2.88	30.6	4.80	18.4
<b>P+ 6 wt% 15A</b>	2.80	31.5	4.92	17.9
<b>Ternary nanocomposites (All-S)</b>				
<b>P+ 2 wt% 15A+ 5 wt% 8900</b>	2.24	39.4	4.52	19.5
<b>P+ 2 wt% 15A+ 10 wt% 8900</b>	2.36	37.4	4.46	19.8
<b>P+ 4 wt% 15A+ 5 wt% 8900</b>	2.36	37.4	4.50	19.6
<b>P+ 4 wt% 15A+ 10 wt% 8900</b>	2.30	38.4	4.46	19.8
<b>P+ 6 wt% 15A+ 5 wt% 8900</b>	2.28	38.7	4.44	19.9
<b>P+ 6 wt% 15A+ 10 wt% 8900</b>	2.34	37.7	4.46	19.8

In the second part of the study, the effects of processing conditions were investigated. Two different screw speeds and processing temperatures were applied while feed rate was kept constant. Nanocomposites were prepared with Cloisite® 15A organoclay, and E-MA-GMA and PP-MAH compatibilizers at specified compositions. Different compatibilizers were used for comparison purposes. Sample compositions were selected as 2 wt% Cloisite® 15A and 5 wt% E-MA-GMA, as well as 1 wt% Cloisite® 15A and 2 wt% PP-MAH.

There are several factors affecting the dispersion of clay platelets such as properties of the polymer matrix, organic modifier of the clay, type and the concentration of the compatibilizer. Although, exfoliation and intercalation mechanism of the organoclay could be determined by these factors, state of exfoliation is also a strong function of processing conditions and mixing protocol [14]. Separation mechanism of the clay

layers is mainly controlled by two factors; the shear stress in the extruder and the diffusion of polymer chains inside clay galleries [43].

Figures 4.6 and 4.7 show XRD diagram of E-MA-GMA and PP-MAH containing nanocomposites prepared at altering processing conditions, respectively. In both two cases, d-spacing values are higher than that of the pure organoclay powder. Moreover, it was observed that as the screw speed was increased the intensity values of the XRD peaks decreased and peaks became broadened. This reduction was more significant for the nanocomposites prepared at low temperatures, indicating the formation of a more delaminated structure at low processing temperatures. It is known a fact that, exfoliated structures can be formed only when the shear stress is sufficient to overcome the electrostatic forces between silicate layers.

Shear stress applied on the polymer is a product of shear rate and melt viscosity. Melt viscosity is inversely proportional to the temperature, therefore as the processing temperature is decreased, melt viscosity increases [104], and at constant shear rate provided by screw speed, the shear stress applied on organoclay increases and exfoliation is promoted. Diffusion is also a function of temperature and as temperature is decreased diffusion of polymer chains become more difficult due to entropic factors. However, in this case it was observed that shear rate and dispersive forces are more important than the diffusion mechanism and decrease in diffusivity owing to low temperature was compensated by high and effective shear forces. Consequently, the best dispersion and delamination was observed in the nanocomposites prepared at 180 °C temperature and 350 rpm screw speed, regardless of the type of compatibilizer and composition used. Several authors also reported that low temperature profile, high screw speed and high polymer viscosity is recommended for enhanced mixing properties [43, 102, 105] and the data of this study are consistent with the literature.

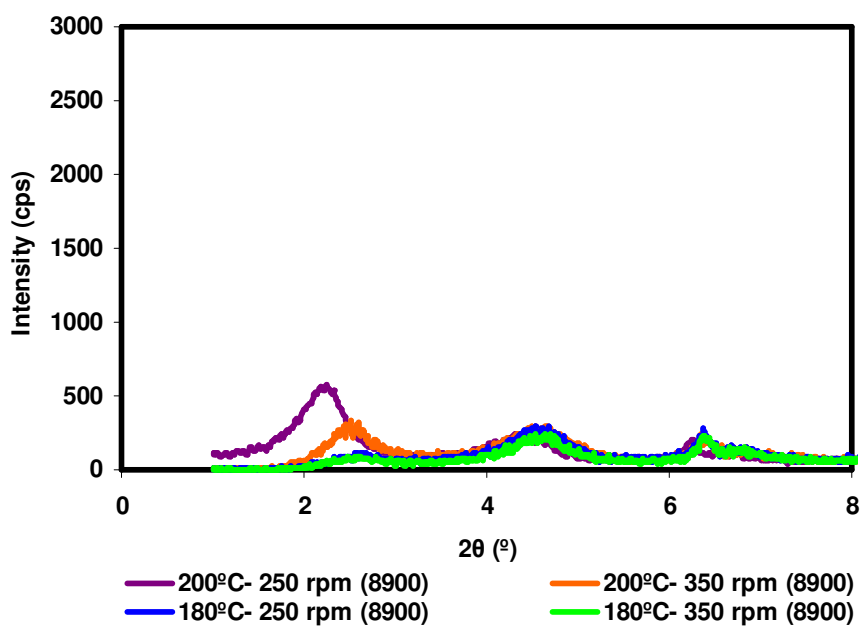


**Figure 4.6** XRD patterns of P- Cloisite® 15A- Lotader® AX8900 at 2 wt% organoclay and 5 wt% compatibilizer loading, effect of processing conditions.

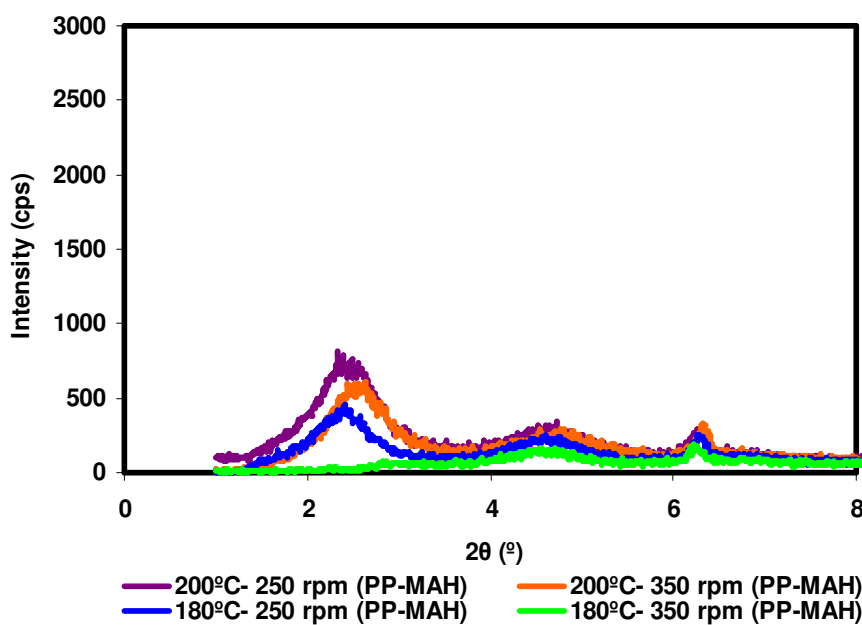


**Figure 4.7** XRD patterns of P- Cloisite® 15A- PP-MAH at 1 wt% organoclay and 2 wt% compatibilizer loading, effect of processing conditions.

**Table 4.2** XRD results, effects of processing conditions.

Processing Condition (°C- rpm)	Peak-I		Peak-II	
	2 $\theta$ (°)	d <sub>001</sub> (Å)	2 $\theta$ (°)	d <sub>002</sub> (Å)
<b>P+ 5 wt % Lotader® AX8900 (E-MA-GMA)+ 2 wt% Cloisite® 15A (All-S)</b>				
200 °C – 250 rpm	2.24	39.4	4.52	19.5
200 °C – 350 rpm	2.51	35.2	4.67	18.9
180 °C – 250 rpm	2.68	32.9	4.54	19.4
180 °C – 350 rpm	2.56	34.5	4.54	19.4
<b>P+ 2 wt % PP-MAH and 1 wt%+ Cloisite® 15A (MB)</b>				
200 °C – 250 rpm	2.34	37.7	4.72	18.7
200 °C – 350 rpm	2.63	33.6	4.54	19.4
180 °C – 250 rpm	2.41	36.6	4.61	19.2
180 °C – 350 rpm	2.87	30.8	4.54	19.4

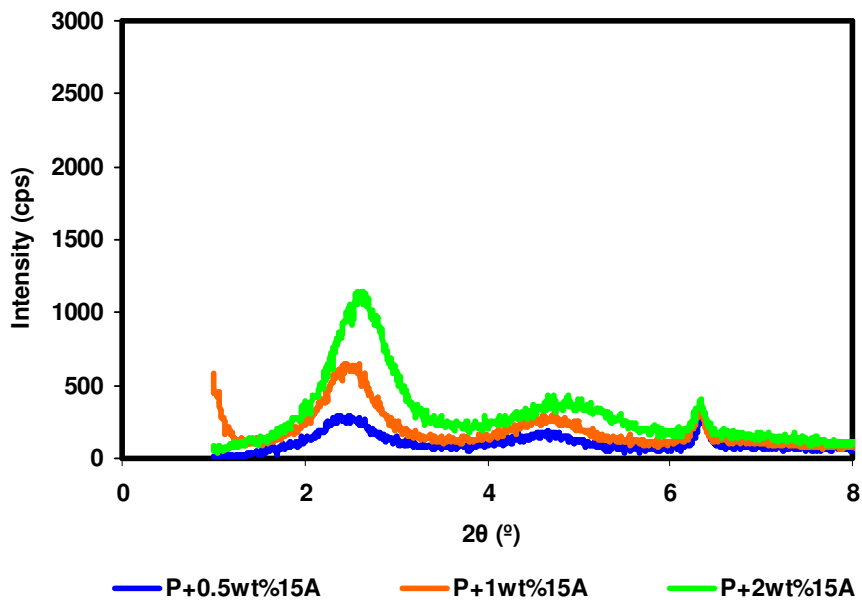
After finding the optimum processing conditions, effect of organoclay to compatibilizer ratio was investigated by using PP-MAH compatibilizer. Low organoclay concentrations between 0.5 to 2.0 wt. percent were tried this time since using clay contents above 2 wt% were found to be nonproductive in the previous experiments. Masterbatch method was applied to the rest of the samples and materials were extruded only once in order to prevent the adverse effects of three subsequent thermal treatments on organoclay structure during compounding.

Figure 4.8 shows the XRD diagram of binary nanocomposites of Cloisite® 15A and P prepared at different clay loadings and Figures 4.9- 4.11 show the XRD patterns of ternary nanocomposites prepared with PP-MAH compatibilizer at different compatibilizer to organoclay ratios of 1, 2, and 3, respectively. For all nanocomposites, the diffraction peaks were shifted to the left with or without compatibilizer as an indication of intercalated structures. For the clay loadings below 2 wt%, the cohesive forces were exceeded by the dispersive and shear forces as previously mentioned. In addition to that, it is clearly observed that as the amount of organoclay was increased from 0.5 wt% to 2 wt% the intensity peak amplitude also increases for both binary and ternary nanocomposites as expected.

The origin of driving force for intercalation in the presence of PP-MAH is the strong hydrogen bonding between maleic anhydride group (or carboxyl group in the case of the hydrolysis of maleic anhydride group) and the oxygen groups of the silicates on the organoclay surface [9, 59]. Interactions between silicate layers were weakened owing to compounding with PP-MAH and organoclay first, and hence the polymer chains were more easily intercalated into the clay galleries under strong shear field [45]. Characteristic structure of the PP-MAH that has both polar part (maleic anhydride group) and non-polar part (polypropylene moiety) was combined in a single chain so that the gap between MMT and polymer could be bridged [106]. Moreover, regarding to the polar character of maleic anhydride, affinity on the silicate surface was created and PP-MAH was employed as a compatibilizer between matrix and the filler [16]. Interaction mechanism between matrix and the filler was also promoted by the miscibility of propylene chains in the PP-MAH structure, otherwise, phase separation would be formed and intercalation mechanism would be diminished due to lack of miscibility.

Significant increase in the d-spacing values was not obtained with addition of compatibilizer when the ternary nanocomposites were concerned. Since mechanical results discussed in section 4.2 indicate remarkable increases with incorporation of PP-MAH compatibilizer, it can be questioned that the orientation of silicate layers on the skin portion and core of the injection molded specimens would be different as stated by Lee et al. [107]. While more stacked platelets are arranged on the skin, delaminated layers would be accommodated in the core section. In TEM images of these nanocomposites, exfoliated zones were also observed.

The effect of compatibilizer to organoclay ratio was not apparent in the XRD diagrams. However, considering the d-spacing values, PP-MAH to organoclay ratio of 3 seemed to have a slightly better effect on the formation of intercalation and, interlayer distance were increased up to 37.1 Å. This result is reasonable owing to the fact that increased proportion of maleic anhydride would form a stronger affinity on the silicate layers and separate them more easily during compounding.



**Figure 4.8** Binary nanocomposites of P and Cloisite® 15A at various compositions.

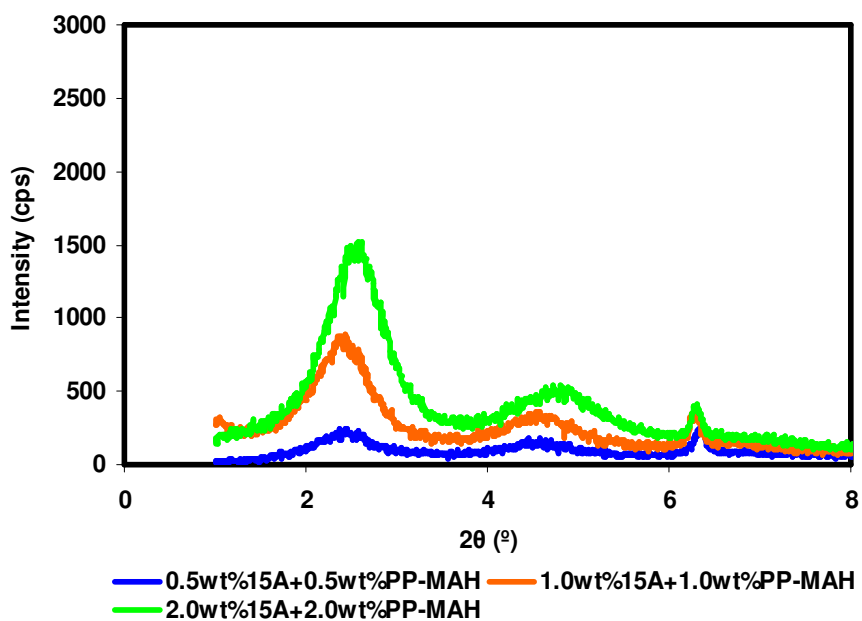


**Figure 4.9** Ternary nanocomposites of P- Cloisite® 15A- PP-MAH prepared at compatibilizer to organoclay ratio of 1.

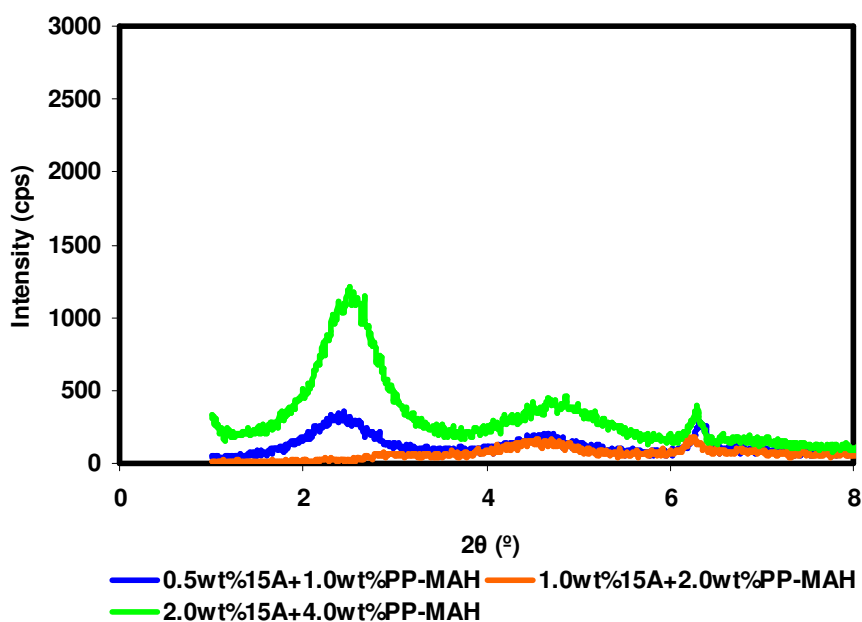


**Figure 4.10** Ternary nanocomposites of P- Cloisite® 15A- PP-MAH prepared at compatibilizer to organoclay ratio of 2.

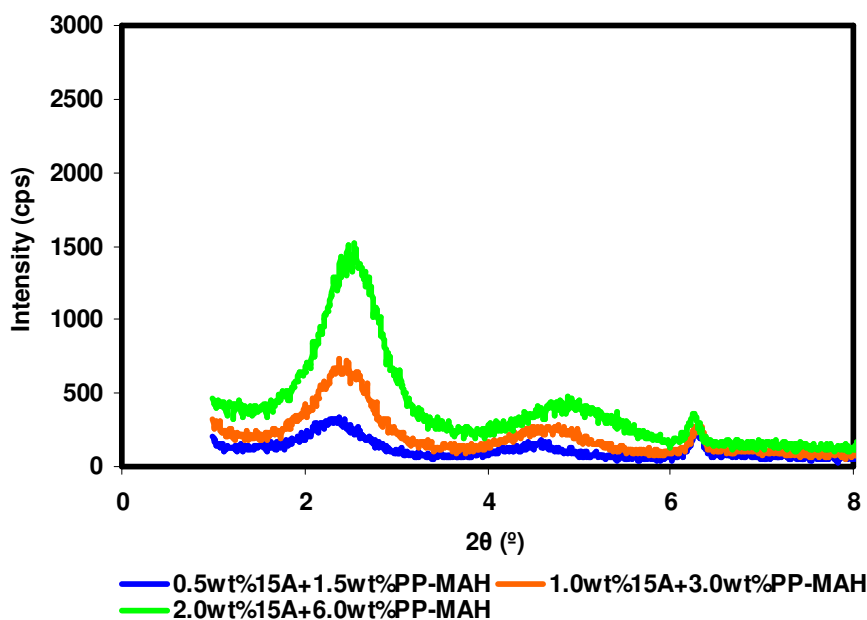


**Figure 4.11** Ternary nanocomposites of P- Cloisite® 15A- PP-MAH prepared at compatibilizer to organoclay ratio of 3.

**Table 4.3** XRD results, effects of PP-MAH to organoclay ratio.

Sample	Peak-I		Peak-II	
	$2\theta$ ( $^{\circ}$ )	$d_{001}$ ( $\text{\AA}$ )	$2\theta$ ( $^{\circ}$ )	$d_{002}$ ( $\text{\AA}$ )
<b>Polymer Matrix</b>				
Recycled Polypropylene (P)	6.34	14.0	-	-
<b>Organoclay</b>				
Cloisite® 15A	2.76	32.0	6.90	12.8
<b>Binary nanocomposites (MB)</b>				
P+ 0.5wt % 15A	2.49	35.4	4.66	18.9
P+ 1.0wt % 15A	2.46	35.9	4.74	18.6
P+ 2.0wt % 15A	2.63	33.6	4.67	18.9
<b>Ternary nanocomposites (MB)</b>				
P+ 0.5wt% PP-MAH+ 0.5wt% 15A	2.45	36.0	4.45	19.8
P+ 1.0wt% PP-MAH+ 1.0wt% 15A	2.44	36.2	4.57	19.3
P+ 2.0wt% PP-MAH+ 2.0wt% 15A	2.61	33.8	4.73	18.7
P+ 1.0wt% PP-MAH+ 0.5wt% 15A	2.45	36.0	4.62	19.1
P+ 2.0wt% PP-MAH+ 1.0wt% 15A	2.87	30.7	4.54	19.4
P+ 4.0wt% PP-MAH+ 2.0wt% 15A	2.50	35.3	4.87	18.1
P+ 1.5wt% PP-MAH+ 0.5wt% 15A	2.38	37.1	4.58	19.3
P+ 3.0wt% PP-MAH+ 1.0wt% 15A	2.38	37.1	4.77	18.5
P+ 6.0wt% PP-MAH+ 2.0wt% 15A	2.55	34.6	4.88	18.1

In the last part of the study, effects of different clay types were investigated. In addition to samples prepared with Cloisite® 15A, nanocomposites were prepared with Cloisite® 25A and Cloisite® 30B at PP-MAH to organoclay ratio of 2 for comparison purposes.

X-Ray Diffraction patterns of Cloisite® 25A and Cloisite® 30B at powder form were shown in Figures 4.12 and 4.13, respectively. Cloisite® 25A has a characteristic peak at  $2\theta=4.9^{\circ}$ , while the characteristic peak of Cloisite® 30B is at  $2\theta=4.92^{\circ}$ .

Nanocomposites prepared with different organoclays are shown in Figures 4.14-4.17 and the d spacing values are listed on Table 4.4.

In Figure 4.14 XRD diagram of binary nanocomposites of Cloisite® 25A and recycled polypropylene are shown, and it was observed that the characteristic peak of Cloisite® 25A was shifted to lower angles as a result of compounding with recycled polypropylene. In the diagrams, two distinct diffraction peaks were observable. The second peak would be emerged due to a second silicate layer since  $2\theta$  value of the second peak was twice the characteristic first peak or it would be representing the unintercalated silicate layers broken down into smaller stacks. In addition to that, incorporation of PP-MAH into ternary nanocomposites prepared with Cloisite® 25A resulted in shifting of the characteristic peak to lower angles as illustrated in Figure 4.15. Higher d-spacing values were obtained, increasing from 18 Å to 37.5 Å for the nanocomposite containing 1 wt% Cloisite® 25A and 2 wt% PP-MAH, indicating high levels of intercalation.

XRD pattern of binary nanocomposites of Cloisite® 30B and recycled polypropylene are shown in Figure 4.16. Broadening of characteristic peak was significant for these systems, and with incorporation of compatibilizer the characteristic peak was completely disappeared and the entire clay structure was seemed to be exfoliated. Good dispersion was expected for the systems containing PP-MAH and Cloisite® 30B since the hydroxyl group in the organoclay structure could open the maleic anhydride ring and attach the bulk chain to its surface resulting with increased interlayer spacing and favored polymer intercalation [108].

According to the data supplied by the producer Cloisite® 15A has the most hydrophobic surface compared to other clays due to absence of polar groups in its structure, and in addition to that, Cloisite® 15A has the largest initial interlayer spacing. Considering the non polar structure of polypropylene and reduced particle-particle attraction due to large interlayer gallery, the best dispersion would be expected in Cloisite® 15A containing nanocomposites. However, that would be an oversimplified approach, since variety of other factors, such as thermodynamic interactions between polymer-organoclay, polymer-compatibilizer and organoclay-compatibilizer as well as organoclay stability and packing density are other important factors on which exfoliation mechanism is highly dependent.

Among the three organoclays utilized, Cloisite® 15A based nanocomposites exhibited mostly intercalated-delaminated structure, while Cloisite® 25A and Cloisite® 30B based nanocomposites were delaminated in a great extent even when

no compatibilizer addition was present. Comparing their structure, Cloisite® 15A consists of two tallow chains and the others accommodate only one tallow. These two long aliphatic chains in the Cloisite® 15A structure would be limiting the entrance of polypropylene macromolecules to the silicate surface more effectively compared to one tailed ones and creating a shielding effect between MMT and polymer and resulting in mostly intercalated structures rather than delaminated [109].

The level of organic loading (MER loading) is another factor affecting the polymer intercalation. It describes the number of milliequivalents of amine salts used per 100 g of clay during cationic exchange reaction with sodium montmorillonite. According to literature, Cloisite® 15A has 125 MER loading while Cloisite® 30B has 90 and it was stated that high or excess amount of surfactant is disadvantageous for dispersion mechanism [109]. The excess amount of surfactant may cover the silicate surface and reduce the polymer clay interaction and hence disturb the exfoliation process. Therefore, one of the reasons of the difference between polymer intercalation with different types of organoclays could be the MER loading.

To conclude on XRD data, excess amount of clay loading would diminish the intercalation mechanism, even in the presence of compatibilizer, especially when the dispersive forces are more important. Besides polymer-organoclay interactions, the processing conditions have significant effects on clay dispersion and increasing screw speed and reducing processing temperature resulted in amplified shear stress on the polymer promoting intercalation. In XRD patterns, the effect of organoclay to compatibilizer ratio was not clearly observed. However, the high affinity at high amount of maleic anhydride content would enhance possible reactions between organoclay and compatibilizer and favor intercalation. Regarding the effects of different clay types, it was observed that the structure and accommodation of alkyl chains are more important than polarity or initial d spacing for an organoclay.

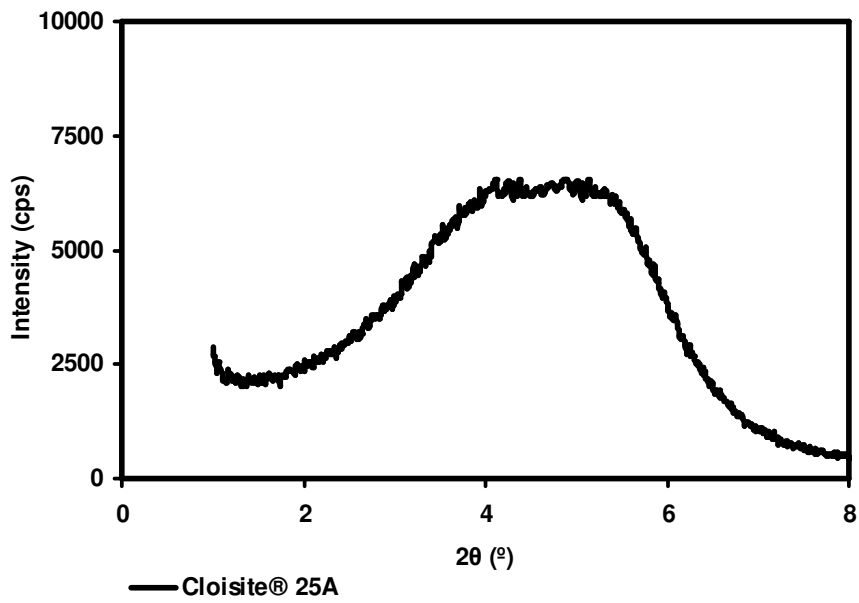


Figure 4.12 XRD pattern of Cloisite® 25A in powder form.

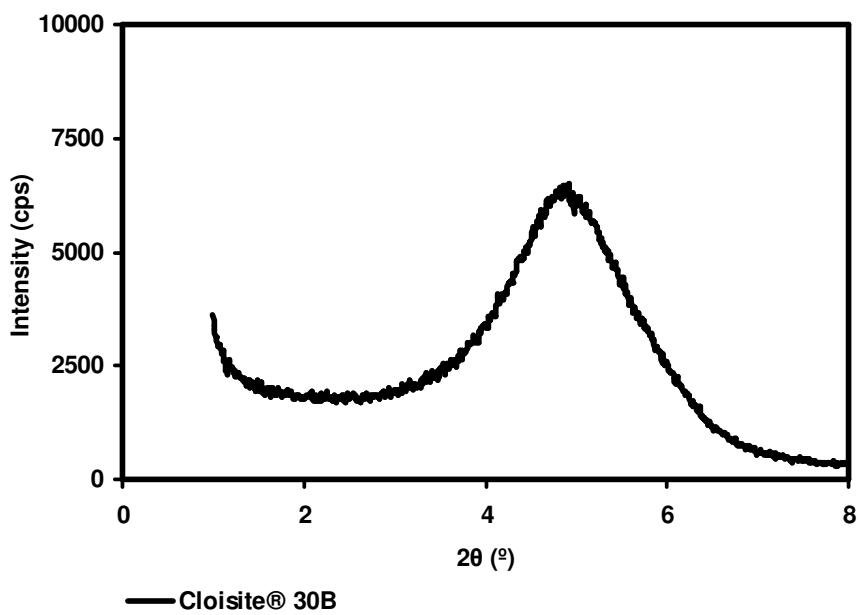
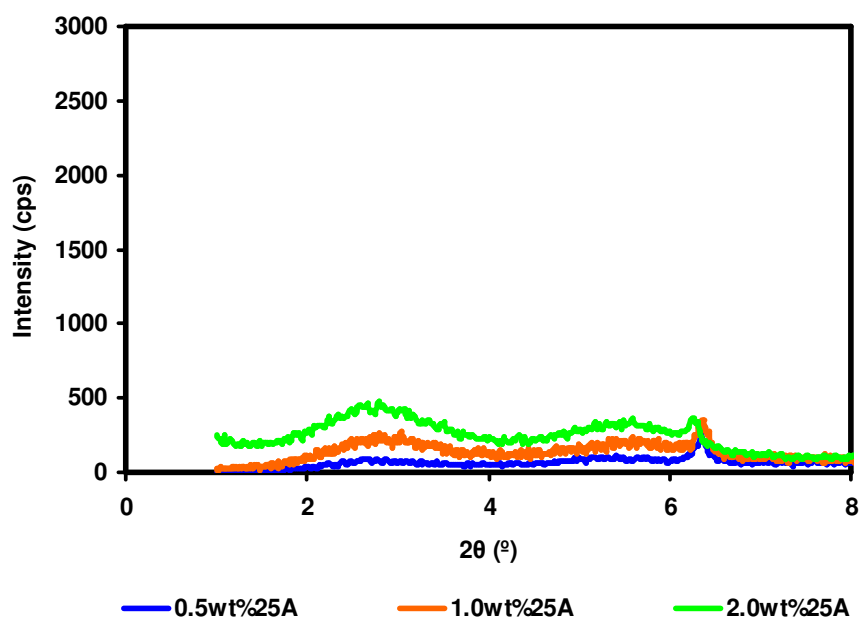
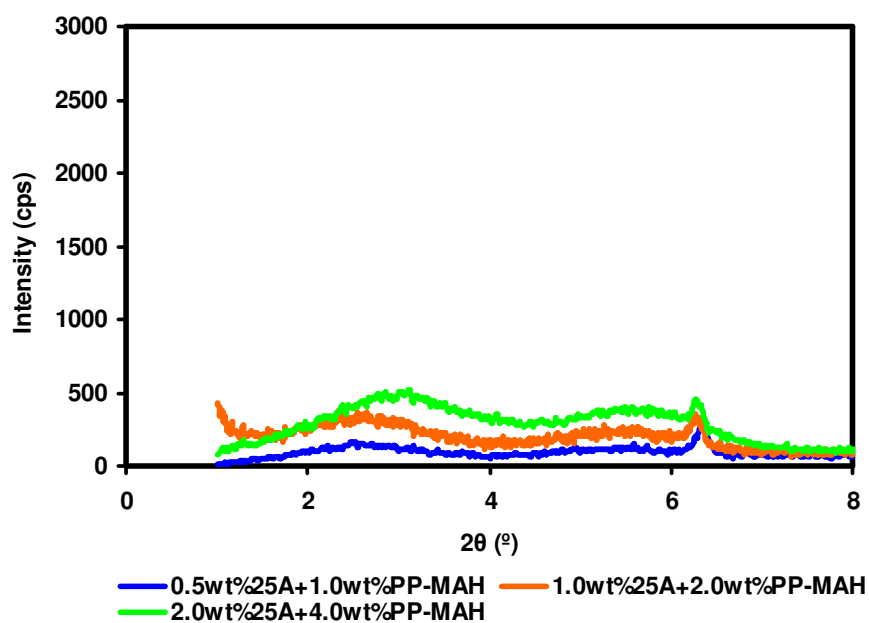


Figure 4.13 XRD pattern of Cloisite® 30B in powder form.



**Figure 4.14** Binary nanocomposites of P- Cloisite® 25A at various clay loadings.



**Figure 4.15** Ternary nanocomposites of P- Cloisite® 25A- PP-MAH prepared at compatibilizer to organoclay ratio of 2 and various clay loadings.

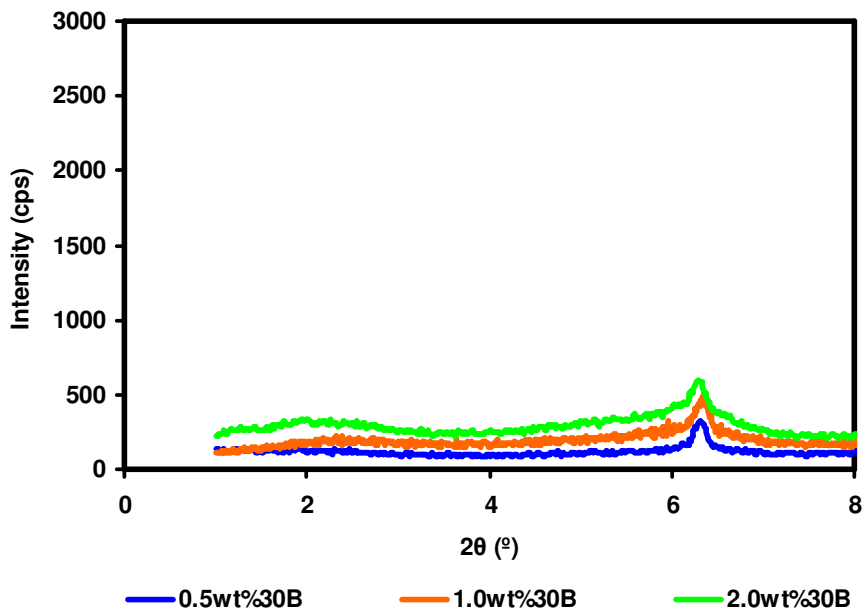


**Figure 4.16** Binary nanocomposites of P- Cloisite® 30B at various clay loadings.

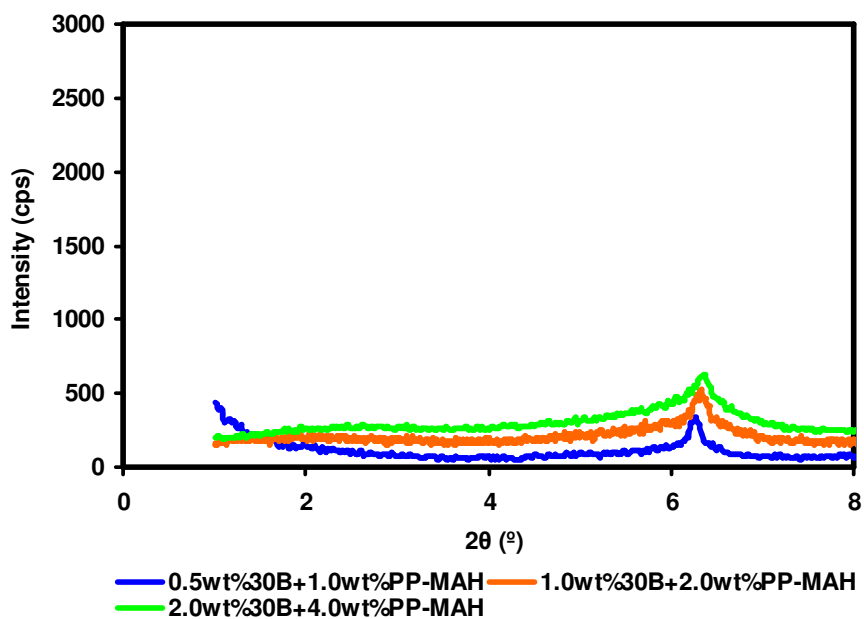


**Figure 4.17** Ternary nanocomposites of P- Cloisite® 30B- PP-MAH prepared at compatibilizer to organoclay ratio of 2 and various clay loadings.

**Table 4.4** XRD results, effects of clay types.

Sample	Peak-I		Peak-II	
	2 $\theta$ ( $^{\circ}$ )	d <sub>001</sub> (Å)	2 $\theta$ ( $^{\circ}$ )	d <sub>002</sub> (Å)
<b>Polymer Matrix</b>				
Recycled Polypropylene (P)	6.34	14.0	-	-
<b>Organoclay</b>				
Cloisite® 25A	4.90	18.0	-	-
Cloisite® 30B	4.92	17.9	-	-
<b>Binary nanocomposites (MB)</b>				
P+ 0.5wt% 25A	2.70	32.7	5.43	16.3
P+ 1.0wt% 25A	3.04	29.0	5.59	15.8
P+ 2.0wt% 25A	2.80	31.5	5.60	15.8
P+ 0.5wt% 30B	1.60	55.2	-	-
P+ 1.0wt% 30B	2.38	37.1	-	-
P+ 2.0wt% 30B	2.26	39.0	-	-
<b>Ternary nanocomposites (MB)</b>				
P+ 0.5wt% PP-MAH+ 0.5 wt% 25A	2.52	35.0	5.60	15.8
P+ 1.0wt% PP-MAH+ 1.0 wt% 25A	2.35	37.5	5.27	16.8
P+ 2.0wt% PP-MAH+ 2.0 wt% 25A	3.12	28.3	5.76	15.3
P+ 0.5wt% PP-MAH+ 0.5 wt% 30B	-	-	-	-
P+ 1.0wt% PP-MAH+ 1.0 wt% 30B	-	-	-	-
P+ 2.0wt% PP-MAH+ 2.0 wt% 30B	-	-	-	-

#### 4.1.2 TEM Analysis

The degree of dispersion or exfoliation of the layered silicate plays an important role in final performance of the materials such as mechanical and thermal expansion properties of polymer nanocomposites. X-Ray Diffraction analysis is useful in characterization of nanostructures and dispersion properties if diffraction peaks are observed in the small angle region. Such peaks represent the d spacing, and presence of ordered-intercalated and ordered-delaminated nanocomposites. However, in the case of disordered structures, XRD peaks become no longer visible due to loss of structural registry or large d spacings or both. In such cases, TEM

analysis is conducted providing definitive information regarding to the structure of the nanocomposites and direct observation of filler arrangements in the composite structure [20].

In the TEM micrographs, the dark areas represent the individual clay layers or agglomerates (tactoids) while rest of gray areas represents the polypropylene matrix. In this study, the white zones in the micrographs are believed to be the dispersed polyethylene phase. In addition to that, clusters of spherical particles were visible as the impurity in the matrix.

It is well known fact that for polypropylene based nanocomposites, generally the layered silicates exhibit a mixed morphology consisting of some exfoliated platelets, but mostly clay particles consisting of multiple platelets, even when compatibilizer is added [40]. In this study, a mixed morphology was also present in the micrographs.

TEM micrograph of recycled polypropylene with Cloisite® 15A but no compatibilizer phase is shown in Figure 4.18. In these micrographs clusters of clay platelets up to 2  $\mu\text{m}$  as well as some exfoliated clay layers are visible. Clay platelets and stacks are mostly covered by a white zone indicating that clay particles were resided mostly inside the polyethylene phase during compounding. Other individual clay layers were dispersed in the polymer matrix. Therefore, dispersion of the particles indicates that the relative affinity of clay platelets was higher for the polyethylene phase when no compatibilizer phase was available. Results are also in agreement with XRD analysis indicating some intercalation of clay layers in the matrix.

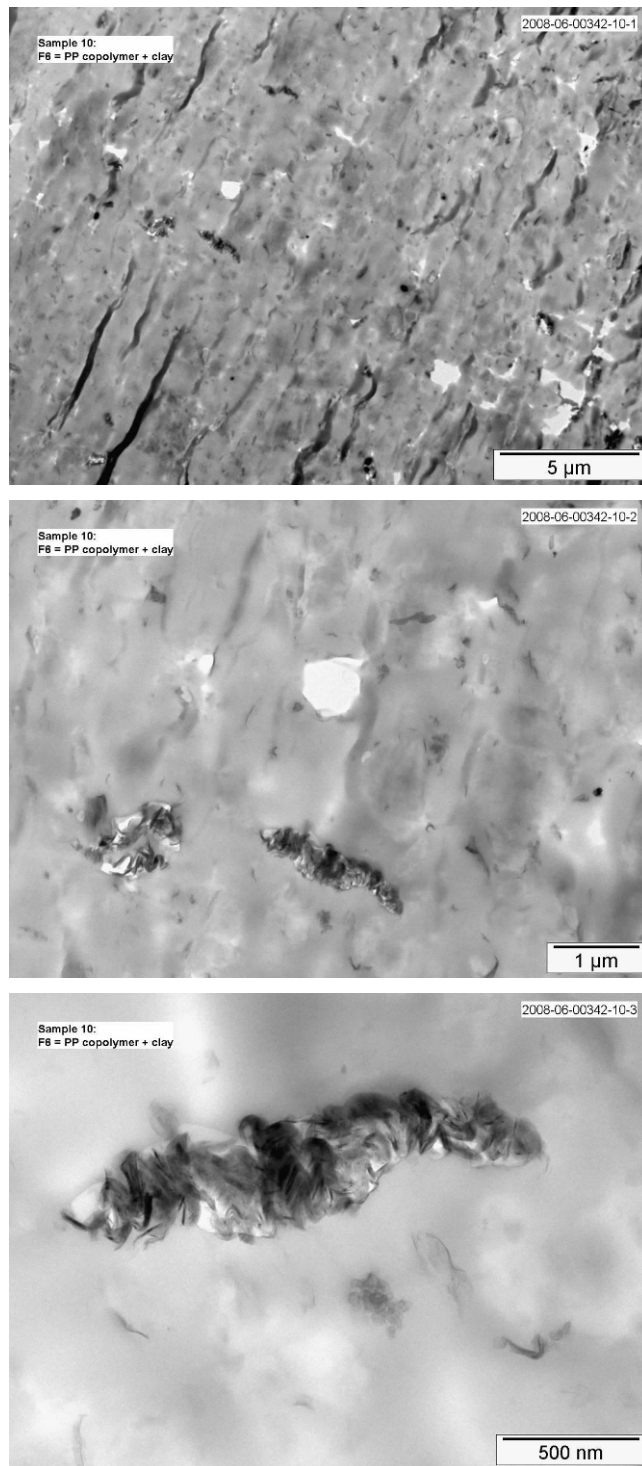
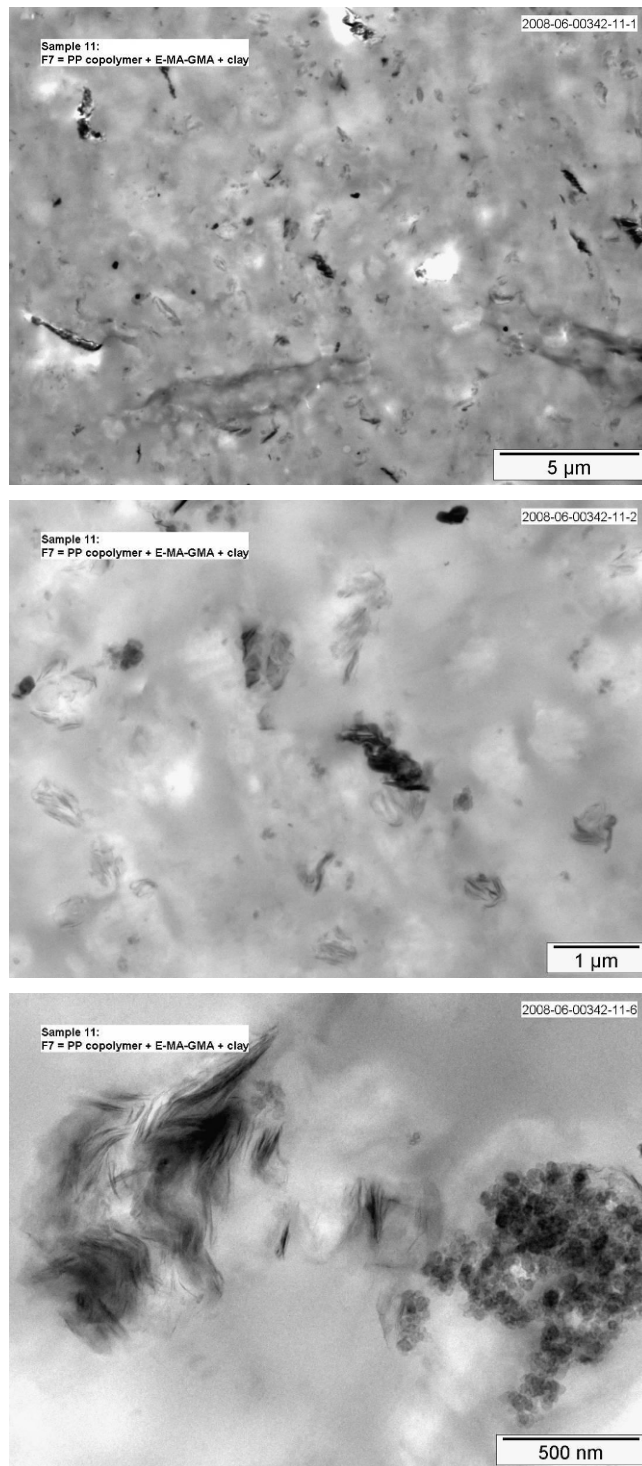


**Figure 4.18** TEM images at different magnifications of the binary nanocomposite containing recycled polypropylene and 2 wt% Cloisite® 15A prepared with MB method.

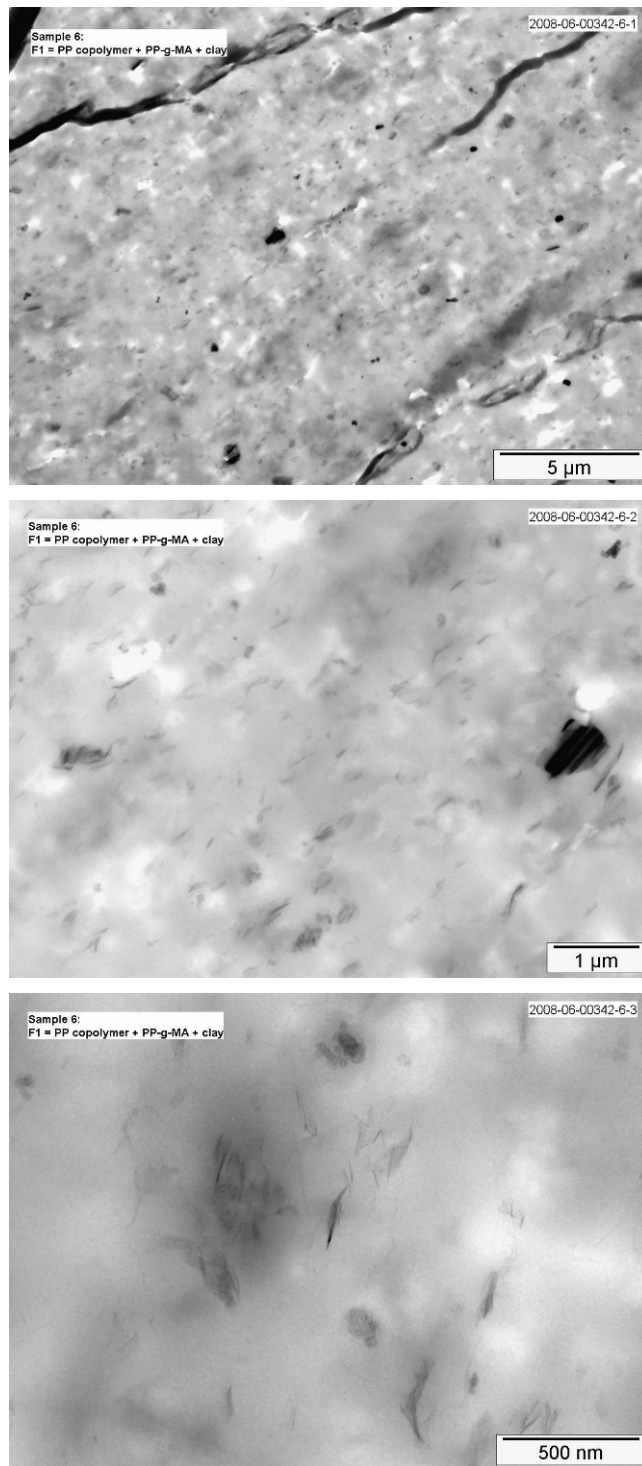
Figure 4.19 shows the micrographs of ternary nanocomposites containing 5 wt% E-MA-GMA and 2 wt% Cloisite® 15A. In the figure, clusters of clay platelets up to 4  $\mu\text{m}$  are visible and the general distribution of clay platelets is between 0.5 to 1  $\mu\text{m}$ . Compared to binary nanocomposite at the same clay loading, the layer thickness is lower and materials are dispersed in the polypropylene matrix more uniformly indicating that the morphology changes from an intercalated structure to a more delaminated morphology as also observed in the XRD patterns. Combining the results of two data, compatibilizing effect of E-MA-GMA was validated.

Figure 4.20 shows the ternary micrographs of nanocomposites containing 6 wt% PP-MAH and 2 wt% Cloisite®15A. In the micrographs, clusters of clay platelets 2  $\mu\text{m}$  in size present. In addition to that, lots of exfoliated platelets with a thickness of a few nanometers were also visible. Silicate layers are dispersed in the polypropylene matrix uniformly rather than being encapsulated by the polyethylene phase. The total dispersion area of clay platelets is significantly increased. This phenomenon explains the improvements in mechanical properties.

Considering the XRD analysis, the last two compositions had similar d spacing values. However, in the TEM images it was observed that the dispersion of clay platelets is much more uniform in the presence of PP-MAH compatibilizer. Consequently, the interactions between the organoclay platelets with PP-MAH, and hence the compatibilizing effect of this elastomer is found to be much significant. Similar results are also obtained in the mechanical properties of these nanocomposites.



**Figure 4.19** TEM micrographs at different magnifications of the ternary nanocomposite, containing recycled polypropylene, 2 wt% Cloisite® 15A and 5 wt% E-MA-GMA prepared with All-S method at 180 °C and 350 rpm screw speed.



**Figure 4.20** TEM micrographs at different magnifications of the ternary nanocomposite containing recycled polypropylene, 2 wt% Cloisite® 15A and 6 wt% PP-MAH prepared with MB method at 180 °C and 350 rpm screw speed.

In Figure 4.21, a nanocomposite containing recycled polypropylene, 1 wt% Cloisite® 15A and 2 wt% PP-MAH having a compatibilizer to organoclay ratio of 2 is shown, while in Figure 4.20, a nanocomposite containing recycled polypropylene, 2 wt% Cloisite® 15A and 6 wt% PP-MAH having a compatibilizer to organoclay ratio of 3 is shown. Comparing these two figures, it was observed that the state of dispersion was greatly enhanced as the compatibilizer to organoclay ratio was increased even in the case of higher organoclay content. Results are in agreement with the ones found by Kim et al. [40], stating that the degree of dispersion and exfoliation of the MMT increases as the ratio of PP-MAH to organoclay increases.

In Figures 4.21-4.23 the effects of organoclay type on the morphology of nanocomposites are compared. Nanocomposites were prepared with Cloisite® 15A, Cloisite® 25A and Cloisite® 30B at 1 wt% loadings, as well as adding 2 wt% PP-MAH compatibilizer, under same processing conditions. XRD results of the nanocomposites revealed that intercalated-delaminated structures were present in the nanocomposites containing Cloisite® 15A, while the silicate layers in other nanocomposites containing Cloisite® 25A and particularly Cloisite® 30B were totally delaminated. However, in the TEM analysis an opposite case was observed. In the TEM micrographs of nanocomposites containing Cloisite® 25A and Cloisite® 30B, clusters of clay platelets as well as some amount of exfoliated particles were visible. In contrast to XRD patterns, in TEM micrographs of nanocomposites containing Cloisite® 30B, agglomerated silicate layers up to 4 µm are visible. Moreover, in nanocomposites containing Cloisite® 25A, parallel multilayered silicate layers up to 2-4 µm are also visible, rather than delaminated structures as predicted from XRD patterns. In addition to that, the best dispersion of this compatibilizer to organoclay ratio was detected for the nanocomposites containing Cloisite® 15A. Silicate layers with a length of 0.5-4 µm are also visible in this case; on the other hand, the total area of exfoliated layers dispersed in the polypropylene matrix is higher compared to other nanocomposites. TEM results are not correlated with XRD results; however, they are in agreement with the mechanical results indicating that the significant improvements were present for nanocomposites containing Cloisite® 15A. These results are attributed to the relative dispersion difference core and the skin regions of the specimen which is commonly observed in polypropylene nanocomposites. In addition to that, the information provided by XRD is more reliable since the samples taken from the core of specimen for TEM analysis reflect only a selected marginal area and dispersion of organoclays might be different in the rest of the specimen.

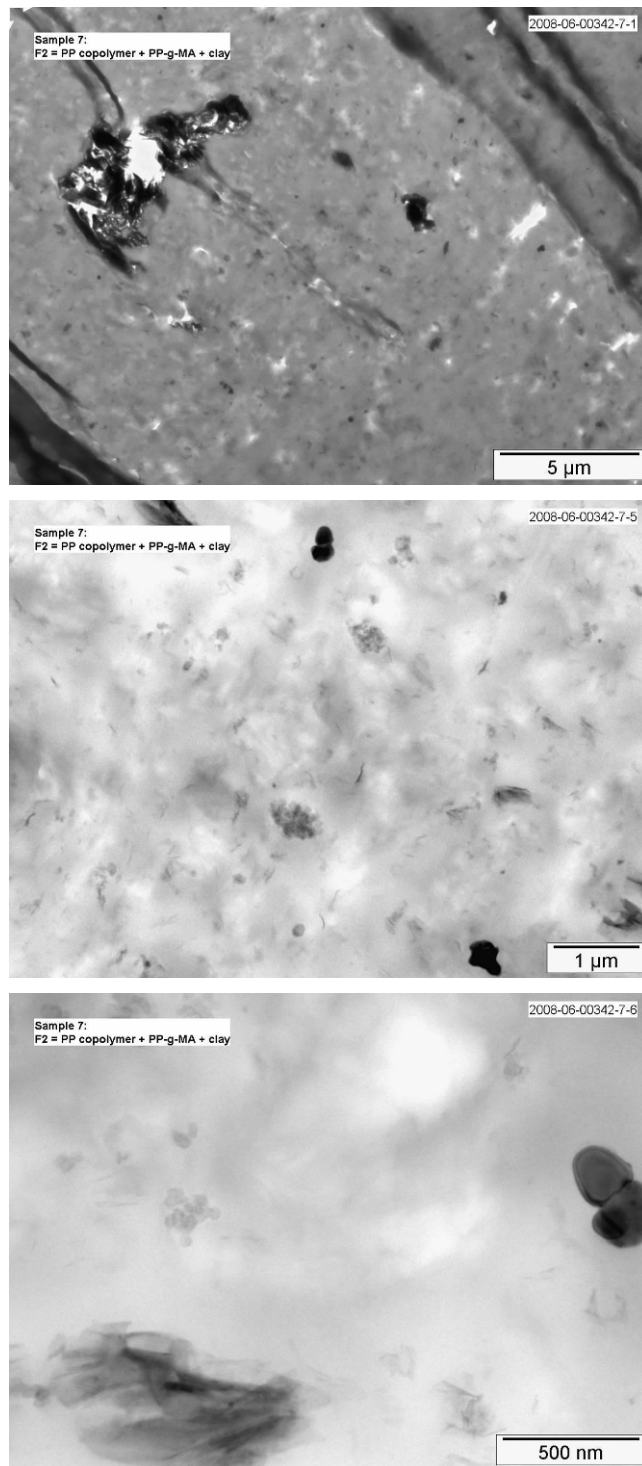


**Figure 4.21** TEM micrographs at different magnifications of the ternary nanocomposite containing recycled polypropylene, 1 wt% Cloisite® 15A and 2 wt% PP-MAH prepared with MB method at 180 °C and 350 rpm screw speed.



**Figure 4.22** TEM micrographs at different magnifications of the ternary nanocomposite containing recycled polypropylene, 1 wt% Cloisite® 25A and 2 wt% PP-MAH prepared with MB method at 180 °C and 350 rpm screw speed.

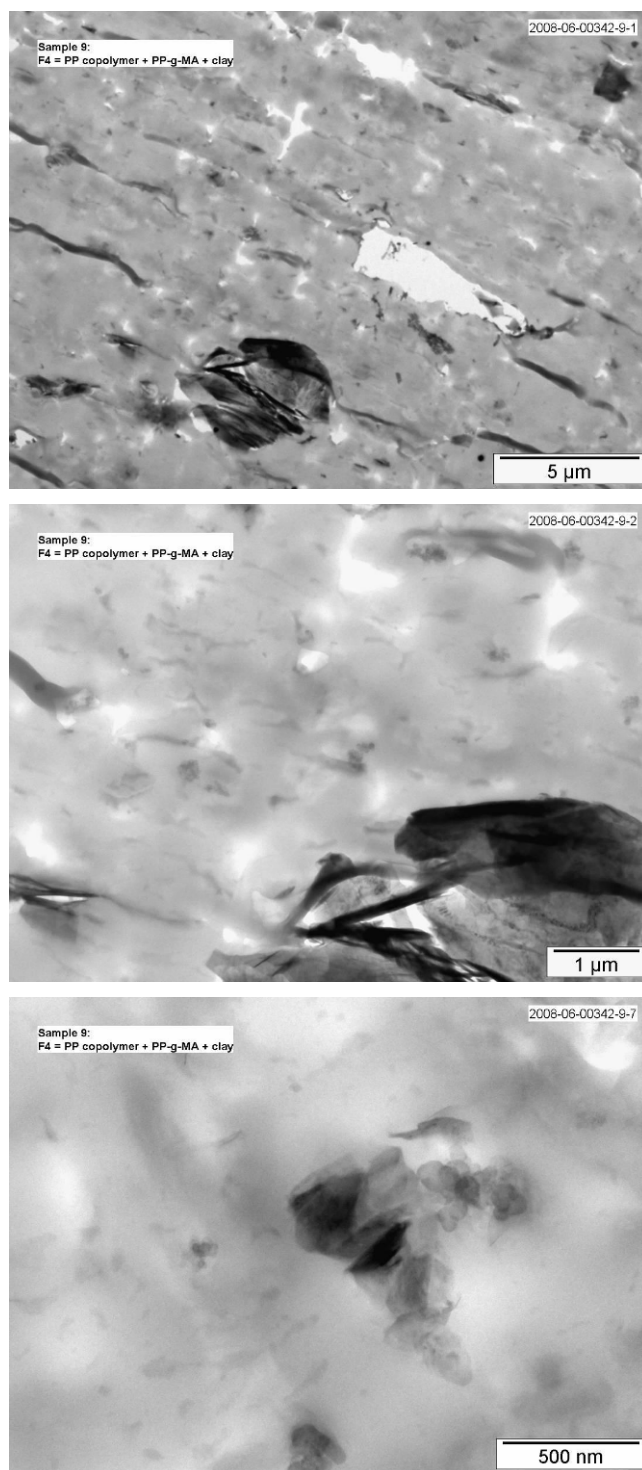


**Figure 4.23** TEM micrographs at different magnifications of the ternary nanocomposite containing recycled polypropylene, 1 wt% Cloisite® 30B and 2 wt% PP-MAH prepared with MB method and 180 °C and 350 rpm screw speed.

### 4.1.3 Scanning Electron Microscopy Analysis (SEM)

SEM analysis was conducted to determine the morphological characteristics of ternary and binary nanocomposites of recycled polypropylene. Moreover the dispersion and particle size of the organoclays and compatibilizers were also examined, since they are intimately related with toughening and reinforcing mechanisms. In order to analyze general morphology, low magnifications and for detailed particle analysis, high magnifications were used. Specimens were subjected to solvent etching prior to analysis to discard polyethylene and compatibilizer phases and obtain contrast for clear observation. Average domain sizes were calculated by Image J program with the aid of Equation 4.1. Approximately 200 to 250 particles were selected for each calculation and the obtained number average area values were then converted to number average diameters by using equation 4.2.

$$\bar{A} = \frac{\sum N_i A_i}{\sum N_i} \quad [4.1]$$

$$\bar{d} = \sqrt{\frac{4\bar{A}}{\pi}} \quad [4.2]$$

where,  $N_i$  is the number of the domains selected with calculated area of  $A_i$ .

The material structure of pristine recycled polypropylene after etching process was porous owing to dispersed polyethylene particles. Particle analyses were implemented to have a general idea, since the homogeneity in the recycled materials was not satisfactory. In this study, it was given importance to take SEM images which reflect the general distribution; however, there is still possibility of observing different distributions in some other parts of the material due to impurities and inadequate homogeneity. Therefore, attaching very precise physical meanings may not be correct in this case. The surface morphologies of the nanocomposites are shown in Figures 4.24- 4.38 and calculated particle domain sizes are given in Table 4.5.

**Table 4.5** SEM results.

Components	Add. Order	Processing Parameters		$\bar{d}$ (nm)
		°C	rpm	
<b>P (not extruded)</b>	-	-	-	<b>386</b>
<b>P (extruded once)</b>	-	180	350	<b>451</b>
<b>P (extruded twice)</b>	-	180	350	<b>579</b>
<b>P- Compatibilizer Blends</b>				
<b>P+ 5 wt% E-MA-GMA</b>	All-S	200	250	<b>553</b>
<b>P+ 10 wt% E-MA-GMA</b>	All-S	200	250	<b>571</b>
<b>P+ 2.0 wt% PP-MAH</b>	All-S	180	350	<b>587</b>
<b>P+ 4.0 wt% PP-MAH</b>	All-S	180	350	<b>536</b>
<b>P+ 6.0 wt% PP-MAH</b>	All-S	180	350	<b>501</b>
<b>P- Clay Binary Nanocomposites</b>				
<b>P+ 2wt% 15A</b>	All-S	200	250	<b>600</b>
<b>P+ 4 wt% 15A</b>	All-S	200	250	<b>585</b>
<b>P+ 6 wt% 15A</b>	All-S	200	250	<b>492</b>
<b>P+ 1.0 wt% 15A</b>	MB	180	350	<b>463</b>
<b>P+ 2.0 wt% 15A</b>	MB	180	350	<b>617</b>
<b>P+ 1.0 wt% 25A</b>	MB	180	350	<b>548</b>
<b>P+ 2.0 wt% 25A</b>	MB	180	350	<b>546</b>
<b>P+ 1.0 wt% 30B</b>	MB	180	350	<b>501</b>
<b>P+ 2.0 wt% 30B</b>	MB	180	350	<b>593</b>
<b>Ternary Nanocomposites (Effect of Processing Conditions)</b>				
<b>P+ 2wt% 15A+ 5wt% E-MA-GMA</b>	All-S	200	350	<b>552</b>
<b>P+ 2wt% 15A+ 5wt% E-MA-GMA</b>	All-S	180	250	<b>527</b>
<b>P+ 2wt% 15A+ 5wt% E-MA-GMA</b>	All-S	180	350	<b>376</b>
<b>P+ 1wt% 15A+ 2wt% PP-MAH</b>	MB	200	250	<b>453</b>
<b>P+ 1wt% 15A+ 2wt% PP-MAH</b>	MB	200	350	<b>532</b>
<b>P+ 1wt% 15A+ 2wt% PP-MAH</b>	MB	180	250	<b>519</b>

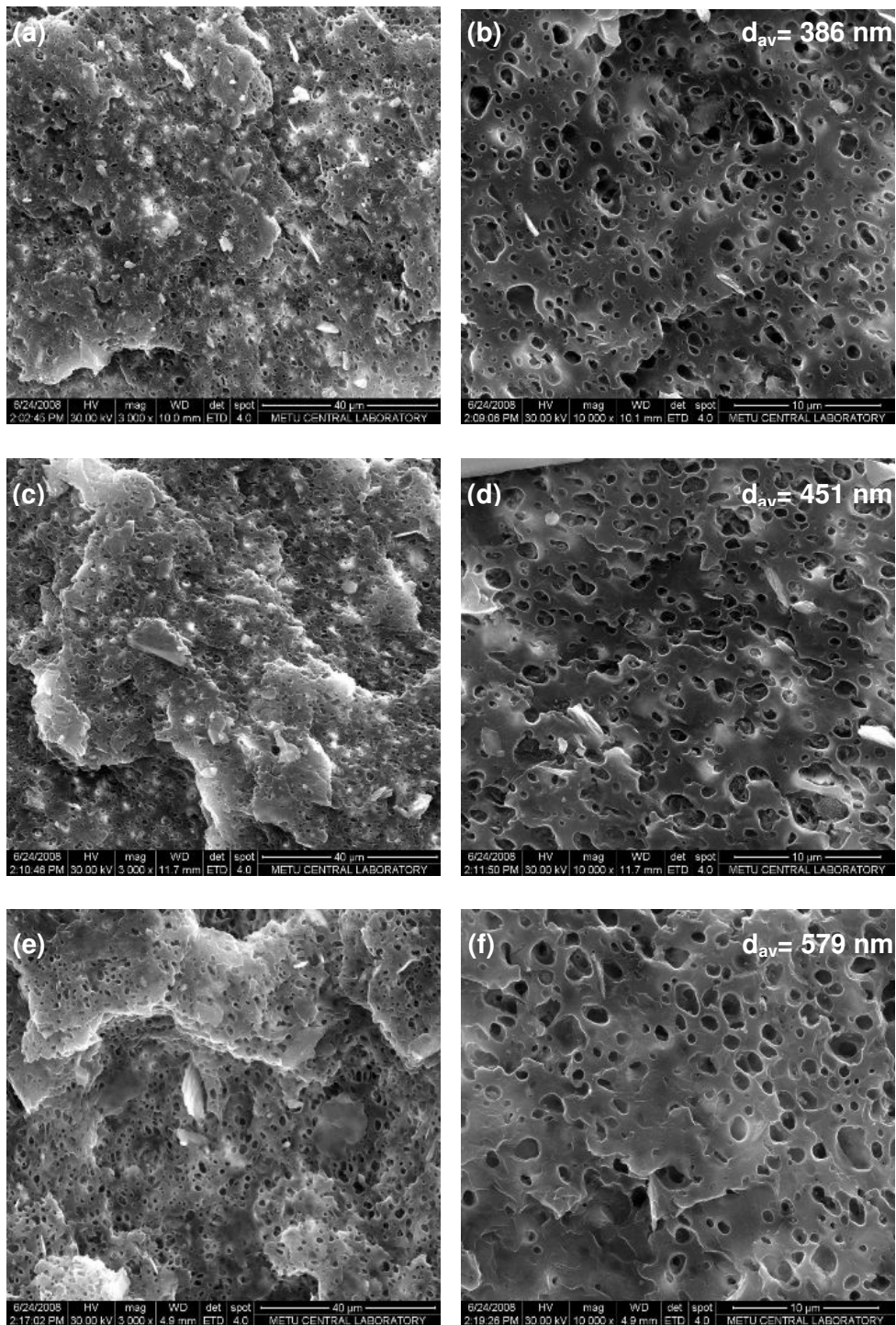
**Table 4.5** SEM results (Cont'd.)

Components	Add. Order	Processing Parameters		$\bar{d}$ (nm)
		$^{\circ}\text{C}$	rpm	
<b>P- Compatibilizer- Clay Ternary Nanocomposites</b>				
<b>P+ 2wt% 15A+ 5wt% E-MA-GMA</b>	All-S	200	250	<b>551</b>
<b>P+ 4wt% 15A+ 5wt% E-MA-GMA</b>	All-S	200	250	<b>421</b>
<b>P+ 6wt% 15A+ 5wt% E-MA-GMA</b>	All-S	200	250	<b>387</b>
<b>P+ 2wt% 15A+ 10wt% E-MA-GMA</b>	All-S	200	250	<b>546</b>
<b>P+ 4wt% 15A+ 10wt% E-MA-GMA</b>	All-S	200	250	<b>576</b>
<b>P+ 6wt% 15A+ 10wt% E-MA-GMA</b>	All-S	200	250	<b>494</b>
<b>P+ 0.5wt% PP-MAH+ 0.5wt% 15A</b>	MB	180	350	<b>503</b>
<b>P+ 1.0wt% PP-MAH+ 1.0wt% 15A</b>	MB	180	350	<b>500</b>
<b>P+ 2.0wt% PP-MAH+ 2.0wt% 15A</b>	MB	180	350	<b>478</b>
<b>P+ 1.0wt% PP-MAH+ 0.5wt% 15A</b>	MB	180	350	<b>553</b>
<b>P+ 2.0wt% PP-MAH+ 1.0wt% 15A</b>	MB	180	350	<b>444</b>
<b>P+ 4.0wt% PP-MAH+ 2.0wt% 15A</b>	MB	180	350	<b>497</b>
<b>P+ 1.5wt% PP-MAH+ 0.5wt% 15A</b>	MB	180	350	<b>536</b>
<b>P+ 3.0wt% PP-MAH+ 1.0wt% 15A</b>	MB	180	350	<b>493</b>
<b>P+ 6.0wt% PP-MAH+ 2.0wt% 15A</b>	MB	180	350	<b>438</b>
<b>P+ 1.0wt% PP-MAH+ 0.5wt% 25A</b>	MB	180	350	<b>552</b>
<b>P+ 2.0wt% PP-MAH+ 1.0wt% 25A</b>	MB	180	350	<b>489</b>
<b>P+ 4.0wt% PP-MAH+ 2.0wt% 25A</b>	MB	180	350	<b>442</b>
<b>P+ 1.0wt% PP-MAH+ 0.5wt% 30B</b>	MB	180	350	<b>557</b>
<b>P+ 2.0wt% PP-MAH+ 1.0wt% 30B</b>	MB	180	350	<b>499</b>
<b>P+ 4.0wt% PP-MAH+ 2.0wt% 30B</b>	MB	180	350	<b>477</b>

Figure 4.24 shows the SEM images of pristine polypropylene that is not extruded, extruded once and twice, respectively. Particle size analysis reveals that pore sizes were increased after the first extrusion and enlarged even further subsequent to second extrusion process. It was observed that small PE domains that were present in the matrix were coagulated and broken into average sized domains after each process. Moreover, the domains were more uniformly distributed with finer interdomain distances.

During blending, the dispersed phases are stretched until fibers are formed, then they are broken into smaller droplets, and finally drops coalesce and form larger particles [110]. Coalescence is known to be arisen owing to the forced collisions of dispersed domains and their recombination [111]. In order to meet the thermodynamic stabilization of the blend systems, components of the mixture tend to create a phase structure with a minimum total free energy, and input of energy is required to form these new surfaces and interfaces [112]. In addition to that, when the rate of coalescence and breakdown are balanced, the equilibrium particle size is achieved [113].

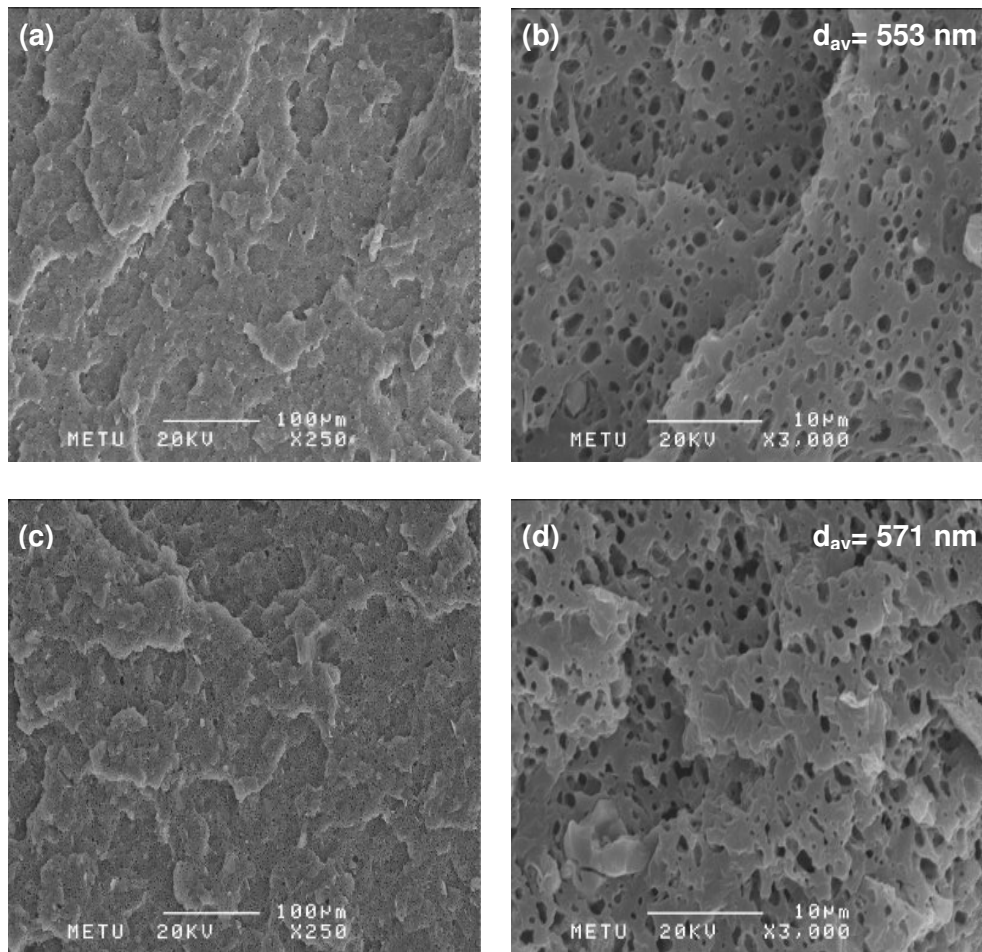
The final domain size is controlled by the viscosity, melt elasticity of the components, shear stresses and rates, mobility of the interface and surface tension [110]. In the case of immiscible blends such as polyethylene and polypropylene the interface is very weak owing to high interfacial tension and it is easy to be broken. Moreover, almost in all incompatible systems coalescence occurs even though small domains are more stable owing to their large surface area. This phenomenon is attributed to the cohesive forces between domains and interfacial mobility of the dispersed phase in terms of statistical theory of the polymer blends [114]. A few excessively large domains in the pristine polymer may be a result of shear intensity which was not adequate to disperse domains homogeneously in the matrix during recycling process. Moreover, considering the increased area of dispersed domains with the application of the extrusion, it can be concluded that, the added energy of mixing during extrusion caused collisions and recombination due to cohesive forces between domains and the weak and mobilized interphase. Since the thermodynamic stabilization was not achieved in the first extrusion step, the domain sizes were further increased after second extrusion.



**Figure 4.24** SEM micrographs of recycled polypropylene a) Not extruded (x3000) b) Not extruded (x10000) c) Extruded once (x3000) d) Extruded once (x10000) e) Extruded twice (x3000) f) Extruded twice (x10000).

Various models of coalescence were developed in the literature. Diffusion of dispersed domains through the matrix is the first step and the second one is collisions between the dispersed domains and the final step is self coagulation. Considering the fast nature of diffusion and coalescence, collision is a relatively slower process and therefore the collision of dispersed phases may be taken as the rate determining step [115]. In Figure 4.25 the morphology of binary blends containing 5 wt% and 10 wt% E-MA-GMA compatibilizer are shown. Adding 5 wt% of elastomer caused a slight decrease in domain size compared to twice extruded pristine polypropylene. The decrease in domain size can be attributed to the reduced possibility of collisions between polyethylene domains due to addition of another elastomeric phase. However, 10 wt% addition of compatibilizer caused increase in the average domain size, since the coalescence of compatibilizer domains became more effective. Moreover, the emerging of enlarged domains compared to the average domain sizes may be a result of inadequate shear intensity which is not sufficient to break down all the domains homogeneously owing to increased compatibilizer content.

According to Figure 4.25, binary blends of E-MA-GMA and recycled polypropylene, the crack lines on the surface of the matrix became shorter and denser with the incorporation of compatibilizer, and they were enhanced further as the added amount of compatibilizer was increased. It is known that the roughness of the surface is an indication of increased amount of energy dissipation during fracture. Addition of elastomeric phase would increase the energy absorption capacity of the matrix. Toughness is also directly related with the energy absorption capability, and mechanical results shown in the subsequent section indicate that the toughness values of these blends increased due to compounding with the compatibilizer phase.



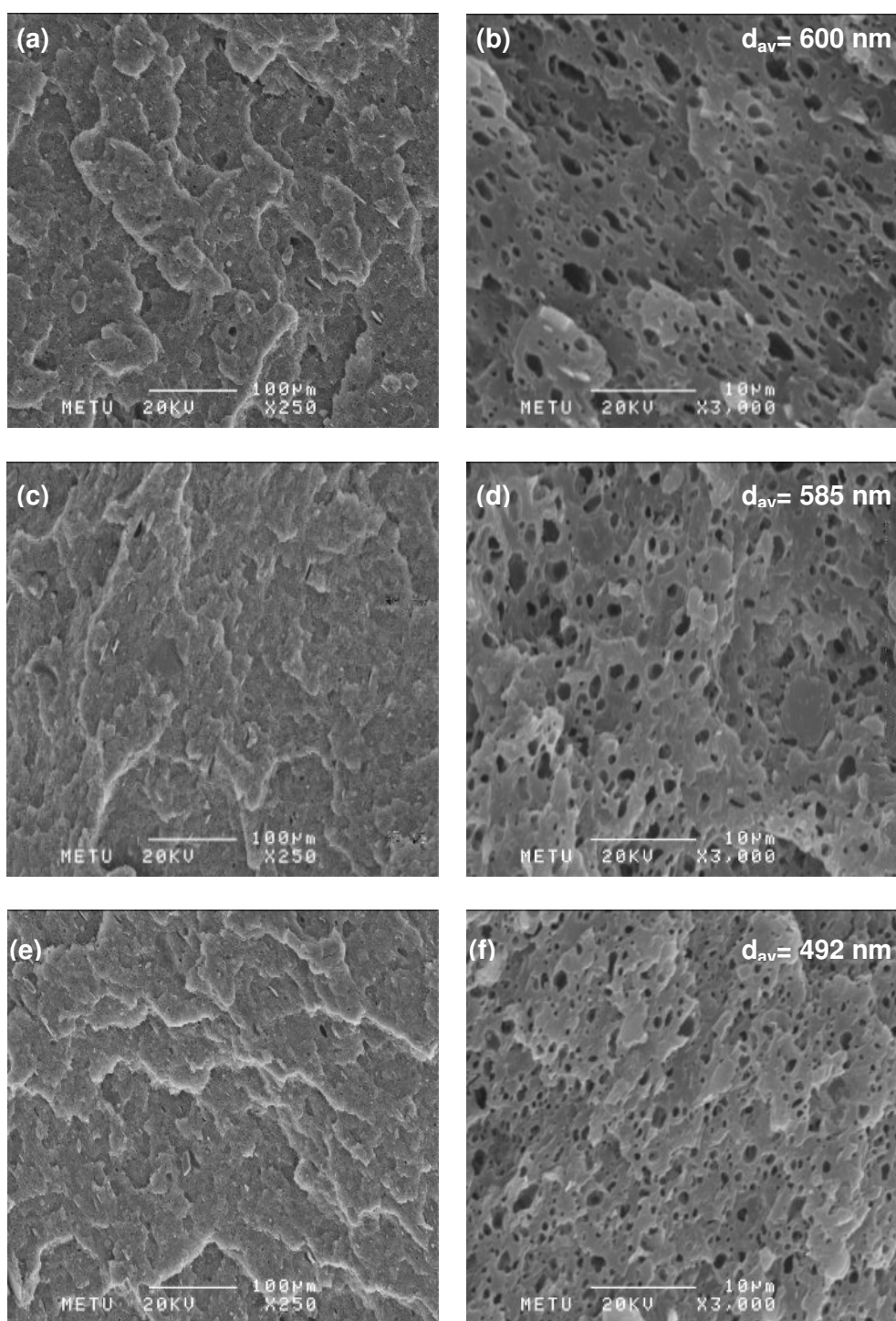
**Figure 4.25** SEM micrographs of binary blends of E-MA-GMA a) 5 wt% (x250) b) 5 wt% (x3000) c) 10 wt% (x250) d) 10 wt% (x3000)

Figure 4.26 shows the binary mixtures of Cloisite® 15A and recycled polypropylene prepared by All-S method at different clay loadings. As clearly observed in the SEM images, increasing clay content from 2 wt% to 6 wt% caused considerable reduction in the size of the polyethylene phase. As stated in the literature, the role of organoclay is very essential for the dispersion of elastomeric phases. The presence of well dispersed organoclay creates a barrier effect and suppresses the agglomeration of the elastomeric domains [53]. The reduction in the size of dispersed domains then can be attributed to the breakage of elastomeric phases into smaller size domains during extrusion and the barrier effect of organoclay that hinders their

recombination. The coalescence of elastomeric phases became more difficult and the domain sizes remained even smaller as the organoclay content was increased.

In Figures 4.27 and 4.28, fracture surface morphology of ternary nanocomposites prepared with E-MA-GMA compatibilizer and Cloisite® 15A organoclay at various loadings and All-S addition order are shown. The reduction of domain size is obvious also in this case, as the organoclay loading is increased. The elastomer domains are larger at 10 wt% compatibilizer content, as in the case of binary blends due to increased elastomer concentration.

There are two main factors affecting the toughness significantly; average domain size and interdomain distances [116]. Considering the lack of homogeneity and the high concentration of the dispersed phase, even in the structure of pristine polymer, it is generally very hard to interpret the effects of interdomain distance for most of the compositions. Therefore, the physical observations are usually attached to the particle size and crack propagation lines. When the toughness values of ternary nanocomposites are examined, the general trend is an inverse relation between toughness and added organoclay amount. SEM images show that the clay particles are dispersed in the polymer matrix and number of clay particles increases at high clay loadings. Moreover, it is observed that when the E-MA-GMA particles are incorporated into the polymer, the silicate layers become closer to each other and create micron sized rough surfaces which might act as crack tips. In addition to that, the circular shape of the elastomeric domains become more formless and a less uniform particle distribution is observed. According to TEM images, silicate layers mostly resided inside the polyethylene domains in the absence of compatibilizer. After adding E-MA-GMA, the compatibilizer domains would be coagulated with polyethylene domains due to compatible ethylene backbone and the affinity of organoclay to matrix would increase. Owing to cohesive forces of organoclay particles, they would form domains of silicate layers inside the matrix.



**Figure 4.26** SEM micrographs of binary nanocomposites of P and Cloisite® 15A prepared by All-S method a) 2 wt% (x250) b) 2 wt% (x3000) c) 4 wt% (x250) d) 4 wt% (x3000) e) 6 wt% (x250) f) 6 wt% (x3000).

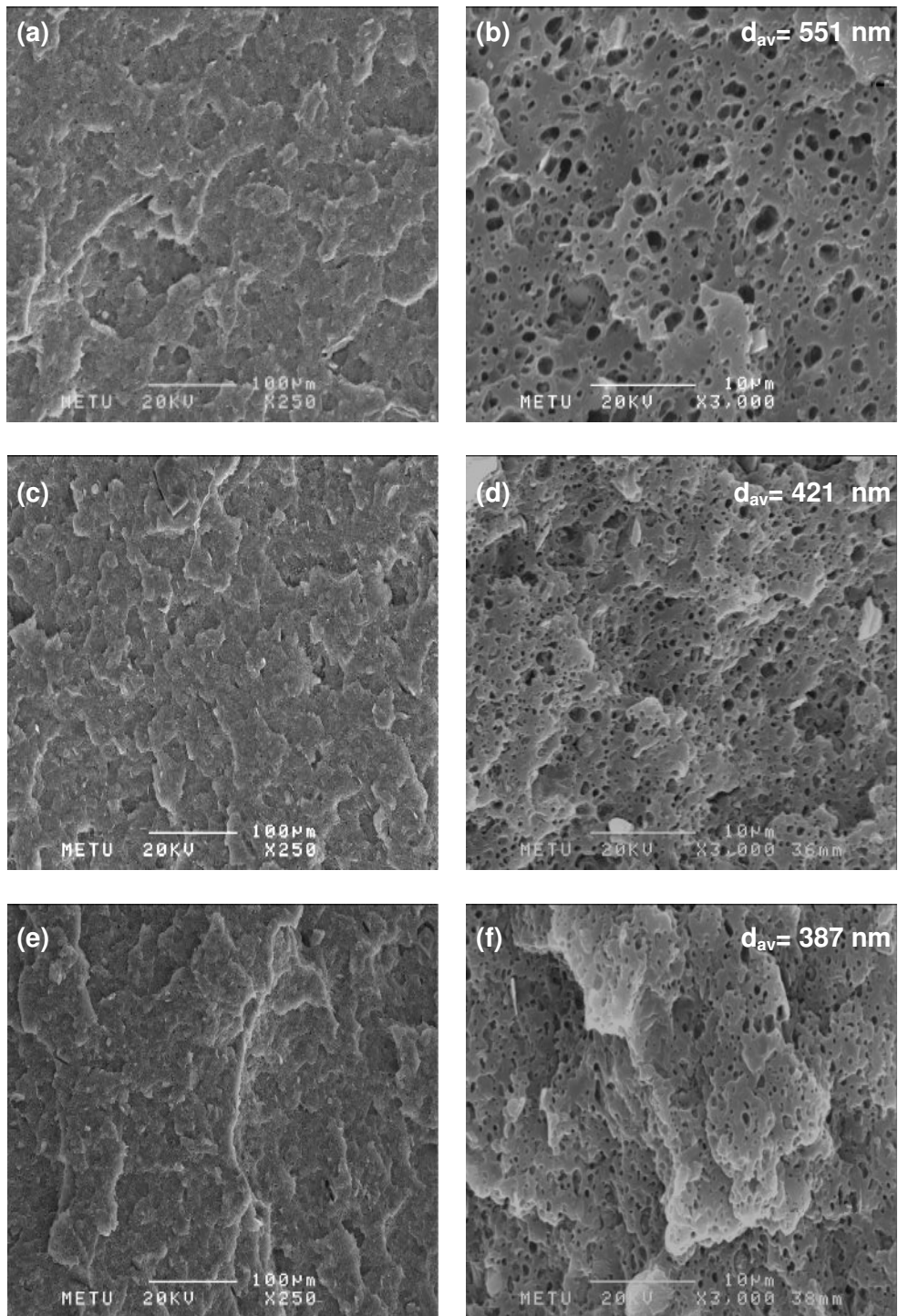


**Figure 4.27** SEM micrographs of ternary nanocomposites containing 5 wt% E-MA-GMA and Cloisite® 15A at various compositions a) 2 wt% 15A (x250) b) 2 wt% (x3000) 15A c) 4 wt% 15A (x250) d) 4 wt% 15A (x3000) e) 6 wt% 15A (x250) f) 6 wt% 15A (x3000).

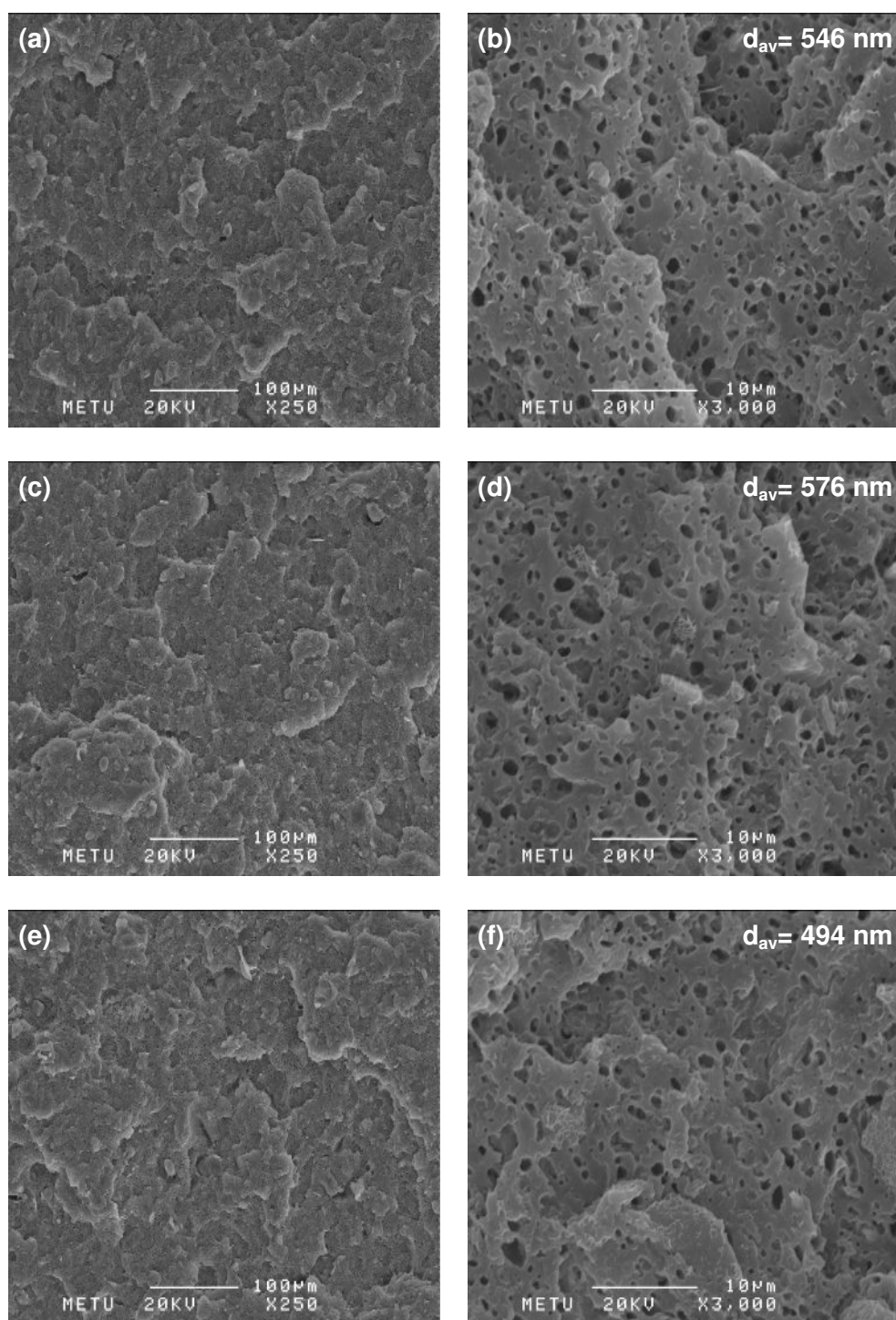


**Figure 4.28** SEM micrographs of ternary nanocomposites containing 10 wt% E-MA-GMA and Cloisite® 15A at various compositions a) 2 wt% 15A (x250) b) 2 wt% (x3000) 15A c) 4 wt% 15A (x250) d) 4 wt% 15A (x3000) e) 6 wt% 15A (x250) f) 6 wt% 15A (x3000).

Effects of processing parameters on the morphologies of the nanocomposites are shown in Figures 4.29 and 4.30. Since polypropylene is a crystalline thermoplastic, the micromorphological structure of the resin such as its crystallinity, crystal size, and degree of orientation depend very much on processing conditions (temperature, flow rate, pressure etc.). Therefore, the processing conditions significantly affect the properties of the polymeric composites and blends [117]. When the nanocomposite prepared with E-MA-GMA compatibilizer at 200 °C temperature and 350 rpm screw speed is examined, almost no change is detected compared to the one prepared at 250 rpm and same processing temperature. However, at lower temperature of 180 °C, a slight decrease in domain size is observed. Results obtained in nanocomposites containing E-MA-GMA compatibilizer are also detected in the nanocomposites containing PP-MAH compatibilizer. These results could be assigned to high matrix viscosity at low temperature profile. Significant effects of shear rate and shear stresses on the homogeneous dispersion of the elastomeric domains are already known [110]. Similarly for nanocomposites prepared at 180°C, the exerted shear stress on the polymer matrix would be higher owing to high matrix viscosity. In addition to that, XRD results also suggest a better dispersion of clay platelets at low processing temperature and high screw speed. In addition to high shear exerted on the polymer, the barrier effect of well dispersed organoclay also contributed to reduction in domain sizes and more uniform domain distribution.

When the toughness values shown later are considered, a general increase is also observed as the temperature profile is decreased and screw speed is increased. There might be two reasons for this result: first one could be the reduction of the domain size of the elastomeric phase affecting toughness properties positively, since the domain sizes are large enough to prevent crack propagation, and interactions with the matrix are higher due to higher interfacial area at this organoclay content; and the second reason is reduced crack propagation possibility owing to good dispersion of organoclay layers.

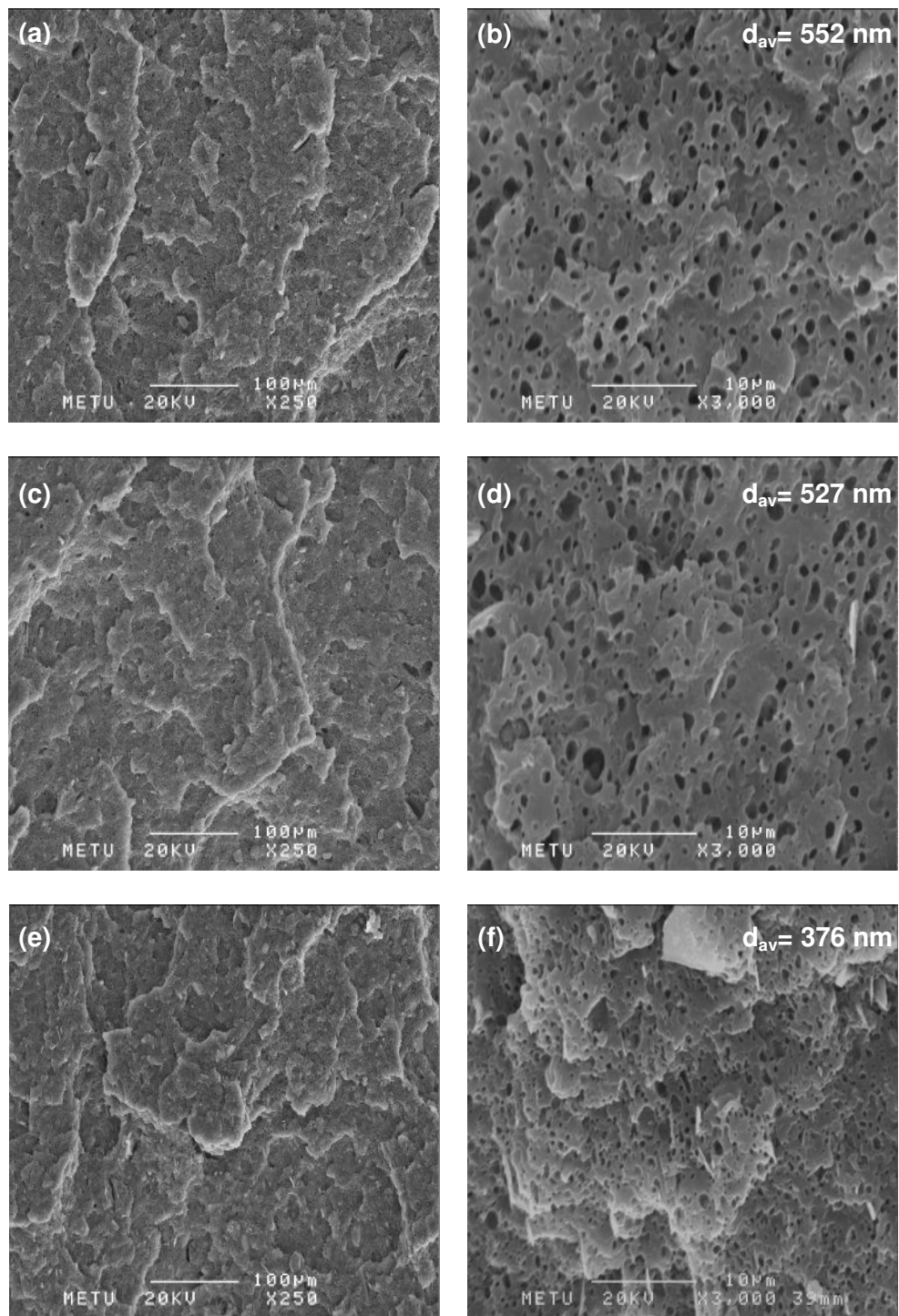


**Figure 4.29** SEM micrographs of ternary nanocomposites containing 2 wt% Cloisite® 15A and 5 wt% E-MA-GMA prepared by All-S method and at various processing conditions a) 200°C-350rpm (x250) b) 200°C-350rpm (x3000) c) 180°C-250rpm (x250) d) 180°C-250rpm (x3000) e) 180°C-350rpm (x250) f) 180°C-350rpm (x3000).

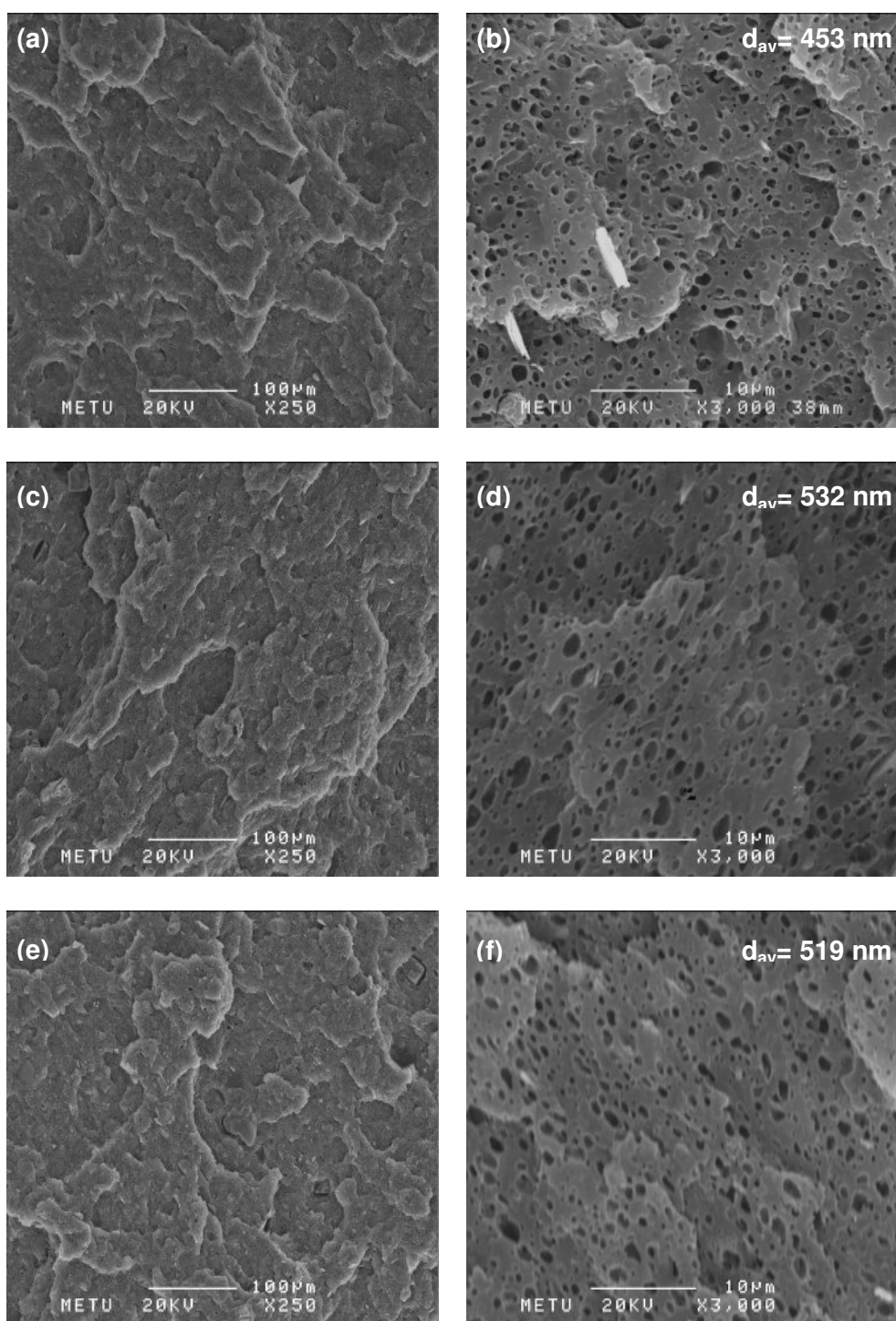


**Figure 4.30** SEM micrographs of ternary nanocomposites containing 1 wt% Cloisite® 15A and 2 wt% PP-MAH prepared by All-S method and at various processing conditions a) 200°C-250rpm (x250) b) 200°C-250rpm (x3000) c) 200°C-350rpm (x250) d) 200°C-350rpm (x3000) e) 180°C-250rpm (x250) f) 180°C-250rpm (x3000).

Effect of PP-MAH compatibilizer to organoclay ratio was investigated in the next part of the study. Figure 4.31 shows the SEM images of binary blends prepared PP-MAH and recycled PP and, Figures 4.32-4.34 illustrate the morphology of the ternary nanocomposites containing PP-MAH and Cloisite® 15A having compatibilizer to organoclay ratio of 1, 2 and 3 respectively.

In the binary blends of PP-MAH and recycled polymer, it is observed that the domain sizes of the elastomeric phases are reduced while the interdomain distances are increased as the PP-MAH content increases. In addition to that, the crack propagation lines became more observable. Li et al. [56] reported that, even though the polyethylene and polypropylene phases in the blend matrix are immiscible, the dynamic mechanical and mechanical properties of the blends exhibit an interfacial interaction between the two phases in the presence of PP-MAH compatibilizer. Therefore, the decrease in the particle size could be attributed to high interfacial adhesion, low interfacial mobility and high matrix viscosity as also indicated by the MFI values shown later. Particle coalescence would partially decrease owing to lower interfacial mobility and high shear, and hence reduction in particle size would occur. Toughness values shown later also increased with PP-MAH addition in accordance with the domain size reduction and increase in interdomain distances. In ternary nanocomposites containing PP-MAH, the reduction of the particle size, uniform distribution of the elastomeric phase and crack propagation lines are also significant.

It is a very well known fact that the presence of an interfacial agent or a compatibilizer can stabilize the morphology in blends and hinder coarsening. This stabilizing effect is believed to occur owing to two reasons: reduced interfacial tension and the accommodation of the compatibilizer at the interface forming a protecting layer which hinders the coalescence [54, 55]. Besides interfacial adhesion, size and uniformity of the dispersed phase are also affected from resulting compatibility [117]. Therefore, the reduction of the domain size in the PP-MAH containing materials could take place due to several reasons. One of the reasons could be the diffusion of PP-MAH particles between the cavities of the dispersed polyethylene phase and polypropylene matrix owing to its low viscosity rather than exhibiting coalescence. Hence, PP-MAH domains would strengthen and immobilize the interface and prevent polyethylene phase coagulation and provide a uniform domain distribution.

Reduction in interfacial tension due to chemical bonding would be expected if one of the phases had polar groups in this blend. However, in literature it is stated that Van Der Waals attraction may also give the sufficient adhesion for toughening, and chemical bonding is not necessary in all cases [118]. Moreover, the presence of chemical functionalities such as carbonyl and hydroxyl groups would promote the interaction of components in polymer blends [119]. Considering chemical compatibility of PP groups of the PP-MAH with the matrix and the functional groups it constitutes, it can be concluded that the PP-MAH provides adhesion between two immiscible phases and enhances interface (i.e. PP and PE) between the matrix and the dispersed phase.

In Figures 4.32 to 4.34 the SEM micrographs of nanocomposites prepared with different Cloisite® 15A organoclay to PP-MAH compatibilizer ratios are shown. When these images are examined it is observed that, uniform domain size and distribution are more remarkable for the nanocomposites having high compatibilizer to organoclay ratio. The best dispersion among all nanocomposites is observed in the nanocomposite containing 6 wt% PP-MAH and 2 wt% Cloisite® 15A. The reduction in particle size and increase in interdomain distances are significant. This composition also has the best mechanical properties and the organoclay layers in the structure are highly exfoliated according to TEM images. These results could be attributed to enhanced adhesion due to the increased amount of PP-MAH and also to the well dispersion of organoclay layers inhibiting possible coagulation of the dispersed phase. Consequently, domains were formed with an optimum domain size and interdomain distances. Moreover, interaction between the maleic anhydride group and the organoclay would cause an increase in viscosity value and reduction in the particle size as a result of application of high shear and enhanced dispersion. When their MFI values shown later are analyzed, a significant reduction in MFI value and hence an increase in the melt viscosity is observed which supports the idea. Basically, as the amount of compatibilizer domains are increased, the possibility of interdomain interaction increases and therefore the viscosity increases. The resultant synergistic effect of adhesion and interactions cause reduction in the domain sizes.

In the final part of the study, the effect of clay type was investigated. Figures 4.35 and 4.36 show the SEM micrographs of binary composites prepared with different organoclays at 1 and 2 wt% clay loadings. In these composites, reduction in domain size at 1 wt% organoclay loading is observed regardless of the type of organoclay.

These results could be a consequence of good dispersion and barrier effect of organoclay layers at low concentration.

In the ternary blends having compatibilizer to PP-MAH ratio 2, as shown in Figures 4.37 and 4.38, the reduction of the domain size is apparent as the additive amount is increased. Enhanced particle uniformity is expected in the nanocomposites containing Cloisite® 30B organoclay owing to good dispersion of organoclay and the possible reactions between maleic anhydride groups of the PP-MAH and the hydroxyl groups of the organoclay. However, all the samples having similar organoclay and PP-MAH loadings represented almost the same dispersion behavior and tortuous crack propagation path independent of the organoclay type. These results are consistent with the impact toughness values shown later where similar trends are also observed with addition of different organoclay types in both binary and ternary nanocomposites.

In conclusion, the dispersion of the elastomeric polyethylene phase is promoted with organoclay and compatibilizer additions. Better dispersion is obtained due to barrier effect of organoclay, enhanced adhesion between matrix and the domains by incorporation of compatibilizer, and increased melt viscosity and hence shear stress on the dispersed phase at low temperatures. Finally, a significant difference on the morphology is not observed with addition of different types of organoclays.

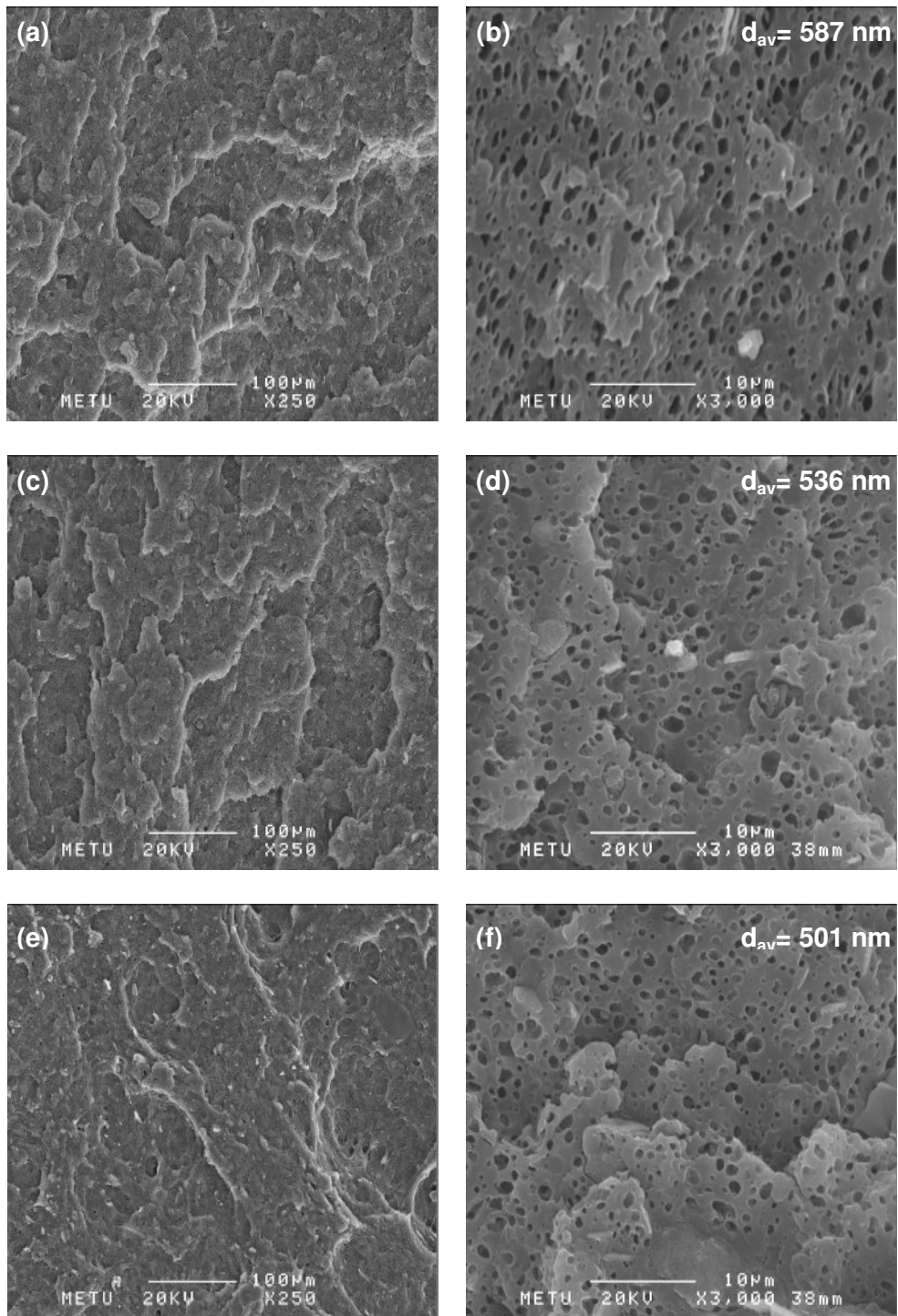


**Figure 4.31** SEM micrographs of binary blends containing PP-MAH at various contents a) 2 wt% (x250) b) 2 wt% (x3000) c) 4 wt% (x250) d) 4 wt% (x3000) e) 6 wt% (x250) f) 6 wt% (x3000).

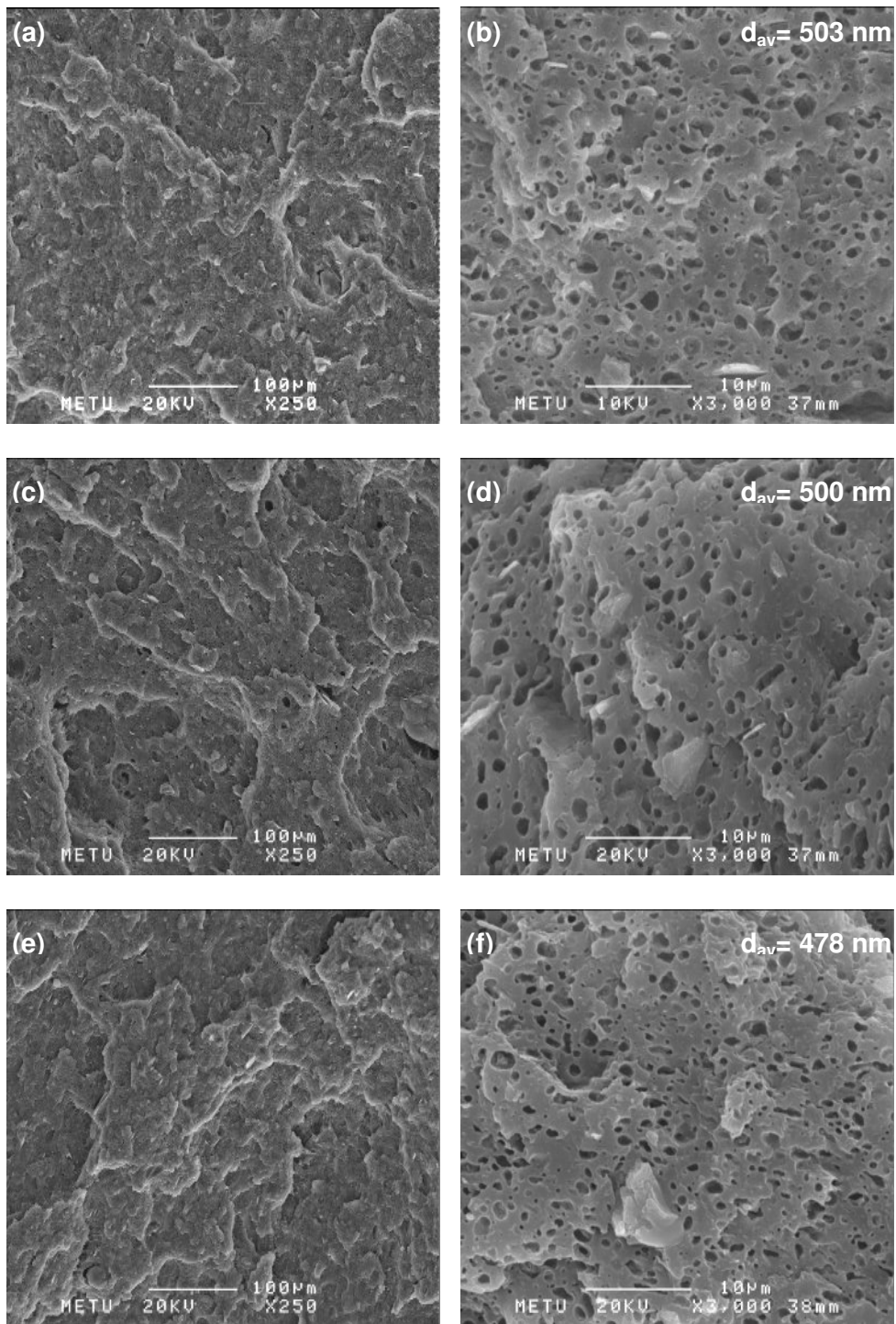


**Figure 4.32** SEM micrographs of ternary nanocomposites prepared with Cloisite® 15A at PP-MAH to organoclay ratio of 1 a)P+0.5wt%PP-MAH+0.5wt%15A (x250) b)P+0.5wt%PP-MAH+0.5wt%15A (x3000) c)P+1.0wt%PP-MAH+1.0wt%15A (x250) d)P+1.0wt%PP-MAH+1.0wt%15A (x3000) e)P+2.0wt%PP-MAH+2.0wt%15A (x250) f)P+2.0wt%PP-MAH+2.0wt%15A (x3000).

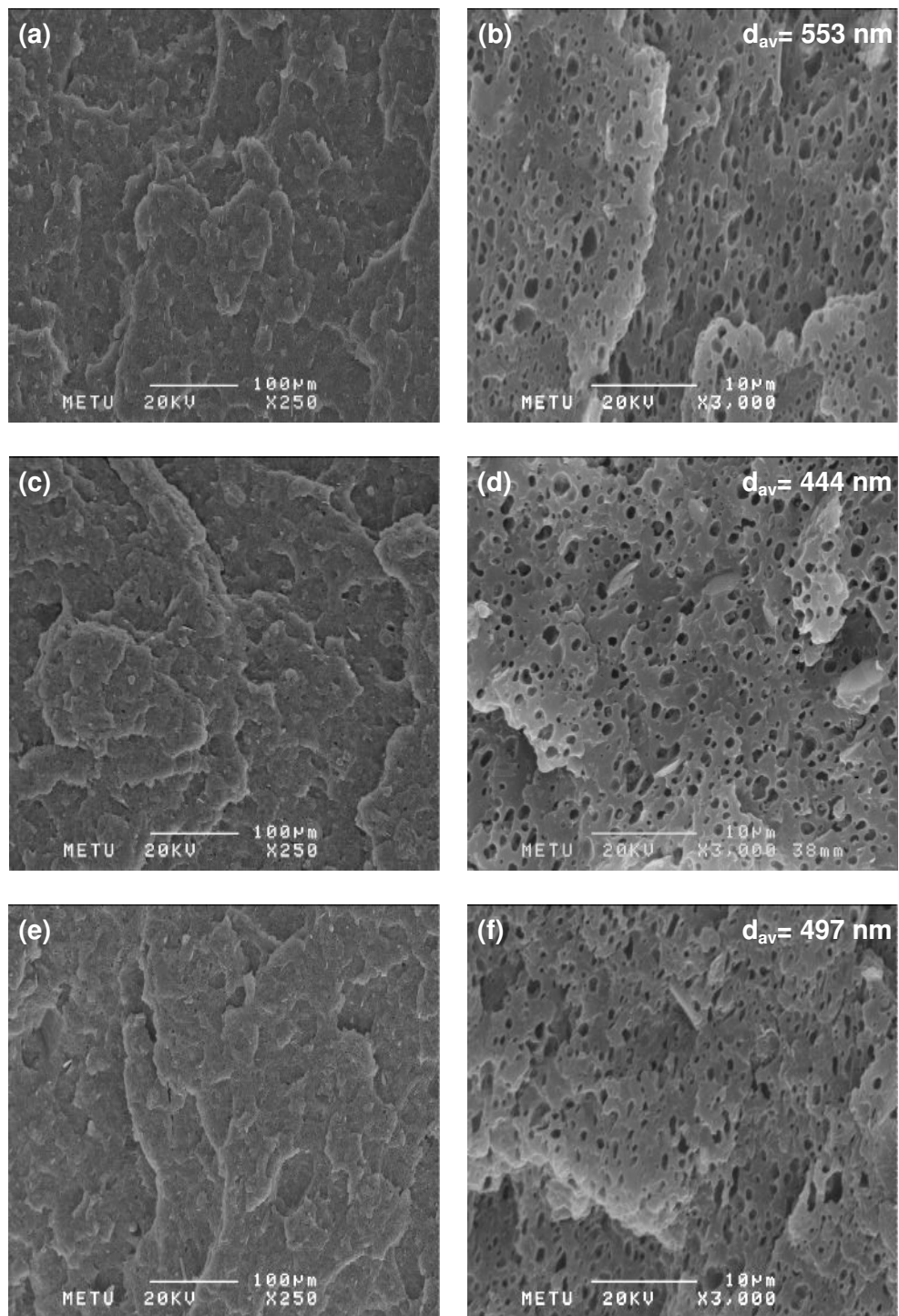


**Figure 4.33** SEM micrographs of ternary nanocomposites prepared with Cloisite® 15A at PP-MAH to organoclay ratio of 2 a)P+1.0wt%PP-MAH+0.5wt%15A (x250) b)P+1.0wt%PP-MAH+0.5wt%15A (x3000) c)P+2.0wt%PP-MAH+1.0wt%15A (x250) d)P+2.0wt%PP-MAH+1.0wt%15A (x3000) e)P+4.0wt%PP-MAH+2.0wt%15A (x250) f)P+4.0wt%PP-MAH+2.0wt%15A (x3000).

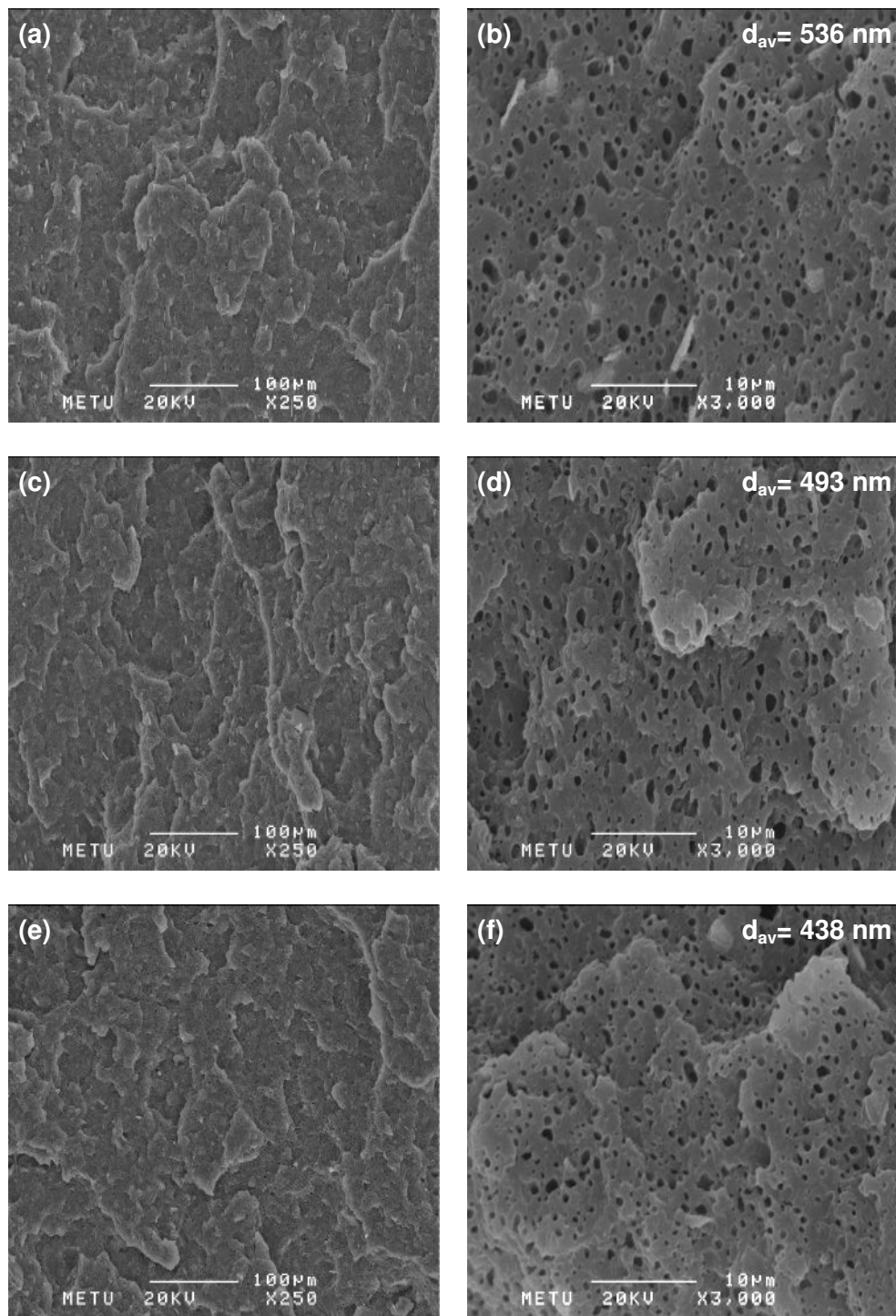


**Figure 4.34** SEM micrographs of ternary nanocomposites prepared with Cloisite® 15A at PP-MAH to organoclay ratio of 3 a)P+1.5wt%PP-MAH+0.5wt%15A (x250) b)P+1.5wt%PP-MAH+0.5wt%15A(x3000) c)P+3.0wt%PP-MAH+1.0wt%15A (x250) d)P+3.0wt%PP-MAH+1.0wt%15A (x3000) e)P+6.0wt%PP-MAH+2.0wt%15A (x250) f)P+6.0wt%PP-MAH+2.0wt%15A (x3000).

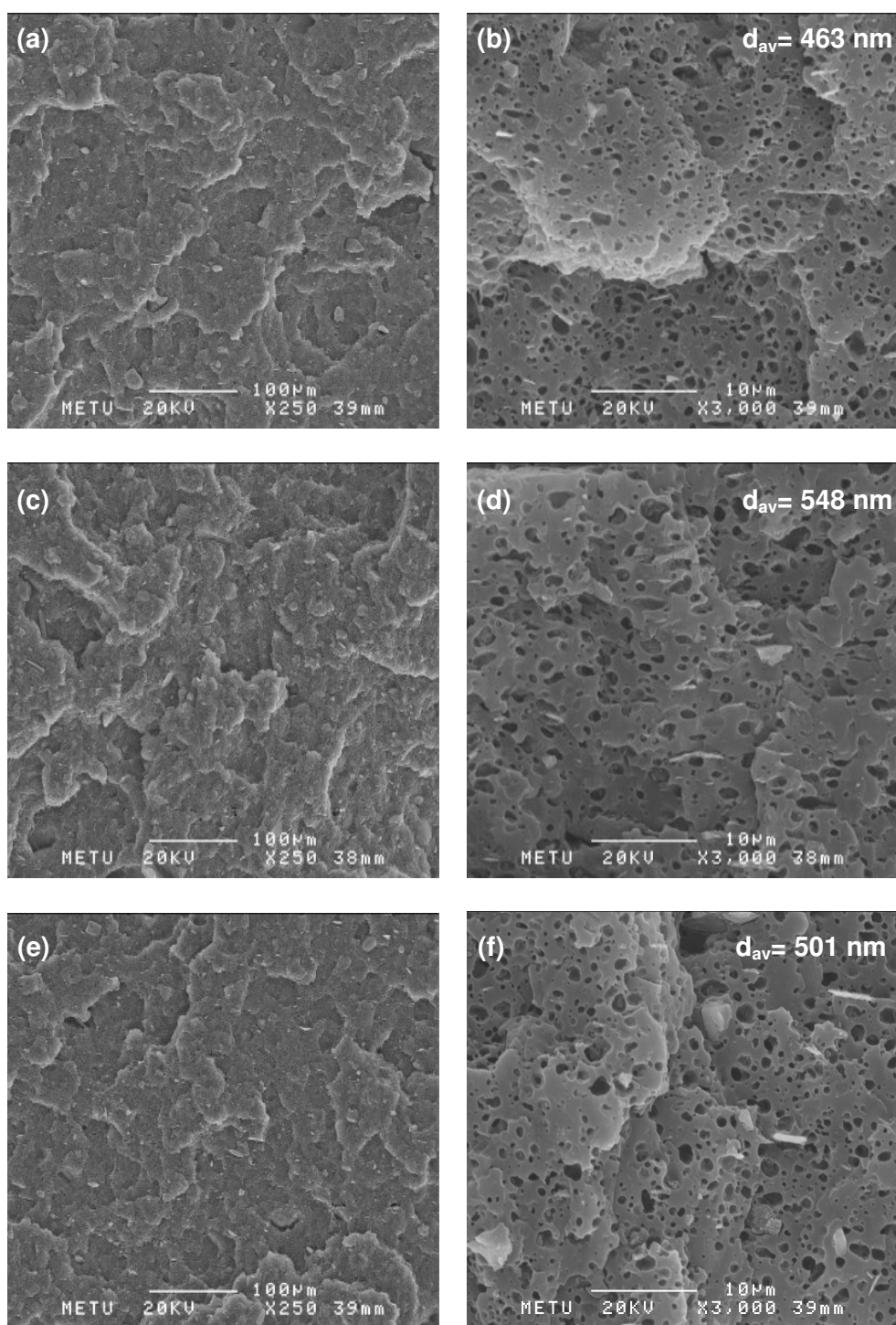


**Figure 4.35** SEM micrographs of binary nanocomposites containing 1 wt% different types of organoclays a) 15A (x250) b) 15A (x3000) c) 25A (x250) d) 25A (x3000) e) 30B (x250) f) 30B (x3000).

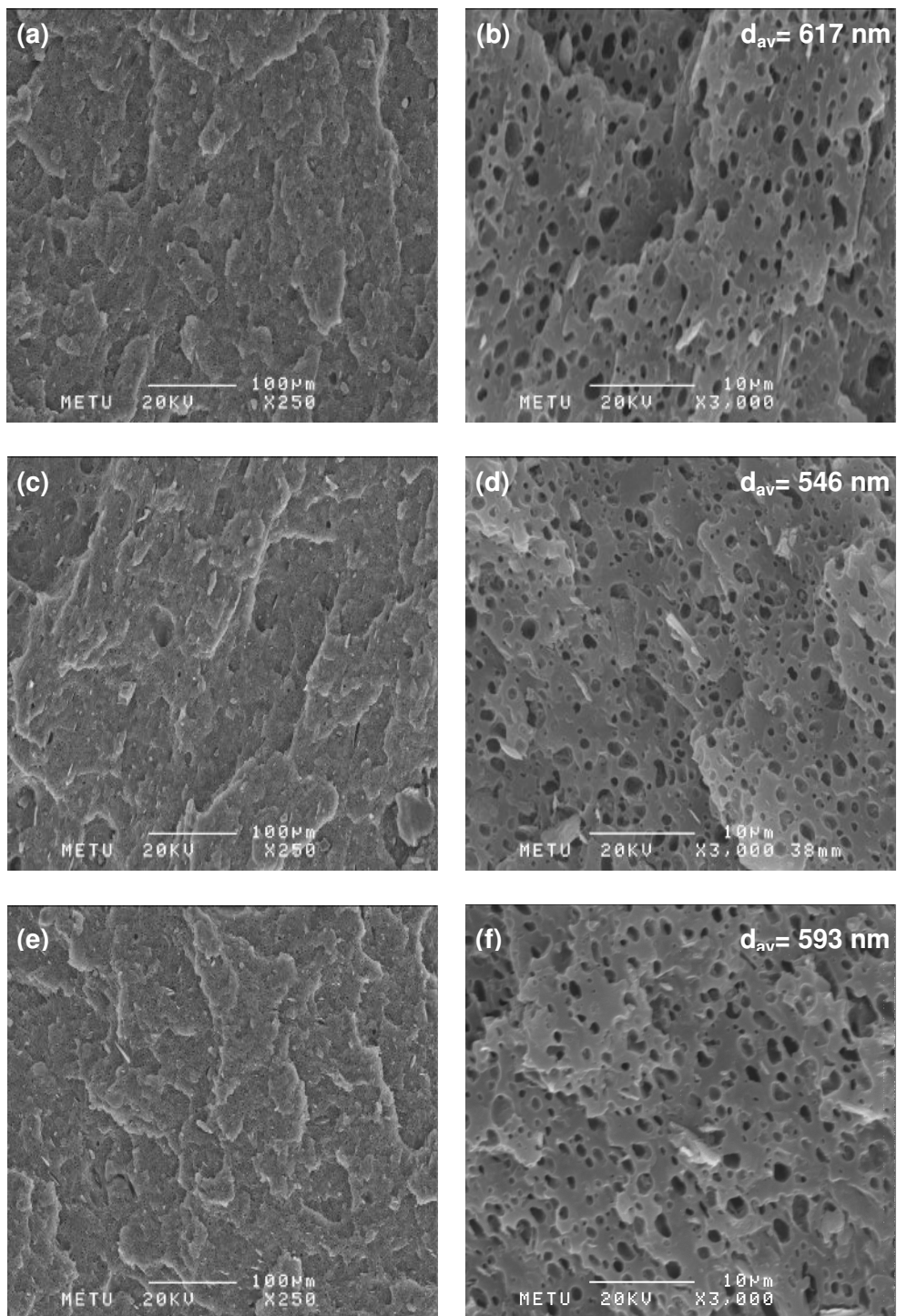


**Figure 4.36** SEM micrographs of binary nanocomposites containing 2 wt% different types of organoclays a) 15A (x250) b) 15A (x3000) c) 25A (x250) d) 25A (x3000) e) 30B (x250) f) 30B (x3000).

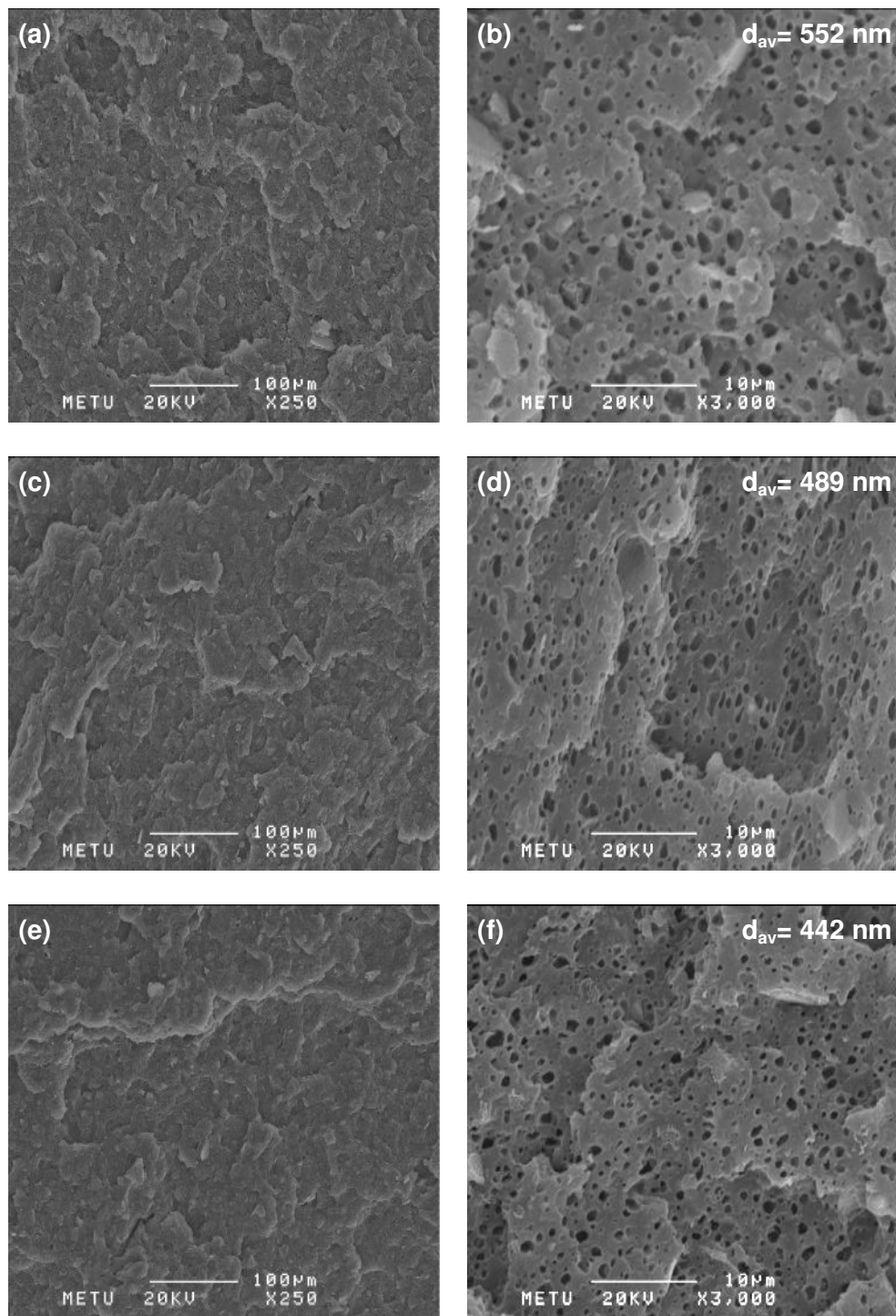


**Figure 4.37** SEM micrographs of ternary nanocomposites prepared Cloisite® 25A at PP-MAH to organoclay ratio of 2 a)P+1.0wt%PP-MAH+0.5wt%25A (x250) b)P+1.0wt%PP-MAH+0.5wt%25A(x3000) c)P+2.0wt%PP-MAH+1.0wt%25A (x250) d)P+2.0wt%PP-MAH+1.0wt%25A (x3000) e)P+4.0wt%PP-MAH+2.0wt%25A (x250) f)P+4.0wt%PP-MAH+2.0wt%25A (x3000).

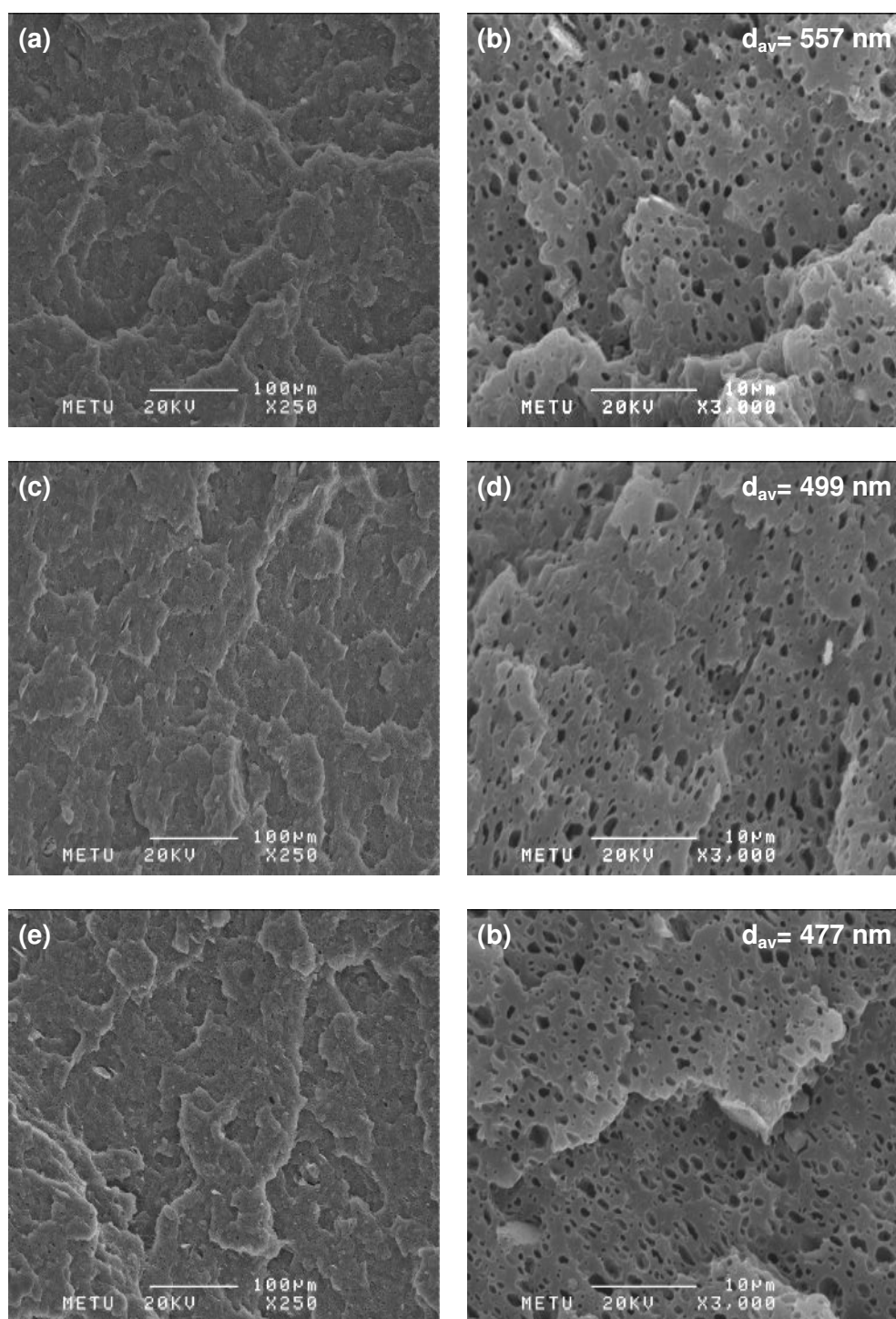


**Figure 4.38** SEM micrographs of ternary nanocomposites prepared Cloisite® 30B at PP-MAH to organoclay ratio of 2 a)P+1.0wt%PP-MAH+0.5wt%30B (x250) b)P+1.0wt%PP-MAH+0.5wt%30B(x3000) c)P+2.0wt%PP-MAH+1.0wt%30B (x250) d)P+2.0wt%PP-MAH+1.0wt%30B (x3000) e)P+4.0wt%PP-MAH+2.0wt%30B (x250) f)P+4.0wt%PP-MAH+2.0wt%30B (x3000).

## **4.2 Mechanical Properties**

Mechanical properties are related with the response and resistance capacity of the materials to load deformation applied in various manners. In this study, tensile and Charpy impact tests were conducted in order to evaluate the degree of improvements in stiffness and toughness properties owing to modifications. The effects of organoclay and compatibilizer compositions, effects of processing conditions, the ratio between the compatibilizer and organoclay as well as organoclay types on performance of the nanocomposites were analyzed.

### **4.2.1 Tensile Tests**

Young's Modulus, tensile stress at yield, tensile strength and elongation at break (%) values were determined from the stress-strain curves of the materials obtained during tensile tests. Stress-strain curves of recycled polypropylene and prepared nanocomposites are shown in Figures 4.40 to 4.63 and their numerical values were given in Appendix A.

Typical stress strain curves of recycled polypropylene used in this study is illustrated in Figure 4.39. According to the figure, material represents a ductile behavior and yields at a specific strain. Yielding was followed by cold drawing and strain hardening due to stretched polymer chains in the direction of load. Recycled polypropylene exhibits similar extension behavior as pure polypropylene does. However, the stiffness value is lower and elongation at break values are higher compared to a pure isotactic polypropylene since recycled polypropylene contains polyethylene domains.

The tensile test values of recycled polypropylene, in neat form, extruded once and twice values were quite similar and Young's Modulus, tensile stress at yield, tensile strength and elongation at break values of the materials were 879.7 MPa, 28.2 MPa, 34.8 MPa and 524%, respectively.

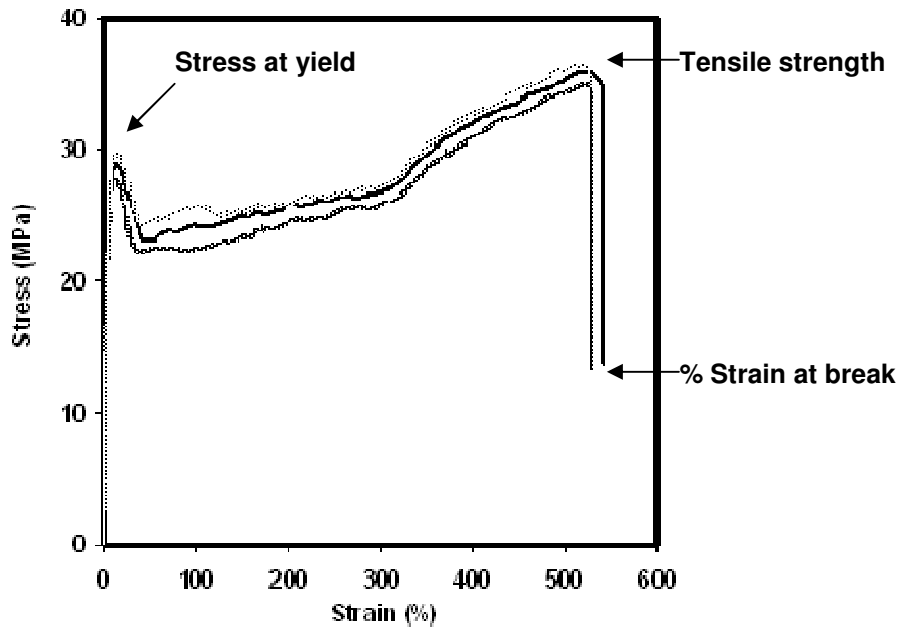


**Figure 4.39** Typical stress-strain curve of recycled polypropylene.

In Figures 4.40-4.43 the tensile properties of blends and nanocomposites prepared with E-MA-GMA type compatibilizer, Cloisite® 15A organoclay and recycled polypropylene at various compositions are shown. Young's Modulus and tensile strength values of binary blends prepared with E-MA-GMA decreased upon addition of compatibilizer. Decrease in the stiffness values of the materials is attributed to the dilution effect of the compatibilizer since E-MA-GMA itself has a lower tensile modulus (measured as 8 MPa) compared to the matrix. Moreover higher % elongation at break and toughness values were detected as a result of incorporation of 5 wt% compatibilizer and further increase was obtained with 10 wt% compatibilizer addition. During elongation, elastomeric phase acts as a stress concentrator and thus yielding or crazing occur around the rubbery phase. Thus, polymer absorbs high amount of energy, avoids highly localized strain and hence may elongate to a greater extent [120]. As the amount of the elastomeric phase is increased the pathway of the crack becomes more tortuous and more energy can be absorbed. Therefore the increase in % elongation at break values was reasonable. On the other hand, as the % elongation at break increases the yield stress values become lower which might be aroused due to the plastic deformation mechanism involving dilatation strain as

mentioned in the literature [110]. Since rubbery phase addition has positive effects on plastic deformation mechanism, the elastic region might become less effective and end up with decrease in stiffness values such as Young's Modulus.

Incorporation of organoclay caused increase in Young's Modulus and tensile stress at yield values, while reduction was observed in % elongation at break and tensile strength values in binary composites except for 2 wt% organoclay content. Enhancement in both modulus and yield stress indicates the reinforcing effect of organoclay owing to its high aspect ratio, platelet structure and large contact area with the polymer matrix [53, 121]. Considering the XRD values, the increase in the d spacing value was observed only in nanocomposites containing 2 wt% organoclay. Since insertation of the polymer chain inside clay galleries leads to an increase in contact area between clay and polymer, the increase in modulus value for this composition is expected. However, with higher concentrations of organoclay (4 wt% and 6 wt%) the XRD peaks were shifted to higher angles indicating reductions in interlayer distance. Then, the enhancement of modulus and yield stress of composites containing 4 wt% and 6 wt% organoclay could have occurred due to two reasons: increased crystallinity and/or reduction in the spherulite size [80, 122]. Silicate layers may act as nucleating agents and promote heterogeneous crystallization [85]. As observed in DSC measurements shown later, increase in crystallinity values were obtained in both polyethylene and polypropylene segments due to addition of organoclay, thus the increase in modulus and yield stress values of composites containing high amounts of organoclay could be due to increased crystallinity. Elongation at break values at higher clay content increased marginally at 2 wt% organoclay loading and then decreased. This increase at 2 wt% loading could be attributed to the good dispersion as observed in the XRD pattern that allows chain mobility under extension. Elongation at break values decrease with reduction of polymer chain mobility owing to presence of clay platelets [123]. In addition, silicate layers can not undergo elongation under applied external stresses due to their rigid structure [110]. Considering possible reduction of the tie chain amount between crystalline domains, the stress could not be transferred through the sample and an early rupture might occur [122]. Regarding to early rupture, material can not reach its ultimate stress value and tensile strength at break value may diminish as also observed in this case.

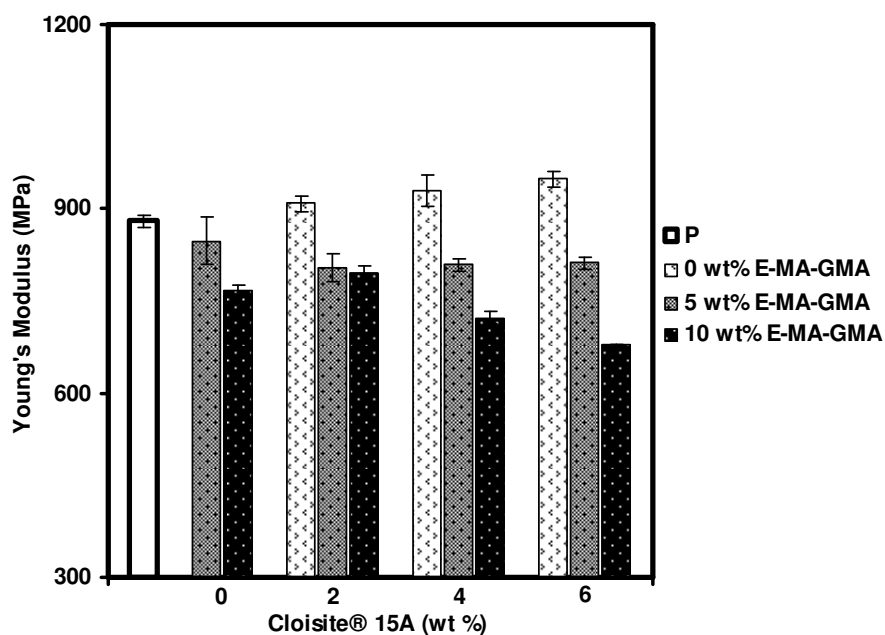


**Figure 4.40** Young's Modulus of blends and nanocomposites prepared with E-MA-GMA compatibilizer (200° C, 250 rpm, All-S).

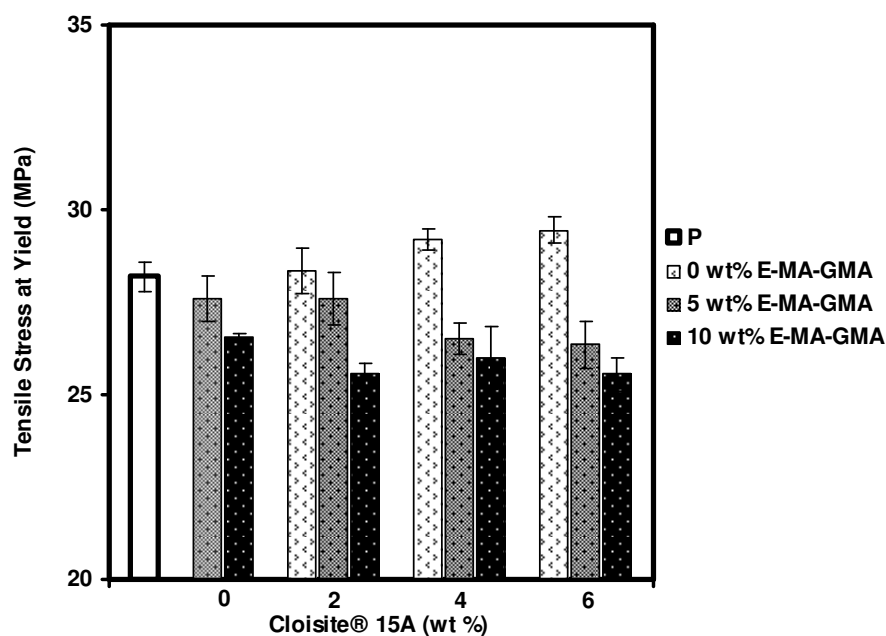


**Figure 4.41** Tensile stress at yield of blends and nanocomposites prepared with E-MA-GMA compatibilizer (200° C, 250 rpm, All-S).

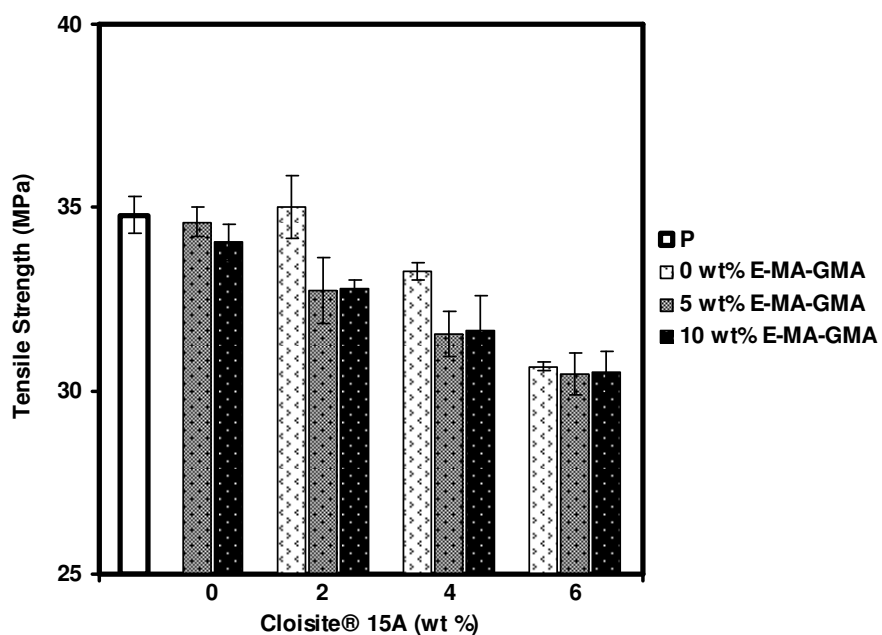


**Figure 4.42** Tensile strength of blends and nanocomposites prepared with E-MA-GMA compatibilizer (200° C, 250 rpm, All-S).

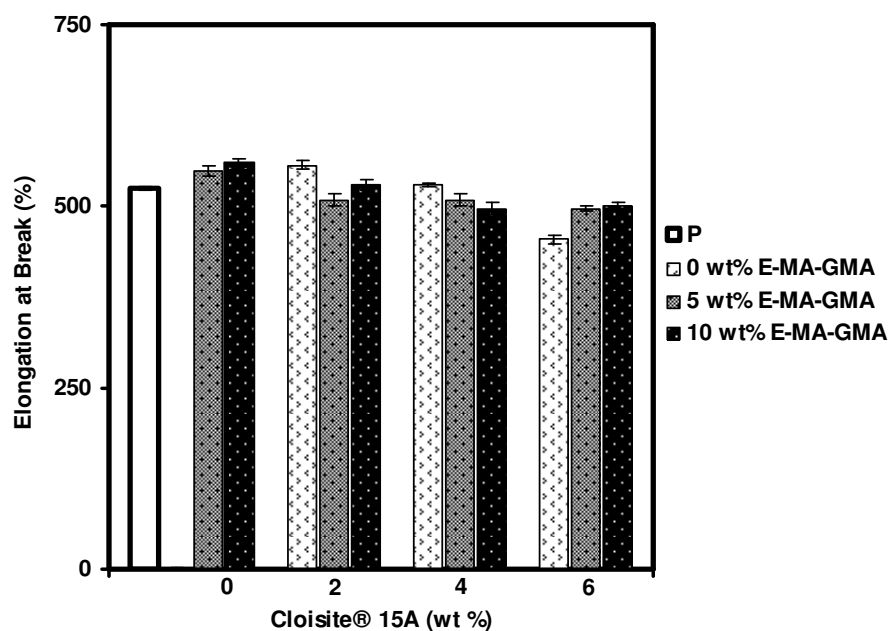


**Figure 4.43** Elongation at break (%) of blends and nanocomposites prepared with E-MA-GMA compatibilizer (200° C, 250 rpm, All-S).

Ternary nanocomposites of E-MA-GMA and Cloisite® 15A exhibit a general reduction trend for tensile properties. The idea behind addition of a compatibilizer phase is to provide better organoclay dispersion and compensate the decrease in the toughness values aroused due to the presence of silicate layers. Young's Modulus and tensile stress at yield values decreased upon compatibilizer addition in ternary nanocomposites and these reductions in the mentioned properties were higher when compatibilizer content was increased to 10 wt%. This result would have occurred due to increased elastomeric domain sizes as observed in SEM values and possible incompatibility between the matrix and the dispersed phase. General decreasing trend was also observed in elongation at break and tensile strength values of ternary nanocomposites. The decrease was more significant when the amount of clay was higher, namely for 4 wt% and 6 wt% clay contents. Immiscible aggregates of clay platelets may act as defects and stress concentrators in the matrix promoting failure mechanism [124]. Moreover, the number of micro voids in the matrix formed due to addition of organoclay would be increased with further addition of organoclay and micro void combination would cause tearing and failure in the matrix. Addition of 10 wt% compatibilizer reduced the negative effect of excess clay incorporation to some extent, however the % elongation at break values were still poor compared to pristine polymer.

The effects of processing conditions on tensile properties of ternary nanocomposites prepared with Cloisite® 15A organoclay, E-MA-GMA or PP-MAH compatibilizer are shown in Figures 4.44-4.47. The first groups in the figures illustrate the nanocomposites with 2 wt% organoclay and 5wt% E-MA-GMA prepared with All-S addition order and second group illustrate nanocomposites containing 1 wt% organoclay and 2 wt% PP-MAH compatibilizer prepared with MB method. Two types of compatibilizers were used in order to analyze whether the same effect could be observed using different types of compatibilizers. Effects of compatibilizers on final mechanical properties were not compared, since elastomer and organoclay compositions and the addition orders were different and incomparable.

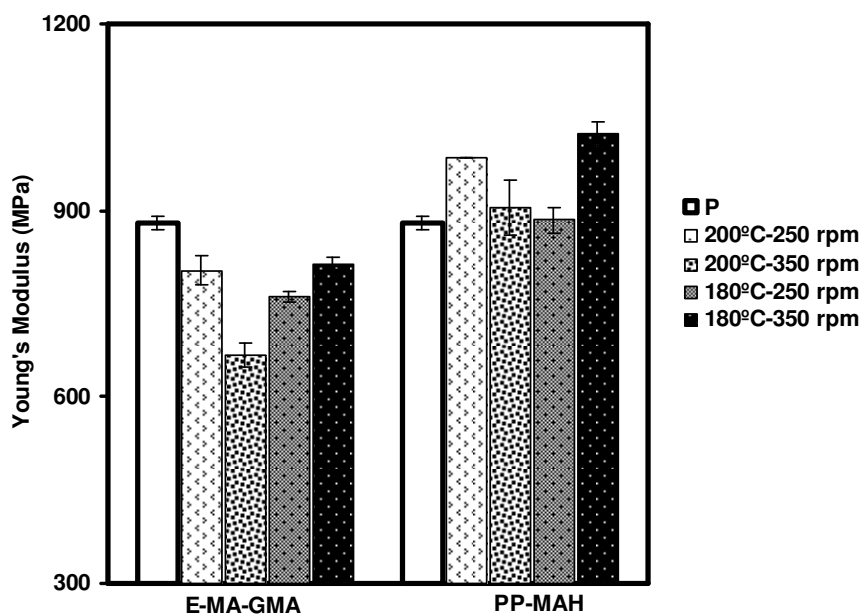


**Figure 4.44** Young's Modulus of nanocomposites containing 5 wt% E-MA-GMA and 2 wt% Cloisite® 15A (on the left) and 2 wt% PP-MAH and 1 wt% Cloisite® 15A (on the right) prepared under different processing conditions.

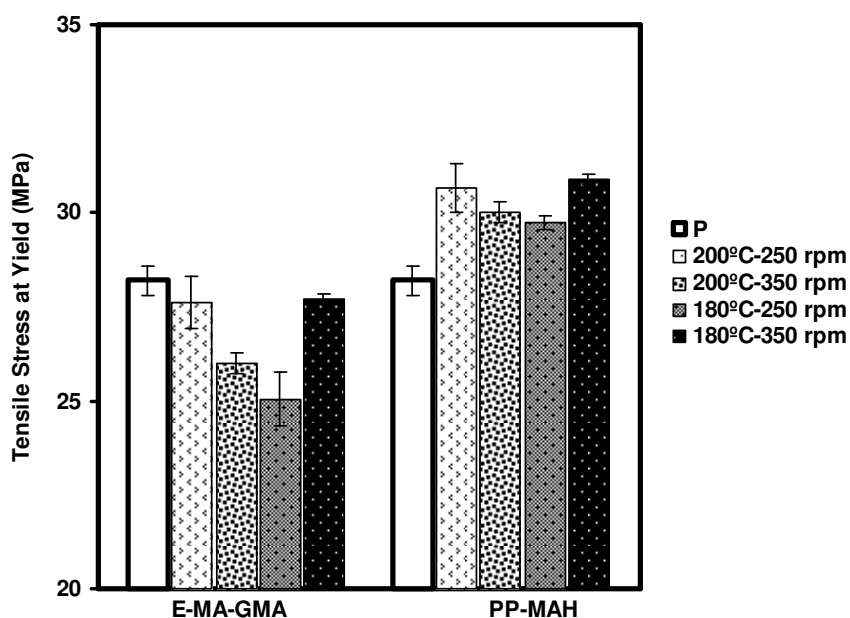


**Figure 4.45** Tensile stress at yield of ternary nanocomposites containing 5 wt% E-MA-GMA and 2 wt% Cloisite® 15A (on the left) and 2 wt% PP-MAH and 1 wt% Cloisite® 15A (on the right) prepared under different processing conditions.

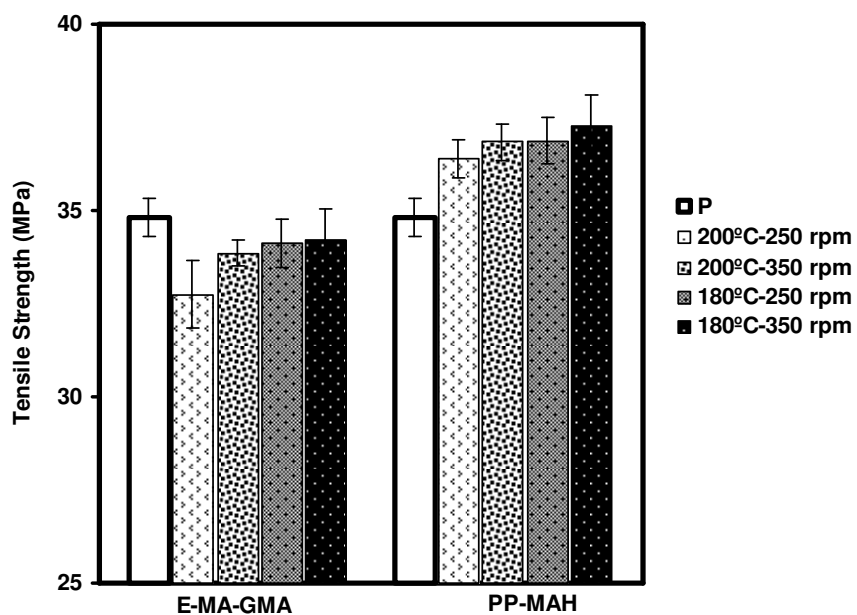


**Figure 4.46** Tensile strength of nanocomposites containing 5 wt% E-MA-GMA and 2 wt% Cloisite® 15A (on the left) and 2 wt% PP-MAH and 1 wt% Cloisite® 15A (on the right) prepared under different processing conditions.

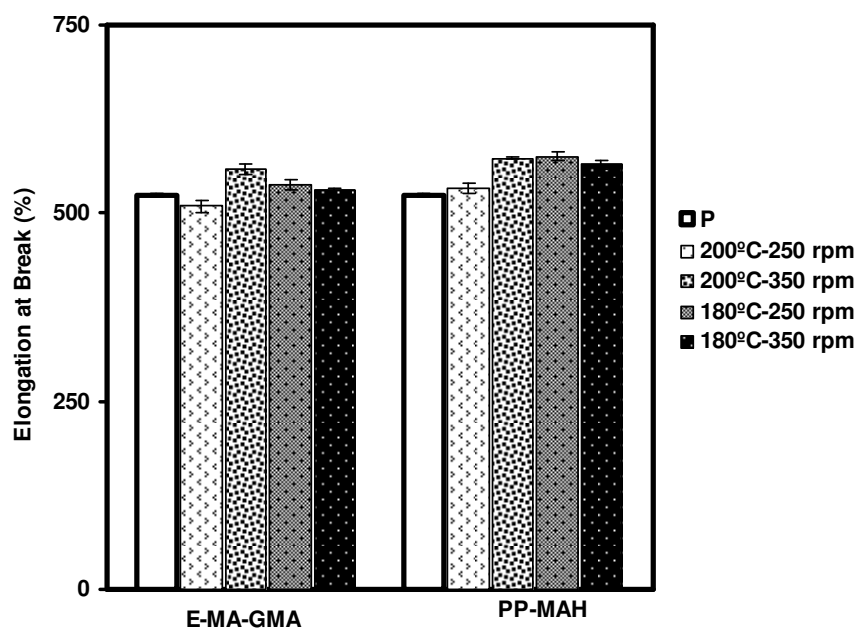


**Figure 4.47** Elongation at break (%) of nanocomposites containing 5 wt% E-MA-GMA and 2 wt% Cloisite® 15A (on the left) and 2 wt% PP-MAH and 1 wt% Cloisite® 15A (on the right) prepared under different processing conditions.

As previously mentioned, clay platelets can either slide apart from each other by the exerted shear stress in the extruder, or diffusion of the polymer chains into silicate layers may cause separation. In nanocomposites prepared with E-MA-GMA, it was observed that the modulus and tensile stress at yield properties decreased with increasing screw speed to 350 rpm at 200°C. Regarding to increased screw speed, the residence time of the material inside the extruder decreases. Moreover, residence time becomes the controlling factor for dispersion when intercalation of polymer inside clay galleries is driven by diffusion [43]. Therefore effective mixing may not be provided, and finally, dispersion of organoclay may be diminished due to inadequate time of mixing necessary for diffusion. Low MFI value and hence high melt viscosity of the polymer matrix could be one of the reasons related with the diffusion problem. When the extruder barrel temperature was decreased to 180°C at 250 rpm screw speed, again the stiffness values decreased. Comparing this result with the result at high temperature, reduction in stiffness can be attributed to lower melt viscosity and reduced shear stress, again diminishing the dispersion of clay platelets at high temperature. Moreover, diffusion of polymer chains would be lower owing to decreased temperature. In the present case, the organophilic environment formed in the interlayer gallery of the silicates by the combination of organic cation and compatibilizer drives the delamination process through thermal diffusion control and makes the mechanical contribution negligible [13]. The best Young's Modulus and tensile stress at yield values were obtained when screw speed was increased to 350 rpm, simultaneously decreasing the temperature to 180° C. The shear stress exerted on the polymer and silicate layer during extrusion could reach a level that compensate for the decreased residence time and diffusive effect which was reduced due to low temperature and high melt viscosity and end up with enhanced stiffness. Elongation at break and tensile strength values were not significantly affected from processing conditions.

Nanocomposites prepared with PP-MAH compatibilizer represent a significant increase in all tensile properties owing to good interaction between polymer and the organoclay. Problems that occurred due to residence time and dispersion in accordance with the changes in processing conditions were also detected in this case, but variations between values were relatively less significant for these nanocomposites, even when they were subjected to extrusion only once. First reason could be the amount of clay added was lower, namely 1 wt%, and therefore agglomeration due to cohesive forces were smaller and dispersion was good. The

second reason could be as a result of masterbatch method that allows expansion of silicate layers before the addition of polymer. In the MB mixing process, PP-MAH chains penetrate into organoclay layer and react with silicate layers. Then the matrix polymer can easily penetrate into thick layer and form a broad interphase [125]. Therefore, polymer chains would have enough time to intercalate inside the clay galleries in a shorter residence time. Increase in % elongation at break for all processing conditions could be due to low clay loading permitting chain mobility and good adhesion between clay layers and matrix enhanced with PP-MAH, leading to reduction of the number of micro voids in the matrix.

Figures 4.48 to 4.51 show the tensile properties of binary blends prepared with PP-MAH compatibilizer. Results indicate that the addition of PP-MAH compatibilizer increases tensile properties. The improvement in tensile strength and Young's Modulus values could be attributed to the higher tensile properties of PP-MAH compared to pristine recycled polymer. Young's Modulus value of PP-MAH was measured as 991 MPa and tensile strength as 32 MPa whereas Young's Modulus of recycled polypropylene is 879.7 MPa and tensile strength is 34.8 MPa. Considering the DSC results of these binary blends, increase in crystallinity, especially in the polypropylene side of the material was observed. Therefore, it can be concluded that PP-MAH strengthened the matrix, increased crystallinity and consequently the mechanical properties were enhanced. Increase in the elongation at break values could be assigned to decreased PE domain size and increased particle domain distance of the polyethylene phase as observed in SEM images as discussed earlier.

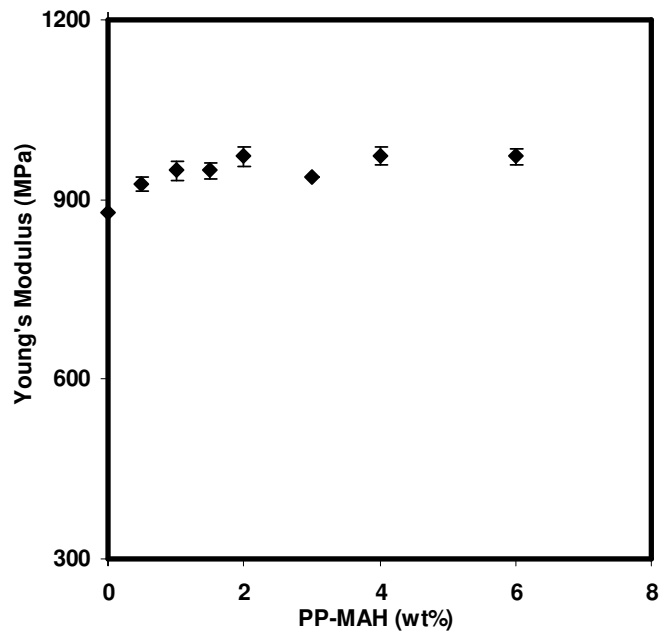


Figure 4.48 Young's Modulus of binary blends containing PP-MAH.

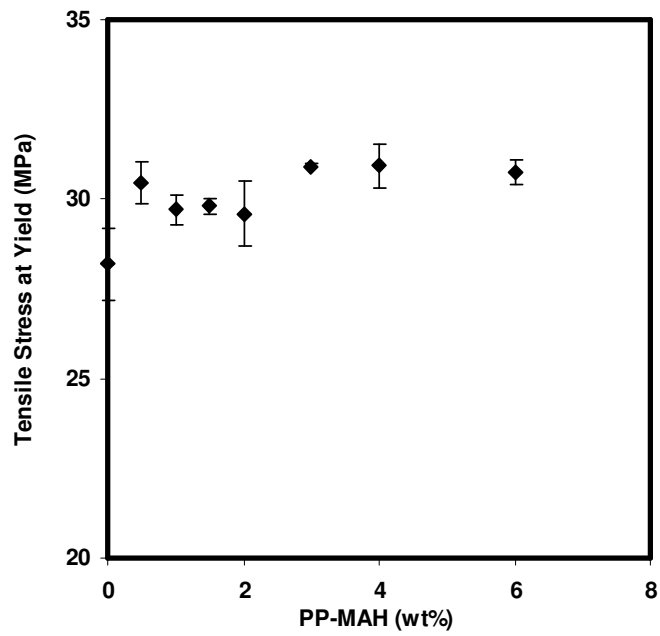
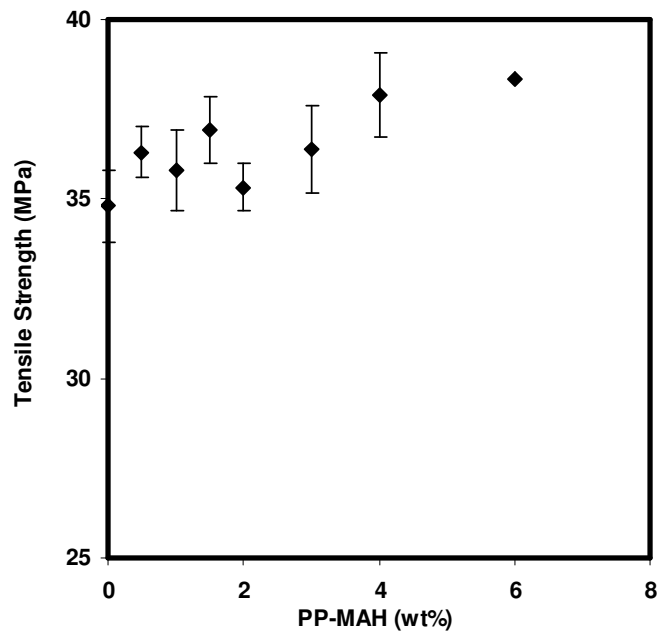
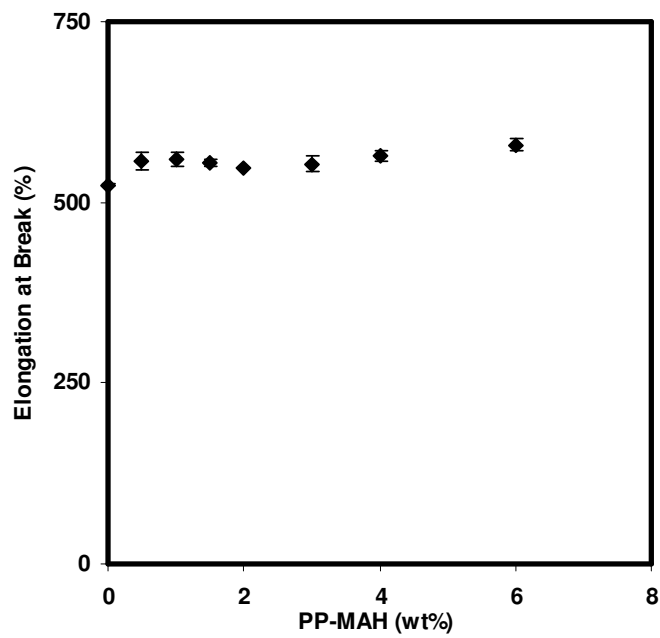


Figure 4.49 Tensile stress at yield of binary blends containing PP-MAH.



**Figure 4.50** Tensile strength of binary blends containing PP-MAH.



**Figure 4.51** Elongation at break (%) of binary blends containing PP-MAH.

The binary nanocomposites of Cloisite® 15A as well as binary nanocomposites of other types of organoclays prepared with masterbatch method are shown in Figures 4.52-4.55. Young's Modulus and tensile strength values were enhanced with organoclay addition and the most remarkable increase was observed at 2 wt% loading. Results indicate that clay was well dispersed in the matrix.

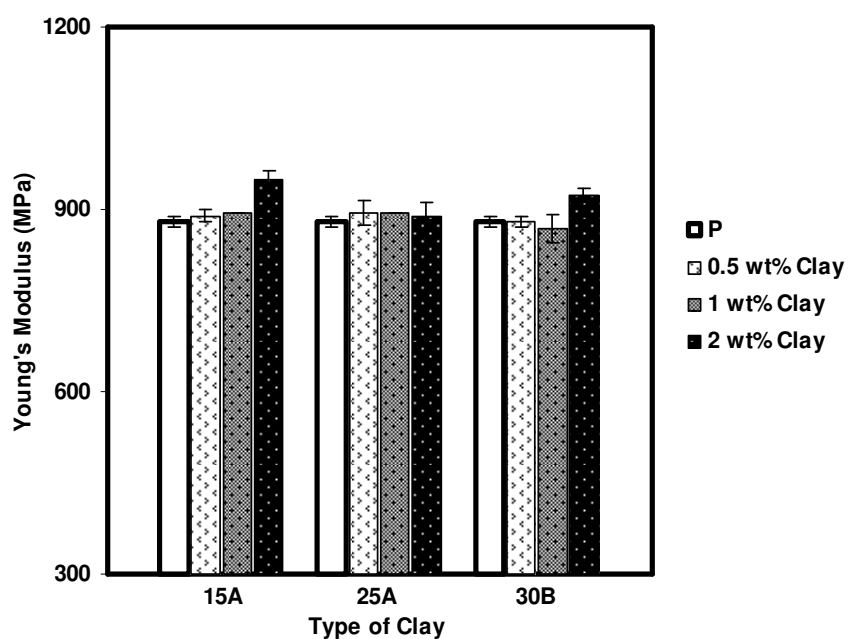


**Figure 4.52** Young's Modulus of binary nanocomposites containing different types of organoclays.

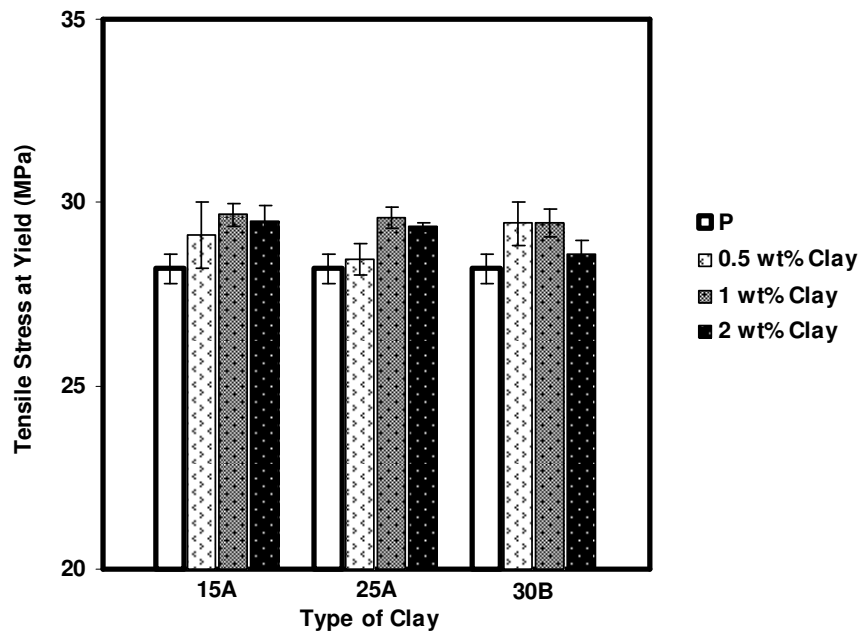


**Figure 4.53** Tensile stress at yield of binary nanocomposites containing different types of organoclays.

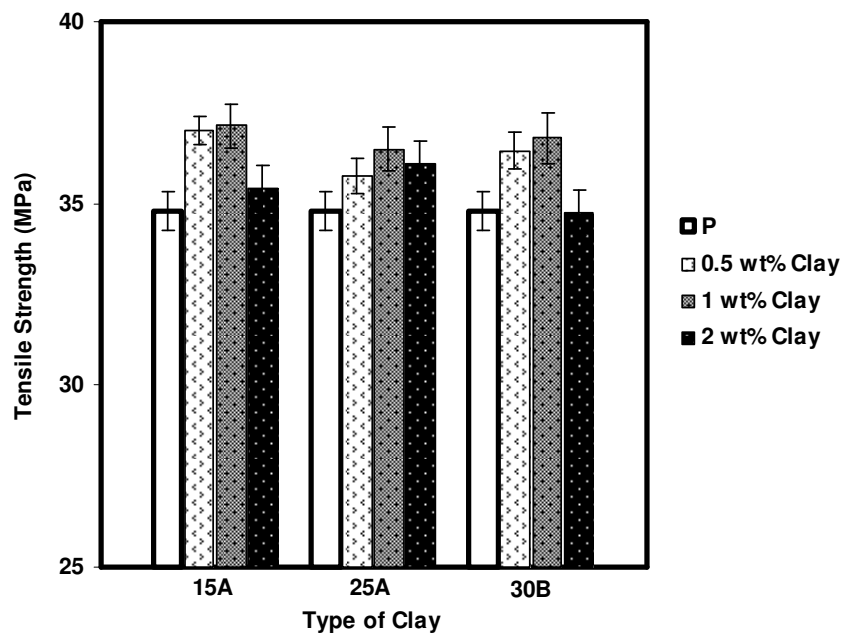


**Figure 4.54** Tensile strength of binary nanocomposites containing different types of organoclays.

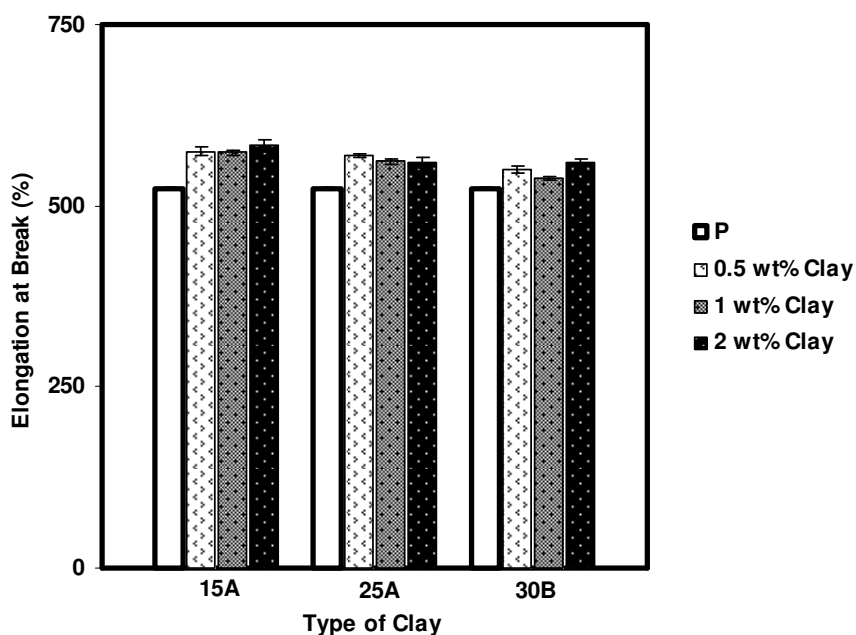


**Figure 4.55** Elongation at break at break (%) of binary nanocomposites containing different types of organoclays.

In Figures 4.56-4.59 the effect of compatibilizer and the ratio of PP-MAH to organoclay are shown. The ratios in the figures indicate the wt% of PP-MAH to organoclay used in the study. It is obvious from the figures that PP-MAH addition as a third component greatly improved tensile properties, especially Young's Modulus. Elastic modulus was higher in the presence of PP-MAH for all filler contents owing to more efficient stress transfer from the polymer matrix to the inorganic filler [43]. As the amount of additive was increased the improvements became more significant.

Enhancement in tensile properties could also be explained considering the blend morphology in the matrix. In the literature, it was reported that organoclay particles could act as a reinforcing agent and also as compatibilizer in a blend system. Interfacial tension, and morphological and mechanical tests applied to polypropylene-polycarbonate immiscible blend revealed that organoclay was located at the interface during compounding [9]. Resultant interfacial activity caused dramatic reduction in interfacial tension and reduction in domain size. Moreover, it was stated that the compatibilizing process was more efficient in the presence of PP-MAH owing to interactions between clay and compatibilizer. Results were confirmed with

mechanical properties, since high increase in elastic modulus was achieved. Considering the same immiscible blend morphology, in the present study, the enhancement in Young's Modulus with simultaneous addition of organoclay and PP-MAH could be attributed to rigid structure of both organoclay and PP-MAH, increase in crystallization and increased adhesion between the PP and PE phases. Moreover, the general increase in elongation at break values could be an indication of previously mentioned reduction in the particle domain and also positive effect of compatibility on crack propagation.

Effect of PP-MAH to organoclay ratio was also investigated, and it was observed that enhancement in tensile properties was better as the ratio between PP-MAH and organoclay was increased. Nanocomposite containing 6 wt% PP-MAH and 2 wt% Cloisite® 15A exhibited 31.7% increase in Young's Modulus which was the highest improvement obtained throughout the study. The same result was also observed in the XRD results, since increased amount of PP-MAH caused better intercalation due to higher affinity and hydrogen bonding. TEM micrographs also revealed that number of the exfoliated zones was increased as the mentioned ratio was increased. In literature, similar results were reported where the organoclay particles were dispersed more uniformly as the ratio of PP-MAH to organoclay was increased. Results were attributed to desired nanoscale dispersion of organoclay achieved with PP-MAH through strong hydrogen bonding between hydroxyl group of silicates and MA group, while relying on chemical similarity of isotactic PP and grafted PP in PP-MAH structure [16, 126]. Besides the improvements in intercalation mechanism, the presence of more PP-MAH would cause higher crystallinity as observed in DSC measurements and also provide stronger adhesion between phases and good stress transfer.

Mechanical properties, especially elongation at break, are very sensitive to adhesion strength between components or partial miscibility at the interface of blend components in phase separated systems [127]. Therefore, increase in the elongation at break values together with the stiffness properties could be assigned to possible increased adhesion provided by both compatibilizer and organoclay system in the PP-MAH containing nanocomposites.

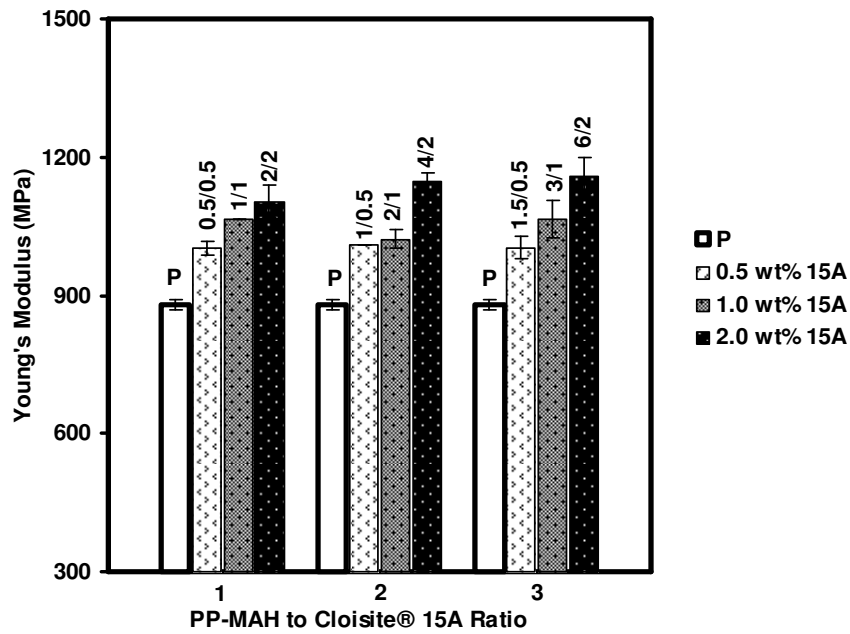


**Figure 4.56** Young's Modulus of ternary nanocomposites prepared with PP-MAH to organoclay ratios of 1, 2 and 3.

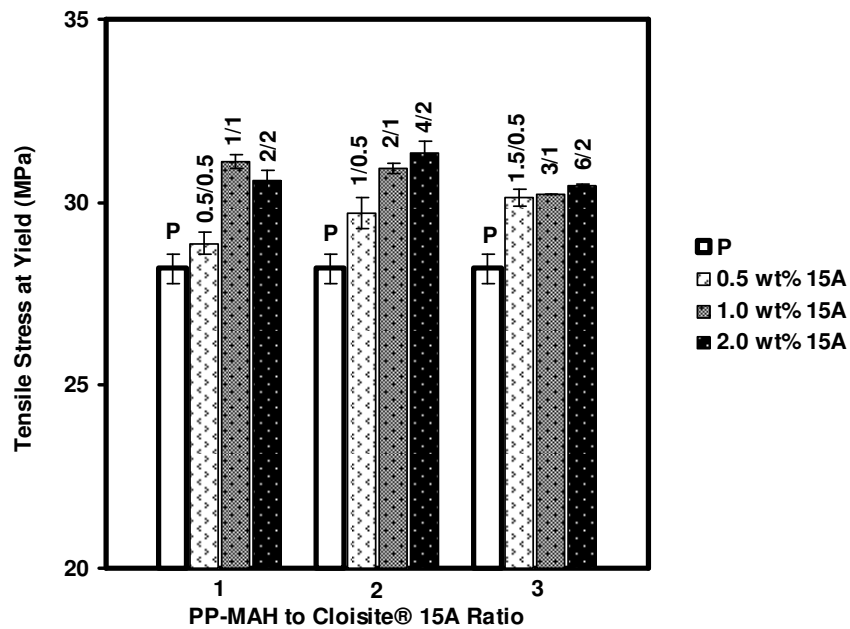


**Figure 4.57** Tensile stress at yield of ternary nanocomposites prepared with PP-MAH to organoclay ratios of 1, 2 and 3.

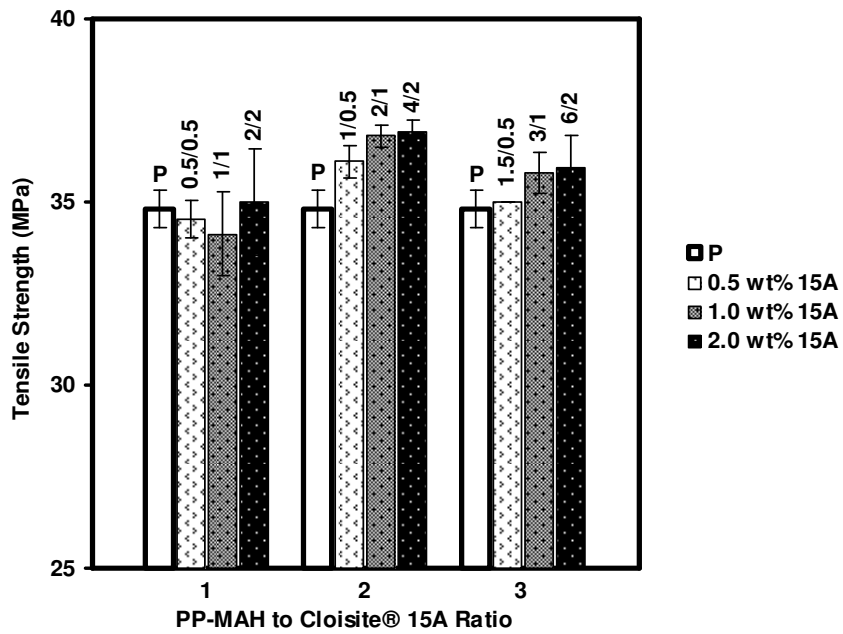


**Figure 4.58** Tensile strength of ternary nanocomposites prepared with PP-MAH to organoclay ratios of 1, 2 and 3.

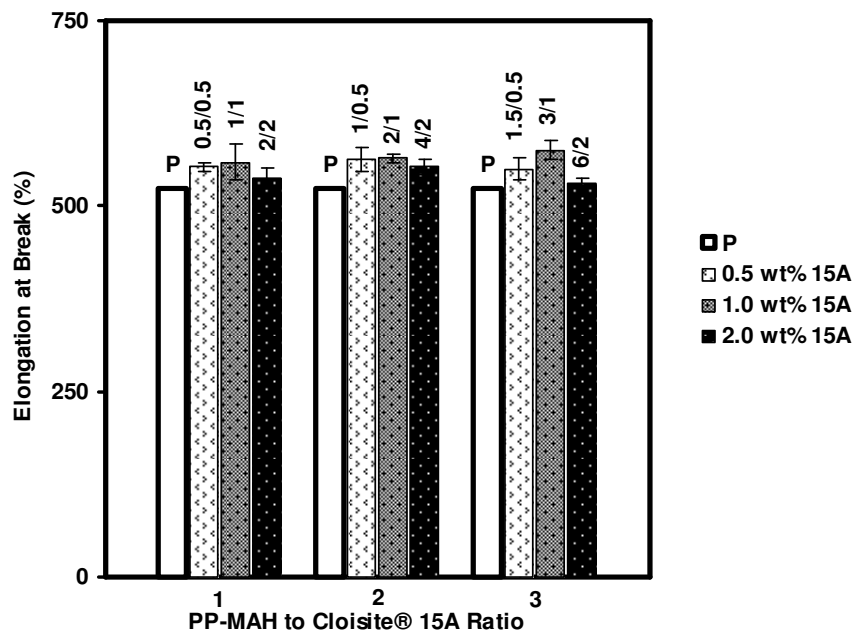


**Figure 4.59** Elongation at break (%) of ternary nanocomposites prepared with PP-MAH to organoclay ratios of 1, 2 and 3.

Finally, the effects of different clay types on mechanical properties studied for PP-MAH to organoclay ratio of 2 and the results are shown in Figures 4.60-4.63. Considering the XRD results, best improvements are expected in the Cloisite® 30B containing nanocomposites since exfoliation was observed in their XRD patterns. In the binary nanocomposites with different types of clay, a general increase in tensile properties was observed and a significant difference between tensile properties was not detected. However, analyzing the figures, Cloisite® 15A and PP-MAH containing ternary nanocomposites exhibited a more significant enhancement in tensile properties. Improvements in nanocomposites were attributed to the flow induced clay orientation during injection molding. Tensile modulus of polymer nanoclay composites is expected to depend on orientation of clay tactoids and orientation of polymer crystallites, besides dispersion of clay, clay loading, degree of crystallinity and interfacial stress transfer mechanisms [109, 128]. Orientation of the filler relative to the applied load dictates the stress transfer mechanism. Misaligned filler, as in an extreme case where filler is perpendicular to the applied load, leads to a mechanism where stress at the interface transforms from a shear mode to a tensile mode which generates a higher concentration of stress in the matrix and less tension in the filler particle, similar to the mechanism of fiber end or platelet edge.

It was also stated that, increased injection shear rate had highly remarkable effect on orientation in the presence of PP-MAH compatibilizer for the nanocomposites prepared with polypropylene and organoclay [128]. Therefore, the remarkable difference between the elastic modulus and yield stress values of the nanocomposites could be explained with addition of PP-MAH and more effective clay orientation for Cloisite® 15A. Moreover, it was also observed that as the amount of clay added was higher, the increase in modulus was more significant. This result could be attributed to the higher filler-filler interactions combined with comparatively lower MFI values as discussed in section 4.4. Higher melt viscosity improved the morphology of the injection molded specimens relating in increased filler orientation and uniform distribution of polyethylene phase [109].

Another reason for the contradiction between XRD and tensile test results could be related to the number of the alkyl chains of the organoclays. One of the studies in the literature conducted with polyethylene and maleic anhydride grafted polyethylene exhibited that the better dispersion and enhanced tensile strength and modulus properties were obtained with organoclay with two alkyl chains rather than one alkyl

chain [129]. In another study, implemented with polyamide-6, it was observed that the results were opposite and they showed that polyamide had relatively better affinity for silicate surface rather than alkyl tail [109]. In the present case, considering the XRD patterns, it was concluded that the entrance of polypropylene chain were hindered by the two long alkyl chains in Cloisite® 15A and therefore better dispersion was obtained in the case of Cloisite® 25A and Cloisite® 30B organoclays that constitutes single alkyl tails.

Some other reason stated in the literature was the high aspect ratio of the clay platelets which creates enhanced reinforcement effect [16, 127]. For the present case, considering applied high shear, the aspect ratio of the Cloisite® 25A and Cloisite® 30B organoclays might be decreased to a value such that the reinforcing effect of the clay might diminish despite their well dispersed delaminated structures. On the other hand, Cloisite® 15A particles that were partially remained as tactoids would have a high aspect ratio that would contribute to the reinforcement. In addition to that, their sizes are not large to act as stress concentrators.

Elongation at break values were similar and enhanced for nanocomposites prepared with each type of organoclay indicating that adhesion between the matrix and the fillers were adequate and a tortuous path for crack propagation was present.

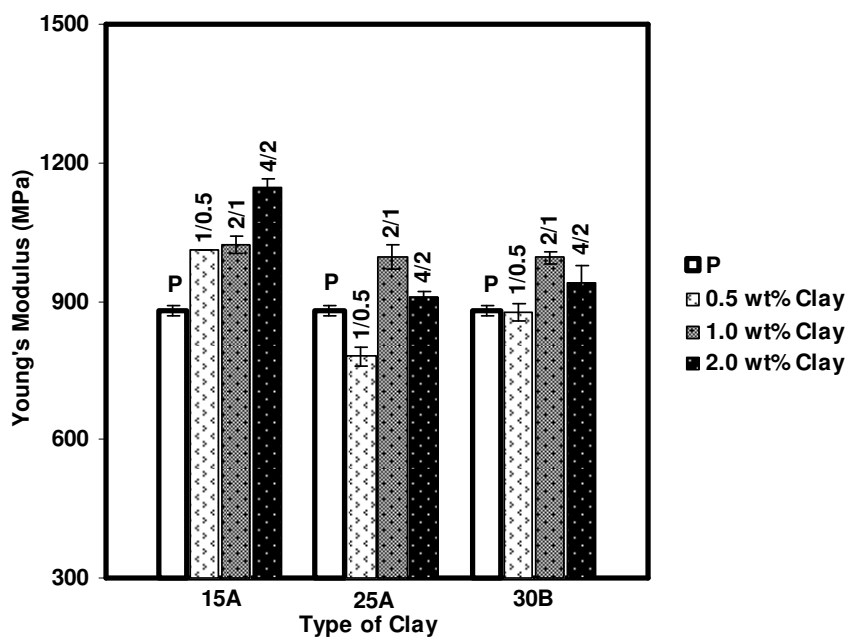


**Figure 4.60** Young's Modulus of ternary nanocomposites prepared with PP-MAH to organoclay ratio of 2 and different types of organoclays (180 °C, 350 rpm, MB).

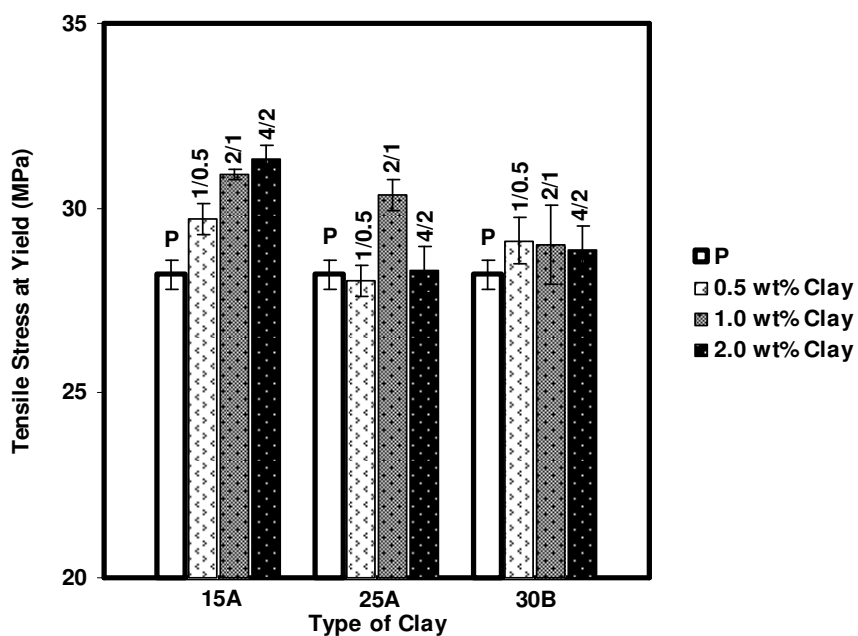


**Figure 4.61** Tensile stress at yield of ternary nanocomposites prepared with PP-MAH to organoclay ratio of 2 and different types of organoclays (180 °C, 350 rpm, MB).

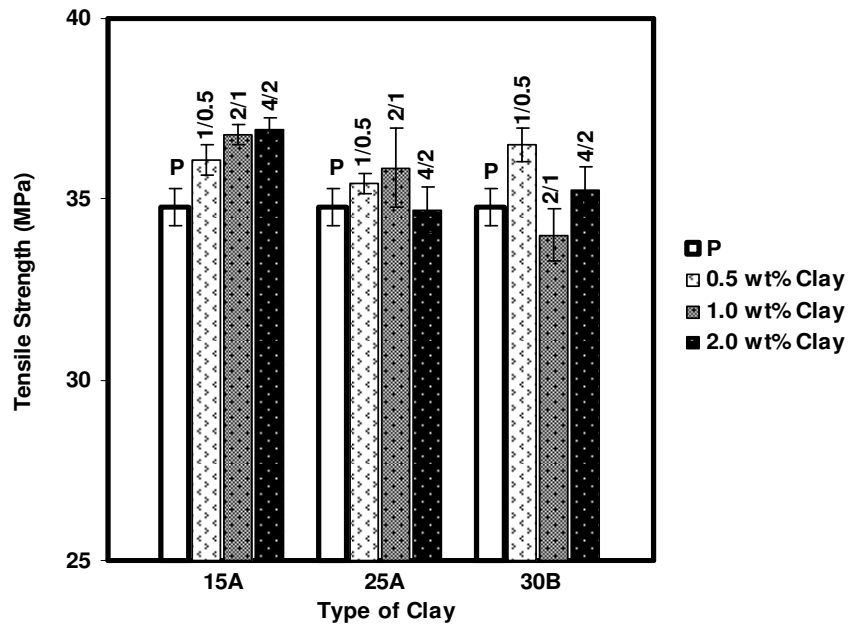


**Figure 4.62** Tensile strength of ternary nanocomposites prepared with PP-MAH to organoclay ratio of 2 and different types of organoclays (180 °C, 350 rpm, MB).

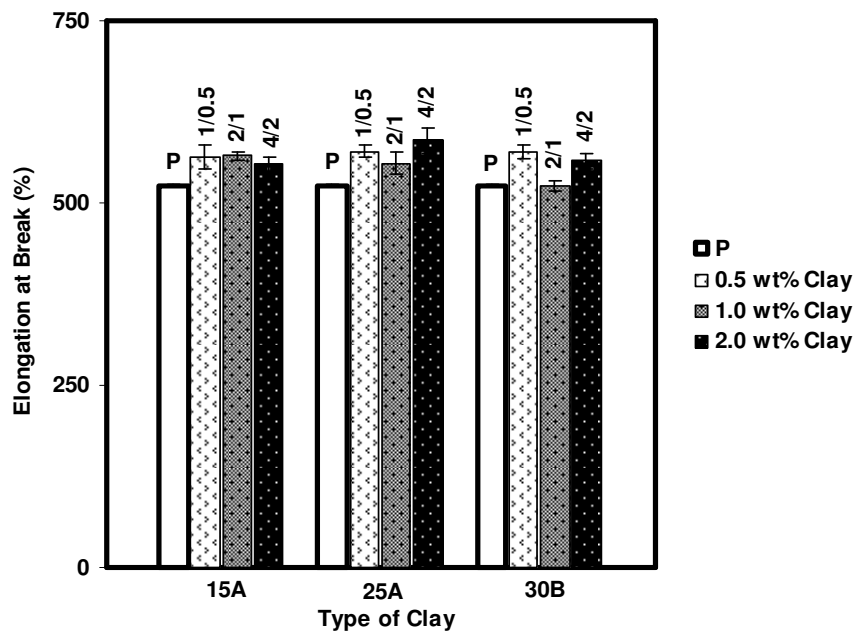


**Figure 4.63** Elongation at break (%) of ternary nanocomposites prepared with PP-MAH to organoclay ratio of 2 and different types of organoclays (180 °C, 350 rpm, MB).

#### 4.2.2 Impact Test

Charpy notched impact tests were carried out for determination of impact strength of the blends and nanocomposites.

The impact properties of semi-crystalline polymers such as polyethylene and polypropylene is fundamentally important regarding to their behaviors under strain which is characterized as ductile at low strain rates while they exhibit brittle response at high strain rates [80].

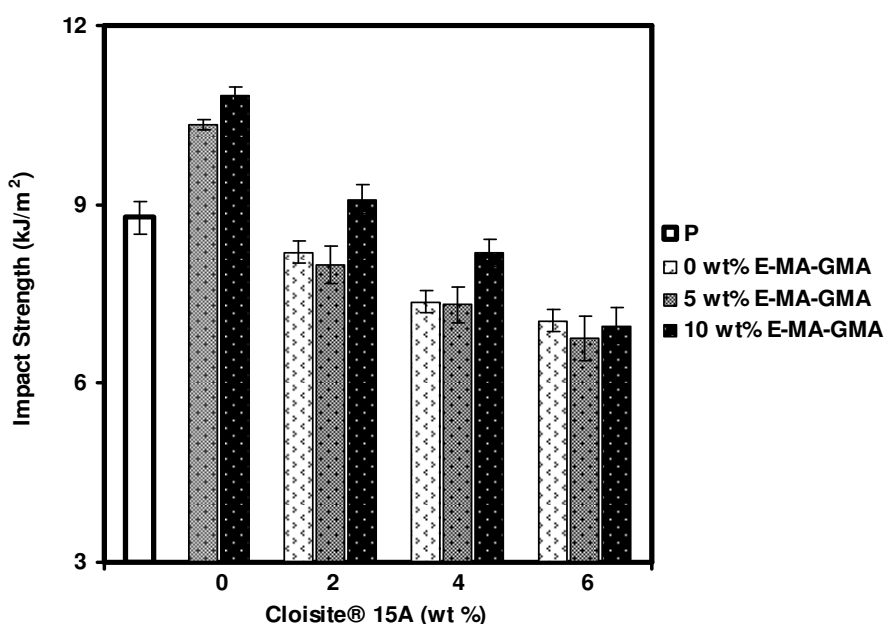
Impact stress generates micro cracks (crazes) on the surface of the rigid polymer and these micro cracks transform into large rapidly moving cracks under applied stress. Sharp points, voids and notches concentrate the stress and initiate the crack propagation. Matrix is teared apart in a single direction beginning from the any inhomogeneity or flaw where the stress may concentrate. Polypropylene and polypropylene nanocomposites have low impact resistance, particularly at low temperatures owing to their relatively high glass transition temperatures. Consequently, they are blended with elastomeric modifiers to improve the impact resistance of the base resin [125]. In a toughened thermoplastic, more energy is required to break the matrix since high unidirectional impact stress can either be converted into small multidirectional stresses or energy of the stress could be absorbed and crack propagation could be stopped by the particle. Uniform size and dispersion of the elastomeric domains, adhesion at the interface of the elastomer and the polymer matrix, interdomain distances and modulus ratio of the matrix and dispersed phase are some of the important factors affecting the toughness [110]. The domain size is mainly dependent on the stabilization of surface mobility and decrease in interfacial tension [110] while interdomain distance is affected by both intrinsic parameters such as interfacial adhesion, modulus of the matrix, ratio between the modulus of the matrix and elastomer domains, and extrinsic parameters such as impact speed, test temperature and deformation mode. The critical interdomain distance becomes higher as the modulus of the elastomeric phase decreases and decreases as the modulus of the matrix increases [59, 130]. In this study, the extrinsic parameters were kept constant; therefore, intrinsic parameters were effective on toughness of the materials.

Figure 4.64 shows the impact resistance of binary blends and ternary nanocomposites prepared with recycled polypropylene, Cloisite® 15A organoclay and E-MA-GMA compatibilizer. In the binary blends with E-MA-GMA compatibilizer, a significant improvement in impact toughness behavior was observed with addition of 5 wt% compatibilizer, and the toughness was further enhanced with 10 wt% compatibilizer addition. Increasing the rubber content of the matrix shifts the brittle-ductile transition temperature to lower temperatures and causes improvement in toughening mechanism [131]. Moreover, toughening could be improved owing to more effectively absorbed and dissipated impact energy by increased number of the compatibilizer domains.

Incorporation of organoclay in polymer matrix decreased the impact strength and reduction became more significant at higher clay content. The chain mobility decreases owing to large surface area of organoclay and the matrix becomes stiffer. [132]. Hence, material fractures in a more brittle manner. In addition to that, SEM images of these composites represented reduction in particle size of the dispersed phase with organoclay addition. This result was attributed to the barrier effect of organoclays. Results in the literature show that presence of small rubber particles in a polypropylene blend enhances toughness and ductility of the material owing to more efficient action of rubbery phase in inducing crazing and/or shear yielding of the matrix. Moreover, formation of cavitations may become easier with accommodation of larger domains [133]. However, an optimum value of domain size exists. When the dimension of the domains in the matrix is smaller than the size of the fracture ligament, the presence of domain can not influence the propagation of cracks and it can only change the rheological properties of the matrix. Therefore the domain size should be big enough to prevent the crack propagation [117]. Considering the literature information it can be concluded that the domain sizes of the rubbery phase in the nanocomposites are not big enough to prevent the crack propagation, especially when the possibility of crack formation is increased due to agglomeration of organoclay at high organoclay concentrations.

E-MA-GMA compatibilizer which has ductile properties was added in order to compensate for the reduction in the impact strength occurring due to organoclay incorporation. In ternary nanocomposites, no remarkable improvement due to compatibilizer addition was observed with 5 wt% compatibilizer addition. However, at 2 wt% and 4 wt% organoclay contents, 10 wt% E-MA-GMA addition prevented the

reduction in impact strength and improved toughness at some extent. On the other hand, at 6 wt% clay content almost no improvement was observed despite the addition of compatibilizer, and the highest reduction among all samples was observed at this clay loading. In the SEM images, micron sized organoclay clusters were observed and they were more observable in the presence of E-MA-GMA. These clusters would act as very sensitive crack tips and decrease impact strength of the material and inhibit the toughening mechanism. For the nanocomposites containing 10 wt% elastomer, these problems were compensated at some extent owing to increased domain sizes and quality of energy absorption capacity, however the toughness of the matrix was still poor compared to pristine polymer. It could be concluded that effect of organoclay loading and dispersion were the controlling factors for the impact properties.



**Figure 4.64** Impact strength of blends and nanocomposites prepared with E-MA-GMA compatibilizer (200° C, 250 rpm, All-S).

The effects of processing conditions on impact strength properties are shown in Figure 4.65. For rubber toughened polymer, brittle-ductile transition temperature can generally be reduced either by increasing elastomer content or by decreasing

elastomer domains [40]. In addition to that, in formation of finer elastic domains and uniform dispersion of elastomeric domains, high shear stresses and melt viscosity play important roles [110]. For both of the compatibilizers, a general trend was an increase in impact strength, as the processing temperature was decreased and screw speed was increased. Ternary nanocomposites containing 5 wt% E-MA-GMA and 2 wt% organoclay represent marginal reduction in domain size of the dispersed phase while nanocomposites containing 2 wt% PP-MAH and 1 wt% organoclay exhibits a more significant reduction in elastomer domain size. Moreover, in XRD patterns of each type of nanocomposite, more delaminated structures were observed at lower processing temperature and higher screw speed. Delamination of organoclay is effective on hindering the coalescence of elastomeric domains by acting as barriers while decreasing the matrix mobility and increasing the interfacial adhesion between the elastomer domains and the matrix [53]. Therefore, increase in melt viscosity and better dispersion of organoclay would be the reasons of reduction in elastomer sizes and improved impact properties compared to the ones having more clay agglomerates.

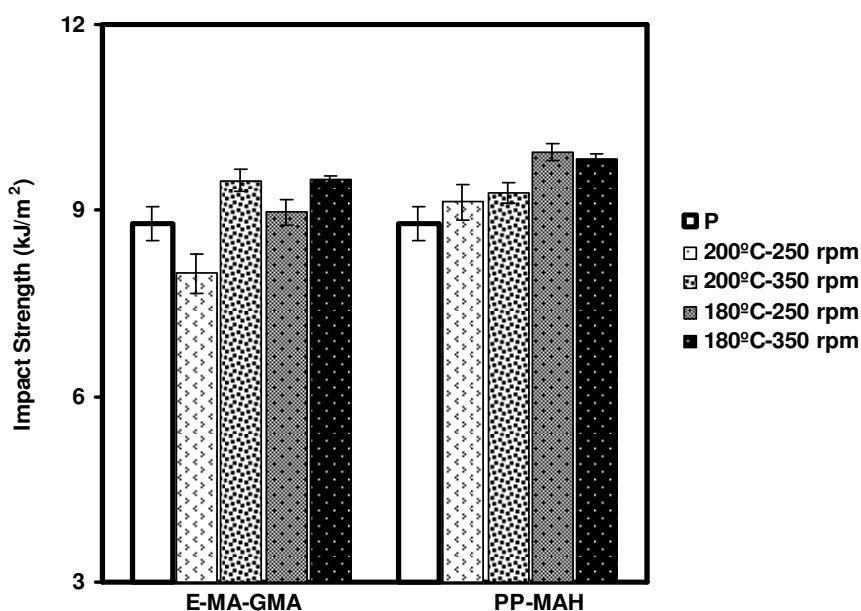


**Figure 4.65** Impact strength of nanocomposites containing 5 wt% E-MA-GMA and 2 wt% Cloisite® 15A (on the left) and 2 wt% PP-MAH and 1 wt% Cloisite® 15A (on the right) prepared under different processing conditions.

In Figure 4.66, the impact strength blends of PP-MAH and recycled polypropylene are shown. Impact strength values of the materials increased as higher amount of PP-MAH was added. The toughening mechanism is different for the PP-MAH compatibilizer, since the modulus of PP-MAH is higher than the matrix material and therefore energy absorption capacity is not high as those of E-MA-GMA or the polyethylene domains. Therefore, improvement in this case would be due to the distribution of force into smaller forces at the tip of the PP-MAH domains and change in the direction of the stress.

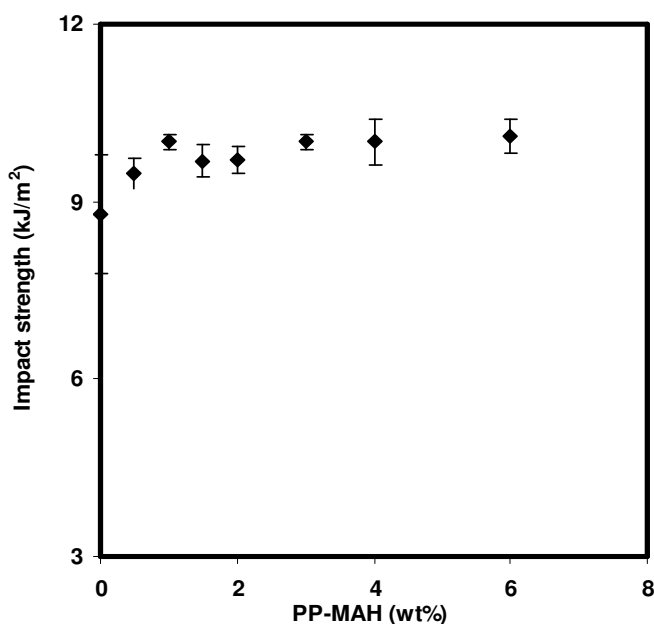


**Figure 4.66** Impact strength of blends containing PP-MAH.

In the binary composites of organoclay and polypropylene, as shown in Figure 4.67, the impact strength first increased up to 1 wt% clay loading and then decreased at 2 wt% organoclay loading when PP-MAH was not added. This result is related with better exfoliation clay particles acting as barrier and retarding the coalescence of the elastomer domains. However, at 2 wt% clay content, the clay platelets would be agglomerated in the matrix and act as crack tips during deformation and reduce the impact strength.

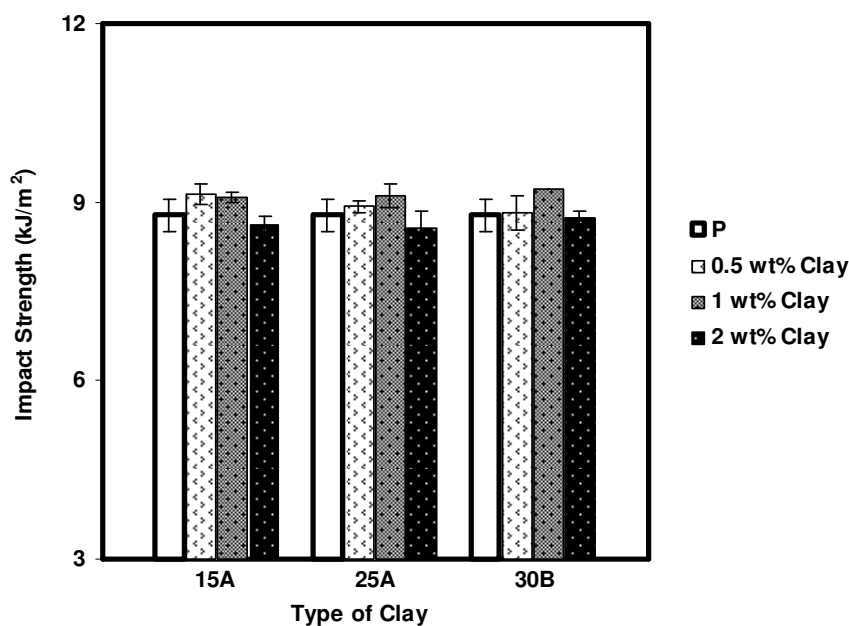


**Figure 4.67** Impact strength of binary nanocomposites containing different types of organoclays. The ratios given are those of PP-MAH to organoclay.

In figure 4.68, the effects of PP-MAH to organoclay ratio on impact properties are shown. Results indicate that the better impact properties were obtained when the ratio was 3, except for the 2 wt% PP-MAH and 1 wt% Cloisite® 15A containing nanocomposite. As previously mentioned, as the amount of PP-MAH was increased the interactions between the clay and the compatibilizer become more effective and organoclay gets dispersed more homogeneously and the coalescence of elastomer domains becomes difficult. Moreover, in the SEM images of nanocomposites containing 6 wt% PP-MAH and 2 wt% Cloisite® 15A, and 2 wt% PP-MAH and 1 wt% Cloisite® 15A prepared at 180 °C temperature and 350 rpm screw speed, a very significant uniform distribution and increase in interparticle distance was observed. Therefore, the results could be attributed to the improved intrinsic properties of the materials when the PP-MAH to organoclay ratio was higher.

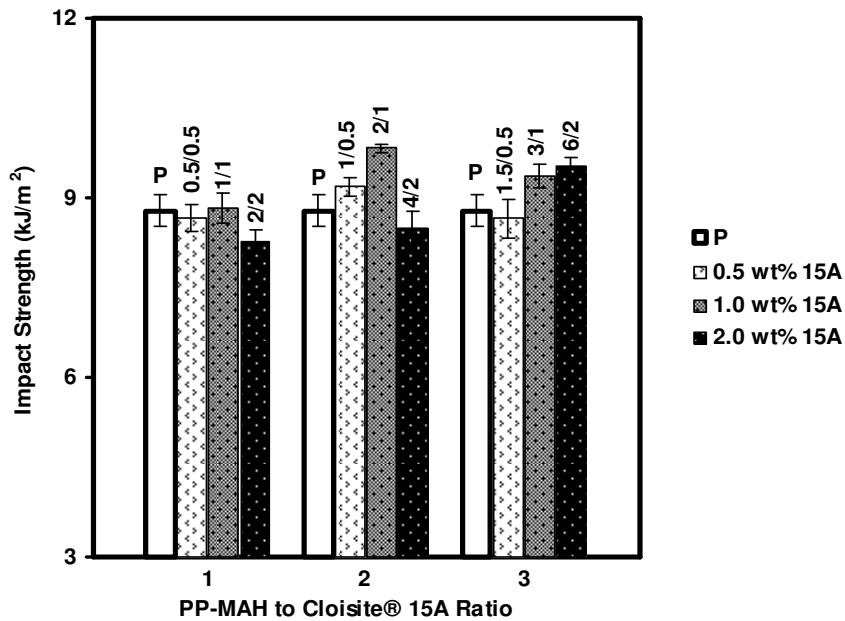


**Figure 4.68** Impact strength of ternary nanocomposites prepared with PP-MAH to organoclay ratios of 1, 2 and 3.

In the last part of the study, the effects of organoclay type on impact properties of nanocomposites were examined. Binary mixtures of recycled polypropylene and different clay types exhibited more or less the same behavior under impact stress. Enhancement in impact strength was developed up to 1 wt% of clay loading and then reduction was observed at 2 wt% organoclay loading in nanocomposites. In SEM micrographs of 1 wt% organoclay containing specimens, decrease in domain size was observed and domain sizes were increased in 2 wt% organoclay content. Results were attributed to the enhanced clay dispersion at low clay loading. Therefore, increase in impact strength could be attributed to the decreased domain size of the dispersed phase.

Considering that the same compatibilizer to organoclay ratio was used in the preparation of ternary nanocomposites, impact strength of nanocomposites containing Cloisite® 15A and Cloisite® 30B increased to a greater extent compared to those with Cloisite® 25A. Improvement in the presence of Cloisite® 30B could be attributed to the exfoliation of clay particles in the presence of PP-MAH and enhanced crack arresting effect. On the other hand, higher impact strength of

Cloisite® 15A containing nanocomposites could be due to improved adhesion properties combined with partial delamination.

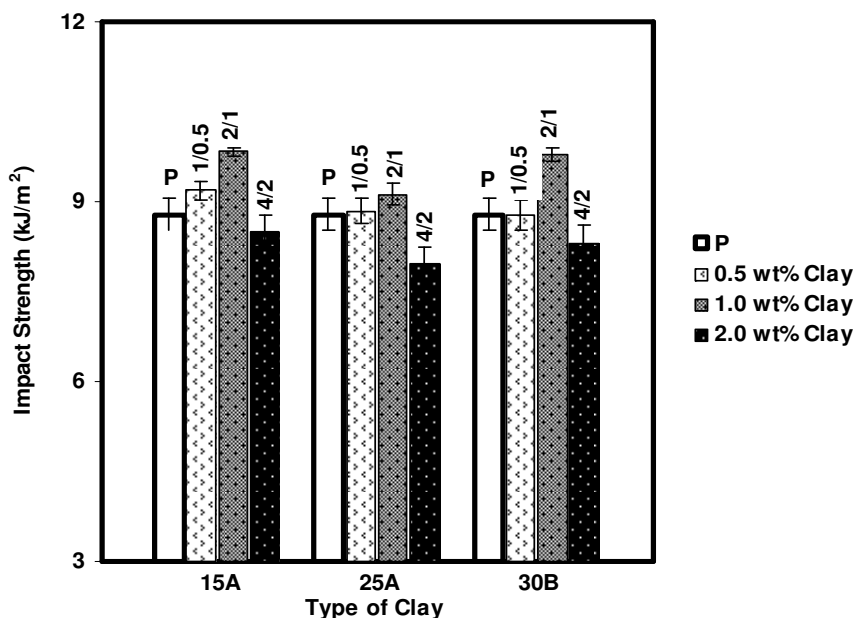


**Figure 4.69** Impact strength of ternary nanocomposites prepared with PP-MAH to organoclay ratio of 2 and different types of organoclays (180 °C, 350 rpm, MB).

Consequently, the most remarkable improvements were obtained at 1 wt% clay loading for each type of organoclay with the presence or absence of PP-MAH. Effect of exfoliation at low clay loading and decreased domain size and increased interdomain distance would be the reason of these results.

### 4.3 Differential Scanning Calorimetry Analysis

DSC analysis was conducted to determine the crystallization behavior of recycled polypropylene and the effects of organoclays and compatibilizers on crystallization during blend and nanocomposite preparation. DSC thermograms of recycled polypropylene as shown in Figure B.1 in Appendix B exhibited two distinct peaks, indicating to two crystalline phases. Two well-separated melting peaks would be assigned for phase separation in the matrix as stated in the literature [134]. First

peak at 127.3 °C was considered as the melting peak of polyethylene phase, and the second peak at 165.2 °C as belong to the polypropylene phase. Glass transition temperatures of both PP and PE phases were not detected in the thermograms, since they were below the room temperature.

The percent crystallinity values of each phase were calculated as the ratio of the heat of fusion of the sample ( $\Delta H_f$ ), divided by the weight fraction of the polymer in the nanocomposite and the heat of fusion of the pure crystalline form of the polymer. Since the weight percent of the phases in the polymer was unknown, it was assumed that, the polymer itself constitutes only one phase in the calculations. Crystallinity of each phase was calculated separately by using heat of fusion ( $\Delta H_f$ ) data of the phases and finally two crystallinity data which belong to polyethylene and polypropylene phases were obtained. The heat of fusion data for pure crystalline form of PE ( $\Delta H_{f, PE}^\circ$ ) and PP ( $\Delta H_{f, PP}^\circ$ ) were taken as 293 J/g and 209 J/g, respectively [94].

Crystallinity of polypropylene segment was fairly low (17.7%) owing to low crystallization rate of 5 °C/min representing a typical behavior of polypropylene without nucleating agent [85].

Melting temperatures of E-MA-GMA and PP-MAH found as 51.9 °C and 164 °C respectively. Calculated % crystallinity values of nanocomposites and blends are given in Tables 4.6-4.9 and related DSC thermographs are shown in Appendix B.

Table 4.6 represents the heat of fusion, melting temperature and % crystallinity values of PE and PP phases inside the recycled polypropylene and also its blends and nanocomposites containing E-MA-GMA and Cloisite® 15A organoclay at different compositions. A significant change in melting temperature and crystallinity were not observed for the entire set of compositions.

Considering the binary blends, the crystallinity of both polypropylene and polyethylene segments was not significantly affected by the addition of E-MA-GMA compatibilizer, and exhibited some marginal reduction in crystallinity. Binary composites of recycled polypropylene and Cloisite® 15A exhibit a general increase in crystallinity in both segments to a small extent. Results were attributed to the presence of platelets dispersed in the matrix promoting heterogeneous nucleation

and increasing the crystallization rate and hence crystallinity [85]. Moreover, as reported in the literature, the organoclay content contributes to the rise of the crystallization temperature and reduction in the crystallite sizes [135]. In addition to these, increase in organoclay content contributed to increase in crystallinity. Similar results were also obtained in the ternary nanocomposites. Finally, melting temperatures of all composites and blends were reduced marginally compared to that of the neat recycled polypropylene.

**Table 4.6** DSC results, Lotader® AX8900 (E-MA-GMA) compatibilizer.

Sample	Peak-I			Peak-II		
	T <sub>m, PE</sub> (°C)	ΔH <sub>1, PE</sub> (J/g)	X <sub>c, PE</sub> (%)	T <sub>m, PP</sub> (°C)	ΔH <sub>1, PP</sub> (J/g)	X <sub>c, PP</sub> (%)
<b>Polymer Matrix</b>						
<b>Recycled Polypropylene (P)</b>	127.3	16.6	5.7	165.2	36.9	17.7
<b>Compatibilizer</b>						
<b>Lotader® AX8900</b>	51.9	23.6	8.1	-	-	-
<b>Binary blends (All-S)</b>						
<b>P+ 5wt% 8900</b>	126.4	15.5	5.6	163.8	35.2	17.7
<b>P+ 10wt% 8900</b>	126.1	14.8	5.6	163.5	35.8	19.0
<b>Binary nanocomposites (All-S)</b>						
<b>P+ 2wt% 15A</b>	126.2	18.5	6.4	163.8	40.4	19.7
<b>P+ 4wt% 15A</b>	126.2	18.1	6.4	163.6	40.3	20.1
<b>P+ 6wt% 15A</b>	126.4	18.0	6.5	163.6	41.9	21.3
<b>Ternary nanocomposites (All-S)</b>						
<b>P+ 2wt%15A+ 5wt% 8900</b>	125.9	18.6	6.8	163.0	42.3	21.7
<b>P+ 2wt%15A+ 10wt% 8900</b>	126.1	17.4	6.8	163.6	38.5	20.9
<b>P+ 4wt%15A+ 5wt% 8900</b>	126.7	17.3	6.5	164.2	38.8	20.4
<b>P+ 4wt%15A+ 10wt% 8900</b>	126.2	15.3	6.1	163.8	34.4	19.1
<b>P+ 6wt%15A+ 5wt% 8900</b>	127.0	14.4	5.5	164.2	33.5	18.0
<b>P+ 6wt%15A+ 10wt% 8900</b>	126.5	17.9	7.3	163.8	38.9	22.1

The effects of processing parameters on crystallinity are shown in Table 4.7 and DSC diagrams are in Appendix B. A significant difference related to processing condition was not observed similar to the results reported in the literature [85]. It should be noted that the final thermal properties depend mostly on the final injection conditions.

**Table 4.7** DSC results, effect of processing conditions.

Sample	Peak-I			Peak-II		
	T <sub>m, PE</sub> (°C)	ΔH <sub>f, PE</sub> (J/g)	X <sub>c, PE</sub> (%)	T <sub>m, PP</sub> (°C)	ΔH <sub>f, PP</sub> (J/g)	X <sub>c, PP</sub> (%)
<b>Polymer Matrix</b>						
<b>Recycled Polypropylene (P)</b>	127.3	16.6	5.7	165.2	36.9	17.7
<b>5 wt % 8900 (E-MA-GMA) and 2 wt% Cloisite® 15A (All-S)</b>						
<b>200 °C – 250 rpm</b>	125.9	18.6	6.8	163.0	42.3	21.7
<b>200 °C – 350 rpm</b>	125.8	19.8	7.3	163.3	40.6	20.9
<b>180 °C – 250 rpm</b>	125.7	19.8	7.3	163.1	46.3	23.8
<b>180 °C – 350 rpm</b>	126.2	18.4	6.8	163.9	39.2	20.2
<b>2 wt% PP-MAH and 1 wt% Cloisite® 15A (MB)</b>						
<b>200 °C – 250 rpm</b>	126.0	18.6	6.5	163.3	44.5	22.0
<b>200 °C – 350 rpm</b>	126.5	16.3	5.7	163.9	38.1	18.8
<b>180 °C – 250 rpm</b>	126.7	17.6	6.2	164.0	41.5	20.5
<b>180 °C – 350 rpm</b>	126.6	17.5	6.2	164.0	41.2	20.3

In binary blends of recycled polypropylene and PP-MAH, as shown in Table 4.8, the crystallinity values of the specimens were higher and, crystallinity was further increased as more compatibilizer was added. This explanation of this result could be due to crystallinity of PP-MAH as well as in the case of organoclay. Increase in crystallinity was specifically significant in the polypropylene segment indicating that presence of PP-MAH mainly affects the polypropylene segments. Also, the crystallinity of PP-MAH would be observed at the same temperature as that of polypropylene.

**Table 4.8** DSC results, effect of PP-MAH to organoclay ratio.

Sample	Peak-I			Peak-II		
	$T_{m, PE}$ (°C)	$\Delta H_{PE}$ (J/g)	$X_{c, PE}$ (%)	$T_{m, PP}$ (°C)	$\Delta H_{PP}$ (J/g)	$X_{c, PP}$ (%)
<b>Polymer Matrix</b>						
<b>Recycled Polypropylene (P)</b>	127.3	16.6	5.7	165.2	36.9	17.7
<b>Compatibilizer</b>						
<b>PP-MAH</b>	-	-	-	164.0	71.8	34.3
<b>Binary blends (MB)</b>						
<b>P+ 0.5 wt% PP-MAH</b>	126.6	20.1	6.9	163.9	41.2	19.8
<b>P+ 1.0 wt% PP-MAH</b>	127.1	16.8	5.8	164.4	38.6	18.7
<b>P+ 2.0 wt% PP-MAH</b>	126.9	17.1	6.0	164.3	41.8	20.4
<b>P+ 3.0 wt% PP-MAH</b>	126.8	15.5	5.4	164.4	37.9	18.7
<b>P+ 4.0 wt% PP-MAH</b>	127.0	16.5	5.9	164.5	42.0	20.9
<b>P+ 6.0 wt% PP-MAH</b>	126.6	17.4	6.3	163.7	44.2	22.5
<b>Binary nanocomposites (MB)</b>						
<b>P+ 0.5 wt% 15A</b>	127.0	16.5	5.7	164.7	37.7	18.1
<b>P+ 1.0 wt% 15A</b>	127.1	16.6	5.7	164.5	34.8	16.8
<b>P+ 2.0 wt% 15A</b>	125.9	20.0	7.0	163.2	45.4	22.2
<b>Ternary nanocomposites (MB)</b>						
<b>P+0.5wt%PP-MAH+0.5wt%15A</b>	127.5	14.2	4.9	165.0	33.3	16.1
<b>P+1.0wt%PP-MAH+1.0wt%15A</b>	127.3	16.5	5.7	164.8	33.7	16.5
<b>P+2.0wt%PP-MAH+2.0wt%15A</b>	127.1	16.6	5.9	164.5	38.9	19.4
<b>P+1.0wt%PP-MAH+0.5wt%15A</b>	126.5	18.6	6.4	164.3	40.8	19.8
<b>P+2.0wt%PP-MAH+1.0wt%15A</b>	126.6	17.5	6.2	164.0	41.2	20.3
<b>P+4.0wt%PP-MAH+2.0wt%15A</b>	127.4	14.8	5.4	165.0	31.3	15.9
<b>P+1.5wt%PP-MAH+0.5wt%15A</b>	127.5	14.5	5.1	165.0	32.2	15.7
<b>P+3.0wt%PP-MAH+1.0wt%15A</b>	126.6	19.1	6.8	164.1	46.5	23.2
<b>P+6.0wt%PP-MAH+2.0wt%15A</b>	126.7	15.9	5.9	163.8	41.8	21.7

Crystallinity of the ternary nanocomposites containing PP-MAH and Cloisite®15A was also higher. The effects of compatibilizer to organoclay ratio were not significant; however, as the ratio became higher, the increase in crystallinity became more detectable, especially in the polypropylene segment. This result would be obtained

due to the crystallinity effect of PP-MAH, whose content was increased as the ratio was increased and relatively better dispersion of organoclays in the presence of PP-MAH affecting the rate of heterogeneous nucleation.

**Table 4.9** DSC results, effect of organoclay type.

Sample	Peak-I			Peak-II		
	T <sub>m, PE</sub> (°C)	ΔH <sub>PE</sub> (J/g)	X <sub>c, PE</sub> (%)	T <sub>m, PP</sub> (°C)	ΔH <sub>PP</sub> (J/g)	X <sub>c, PP</sub> (%)
<b>Polymer Matrix</b>						
<b>Recycled Polypropylene (P)</b>	127.3	16.6	5.7	165.2	36.9	17.7
<b>Compatibilizer</b>						
<b>PP-MAH</b>	-	-	-	164.0	71.8	34.3
<b>Binary nanocomposites (MB)</b>						
<b>P+ 0.5wt% 25A</b>	127.0	16.6	5.7	164.2	39.0	18.8
<b>P+ 1.0wt% 25A</b>	126.4	17.0	5.9	163.8	39.8	19.2
<b>P+ 2.0wt% 25A</b>	126.6	19.8	6.9	163.9	46.0	22.4
<b>P+ 0.5wt% 30B</b>	126.5	19.2	6.6	164.2	45.5	21.9
<b>P+ 1.0wt% 30B</b>	126.1	19.0	6.5	163.6	43.8	21.2
<b>P+ 2.0wt% 30B</b>	126.7	17.9	6.2	164.0	41.2	20.1
<b>Ternary nanocomposites (MB)</b>						
<b>P+1.0wt%PP-MAH+0.5wt%25A</b>	126.7	17.5	6.1	163.6	41.5	20.2
<b>P+2.0wt%PP-MAH+1.0wt%25A</b>	127.8	16.6	5.8	165.2	33.1	16.3
<b>P+4.0wt%PP-MAH+2.0wt%25A</b>	126.7	17.9	6.5	163.8	45.6	23.2
<b>P+1.0wt%PP-MAH+0.5wt%30B</b>	126.9	17.4	6.0	164.5	40.2	19.5
<b>P+2.0wt%PP-MAH+1.0wt%30B</b>	127.6	13.3	4.7	164.9	32.1	15.8
<b>P+4.0wt%PP-MAH+2.0wt%30B</b>	126.9	16.2	5.9	164.2	40.3	20.5

Finally, the effects of clay type on crystallization behavior of recycled polypropylene were investigated and the results are given in Table 4.9 and the detailed DSC diagrams are in Appendix B. Significant effects of clay type in binary and ternary nanocomposites were not observed, even though Cloisite® 30B exhibited better dispersion in XRD results and better crystallization effect was expected in this clay

type. Consequently, it was concluded that each clay type had similar effect on nucleation of recycled polypropylene in the presence or absence of PP-MAH.

#### **4.4 Melt Flow Index Analysis**

Melt flow index measurements were performed at 180 °C under a specified load of 2.16 kg. Melt flow index is a parameter that is inversely proportional to the melt viscosity of the materials. Molecular weight of the matrix, presence of additives, interactions between the components, degree of chain branching as well as processing parameters are the main factors affecting the MFI values.

In Table 4.10 the MFI values of recycled polypropylene (neat and extruded forms) compatibilizers used during study, and blends and nanocomposites prepared with E-MA-GMA elastomer and Cloisite® 15A organoclay are shown. MFI of recycled polypropylene was reduced after the first extrusion and remained almost constant after second extrusion. Considering the SEM images, this could have resulted from uniform distribution of the polyethylene phase owing to effective mixing and hence increased interaction between phases causing increase in melt viscosity. MFI values were not significantly altered upon E-MA-GMA compatibilizer addition. This result is due to the closeness of the MFI values of matrix and compatibilizer and the amount of additive which was small to affect the flow properties. Incorporation of organoclay decreased the melt viscosity until 4 wt% organoclay content and then increased at 6 wt% addition. Clay platelets restrict the motion of polymer chains during flow and generally increase the melt viscosity. Slip between the matrix material and the clay platelets during high shear was reported as one of the possibilities to this contradiction [136]. Moreover, increase in melt viscosity after 4 wt% clay loading could be attributed to dominating hindrance effect of clay agglomerates at higher clay loading. In ternary nanocomposites, a general trend was an increase in melt viscosity except for the one containing 2 wt% organoclay and 5 wt% E-MA-GMA. Increase in melt viscosity in the ternary nanocomposites could be an indication of interactions between the E-MA-GMA and organoclay restricting the chain mobility. For the nanocomposite containing 2 wt% organoclay and 5 wt% E-MA-GMA the slippage effect between the clay particles and matrix dominated the interactions between the compatibilizer and the organoclay and resulted in higher MFI (lower melt viscosity).

**Table 4.10** MFI results, Lotader® AX8900 (E-MA-GMA) compatibilizer.

Sample	P Concentration (wt %)	MFI (g/10 min)	St. D.
<b>Polymer Matrix</b>			
P (not extruded)	100	3.91	0.08
P (extruded once)	100	3.69	0.06
P (extruded twice)	100	3.64	0.11
<b>Compatibilizers</b>			
E-MA-GMA	100	7.3	0.27
PP-MAH	100	107.2	9.33
<b>Binary blends (All-S)</b>			
P+ 5 wt% E-MA-GMA	95	3.49	0.04
P+ 10 wt% E-MA-GMA	90	3.65	0.04
<b>Binary nanocomposites (All-S)</b>			
P+ 2 wt% 15A	98	3.80	0.06
P+ 4 wt% 15A	96	3.86	0.03
P+ 6 wt% 15A	94	3.24	0.05
<b>Ternary nanocomposites (All-S)</b>			
P+ 2wt% 15A+ 5wt% E-MA-GMA	93	4.07	0.06
P+ 2wt% 15A+ 10wt% E-MA-GMA	88	2.52	0.04
P+ 4wt% 15A+ 5wt% E-MA-GMA	91	2.48	0.02
P+ 4wt% 15A+ 10wt% E-MA-GMA	86	1.81	0.01
P+ 6wt% 15A+ 5wt% E-MA-GMA	89	2.23	0.01
P+ 6wt% 15A+ 10wt% E-MA-GMA	84	1.60	0.01

MFI measurements for determining the effects of processing conditions were conducted with only one composition of 1 wt% Cloisite® 15A and 2 wt% PP-MAH. It was observed that at low processing temperature and high screw speed the melt viscosity was higher as shown in Table 4.11. Results were in correlation with the XRD patterns of the nanocomposites, pointing out the enhanced dispersion and hence interactions between the matrix and silicate layers owing to effective mixing under high shear.

**Table 4.11** MFI results, effect of processing conditions.

Sample	P Concentration (wt %)	MFI (g/10 min)	St. D.
<b>P+ 2 wt% PP-MAH+ 1 wt% Cloisite® 15A (MB)</b>			
200 °C – 250 rpm	97	3.69	0.05
200 °C – 350 rpm	97	3.79	0.05
180 °C – 250 rpm	97	3.53	0.02
180 °C – 350 rpm	97	3.50	0.01

Table 4.12 shows the MFI values of blends and nanocomposites prepared with PP-MAH and Cloisite® 15A, Cloisite® 25A and Cloisite® 30B. In the binary blends of PP-MAH and recycled polypropylene, increase in MFI values was expected owing to high melt flow index of PP-MAH itself. However, specifically at 6 wt% compatibilizer concentration the MFI was decreased. As previously mentioned, despite the non polar structures of constituents in the recycled polymer matrix and immiscibility between the phases, improved interfacial interactions were suggested with incorporation of PP-MAH compatibilizer in the literature [56]. Therefore, reduction in the melt viscosity could be assigned for these enhanced interactions between polyethylene and polypropylene phases in the presence of PP-MAH. This result could also explain the size reduction in the elastomeric domains observed in the SEM images at 6 wt% PP-MAH loading and relative increase in mechanical properties at this PP-MAH content.

Reduction in MFI was also observed in the ternary nanocomposites prepared with PP-MAH and Cloisite® 15A. Decrease in the MFI was much significant compared to binary blends of PP-MAH and recycled polypropylene owing to the interactions between compatibilizer and organoclay surface hindering the flow of the polymer chains. In addition to that, as the ratio between compatibilizer and organoclay was increased, the decrease in MFI values was more observable indicating that enhanced interactions between organoclay and compatibilizer were present.

In the last part of the study, the effect of organoclay type on flow properties was investigated and results are shown in Table 4.12. Increase in MFI values at 1 and 2

wt% organoclay loading was observed in binary nanocomposites prepared with all types of organoclays. However, in ternary nanocomposites, reduction in MFI was more significant for the ones constituting Cloisite® 15A. This result could be attributed to the greater intermolecular interactions between the Cloisite® 15A and the PP-MAH compared to other organoclays impeding the segmental motion and flow tendency of polymer chains.

**Table 4.12** MFI results, effect of PP-MAH to organoclay ratio and organoclay type.

Sample	P Concentration (wt %)	MFI (g/10 min)	St. D.
<b>Binary blends (MB)</b>			
P+ 2.0 wt% PP-MAH	98	3.45	0.02
P+ 4.0 wt% PP-MAH	96	3.46	0.04
P+ 6.0 wt% PP-MAH	94	3.25	0.03
<b>Binary nanocomposites (MB)</b>			
P+ 1.0 wt% 15A	99	3.98	0.02
P+ 2.0 wt% 15A	98	3.82	0.05
P+ 1.0 wt% 25A	99	4.02	0.07
P+ 2.0 wt% 25A	98	3.90	0.04
P+ 1.0 wt% 30B	99	3.60	0.05
P+ 2.0 wt% 30B	98	3.70	0.05
<b>Ternary nanocomposites (MB)</b>			
P+ 1.0wt% PP-MAH+ 1.0wt% 15A	98	3.63	0.04
P+ 2.0wt% PP-MAH+ 2.0wt% 15A	96	3.22	0.04
P+ 2.0wt% PP-MAH+ 1.0wt% 15A	97	3.50	0.01
P+ 4.0wt% PP-MAH+ 2.0wt% 15A	94	2.91	0.02
P+ 3.0wt% PP-MAH+ 1.0wt% 15A	96	3.48	0.04
P+ 6.0wt% PP-MAH+ 2.0wt% 15A	92	2.89	0.02
P+ 2.0wt% PP-MAH+ 1.0wt% 25A	97	3.51	0.05
P+ 4.0wt% PP-MAH+ 2.0wt% 25A	94	3.07	0.03
P+ 2.0wt% PP-MAH+ 1.0wt% 30B	97	3.58	0.05
P+ 4.0wt% PP-MAH+ 2.0wt% 30B	94	3.26	0.05

## CHAPTER 5

### CONCLUSIONS

Polymer blends and nanocomposites were prepared by melt compounding method in order to improve the mechanical properties of a recycled grade polypropylene. The effects of concentrations as well as the types of organoclays and compatibilizers, effect of processing conditions and the ratio of the compatibilizer to organoclay on the morphology and mechanical, thermal and flow properties were investigated.

At 2 wt% Cloisite® 15A content, intercalation ability of polymer chains was present. In addition to that, dispersion mechanism was improved with the addition of E-MA-GMA phase. However, amounts of clay loading over 2 wt% diminished the intercalation mechanism even in the presence of the compatibilizer. Owing to the nucleating effect of organoclay, the crystallinity and hence the stiffness were improved at high clay loadings. However, the reduction in the domain size and the existing micro cracks formed as a consequence of clay agglomerates depleted the impact strength. In the binary blends of E-MA-GMA and recycled polypropylene, the toughness was improved as a result of increased energy absorbing capacity of the matrix, on the other hand, addition of organoclay at high loadings as a third component lowered both the tensile and the impact properties.

Besides the polymer-organoclay and the compatibilizer-organoclay interactions, processing conditions significantly affected the morphology and material properties. In the XRD patterns, remarkable reduction in intensity values were observed as extrusion temperature was decreased and screw speed was increased as a result of partial delamination. In SEM micrographs, reduction in domain size and uniform distribution of rubber domains were also observed in specimens prepared with both PP-MAH and E-MA-GMA compatibilizers. When processing temperature was decreased simultaneously with increasing screw speed, significant improvements in both tensile and impact properties were observed as a result of dominating dispersive forces at high shear medium and hence improved organoclay dispersion.

In the XRD patterns of ternary nanocomposites prepared with PP-MAH and Cloisite® 15A, the peaks shifted to lower angles and decreased in intensity. Intercalation ability of PP-MAH compatibilizer was obvious, and as the PP-MAH to organoclay ratio was increased, more effective dispersion was observed in both XRD patterns and TEM micrographs. Interactions between organoclay and polymer were improved as a consequence of higher affinity and hydrogen bonding between the maleic anhydride group and the silicate surfaces as well as the chemical compatibility between the isotactic polypropylene matrix and polypropylene present in the compatibilizer structure.

Tensile properties of recycled polypropylene matrix were improved with incorporation of PP-MAH compatibilizer. This result was attributed to the higher crystallinity of PP-MAH as observed in DSC analysis, and also higher tensile properties compared to recycled polypropylene. In addition to that, domain size of polyethylene phase was reduced and hence the impact strength also enhanced. Considering the MFI values of binary blends prepared with PP-MAH, the MFI of the blends decreased, although the MFI value of PP-MAH was higher than that of the matrix. This result was assigned to increased adhesion and decreased interface mobility between the immiscible polyethylene and polypropylene phases in the presence of PP-MAH.

Improvement in tensile properties for the ternary nanocomposites prepared with PP-MAH and organoclays were much more significant. Reduction in domain size and increased interdomain distance in the SEM images of these ternary nanocomposites were apparent. The barrier effect of organoclay and the improvement in adhesion between the phases due to compatibilizer and organoclay addition would be the main reason behind the simultaneous improvements of all properties in these nanocomposites.

In the last part of the study, the effects of organoclay type were investigated. In binary nanocomposites prepared with Cloisite® 15A, Cloisite® 25A and Cloisite® 30B and recycled polypropylene, intercalation of organoclay layers was observed. Since the organoclay content was low, the dispersive forces easily overcame the cohesive forces between the clay platelets for all nanoclay types. Tensile properties were also improved to a small extent due to nucleating ability of organoclays and hence the increased crystallinity. In addition to that, reduction in particle size was observed in SEM images of nanocomposites containing 1 wt% organoclay of each

type and the best improvement in impact strength was also detected in these nanocomposites regardless of the organoclay type.

In ternary nanocomposites prepared with PP-MAH compatibilizer at specified composition, Cloisite® 15A exhibited intercalated-delaminated structure, whereas in XRD patterns of Cloisite® 25A and particularly Cloisite® 30B exfoliated structures were determined. In TEM micrographs, the results were contradictory, since each type of clay exhibited the same intercalated delaminated structure and even the number of the delaminated zones was higher in the micrographs of Cloisite® 15A. XRD results were found to be more, reliable since TEM analysis represents only a minor part of the specimen.

Improvement in tensile properties of nanocomposites containing Cloisite® 15A was greater compared to nanocomposites prepared with the other organoclays. According to the XRD results, the best improvement was expected in the case of Cloisite® 30B, since the organoclay layers were completely exfoliated and hence the interaction between the silicate layers and polymer was maximized. Contradiction between the XRD and tensile results was assigned to two main reasons. First one is the orientation of organoclay in the specimens during injection molding. The silicate layers of Cloisite® 15A would be oriented during the injection process, and even though the structure was less exfoliated compared to other organoclays, the tensile properties in the direction of injection would be greater. Second reason is due to the dimensions of the fillers: the aspect ratio of organoclay platelets of Cloisite® 25A and Cloisite® 30B would become smaller under high shear media as observed for Cloisite® 25A and Cloisite® 30B containing nanocomposites and the reinforcing effect of the fillers would be lower even though they were delaminated.

Finally, the best improvement in mechanical properties were obtained for the nanocomposites containing 6 wt% PP-MAH and 2 wt% Cloisite® 15A with %31.5 increase in Young's Modulus, %7.8 increase in tensile stress at yield, %3.2 tensile strength, % 1.4 elongation at break and % 8.5 impact strength.

## REFERENCES

1. Kaw A.K., "Mechanics of Composite Materials", 2<sup>nd</sup> Edition, CRS Press, Boca Raton, Fla., 2006.
2. Starr F.L., "Composites: A Profile of the Worldwide Reinforced Plastics Industry, Markets and Suppliers", 3<sup>rd</sup> Edition, Elsevier, Kidlington, Oxford, UK, 1999.
3. Matthews F.L., Rowlings R.D., "Composite Materials, Engineering & Science", Chapman & Hall, London, New York, 1994.
4. Lubin G., "Handbook of Composites", Van Nostrand Reinhold, New York, 1982.
5. Fischer H., Materials Science and Engineering, C 23, 763–772, 2003.
6. Ajayan P.M., Schadler L.S., Braun P.V., "Nanocomposite Science and Technology", Wiley-VCH, Weinheim, Great Britain, 2003.
7. Mai Y.W., Yu Z.Z., "Polymer Nanocomposites", CRS Press, Boca Raton, Fla., Woodhead, Cambridge, England, 2006.
8. Vaia R.A., Ishii H., Giannelis E.P., Chemistry of Materials, 5, 1694-6, 1993.
9. Ray S.S., Okamoto M., Progress in Polymer Science, 28, 1539-1641, 2003.
10. Manias E., Touny A., Wu L., Strawhecker K., Lu B., Chung T.C., Chemistry of Materials, 13, 3516-3523, 2001.
11. Alexandre M., Dubois P., Materials Science and Engineering, 28, 1-63, 2000.
12. Zanetti M., Lomakin S. and Camino G., Macromolecular Materials and Engineering, 279, 1-9, 2000.
13. Giannelis E.P., Krishnamoorti R., Manias E., Advances in Polymer Science, 138, 107-147, 1999.
14. Lertwimolnun W., Vergnes B., Polymer Engineering Science, 46, 314-323, 2006.

15. Karian H.G., "Handbook of Polypropylene and Polypropylene Composites", Marcel Dekker Incorporated, New York, 1999.
16. Kim D.H., Fasulo P.D., Rodgers W.R., Paul D.R., Polymer, 48, 5308-5323, 2007.
17. Albano C., Gonzalez J., Ichazo M., Rosales C., Urbina de Navarro C., Parra C., Composite Structures, 48, 49-58, 2000.
18. Chawla K., "Composite Materials Science and Engineering", 2<sup>nd</sup> Ed., Springer - Verlag, New York, 1998.
19. Rosen S.L., "Fundamental Principles of Polymeric Materials", Wiley, New York, 1982.
20. Gilman J.W., Jackson C.L., Morgan A.B., Harris R., Chemistry of. Materials, 12, 1866-1873, 2000.
21. Lebaron P.C., Wang Z., Pinnavaia T., Journal of Applied Clay Science, 15, 11-29, 1999.
22. Kornmann, X., PhD Thesis, Synthesis and Characterization of Thermoset-clay Nanocomposites, Division of Polymer Engineering, Luleå University of Technology: Luleå, Sweden, 2001.
23. Simon G.P., "Polymer Characterization Techniques and Their Applications to Blends", Oxford University Press, 2003.
24. Ultracki, "L.A, Polymer Blends Handbook", Kluwer Academic Publishers, Dordrecht, 2002.
25. Harper, C.A., "Modern Plastics Handbook", McGraw-Hill Professional Publishing, Blacklick, OH, USA, 2000.
26. Mantia F., "Handbook of Plastics Recycling", Rapra Technology Limited, Shawbury, 2002.
27. Maier C., Calafut T., "Polypropylene - The Definitive User's Guide and Databook", William Andrew Publishing, 1998.
28. Vasile C., "Handbook of Polyolefins", 2<sup>nd</sup> Edition, CRC Press, 2000.

29. Kroschwitz J.I., Mark H.F., "Encyclopedia of Polymer Science and Technology", 3<sup>rd</sup> Ed., Wiley Interscience, 2003.
30. Van der Vegt A.K., "From Polymers to Plastics", Delft University Press, Delft, The Netherlands, 2002.
31. Tripathi D., "Practical Guide to Polypropylene", 1<sup>st</sup> Edition, Rapra Technology Ltd., UK, 2002.
32. Blom H.P., Teh J.W., Rudin A., Journal of Applied Polymer Science, 70, 2081-2095, 1998.
33. Peacock A.J., "Handbook of Polyethylene: Structures, Properties, and Applications", CRC Press, 2000.
34. Kroschwitz J.I., "Concise Encyclopedia of Polymer Science and Engineering", Wiley-Interscience Publication, New York, 1990.
35. Jancar J., Dibenedetto A.T., Journal of Material Science, 29, 4651-4658, 1994.
36. Jang B.Z., Uhlmann D.R., Vander Sande J.B., Journal of Applied Polymer Science, 30, 2485-2504, 1985.
37. Long Y., Shanks R.A., Journal of Applied Polymer Science, 62, 639-646, 1996.
38. Ou Y.C., Guo T.T., Fang X.P., Yu Z.Z., Journal of Applied Polymer Science, 74, 2397-2403, 1999.
39. Li Y., Wei G.X., Sue H.J., Journal of Material Science, 37, 2447-2459, 2002.
40. Kim D.H., Fasulo P.D., Rodgers W.R., Paul D.R., Polymer, 48, 5960-5978, 2007.
41. Lei S.G., Hoa S.V., Ton-That, M.T, Composites Science and Technology, 66, 1274-1279, 2006.
42. Garcia Lopez D., Gobernado Mitre I., Merino J.C., Pastor J.M., Polymer Bulletin, 59, 667-676, 2007.
43. Modesti M., Lorenzetti A., Bon D., Besco S., Polymer, 46, 10237-10245, 2005.

44. Usuki A., Kato M., Okada A., Kurauchi T., *Journal of Applied Polymer Science*, 63, 137, 1997.
45. Kawasumi M., Hasegawa N., Kato M., Usuki A., Okada A., *Macromolecules*, 30, 6333, 1997.
46. Leuteritz A., Pospiech D., Kretzschmar B., Willeke M., Jehnichen D., Jentsch U., *Advanced Engineering Materials*, 9, 678–681, 2003.
47. Kaempfer D., Thomann R., Mulhaupt R., *Polymer*, 43, 2909–2916, 2002.
48. Mehrabzadeh M., Hossein N.K., *Journal of Applied Polymer Science*, 72, 1257–1265, 1999.
49. Zhao R.F., Dai G., *Journal of Applied Polymer Science*, 86, 2486–2491, 2002.
50. Hasegawa N., Usuki A., *Journal of Applied Polymer Science*, 93, 464-470, 2004.
51. Wang K., Wu J.S., Zeng H.M., *Composite Science Technology*, 61, 1529-1583, 2001.
52. Yin B., Zhao Y., Pan M.M., Yang M.B., *Polymers for Advanced Technologies*, 18, 439-445, 2007.
53. Hassan A., Othman N., Wahit M.U., Wei L.J., Rahmat A.R., Ishak Z.A.M., *Macromolecular Symposia*, 239, 182-191, 2006.
54. Baker W.E., Scott C.E., Hu G.H., “Reactive Polymer Blending”, Hanser, Munich, Germany, 2001.
55. Macosko C.W., Guegan P., Khandpur A.K, *Macromolecules*, 29, 5590-5598, 1996.
56. Li S., Jarvela P.K., Jarvela A.P., *Polymer Engineering and Science*, 37, 1997.
57. The Dow Chemical Company, “<http://www.dow.com>”, last accessed; 15<sup>th</sup> July 2008.
58. Kato M., Usuki A., Okada, A., Kurauchi T., *Journal of Applied Polymer Science*, 63, 137-139, 1997.

59. Liu X., Wu Q., *Polymer*, 42, 10013-10019, 2001.
60. Hasegawa N., Okamoto H., Kawasumi M., Kato M., Tsukigase A., Usuki A., *Macromolecular. Materials and Engineering*, 280/281, 76-79, 2000.
61. Tadmor Z., Gogos C.G., "Principles of Polymer Processing", Wiley, New York, 1979.
62. Middleman S., "Fundamentals of Polymer Processing", McGraw-Hill, New York, 1997.
63. Ram A., "Fundamentals of Polymer Engineering", Plenum Press, New York, 1997.
64. Rosato D.V., "Extruding Plastics - A Practical Processing Handbook", Springer, Verlag, 1998.
65. Todd D.B., "Plastics Compounding-Equipment and Processing", Hanser Publishers, Munich, 1998.
66. Margolis J.M., "Engineering Plastics Handbook", McGraw-Hill, New York, 2006.
67. Shigley J.E., Mischke C.R., Brown T.H., "Standard Handbook of Machine Design", McGraw-Hill, New York, 2004.
68. Seymour R.B., "Polymer Chemistry: An Introduction", 4<sup>th</sup> Edition, Marrel Dekker, New York, 1996.
69. Fried J. R., "Polymer Science and Technology", 2<sup>nd</sup> Edition, Prentice Hall Publications, USA, 2003.
70. Sandler S.R., "Polymer Synthesis and Characterization: A Laboratory Manual", Academic Press, San Diego, 1998.
71. Billmeyer F.W., "Textbook of Polymer Science", John Wiley & Sons, New York, 1984.
72. Crompton T.R., "Polymer Reference Handbook", Rapra Technology Limited, Shawbury, 2006.

73. Chou, N.J., Kowalczyk, S.P., Saraf, R., Tong, H.M., "Characterization of Polymers", Manning Publication, 1994.
74. Cao G., "Nanostructures and Nanomaterials: Synthesis, Properties and Applications", Imperial College Press, 2004.
75. Ramakrishna, S., "An Introduction to Electrospinning and Nanofibers", River Edge, NJ, USA: World Scientific Publishing Company, 2005.
76. Sperling, L.H., "Introduction to Physical Polymer Science", 4<sup>th</sup> Edition, Wiley, 2006.
77. Callister W., "Materials Science and Engineering: An Introduction", 4<sup>th</sup> Edition, John-Wiley & Sons, USA, 1997.
78. Goodhew P.J., Humphreys F.J., Beanland R., "Electron Microscopy and Analysis", 3<sup>rd</sup> Edition, Taylor & Francis, 1975.
79. Shenoy A.V., "Rheology of Filled Polymer Systems", Kluwer Academic Publishers, Dordrecht, 1999.
80. Deshmane C., Yuan Q., Perkins R.S., Misra R.D.K, Materials Science and Engineering, A458, 150-157, 2007.
81. Zhang Q., Fu Q., Jiang L., Lei Y., Polymer International, 49, 1561-1564, 2000.
82. Gianelli W., Ferrara G., Camino G., Pellegatti G., Rosenthal J., Trombini R.C., Polymer, 46, 7037-7046, 2005.
83. Ton-That M. T., Perrin-Sarazin F., Cole K. C., Bureau M. N., Denault J., Polymer Engineering and Science, 44, 1212-1219, 2004.
84. Lertwimolnun W., Vergnes B., Polymer, 46, 3462-3471, 2005.
85. Modesti M., Lorenzetti A., Bon D., Besco S., Polymer Degradation and Stability, 91, 672-680, 2006.
86. Deenadayalan E., Vidhate S., Lele A., Polymer International, 55, 1270-1276, 2006.

87. Lim J.W., Hassan A., Rahmat A.R., Wahit M.U, Polymer-Plastics Technology and Engineering, 47, 411- 419, 2008.
88. Zhu L., Xanthos M., Journal of Applied Polymer Science, 93, 1891-1899, 2004.
89. Southern Clay Products, "<http://www.scprod.com>", last accessed; 15<sup>th</sup> of July, 2008.
90. Arkema Inc., "<http://www.arkema-inc.com>", last accessed; 15<sup>th</sup> July, 2008.
91. Polyram, "<http://www.polyram.co.il>", last accessed; 15<sup>th</sup> July, 2008.
92. ISO 527, International Organization for Standardization - Plastics, "Determination of Tensile Properties" & "Test Conditions for Molding and Extrusion Plastics".
93. ISO 179, International Organization for Standardization - Plastics, "Determination of Charpy Impact Properties".
94. Chen J.H., Zhong J.C., Cai Y.H., Su W.B., Yang Y.B., Polymer, 48, 2946-2957, 2007.
95. ISO 1133, International Organization for Standardization-Plastics, "Determination of Melt Volume Flow Rate (MVR), Melt Mass Flow Rate (MFR) of Thermoplastics Materials".
96. Brindley G. W., Brown G., "Crystal Structures of Clay Minerals and their X-Ray Identification", Mineralogical Society, London, 1980.
97. Park K.W., Chowdhury S.R., Park C.C, Kim G.H., Journal of Applied Polymer Science, 104, 3879-3885, 2007.
98. Mirzadeh A., Kokabi M., European Polymer Journal, 43, 3757-3765, 2007.
99. González I., Eguiazábal J.I., Nazábal J., Composites Science and Technology, 66, 1833-1843, 2006.
100. Marchant D., Jayaraman K., Industrial and Engineering Chemistry Research, 41, 6402-6408, 2002.
101. Chang Y.W., Lee D., Bae S.Y., Polymer International, 55, 184-189, 2006.

102. Kim S.W., Jo W.H., Lee M.S., Ko M.B., Jho J.Y., *Polymer Journal*, 34, 103-111, 2002.
103. Pozsgay A., Frater T., Papp L., Sajó I., Pukanszky B., *Journal of Macromolecular Science, Part B*, 41, 1249, 2002.
104. McCabe W.L., Smith J.C., Harriott P., "Unit Operations of Chemical Engineering", 7<sup>th</sup> Edition, McGraw Hill, Boston, 2005.
105. Yilmazer U, Cansever M., *Polymer Composites*, 23, 61-71, 2002.
106. Chung Y.C., Cho T.K., and Chun B.C., *Fibers and Polymers*, 9, 7-14, 2008.
107. Lee H.S., Fasulo P.D., Rodgers W.R., Paul D.R., *Polymer*, 46, 11673, 2005.
108. Lee, J.W., Lim Y.T, Park O.O., *Polymer Bulletin* 45, 191-198, 2000.
109. Fornes T.D., Yoon P.J., Hunter D.L., Keskkula H., Paul D.R., *Polymer*, 43, 5915-5933, 2002.
110. Contreras V., Cafiero M., Da Silva S., Rosales C., Perera R. and Matos M., *Polymer Engineering and Science*, 46, 1111-1120, 2006.
111. Plochocki A.P., Dagli S.S., Andrews R.D., *Polymer Engineering Science*, 30, 741, 1990.
112. Pukanszky B., Tudos F., Kolarik J., Lednický F., *Polymer Composites*, 11, 98, 1990.
113. Tokita N., *Rubber Chem. Technology*, 50, 292, 1977.
114. Jose S., Aprem A.S, Francis B., Chandy M.C., Werner P., Alstaedt V., Thomas S., *European Polymer Journal*, 40, 2105-2115, 2004.
115. Walsh D.J, Higgins J.S., *Polymer*, 23, 336, 1982.
116. Kelnar I., Kotek J., Kaprálková L., Munteanu B.S., *Journal of Applied Polymer Science*, 96, 288-293, 2005.
117. Liang J. Z., Li R. K. Y., *Journal of Applied Polymer Science*, 77, 409-417, 2000.

118. Wu S., *Polymer Engineering Science*, 27, 335, 1987.
119. Arcana I.M., Bundjali B., Yudistra I., Jariah B., Sukria L., *Polymer Journal*, 39, 1337-1344, 2007.
120. Kim G.M., Michler G. H., Rösch J. and Mülhaupt R., *Acta Polymerica*, 49, 88-95, 1998.
121. Chow, W. S., Mohd Ishak Z. A., Karger-Kocsis J., Apostolov A. A., Ishiaku U. S., *Polymer*, 44, 7427, 2003.
122. Vlasveld D.P.N, Vaidya S.G., Bersee H.E.N, Picken S.J, *Polymer*, 46, 3452-3461, 2005.
123. Saminathan K., Selvakumar P., Bhatnagar N., *Polymer Testing*, 27, 296-307, 2008.
124. Solomon M.J., Somwangthanaroj A, "Intercalated Polypropylene Nanocomposites," *Dekker Encyclopedia of Nanoscience and Nanotechnology*, Marcel Dekker, 1483-1490, 2004.
125. Lim J.W., Hassan A., Rahmat A.R., Wahit M.U., *Journal of Applied Polymer Science*, 99, 3441-3450, 2006.
126. Hasegawa N., Okamoto H., Kawasumi M., Usuki A., *Journal of Applied Polymer Science*, 74, 3359, 1999.
127. Nielsen L.E., Landel R.F., "Mechanical Properties of Polymers and Composites", 2<sup>nd</sup> Edition, Marcel Dekker Inc., USA, 1994.
128. Galgali G., Agarwal S., Lele A., *Polymer*, 45, 6059-6069, 2004.
129. Hotta S., Paul D. R., *Polymer*, 45, 7639-7654, 2004.
130. Jiang W., Liu C. H., Wang Z. G., An L. J., Liang H. J., Jiang B.Z., Wang X. H. And Zhang H. X., *Polymer*, 39, 3285-3288, 1998.
131. Van der Wal A., Nijhof R., Gaymans R., *Polymer*, 40, 6031-6044, 1990.

132. Tjong S.C., Bao S.P., *Journal of Polymer Science, Part B, Polymer Physics*, 43, 585-595, 2005.
133. Van der Wal, A., Gaymans, R., *Journal of Polymer*, 40, 6067, 1999.
134. Rachtanapun P., Selke S. E. M., Matuana L. M., *Journal of Applied Polymer Science*, 88, 2842, 2003.
135. Qin H., Su Q., Zhang S., Zhao B., Yang M., *Polymer*, 44, 7533-7538, 2003.
136. Cho J.W., Paul D.R., *Polymer*, 42, 1083-1094, 2001.

## APPENDIX A

### MECHANICAL TEST RESULTS

**Table A.1** Young's Modulus data and standard deviations for all compositions.

Components	Add. Order	Processing Parameters		Young's Modulus (MPa)	
		°C	rpm	Value	St. D.
<b>P</b>	-	-		<b>879.7</b>	<b>± 9.9</b>
<b>P- Compatibilizer Blends</b>					
<b>P+ 5 wt% E-MA-GMA</b>	All-S	200	250	<b>847.4</b>	<b>± 38.7</b>
<b>P+ 10 wt% E-MA-GMA</b>	All-S	200	250	<b>766.8</b>	<b>± 8.6</b>
<b>P+ 0.5 wt% PP-MAH</b>	All-S	180	350	<b>926.3</b>	<b>± 12.5</b>
<b>P+ 1.0 wt% PP-MAH</b>	All-S	180	350	<b>948.6</b>	<b>± 16.2</b>
<b>P+ 1.5 wt% PP-MAH</b>	All-S	180	350	<b>948.6</b>	<b>± 13.2</b>
<b>P+ 2.0 wt% PP-MAH</b>	All-S	180	350	<b>972.0</b>	<b>± 17.0</b>
<b>P+ 3.0 wt% PP-MAH</b>	All-S	180	350	<b>937.1</b>	<b>± 0.0</b>
<b>P+ 4.0 wt% PP-MAH</b>	All-S	180	350	<b>972.2</b>	<b>± 14.0</b>
<b>P+ 6.0 wt% PP-MAH</b>	All-S	180	350	<b>972.0</b>	<b>± 13.9</b>
<b>P- Clay Binary Nanocomposites</b>					
<b>P+ 2 wt% 15A</b>	All-S	200	250	<b>908.5</b>	<b>± 12.0</b>
<b>P+ 4 wt% 15A</b>	All-S	200	250	<b>930.3</b>	<b>± 25.7</b>
<b>P+ 6 wt% 15A</b>	All-S	200	250	<b>948.6</b>	<b>± 13.2</b>
<b>P+ 0.5 wt% 15A</b>	MB	180	350	<b>889.6</b>	<b>± 10.0</b>
<b>P+ 1.0 wt% 15A</b>	MB	180	350	<b>894.6</b>	<b>± 0.0</b>
<b>P+ 2.0 wt% 15A</b>	MB	180	350	<b>948.6</b>	<b>±16.2</b>
<b>P+ 0.5 wt% 25A</b>	MB	180	350	<b>894.9</b>	<b>± 20.4</b>
<b>P+ 1.0 wt% 25A</b>	MB	180	350	<b>894.6</b>	<b>± 0.0</b>
<b>P+ 2.0 wt% 25A</b>	MB	180	350	<b>888.3</b>	<b>± 23.5</b>
<b>P+ 0.5 wt% 30B</b>	MB	180	350	<b>879.7</b>	<b>± 9.9</b>
<b>P+ 1.0 wt% 30B</b>	MB	180	350	<b>868.7</b>	<b>± 22.5</b>
<b>P+ 2.0 wt% 30B</b>	MB	180	350	<b>922.6</b>	<b>± 12.5</b>

**Table A.1** Young's Modulus data and standard deviations for all compositions (Cont'd).

Components	Add. Order	Processing Parameters		Young's Modulus (MPa)		
		°C	rpm	Value	St. D.	
<b>P- Compatibilizer- Clay Ternary Nanocomposites</b>						
<b>P+2wt%15A+ 5wt%E-MA-GMA</b>	All-S	200	250	<b>803.6</b>	<b>± 23.2</b>	
<b>P+2wt%15A+ 10wt%E-MA-GMA</b>	All-S	200	250	<b>795.3</b>	<b>± 11.4</b>	
<b>P+4wt%15A+ 5wt%E-MA-GMA</b>	All-S	200	250	<b>808.9</b>	<b>± 9.6</b>	
<b>P+4wt%15A+ 10wt%E-MA-GMA</b>	All-S	200	250	<b>722.3</b>	<b>± 9.4</b>	
<b>P+6wt%15A+ 5wt%E-MA-GMA</b>	All-S	200	250	<b>811.7</b>	<b>± 9.6</b>	
<b>P+6wt%15A+ 10wt%E-MA-GMA</b>	All-S	200	250	<b>678.6</b>	<b>± 0.0</b>	
<b>P+0.5wt%PP-MAH+ 0.5wt%15A</b>	MB	180	350	<b>1000.8</b>	<b>± 14.5</b>	
<b>P+1.0wt%PP-MAH+ 1.0wt%15A</b>	MB	180	350	<b>1063.8</b>	<b>± 0.0</b>	
<b>P+2.0wt%PP-MAH+ 2.0wt%15A</b>	MB	180	350	<b>1104.3</b>	<b>± 35.0</b>	
<b>P+1.0wt%PP-MAH+ 0.5wt%15A</b>	MB	180	350	<b>1009.2</b>	<b>± 0.0</b>	
<b>P+2.0wt%PP-MAH+ 1.0wt%15A</b>	MB	180	350	<b>1022.5</b>	<b>± 18.8</b>	
<b>P+4.0wt%PP-MAH+ 2.0wt%15A</b>	MB	180	350	<b>1146.6</b>	<b>± 19.1</b>	
<b>P+1.5wt%PP-MAH+ 0.5wt%15A</b>	MB	180	350	<b>1003.3</b>	<b>± 24.7</b>	
<b>P+3.0wt%PP-MAH+ 1.0wt%15A</b>	MB	180	350	<b>1064.6</b>	<b>± 40.7</b>	
<b>P+6.0wt%PP-MAH+ 2.0wt%15A</b>	MB	180	350	<b>1158.6</b>	<b>± 39.4</b>	
<b>P+1.0wt%PP-MAH+ 0.5wt%25A</b>	MB	180	350	<b>779.8</b>	<b>± 20.0</b>	
<b>P+2.0wt%PP-MAH+ 1.0wt%25A</b>	MB	180	350	<b>997.0</b>	<b>± 25.9</b>	
<b>P+4.0wt%PP-MAH+ 2.0wt%25A</b>	MB	180	350	<b>908.5</b>	<b>± 12.0</b>	
<b>P+1.0wt%PP-MAH+ 0.5wt%30B</b>	MB	180	350	<b>875.0</b>	<b>± 19.5</b>	
<b>P+2.0wt%PP-MAH+ 1.0wt%30B</b>	MB	180	350	<b>994.1</b>	<b>±13.8</b>	
<b>P+4.0wt%PP-MAH+ 2.0wt%30B</b>	MB	180	350	<b>938.3</b>	<b>± 39.6</b>	
<b>Ternary Nanocomposites (Effect of Processing Conditions)</b>						
<b>P+2wt%15A+ 5wt%E-MA-GMA</b>	All-S	200	350	<b>667.5</b>	<b>± 19.9</b>	
<b>P+2wt%15A+ 5wt%E-MA-GMA</b>	All-S	180	250	<b>761.9</b>	<b>± 8.6</b>	
<b>P+2wt%15A+ 5wt%E-MA-GMA</b>	All-S	180	350	<b>814.4</b>	<b>± 9.6</b>	
<b>P+1wt%15A+ 2wt%PP-MAH</b>	MB	200	250	<b>984.0</b>	<b>± 0.0</b>	
<b>P+1wt%15A+ 2wt%PP-MAH</b>	MB	200	350	<b>905.9</b>	<b>± 44.1</b>	
<b>P+1wt%15A+ 2wt%PP-MAH</b>	MB	180	250	<b>884.9</b>	<b>± 20.3</b>	

**Table A.2** Tensile stress at yield data and standard deviations for all compositions.

Components	Add. Order	Processing Parameters		Tensile Stress at Yield (MPa)	
		°C	rpm	Value	St. D.
<b>P</b>	-	-	-	<b>28.2</b>	<b>±0.4</b>
<b>P- Compatibilizer Blends</b>					
<b>P+ 5 wt% E-MA-GMA</b>	All-S	200	250	<b>27.6</b>	<b>±0.6</b>
<b>P+ 10 wt% E-MA-GMA</b>	All-S	200	250	<b>26.5</b>	<b>±0.1</b>
<b>P+ 0.5 wt% PP-MAH</b>	All-S	180	350	<b>30.5</b>	<b>±0.6</b>
<b>P+ 1.0 wt% PP-MAH</b>	All-S	180	350	<b>29.7</b>	<b>±0.4</b>
<b>P+ 1.5 wt% PP-MAH</b>	All-S	180	350	<b>29.8</b>	<b>±0.2</b>
<b>P+ 2.0 wt% PP-MAH</b>	All-S	180	350	<b>29.6</b>	<b>±0.9</b>
<b>P+ 3.0 wt% PP-MAH</b>	All-S	180	350	<b>30.9</b>	<b>±0.1</b>
<b>P+ 4.0 wt% PP-MAH</b>	All-S	180	350	<b>30.9</b>	<b>±0.6</b>
<b>P+ 6.0 wt% PP-MAH</b>	All-S	180	350	<b>30.8</b>	<b>±0.3</b>
<b>P- Clay Binary Nanocomposites</b>					
<b>P+ 2wt% 15A</b>	All-S	200	250	<b>28.3</b>	<b>±0.6</b>
<b>P+ 4 wt% 15A</b>	All-S	200	250	<b>29.2</b>	<b>±0.3</b>
<b>P+ 6 wt% 15A</b>	All-S	200	250	<b>29.5</b>	<b>±0.3</b>
<b>P+ 0.5 wt% 15A</b>	MB	180	350	<b>29.1</b>	<b>±0.9</b>
<b>P+ 1.0 wt% 15A</b>	MB	180	350	<b>29.7</b>	<b>±0.3</b>
<b>P+ 2.0 wt% 15A</b>	MB	180	350	<b>29.5</b>	<b>±0.4</b>
<b>P+ 0.5 wt% 25A</b>	MB	180	350	<b>28.5</b>	<b>±0.4</b>
<b>P+ 1.0 wt% 25A</b>	MB	180	350	<b>29.6</b>	<b>±0.3</b>
<b>P+ 2.0 wt% 25A</b>	MB	180	350	<b>29.3</b>	<b>±0.1</b>
<b>P+ 0.5 wt% 30B</b>	MB	180	350	<b>29.4</b>	<b>±0.6</b>
<b>P+ 1.0 wt% 30B</b>	MB	180	350	<b>29.5</b>	<b>±0.4</b>
<b>P+ 2.0 wt% 30B</b>	MB	180	350	<b>28.6</b>	<b>±0.4</b>

**Table A.2** Tensile stress at yield data and standard deviations for all the compositions (Cont'd.)

Components	Add. Order	Processing Parameters		Tensile Stress at Yield (MPa)	
		°C	rpm	Value	St. D.
<b>P- Compatibilizer- Clay Ternary Nanocomposites</b>					
<b>P+2wt%15A+ 5wt%E-MA-GMA</b>	All-S	200	250	<b>27.6</b>	<b>±0.7</b>
<b>P+2wt%15A+ 10wt%E-MA-GMA</b>	All-S	200	250	<b>25.6</b>	<b>±0.3</b>
<b>P+4wt%15A+ 5wt%E-MA-GMA</b>	All-S	200	250	<b>26.5</b>	<b>±0.4</b>
<b>P+4wt%15A+ 10wt%E-MA-GMA</b>	All-S	200	250	<b>26.0</b>	<b>±0.8</b>
<b>P+6wt%15A+ 5wt%E-MA-GMA</b>	All-S	200	250	<b>26.4</b>	<b>±0.6</b>
<b>P+6wt%15A+ 10wt%E-MA-GMA</b>	All-S	200	250	<b>25.6</b>	<b>±0.4</b>
<b>P+0.5wt%PP-MAH+ 0.5wt%15A</b>	MB	180	350	<b>28.9</b>	<b>±0.3</b>
<b>P+1.0wt%PP-MAH+ 1.0wt%15A</b>	MB	180	350	<b>31.1</b>	<b>±0.2</b>
<b>P+2.0wt%PP-MAH+ 2.0wt%15A</b>	MB	180	350	<b>30.6</b>	<b>±0.3</b>
<b>P+1.0wt%PP-MAH+ 0.5wt%15A</b>	MB	180	350	<b>29.7</b>	<b>±0.4</b>
<b>P+2.0wt%PP-MAH+ 1.0wt%15A</b>	MB	180	350	<b>30.9</b>	<b>±0.1</b>
<b>P+4.0wt%PP-MAH+ 2.0wt%15A</b>	MB	180	350	<b>31.4</b>	<b>±0.3</b>
<b>P+1.5wt%PP-MAH+ 0.5wt%15A</b>	MB	180	350	<b>30.1</b>	<b>±0.2</b>
<b>P+3.0wt%PP-MAH+ 1.0wt%15A</b>	MB	180	350	<b>30.2</b>	<b>±0.0</b>
<b>P+6.0wt%PP-MAH+ 2.0wt%15A</b>	MB	180	350	<b>30.4</b>	<b>±0.1</b>
<b>P+1.0wt%PP-MAH+ 0.5wt%25A</b>	MB	180	350	<b>28.0</b>	<b>±0.4</b>
<b>P+2.0wt%PP-MAH+ 1.0wt%25A</b>	MB	180	350	<b>30.4</b>	<b>±0.4</b>
<b>P+4.0wt%PP-MAH+ 2.0wt%25A</b>	MB	180	350	<b>28.3</b>	<b>±0.6</b>
<b>P+1.0wt%PP-MAH+ 0.5wt%30B</b>	MB	180	350	<b>29.1</b>	<b>±0.6</b>
<b>P+2.0wt%PP-MAH+ 1.0wt%30B</b>	MB	180	350	<b>29.0</b>	<b>±1.1</b>
<b>P+4.0wt%PP-MAH+ 2.0wt%30B</b>	MB	180	350	<b>28.9</b>	<b>±0.6</b>
<b>Ternary Nanocomposites (Effect of Processing Conditions)</b>					
<b>P+2wt%15A+ 5wt%E-MA-GMA</b>	All-S	200	350	<b>26.0</b>	<b>±0.3</b>
<b>P+2wt%15A+ 5wt%E-MA-GMA</b>	All-S	180	250	<b>25.1</b>	<b>±0.7</b>
<b>P+2wt%15A+ 5wt%E-MA-GMA</b>	All-S	180	350	<b>27.7</b>	<b>±0.1</b>
<b>P+1wt%15A+ 2wt%PP-MAH</b>	MB	200	250	<b>30.7</b>	<b>±0.6</b>
<b>P+1wt%15A+ 2wt%PP-MAH</b>	MB	200	350	<b>30.0</b>	<b>±0.3</b>
<b>P+1wt%15A+ 2wt%PP-MAH</b>	MB	180	250	<b>29.8</b>	<b>±0.2</b>

**Table A.3** Tensile strength data and standard deviations for all compositions.

Components	Add. Order	Processing Parameters		Tensile Strength at Break (MPa)	
		°C	rpm	Value	St. D.
<b>P</b>	-	-	-	<b>34.8</b>	<b>±0.5</b>
<b>P- Compatibilizer Blends</b>					
<b>P+ 5 wt% E-MA-GMA</b>	All-S	200	250	<b>34.6</b>	<b>±0.4</b>
<b>P+ 10 wt% E-MA-GMA</b>	All-S	200	250	<b>34.1</b>	<b>±0.5</b>
<b>P+ 0.5 wt% PP-MAH</b>	All-S	180	350	<b>36.3</b>	<b>±0.7</b>
<b>P+ 1.0 wt% PP-MAH</b>	All-S	180	350	<b>35.8</b>	<b>±1.1</b>
<b>P+ 1.5 wt% PP-MAH</b>	All-S	180	350	<b>36.9</b>	<b>±0.9</b>
<b>P+ 2.0 wt% PP-MAH</b>	All-S	180	350	<b>35.3</b>	<b>±0.6</b>
<b>P+ 3.0 wt% PP-MAH</b>	All-S	180	350	<b>36.4</b>	<b>±1.2</b>
<b>P+ 4.0 wt% PP-MAH</b>	All-S	180	350	<b>37.9</b>	<b>±1.2</b>
<b>P+ 6.0 wt% PP-MAH</b>	All-S	180	350	<b>38.4</b>	<b>±0.2</b>
<b>P- Clay Binary Nanocomposites</b>					
<b>P+ 2wt% 15A</b>	All-S	200	250	<b>35.0</b>	<b>±0.8</b>
<b>P+ 4 wt% 15A</b>	All-S	200	250	<b>33.3</b>	<b>±0.2</b>
<b>P+ 6 wt% 15A</b>	All-S	200	250	<b>30.7</b>	<b>±0.1</b>
<b>P+ 0.5 wt% 15A</b>	MB	180	350	<b>37.0</b>	<b>±0.4</b>
<b>P+ 1.0 wt% 15A</b>	MB	180	350	<b>37.1</b>	<b>±0.6</b>
<b>P+ 2.0 wt% 15A</b>	MB	180	350	<b>35.4</b>	<b>±0.7</b>
<b>P+ 0.5 wt% 25A</b>	MB	180	350	<b>35.8</b>	<b>±0.5</b>
<b>P+ 1.0 wt% 25A</b>	MB	180	350	<b>36.5</b>	<b>±0.6</b>
<b>P+ 2.0 wt% 25A</b>	MB	180	350	<b>36.1</b>	<b>±0.6</b>
<b>P+ 0.5 wt% 30B</b>	MB	180	350	<b>36.5</b>	<b>±0.5</b>
<b>P+ 1.0 wt% 30B</b>	MB	180	350	<b>36.8</b>	<b>±0.7</b>
<b>P+ 2.0 wt% 30B</b>	MB	180	350	<b>34.8</b>	<b>±0.6</b>

**Table A.3** Tensile strength data and standard deviations for all compositions (Cont'd.)

Components	Add. Order	Processing Parameters		Tensile Strength at Break (MPa)	
		°C	rpm	Value	St. D.
<b>P- Compatibilizer- Clay Ternary Nanocomposites</b>					
<b>P+2wt%15A+ 5wt%E-MA-GMA</b>	All-S	200	250	<b>32.7</b>	<b>±0.9</b>
<b>P+2wt%15A+ 10wt%E-MA-GMA</b>	All-S	200	250	<b>32.8</b>	<b>±0.2</b>
<b>P+4wt%15A+ 5wt%E-MA-GMA</b>	All-S	200	250	<b>31.5</b>	<b>±0.6</b>
<b>P+4wt%15A+ 10wt%E-MA-GMA</b>	All-S	200	250	<b>31.7</b>	<b>±0.9</b>
<b>P+6wt%15A+ 5wt%E-MA-GMA</b>	All-S	200	250	<b>30.5</b>	<b>±0.6</b>
<b>P+6wt%15A+ 10wt%E-MA-GMA</b>	All-S	200	250	<b>30.5</b>	<b>±0.6</b>
<b>P+0.5wt%PP-MAH+ 0.5wt%15A</b>	MB	180	350	<b>34.5</b>	<b>±0.5</b>
<b>P+1.0wt%PP-MAH+ 1.0wt%15A</b>	MB	180	350	<b>34.1</b>	<b>±1.1</b>
<b>P+2.0wt%PP-MAH+ 2.0wt%15A</b>	MB	180	350	<b>35.0</b>	<b>±1.4</b>
<b>P+1.0wt%PP-MAH+ 0.5wt%15A</b>	MB	180	350	<b>36.1</b>	<b>±0.4</b>
<b>P+2.0wt%PP-MAH+ 1.0wt%15A</b>	MB	180	350	<b>36.8</b>	<b>±0.3</b>
<b>P+4.0wt%PP-MAH+ 2.0wt%15A</b>	MB	180	350	<b>36.9</b>	<b>±0.3</b>
<b>P+1.5wt%PP-MAH+ 0.5wt%15A</b>	MB	180	350	<b>35.0</b>	<b>±0.0</b>
<b>P+3.0wt%PP-MAH+ 1.0wt%15A</b>	MB	180	350	<b>35.8</b>	<b>±0.6</b>
<b>P+6.0wt%PP-MAH+ 2.0wt%15A</b>	MB	180	350	<b>35.9</b>	<b>±0.9</b>
<b>P+1.0wt%PP-MAH+ 0.5wt%25A</b>	MB	180	350	<b>35.4</b>	<b>±0.3</b>
<b>P+2.0wt%PP-MAH+ 1.0wt%25A</b>	MB	180	350	<b>35.9</b>	<b>±1.1</b>
<b>P+4.0wt%PP-MAH+ 2.0wt%25A</b>	MB	180	350	<b>34.7</b>	<b>±0.6</b>
<b>P+1.0wt%PP-MAH+ 0.5wt%30B</b>	MB	180	350	<b>36.5</b>	<b>±0.5</b>
<b>P+2.0wt%PP-MAH+ 1.0wt%30B</b>	MB	180	350	<b>34.0</b>	<b>±0.7</b>
<b>P+4.0wt%PP-MAH+ 2.0wt%30B</b>	MB	180	350	<b>35.2</b>	<b>±0.7</b>
<b>Ternary Nanocomposites (Effect of Processing Conditions)</b>					
<b>P+2wt%15A+ 5wt%E-MA-GMA</b>	All-S	200	350	<b>33.9</b>	<b>±0.3</b>
<b>P+2wt%15A+ 5wt%E-MA-GMA</b>	All-S	180	250	<b>34.1</b>	<b>±0.6</b>
<b>P+2wt%15A+ 5wt%E-MA-GMA</b>	All-S	180	350	<b>34.2</b>	<b>±0.9</b>
<b>P+1wt%15A+ 2wt%PP-MAH</b>	MB	200	250	<b>36.4</b>	<b>±0.5</b>
<b>P+1wt%15A+ 2wt%PP-MAH</b>	MB	200	350	<b>36.8</b>	<b>±0.5</b>
<b>P+1wt%15A+ 2wt%PP-MAH</b>	MB	180	250	<b>36.9</b>	<b>±0.6</b>

**Table A.4** Elongation at break (%) data and standard deviations for all compositions.

Components	Add. Order	Processing Parameters		Elongation at Break (%)	
		°C	rpm	Value	St. D.
<b>P</b>	-	-	-	<b>524.4</b>	<b>±2.0</b>
<b>P- Compatibilizer Blends</b>					
<b>P+ 5 wt% E-MA-GMA</b>	All-S	200	250	<b>548.8</b>	<b>±7.3</b>
<b>P+ 10 wt% E-MA-GMA</b>	All-S	200	250	<b>559.6</b>	<b>±6.2</b>
<b>P+ 0.5 wt% PP-MAH</b>	All-S	180	350	<b>558.0</b>	<b>±12.1</b>
<b>P+ 1.0 wt% PP-MAH</b>	All-S	180	350	<b>559.0</b>	<b>±10.1</b>
<b>P+ 1.5 wt% PP-MAH</b>	All-S	180	350	<b>554.2</b>	<b>±4.7</b>
<b>P+ 2.0 wt% PP-MAH</b>	All-S	180	350	<b>548.3</b>	<b>±4.2</b>
<b>P+ 3.0 wt% PP-MAH</b>	All-S	180	350	<b>553.4</b>	<b>±10.5</b>
<b>P+ 4.0 wt% PP-MAH</b>	All-S	180	350	<b>564.0</b>	<b>±7.7</b>
<b>P+ 6.0 wt% PP-MAH</b>	All-S	180	350	<b>579.7</b>	<b>±8.4</b>
<b>P- Clay Binary Nanocomposites</b>					
<b>P+ 2 wt% 15A</b>	All-S	200	250	<b>557.0</b>	<b>±5.7</b>
<b>P+ 4 wt% 15A</b>	All-S	200	250	<b>530.5</b>	<b>±2.5</b>
<b>P+ 6 wt% 15A</b>	All-S	200	250	<b>455.0</b>	<b>±6.0</b>
<b>P+ 0.5 wt% 15A</b>	MB	180	350	<b>574.5</b>	<b>±6.2</b>
<b>P+ 1.0 wt% 15A</b>	MB	180	350	<b>573.2</b>	<b>±4.1</b>
<b>P+ 2.0 wt% 15A</b>	MB	180	350	<b>582.7</b>	<b>±8.4</b>
<b>P+ 0.5 wt% 25A</b>	MB	180	350	<b>569.1</b>	<b>±3.5</b>
<b>P+ 1.0 wt% 25A</b>	MB	180	350	<b>561.0</b>	<b>±3.5</b>
<b>P+ 2.0 wt% 25A</b>	MB	180	350	<b>558.9</b>	<b>±7.0</b>
<b>P+ 0.5 wt% 30B</b>	MB	180	350	<b>550.2</b>	<b>±4.2</b>
<b>P+ 1.0 wt% 30B</b>	MB	180	350	<b>537.6</b>	<b>±2.1</b>
<b>P+ 2.0 wt% 30B</b>	MB	180	350	<b>559.6</b>	<b>±4.7</b>

**Table A.4** Elongation at break (%) data and standard deviations for all compositions (Cont'd.)

Components	Add. Order	Processing Parameters		Elongation at Break (%)	
		°C	rpm	Value	St. D.
<b>P- Compatibilizer- Clay Ternary Nanocomposites</b>					
<b>P+2wt%15A+ 5wt%E-MA-GMA</b>	All-S	200	250	<b>509.2</b>	<b>±7.7</b>
<b>P+2wt%15A+ 10wt%E-MA-GMA</b>	All-S	200	250	<b>529.0</b>	<b>±7.0</b>
<b>P+4wt%15A+ 5wt%E-MA-GMA</b>	All-S	200	250	<b>508.5</b>	<b>±8.6</b>
<b>P+4wt%15A+ 10wt%E-MA-GMA</b>	All-S	200	250	<b>496.7</b>	<b>±8.2</b>
<b>P+6wt%15A+ 5wt%E-MA-GMA</b>	All-S	200	250	<b>496.6</b>	<b>±3.2</b>
<b>P+6wt%15A+ 10wt%E-MA-GMA</b>	All-S	200	250	<b>500.0</b>	<b>±5.9</b>
<b>P+0.5wt%PP-MAH+ 0.5wt%15A</b>	MB	180	350	<b>552.9</b>	<b>±6.0</b>
<b>P+1.0wt%PP-MAH+ 1.0wt%15A</b>	MB	180	350	<b>559.6</b>	<b>±23.8</b>
<b>P+2.0wt%PP-MAH+ 2.0wt%15A</b>	MB	180	350	<b>537.6</b>	<b>±14.3</b>
<b>P+1.0wt%PP-MAH+ 0.5wt%15A</b>	MB	180	350	<b>562.5</b>	<b>±16.1</b>
<b>P+2.0wt%PP-MAH+ 1.0wt%15A</b>	MB	180	350	<b>565.1</b>	<b>±5.7</b>
<b>P+4.0wt%PP-MAH+ 2.0wt%15A</b>	MB	180	350	<b>552.9</b>	<b>±11.0</b>
<b>P+1.5wt%PP-MAH+ 0.5wt%15A</b>	MB	180	350	<b>549.5</b>	<b>±15.0</b>
<b>P+3.0wt%PP-MAH+ 1.0wt%15A</b>	MB	180	350	<b>575.7</b>	<b>±11.7</b>
<b>P+6.0wt%PP-MAH+ 2.0wt%15A</b>	MB	180	350	<b>531.9</b>	<b>±6.5</b>
<b>P+1.0wt%PP-MAH+ 0.5wt%25A</b>	MB	180	350	<b>570.7</b>	<b>±8.7</b>
<b>P+2.0wt%PP-MAH+ 1.0wt%25A</b>	MB	180	350	<b>554.9</b>	<b>±16.1</b>
<b>P+4.0wt%PP-MAH+ 2.0wt%25A</b>	MB	180	350	<b>585.5</b>	<b>±18.1</b>
<b>P+1.0wt%PP-MAH+ 0.5wt%30B</b>	MB	180	350	<b>569.8</b>	<b>±9.4</b>
<b>P+2.0wt%PP-MAH+ 1.0wt%30B</b>	MB	180	350	<b>523.7</b>	<b>±7.7</b>
<b>P+4.0wt%PP-MAH+ 2.0wt%30B</b>	MB	180	350	<b>557.4</b>	<b>±10.4</b>
<b>Ternary Nanocomposites (Effect of Processing Conditions)</b>					
<b>P+2wt%15A+ 5wt%E-MA-GMA</b>	All-S	200	350	<b>557.6</b>	<b>±7.1</b>
<b>P+2wt%15A+ 5wt%E-MA-GMA</b>	All-S	180	250	<b>537.3</b>	<b>±6.5</b>
<b>P+2wt%15A+ 5wt%E-MA-GMA</b>	All-S	180	350	<b>530.5</b>	<b>±2.0</b>
<b>P+1wt%15A+ 2wt%PP-MAH</b>	MB	200	250	<b>532.5</b>	<b>±7.0</b>
<b>P+1wt%15A+ 2wt%PP-MAH</b>	MB	200	350	<b>572.7</b>	<b>±1.0</b>
<b>P+1wt%15A+ 2wt%PP-MAH</b>	MB	180	250	<b>575.2</b>	<b>±5.2</b>

**Table A.5** Impact strength data and standard deviations for all compositions.

Components	Add. Order	Processing Parameters		Impact Strength (kJ/m <sup>2</sup> )	
		°C	rpm	Value	St. D.
<b>P</b>	-	-	-	<b>8.781</b>	<b>±0.270</b>
<b>P- Compatibilizer Blends</b>					
<b>P+ 5 wt% E-MA-GMA</b>	All-S	200	250	<b>10.333</b>	<b>±0.091</b>
<b>P+ 10 wt% E-MA-GMA</b>	All-S	200	250	<b>10.836</b>	<b>±0.141</b>
<b>P+ 0.5 wt% PP-MAH</b>	All-S	180	350	<b>9.477</b>	<b>±0.266</b>
<b>P+ 1.0 wt% PP-MAH</b>	All-S	180	350	<b>10.010</b>	<b>±0.126</b>
<b>P+ 1.5 wt% PP-MAH</b>	All-S	180	350	<b>9.688</b>	<b>±0.265</b>
<b>P+ 2.0 wt% PP-MAH</b>	All-S	180	350	<b>9.703</b>	<b>±0.237</b>
<b>P+ 3.0 wt% PP-MAH</b>	All-S	180	350	<b>10.010</b>	<b>±0.126</b>
<b>P+ 4.0 wt% PP-MAH</b>	All-S	180	350	<b>10.010</b>	<b>±0.378</b>
<b>P+ 6.0 wt% PP-MAH</b>	All-S	180	350	<b>10.115</b>	<b>±0.290</b>
<b>P- Clay Binary Nanocomposites</b>					
<b>P+ 2 wt% 15A</b>	All-S	200	250	<b>8.198</b>	<b>±0.180</b>
<b>P+ 4 wt% 15A</b>	All-S	200	250	<b>7.365</b>	<b>±0.188</b>
<b>P+ 6 wt% 15A</b>	All-S	200	250	<b>7.055</b>	<b>±0.177</b>
<b>P+ 0.5 wt% 15A</b>	MB	180	350	<b>9.135</b>	<b>±0.180</b>
<b>P+ 1.0 wt% 15A</b>	MB	180	350	<b>9.083</b>	<b>±0.090</b>
<b>P+ 2.0 wt% 15A</b>	MB	180	350	<b>8.609</b>	<b>±0.154</b>
<b>P+ 0.5 wt% 25A</b>	MB	180	350	<b>8.922</b>	<b>±0.104</b>
<b>P+ 1.0 wt% 25A</b>	MB	180	350	<b>9.102</b>	<b>±0.200</b>
<b>P+ 2.0 wt% 25A</b>	MB	180	350	<b>8.563</b>	<b>±0.272</b>
<b>P+ 0.5 wt% 30B</b>	MB	180	350	<b>8.821</b>	<b>±0.287</b>
<b>P+ 1.0 wt% 30B</b>	MB	180	350	<b>9.219</b>	<b>±0.000</b>
<b>P+ 2.0 wt% 30B</b>	MB	180	350	<b>8.735</b>	<b>±0.111</b>

**Table A.5** Impact strength data and standard deviations for all the compositions (Cont'd).

Components	Add. Order	Processing Parameters		Impact Strength (kJ/m <sup>2</sup> )	
		°C	rpm	Value	St. D.
<b>P- Compatibilizer- Clay Ternary Nanocomposites</b>					
<b>P+2wt%15A+ 5wt%E-MA-GMA</b>	All-S	200	250	<b>7.985</b>	<b>±0.307</b>
<b>P+2wt%15A+ 10wt%E-MA-GMA</b>	All-S	200	250	<b>9.086</b>	<b>±0.240</b>
<b>P+4wt%15A+ 5wt%E-MA-GMA</b>	All-S	200	250	<b>7.321</b>	<b>±0.295</b>
<b>P+4wt%15A+ 10wt%E-MA-GMA</b>	All-S	200	250	<b>8.189</b>	<b>±0.242</b>
<b>P+6wt%15A+ 5wt%E-MA-GMA</b>	All-S	200	250	<b>6.750</b>	<b>±0.379</b>
<b>P+6wt%15A+ 10wt%E-MA-GMA</b>	All-S	200	250	<b>6.961</b>	<b>±0.298</b>
<b>P+0.5wt%PP-MAH+ 0.5wt%15A</b>	MB	180	350	<b>8.667</b>	<b>±0.222</b>
<b>P+1.0wt%PP-MAH+ 1.0wt%15A</b>	MB	180	350	<b>8.844</b>	<b>±0.254</b>
<b>P+2.0wt%PP-MAH+ 2.0wt%15A</b>	MB	180	350	<b>8.271</b>	<b>±0.188</b>
<b>P+1.0wt%PP-MAH+ 0.5wt%15A</b>	MB	180	350	<b>9.188</b>	<b>±0.156</b>
<b>P+2.0wt%PP-MAH+ 1.0wt%15A</b>	MB	180	350	<b>9.833</b>	<b>±0.072</b>
<b>P+4.0wt%PP-MAH+ 2.0wt%15A</b>	MB	180	350	<b>8.500</b>	<b>±0.267</b>
<b>P+1.5wt%PP-MAH+ 0.5wt%15A</b>	MB	180	350	<b>8.656</b>	<b>±0.325</b>
<b>P+3.0wt%PP-MAH+ 1.0wt%15A</b>	MB	180	350	<b>9.365</b>	<b>±0.188</b>
<b>P+6.0wt%PP-MAH+ 2.0wt%15A</b>	MB	180	350	<b>9.531</b>	<b>±0.155</b>
<b>P+1.0wt%PP-MAH+ 0.5wt%25A</b>	MB	180	350	<b>8.844</b>	<b>±0.205</b>
<b>P+2.0wt%PP-MAH+ 1.0wt%25A</b>	MB	180	350	<b>9.125</b>	<b>±0.179</b>
<b>P+4.0wt%PP-MAH+ 2.0wt%25A</b>	MB	180	350	<b>7.969</b>	<b>±0.270</b>
<b>P+1.0wt%PP-MAH+ 0.5wt%30B</b>	MB	180	350	<b>8.781</b>	<b>±0.251</b>
<b>P+2.0wt%PP-MAH+ 1.0wt%30B</b>	MB	180	350	<b>9.797</b>	<b>±0.110</b>
<b>P+4.0wt%PP-MAH+ 2.0wt%30B</b>	MB	180	350	<b>8.302</b>	<b>±0.307</b>
<b>Ternary Nanocomposites (Effect of Processing Conditions)</b>					
<b>P+2wt%15A+ 5wt%E-MA-GMA</b>	All-S	200	350	<b>9.477</b>	<b>±0.177</b>
<b>P+2wt%15A+ 5wt%E-MA-GMA</b>	All-S	180	250	<b>8.969</b>	<b>±0.205</b>
<b>P+2wt%15A+ 5wt%E-MA-GMA</b>	All-S	180	350	<b>9.500</b>	<b>±0.051</b>
<b>P+1wt%15A+ 2wt%PP-MAH</b>	MB	200	250	<b>9.136</b>	<b>±0.290</b>
<b>P+1wt%15A+ 2wt%PP-MAH</b>	MB	200	350	<b>9.274</b>	<b>±0.168</b>
<b>P+1wt%15A+ 2wt%PP-MAH</b>	MB	180	250	<b>9.953</b>	<b>±0.136</b>

## APPENDIX B

### DSC ANALYSIS

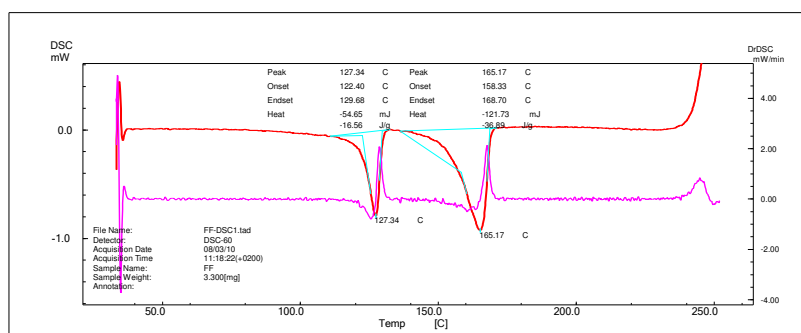


Figure B.1 DSC thermogram of recycled polypropylene.

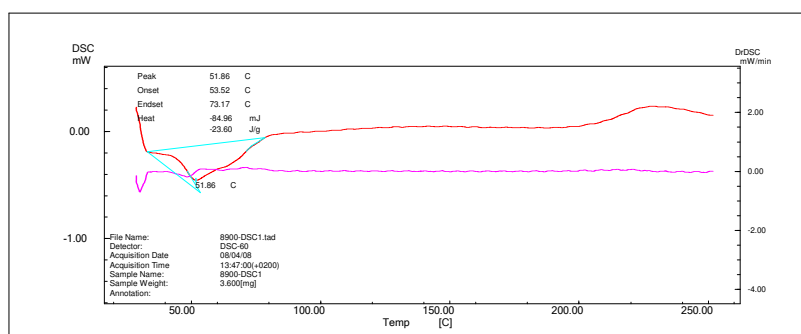


Figure B.2 DSC thermogram of Lotader® AX8900 (E-MA-GMA).

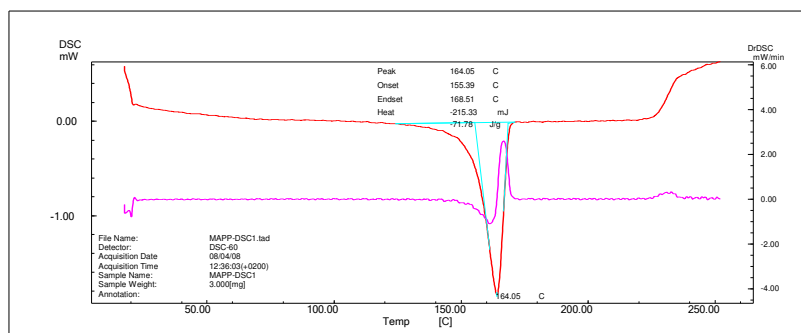


Figure B.3 DSC thermogram of PP-MAH.

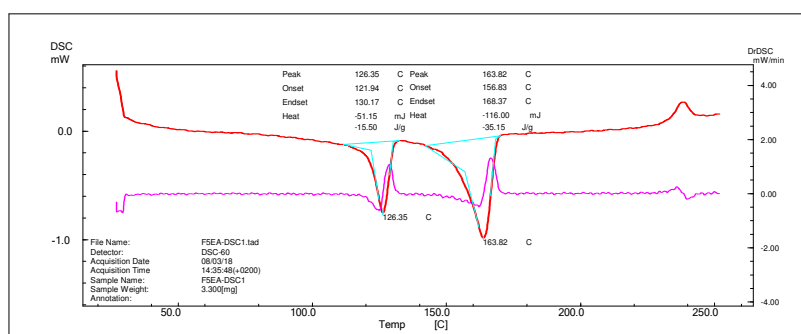


Figure B.4 DSC thermogram of binary blend containing 5 wt% E-MA-GMA.

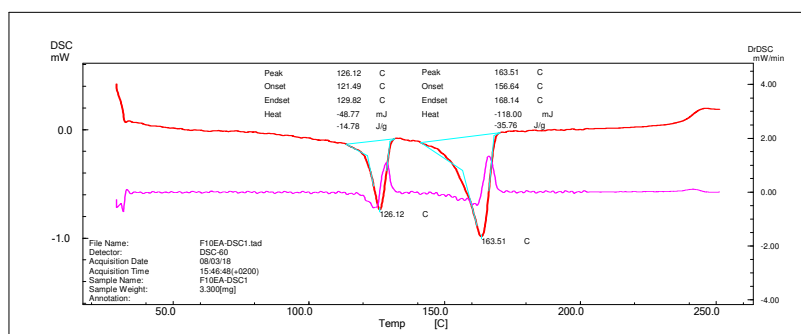
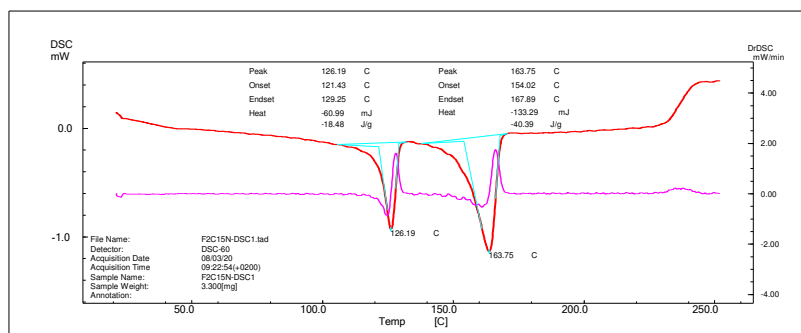
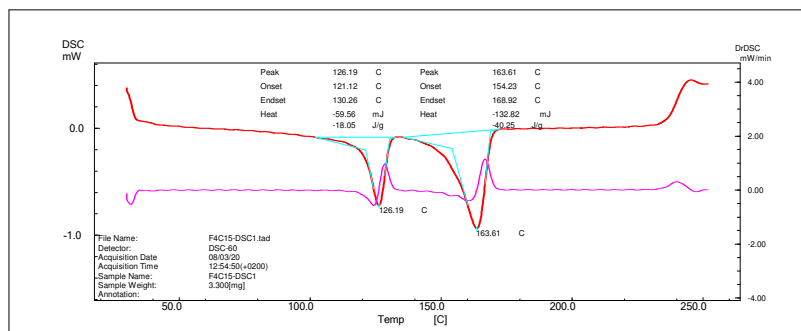


Figure B.5 DSC thermogram of binary blend containing 10 wt% E-MA-GMA.



**Figure B.6** DSC thermogram of binary nanocomposite containing 2 wt% Cloisite® 15A (All-S).



**Figure B.7** DSC thermogram of binary nanocomposite containing 4 wt% Cloisite® 15A.

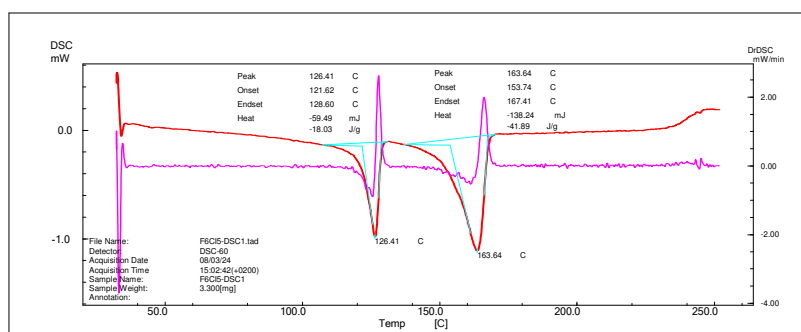


**Figure B.8** DSC thermogram of binary nanocomposite containing 6 wt% Cloisite® 15A.

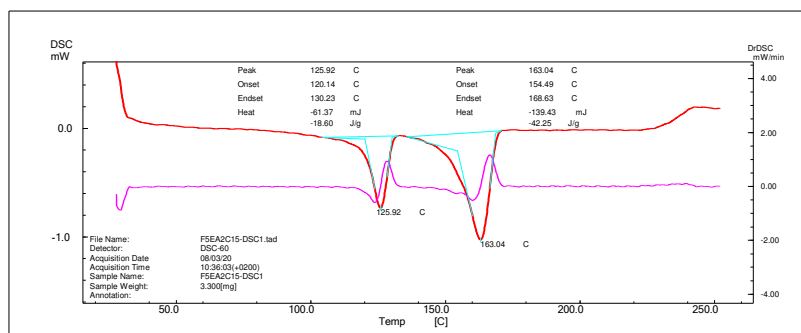


**Figure B.9** DSC thermogram of ternary nanocomposite containing 2 wt% Cloisite® 15A and 5 wt% E-MA-GMA prepared at 200 °C temperature and 250 rpm.

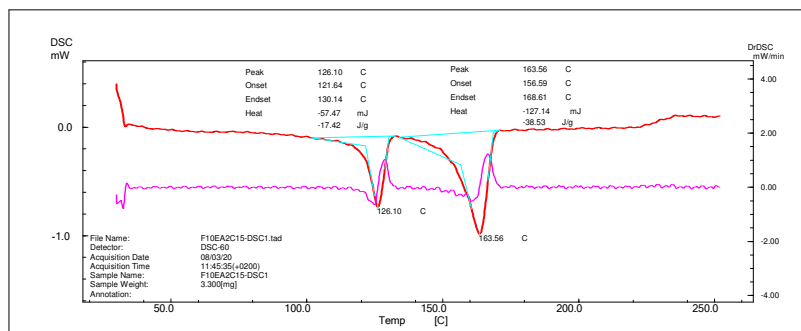


**Figure B.10** DSC thermogram of ternary nanocomposite containing 2 wt% Cloisite® 15A and 10 wt% E-MA-GMA.

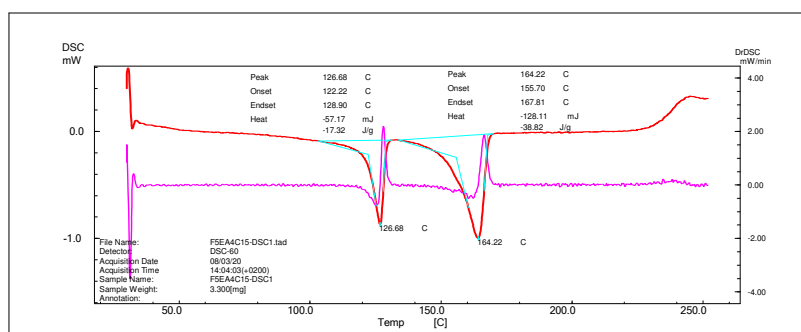


**Figure B.11** DSC thermogram of ternary nanocomposite containing 4 wt% Cloisite® 15A and 5 wt% E-MA-GMA.

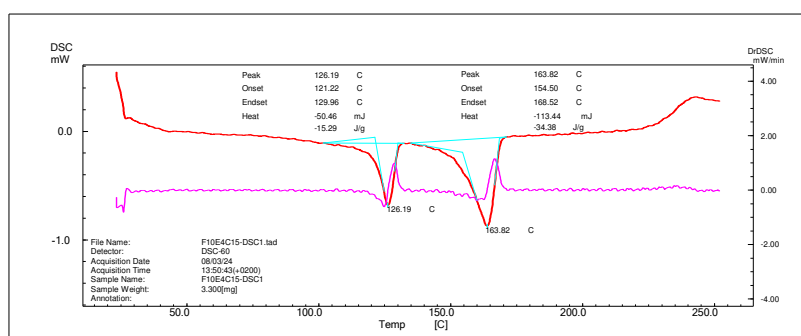


**Figure B.12** DSC thermogram of ternary nanocomposite containing 4 wt% Cloisite® 15A and 10 wt% E-MA-GMA.

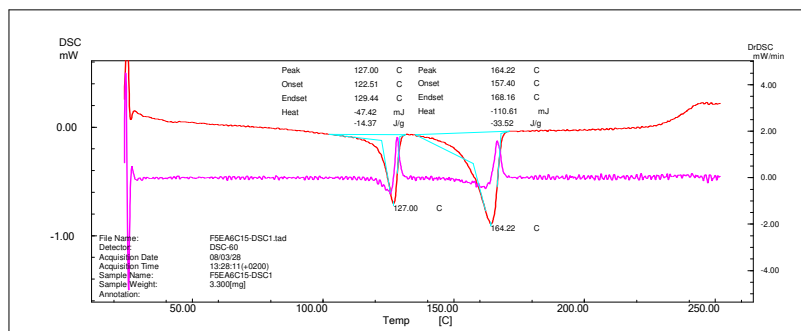


**Figure B.13** DSC thermogram of ternary nanocomposite containing 6 wt% Cloisite® 15A and 5 wt% E-MA-GMA.

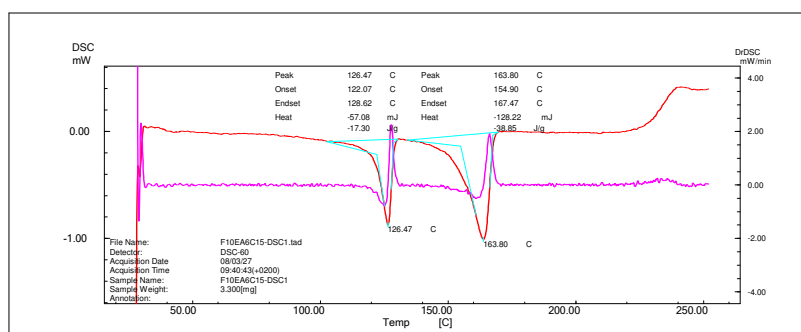


**Figure B.14** DSC thermogram of ternary nanocomposite containing 6 wt% Cloisite® 15A and 10 wt% E-MA-GMA.

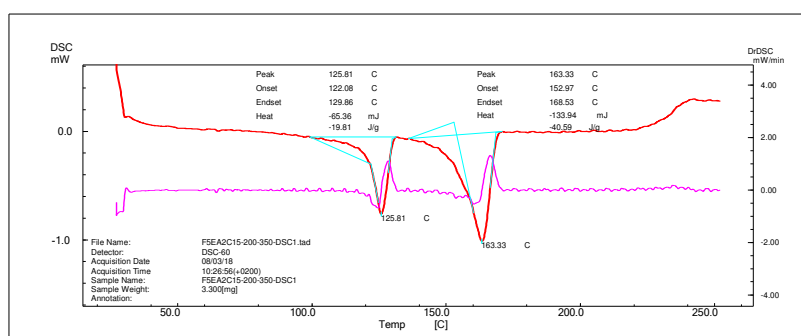


**Figure B.15** DSC thermogram of ternary nanocomposite containing 2 wt% Cloisite® 15A and 5 wt% E-MA-GMA prepared at 200 °C temperature and 350 rpm.

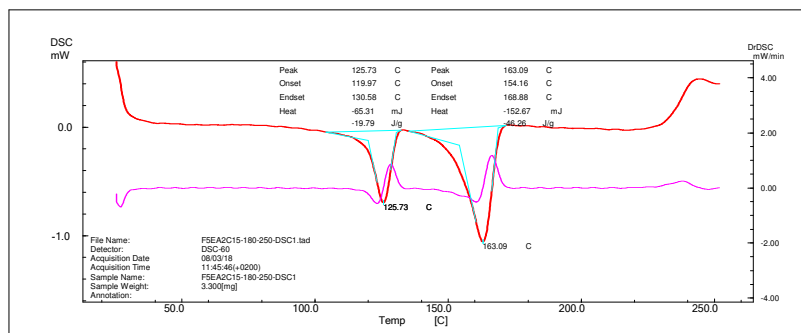


**Figure B.16** DSC thermogram of ternary nanocomposite containing 2 wt% Cloisite® 15A and 5 wt% E-MA-GMA prepared at 180 °C temperature and 250 rpm.

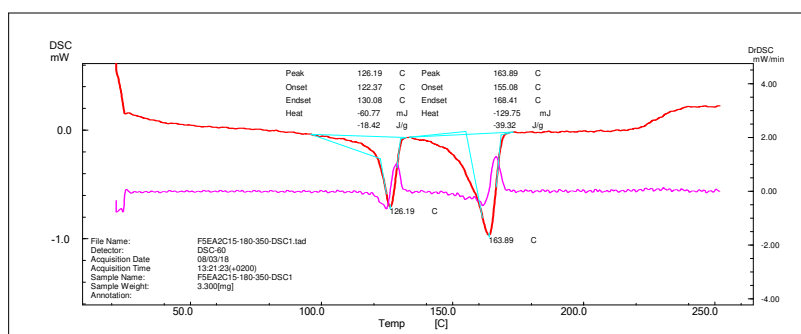


**Figure B.17** DSC thermogram of ternary nanocomposite containing 2 wt% Cloisite® 15A and 5 wt% E-MA-GMA prepared at 180 °C temperature and 350 rpm.

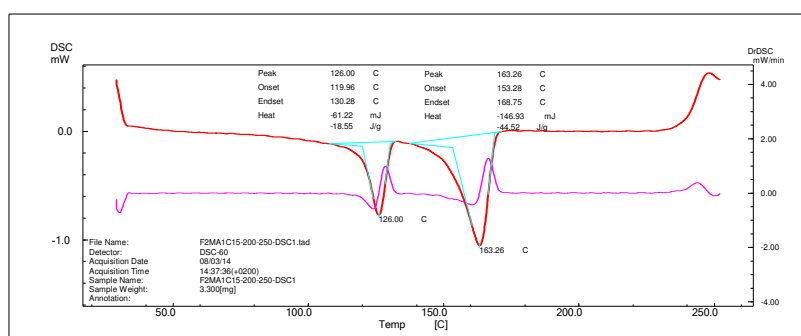


**Figure B.18** DSC thermogram of ternary nanocomposite containing 1 wt% Cloisite® 15A and 2 wt% PP-MAH prepared at 200 °C temperature and 250 rpm.

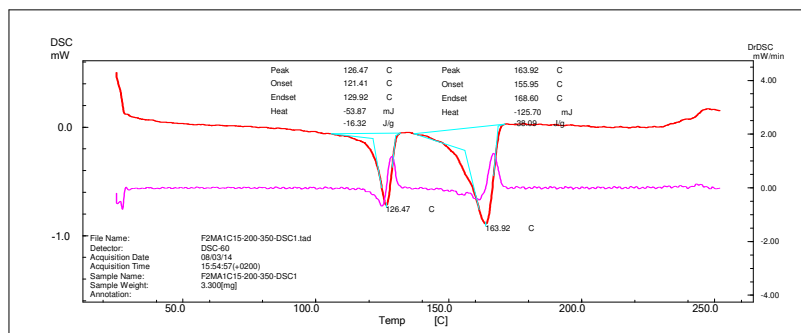


**Figure B.19** DSC thermogram of ternary nanocomposite containing 1 wt% Cloisite® 15A and 2 wt% PP-MAH prepared at 200 °C temperature and 350 rpm.

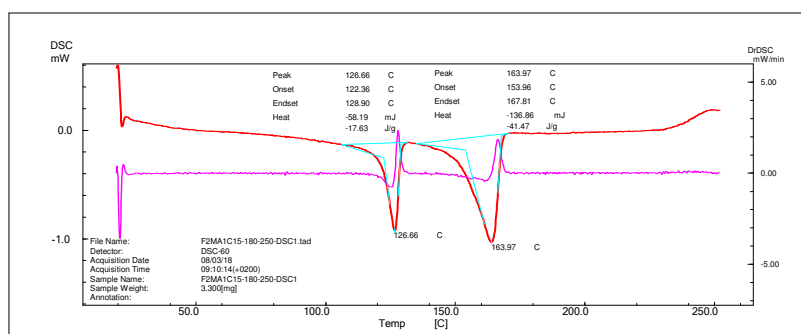


**Figure B.20** DSC thermogram of ternary nanocomposite containing 1 wt% Cloisite® 15A and 2 wt% PP-MAH prepared at 180 °C temperature and 250 rpm.

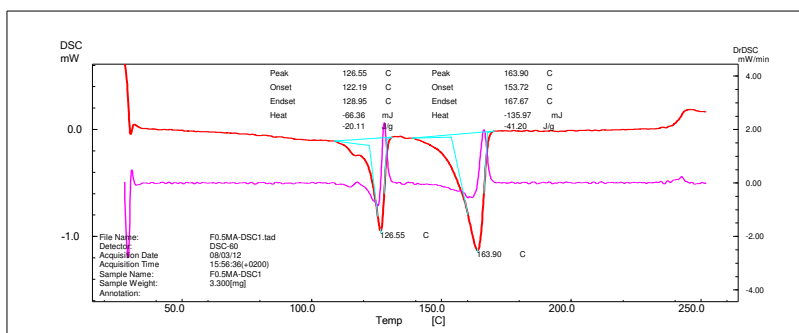


Figure B.21 DSC thermogram of binary blend containing 0.5 wt% PP-MAH.

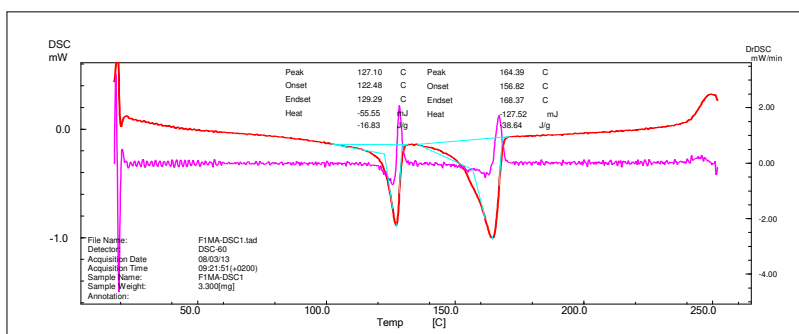


Figure B.22 DSC thermogram of binary blend containing 1 wt% PP-MAH.

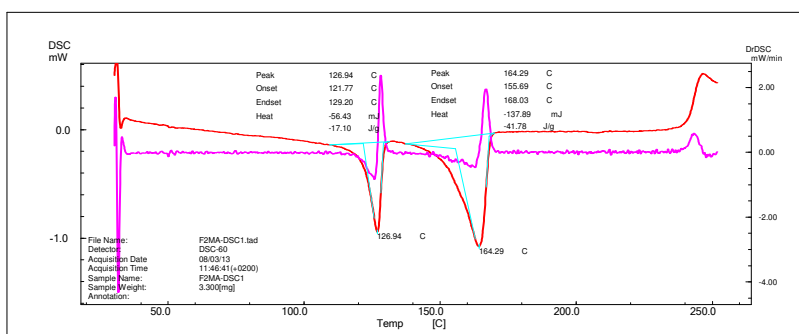


Figure B.23 DSC thermogram of binary blend containing 2 wt% PP-MAH.

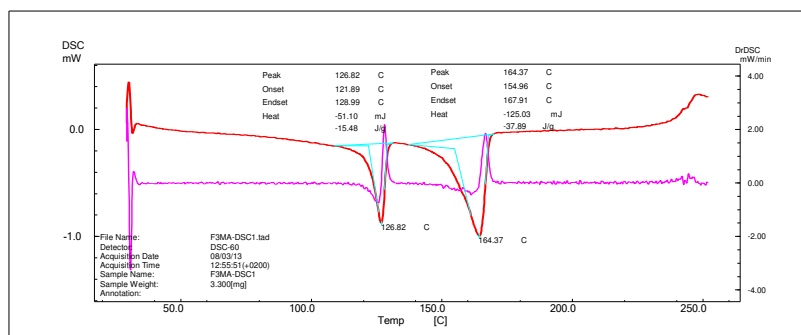


Figure B.24 DSC thermogram of binary blend containing 3 wt% PP-MAH.

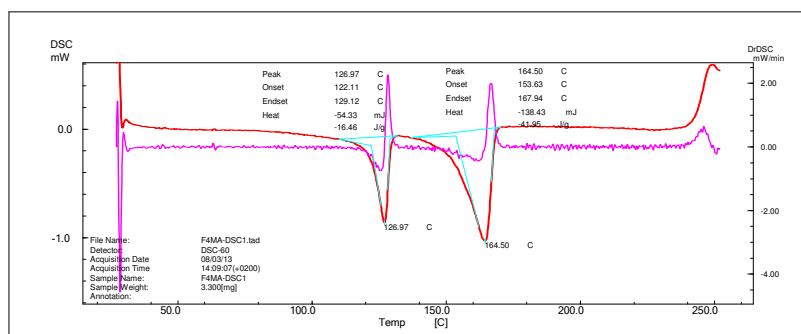


Figure B.25 DSC thermogram of binary blend containing 4 wt% PP-MAH.

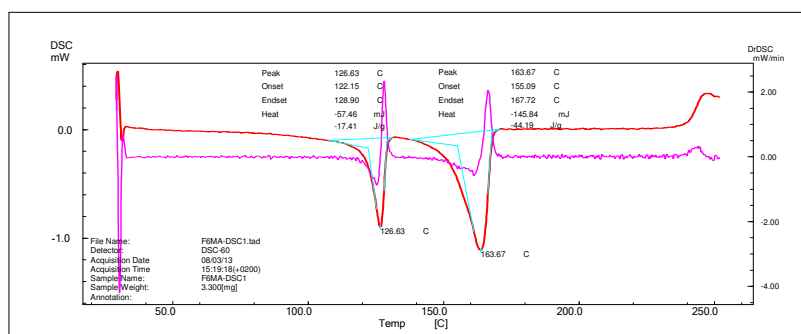
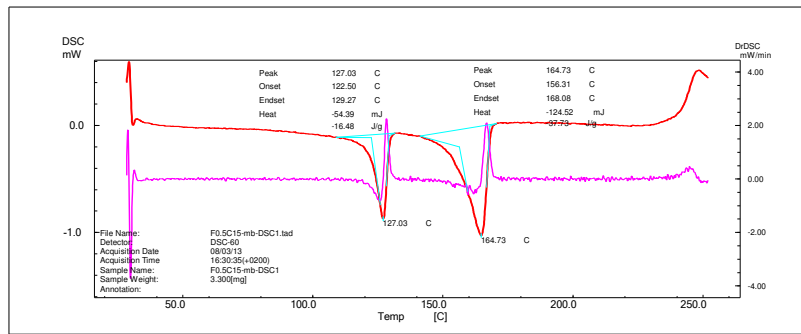
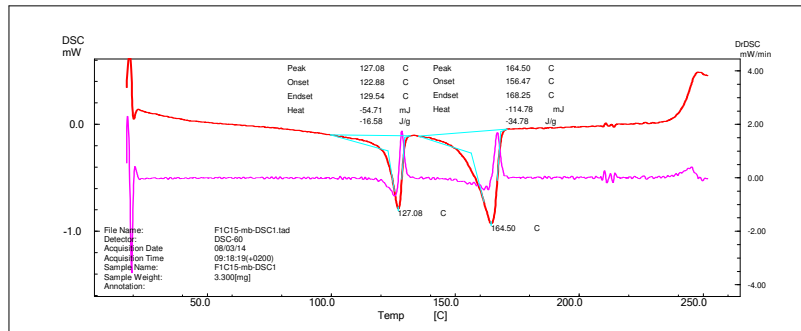


Figure B.26 DSC thermogram of binary blend containing 6 wt% PP-MAH.



**Figure B.27** DSC thermogram of binary nanocomposite containing 0.5 wt% Cloisite® 15A.



**Figure B.28** DSC thermogram of binary nanocomposite containing 1 wt% Cloisite® 15A.

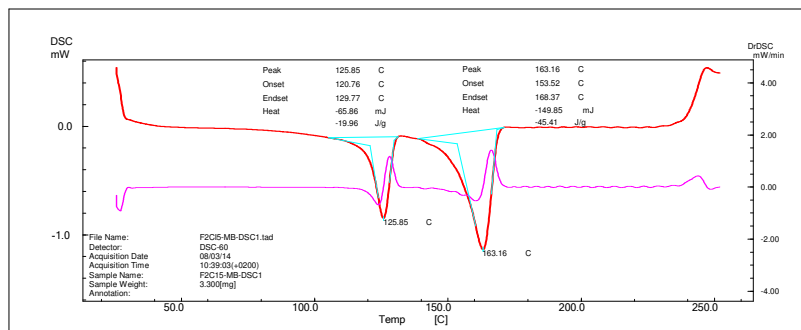


**Figure B.29** DSC thermogram of binary nanocomposite containing 2 wt% Cloisite® 15A (MB).

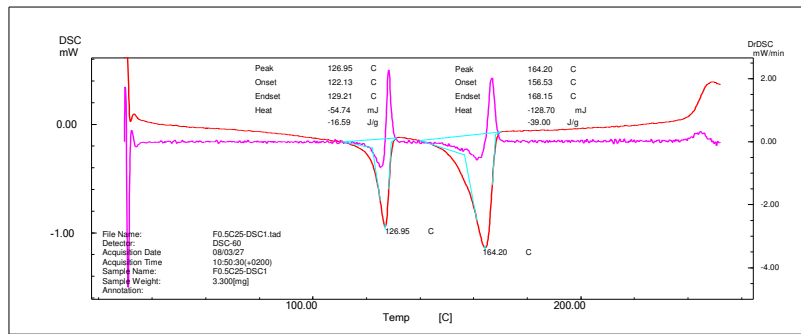


**Figure B.30** DSC thermogram of binary nanocomposite containing 0.5 wt% Cloisite® 25A.

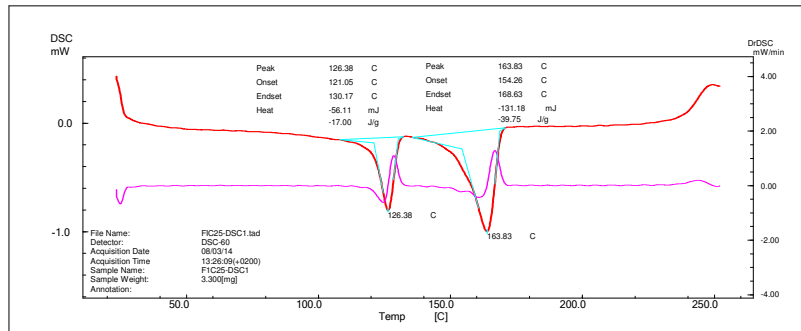


**Figure B.31** DSC thermogram of binary nanocomposite containing 1 wt% Cloisite® 25A.

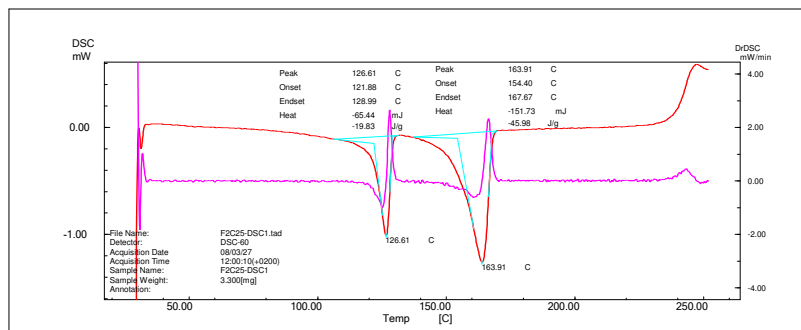


**Figure B.32** DSC thermogram of binary nanocomposite containing 2 wt% Cloisite® 25A.

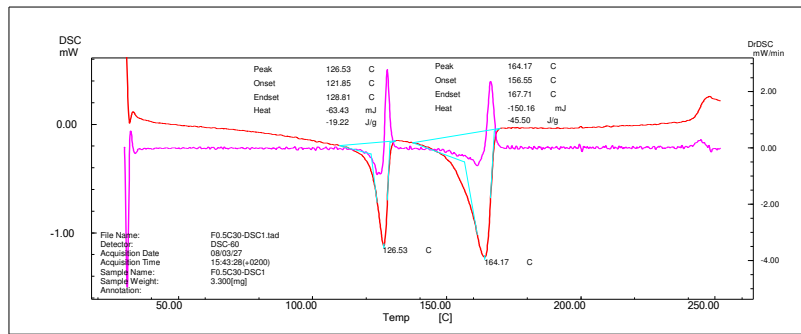


**Figure B.33** DSC thermogram of binary nanocomposite containing 0.5 wt% Cloisite® 30B.

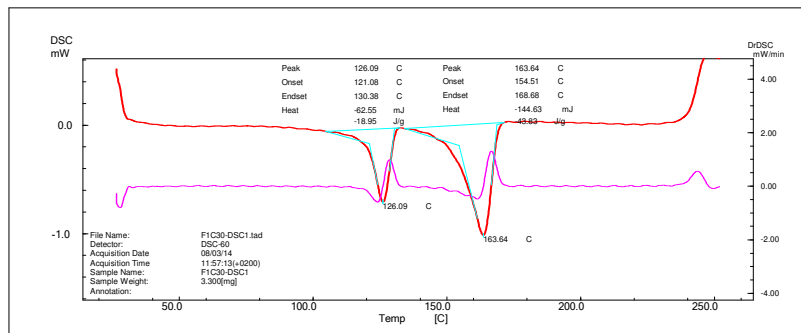


**Figure B.34** DSC thermogram of binary nanocomposite containing 1 wt% Cloisite® 30B.

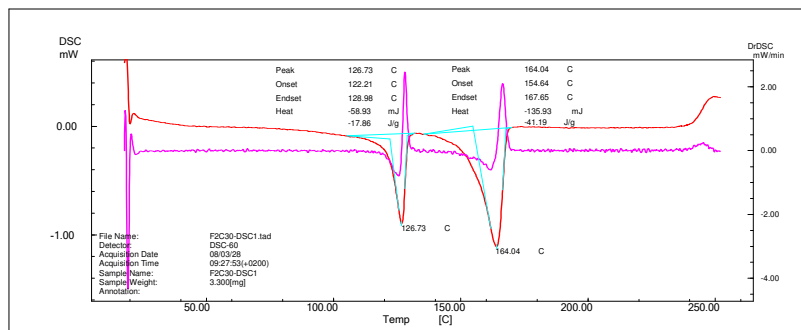


**Figure B.35** DSC thermogram of binary nanocomposite containing 2 wt% Cloisite® 30B.

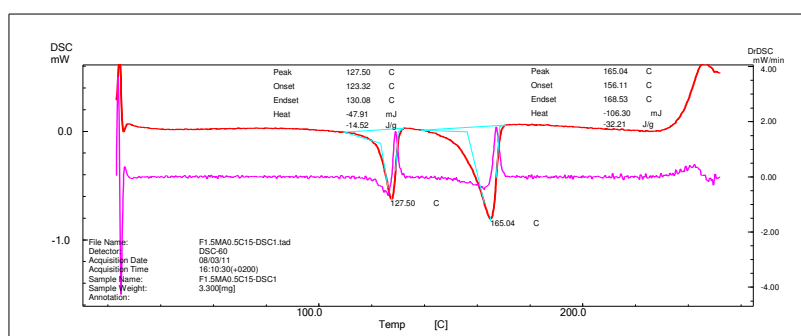


**Figure B.36** DSC thermogram of ternary nanocomposite containing 0.5 wt% Cloisite® 15A and 0.5 wt% PP-MAH.

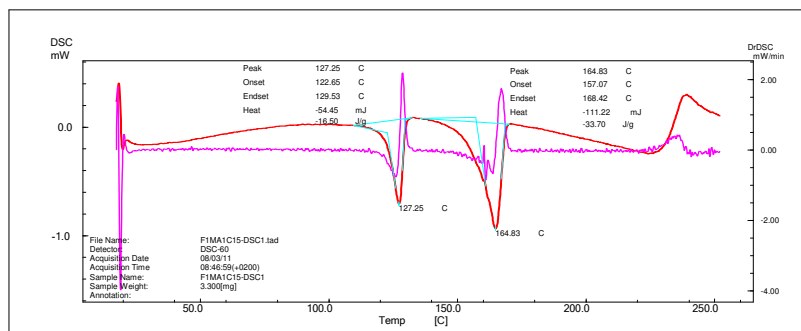


**Figure B.37** DSC thermogram of ternary nanocomposite containing 1 wt% Cloisite® 15A and 1 wt% PP-MAH.

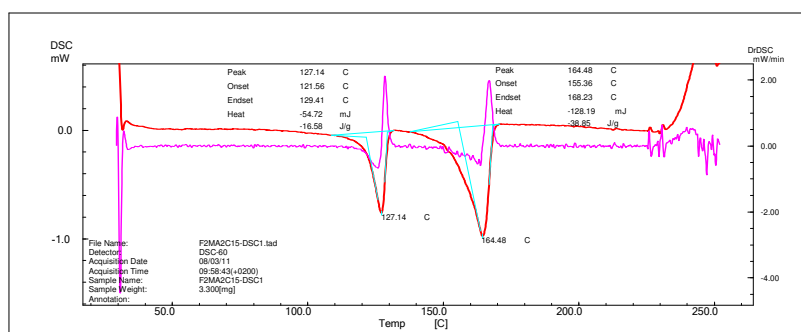


**Figure B.38** DSC thermogram of ternary nanocomposite containing 2 wt% Cloisite® 15A and 2 wt% PP-MAH.

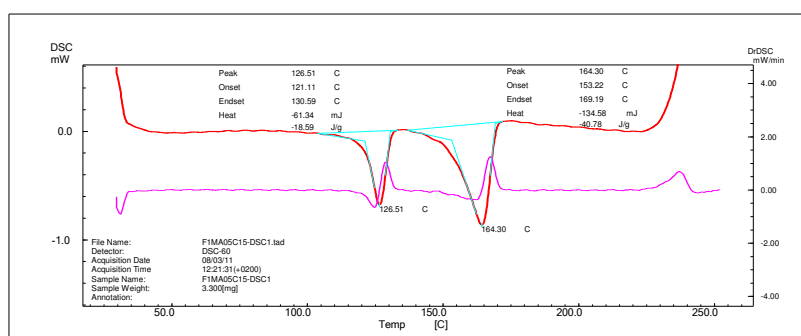


**Figure B.39** DSC thermogram of ternary nanocomposite containing 0.5 wt% Cloisite® 15A and 1 wt% PP-MAH.

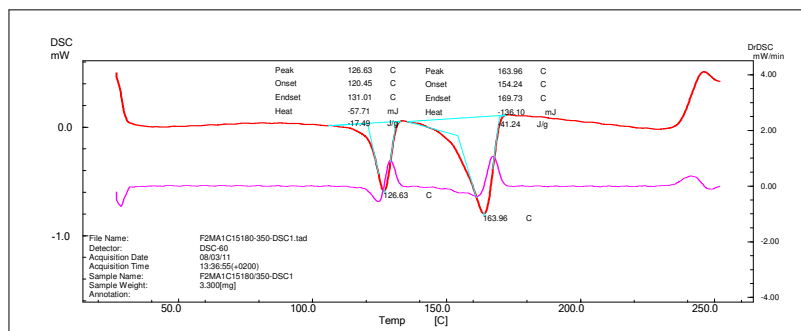


**Figure B.40** DSC thermogram of ternary nanocomposite containing 1 wt% Cloisite® 15A and 2 wt% PP-MAH, prepared at 180 °C and 350 rpm.

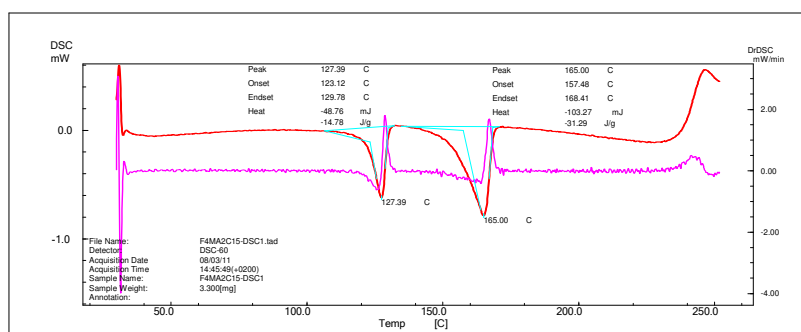


**Figure B.41** DSC thermogram of ternary nanocomposite containing 2 wt% Cloisite® 15A and 4 wt% PP-MAH.

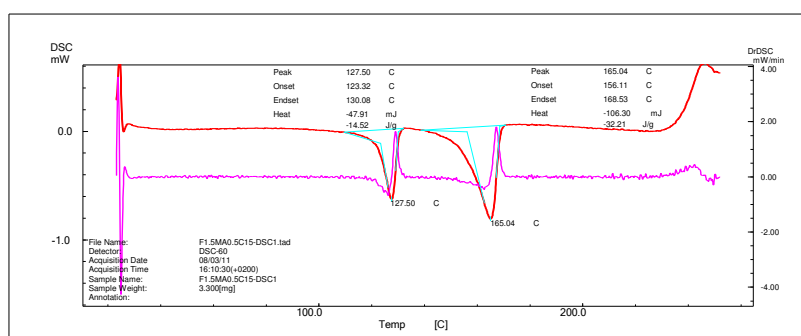


**Figure B.42** DSC thermogram of ternary nanocomposite containing 0.5 wt% Cloisite® 15A and 1.5 wt% PP-MAH.

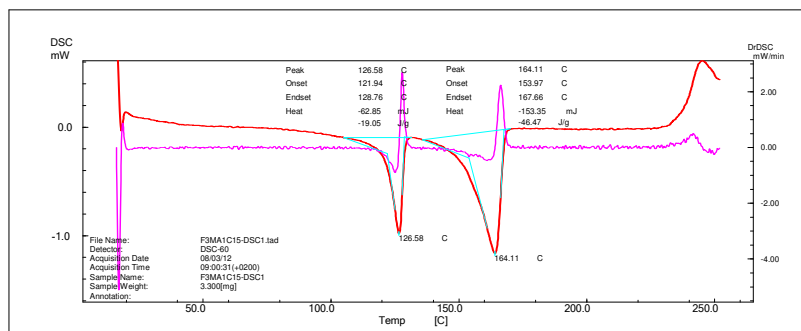


**Figure B.43** DSC thermogram of ternary nanocomposite containing 1 wt% Cloisite® 15A and 3 wt% PP-MAH.

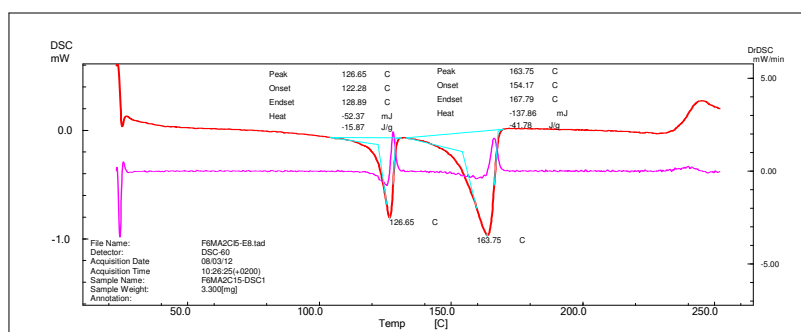


**Figure B.44** DSC thermogram of ternary nanocomposite containing 2 wt% Cloisite® 15A and 6 wt% PP-MAH.

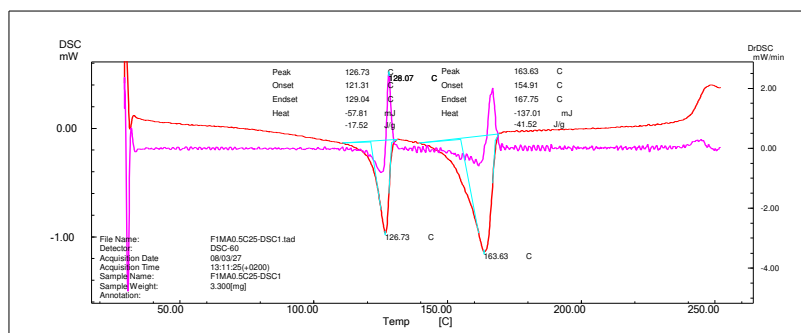


**Figure B.45** DSC thermogram of ternary nanocomposite containing 0.5 wt% Cloisite® 25A and 1 wt% PP-MAH.

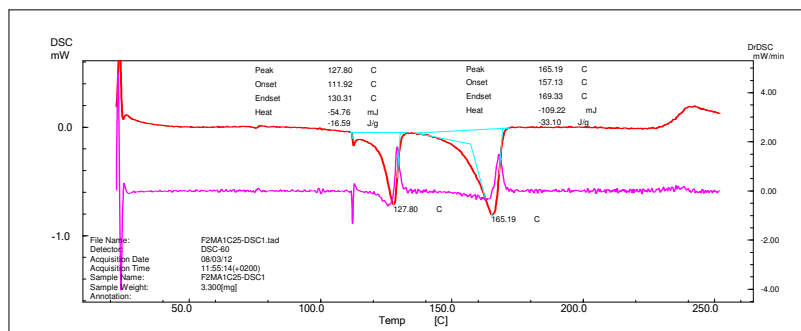


**Figure B.46** DSC thermogram of ternary nanocomposite containing 1 wt% Cloisite® 25A and 2 wt% PP-MAH.

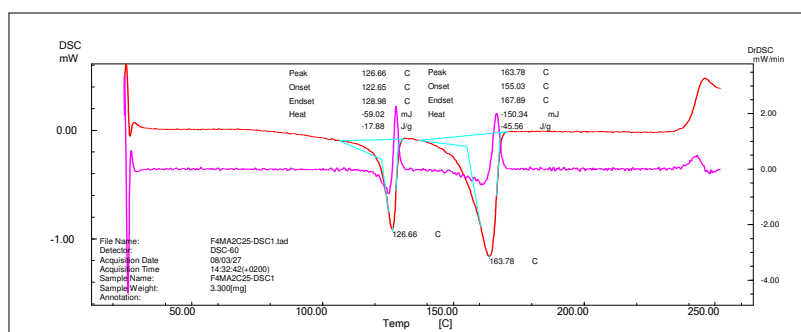


**Figure B.47** DSC thermogram of ternary nanocomposite containing 2 wt% Cloisite® 25A and 4 wt% PP-MAH.

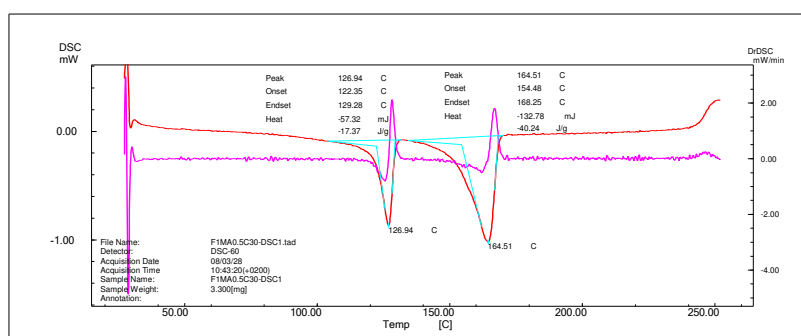


**Figure B.48** DSC thermogram of ternary nanocomposite containing 0.5 wt% Cloisite® 30B and 1 wt% PP-MAH.

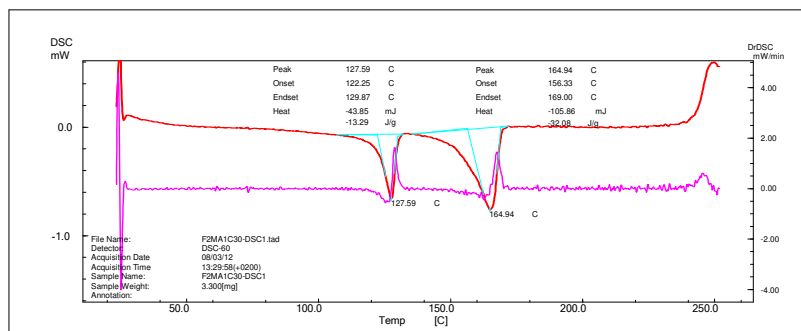


**Figure B.49** DSC thermogram of ternary nanocomposite containing 1 wt% Cloisite® 30B and 2 wt% PP-MAH

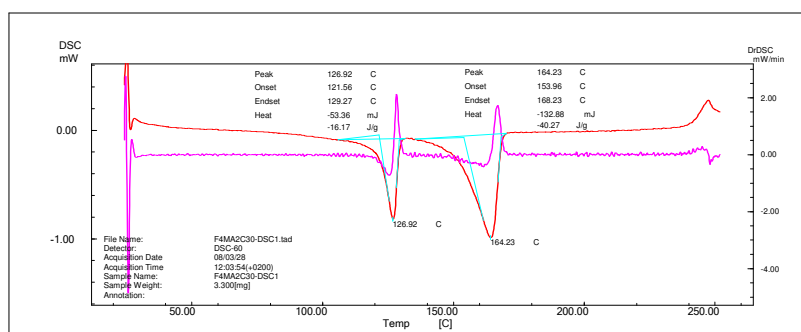


**Figure B.50** DSC thermogram of ternary nanocomposite containing 2 wt% Cloisite® 30B and 4 wt% PP-MAH.